THE JOURNAL
OF
CHEMICAL PHYSICS

VOLUME 18, NUMBER 11 NOVEMBER, 1950

Light Scattering by Concentrated Polymer Solutions*

P. DEBYE AND A. M. BUECHE**
Department of Chemistry, Cornell University, Ithaca, New York
(Received April 24, 1950)

The light scattered by benzene solutions of polystyrene up to a volume fraction of polymer of 0.62 has been measured. The results are compared with what was to be expected on the basis of recent thermodynamic theories for polymer solutions.

This comparison has led to the recognition of a new and rapid method for estimating molecular weights. The method also seems to be a convenient one for obtaining thermodynamic information.

WE have recently measured the 90° light scattering of polystyrene solutions in benzene up to a volume fraction of polymer $v_2=0.62$. The data are compared with the curves to be expected on the basis of current thermodynamic theories. A new method for the determination of molecular weights is indicated. The method is general and appears to be an easy and rapid one for obtaining thermodynamic information about concentrated as well as dilute solutions.

EXPERIMENTAL

A sample of Dow Styron, having an intrinsic viscosity at 35°C in benzene of 1.0, was carefully washed with freshly distilled methyl alcohol to remove dust and was dried in vacuum. Portions of this sample were weighed into test tubes to be used in our light scattering apparatus, different amounts of benzene were added and the tubes sealed off. They were then heated to about 100°C for several days until the polymer and solvent were homogeneously mixed. After cooling to room temperature the 90° scattering, for $\lambda=4358$A, was measured in an apparatus[1] described elsewhere. Since the dissymmetry of scattering for this sample is small, it was neglected and the 90° values were used to calculate the turbidities, τ_0, of the solutions. The data are shown in Fig. 1. The value at $v_2=0$ is that obtained with the tubes filled with benzene and represents the scattering of benzene plus a small amount of stray light in the instrument.

The curve obtained shows the usual rapid increase of τ_0 in the low concentration region. This initial slope is proportional to the weight average molecular weight of the polymer. Data in this region have been used many times in the past for molecular weight determinations.[2] The curve then goes through a rather sharp maximum and finally remains almost constant after about $v_2=0.4$. This maximum is of considerable importance. Its use in the determination of molecular weights will be discussed in the next section.

DISCUSSION

It has been shown[3] that the total turbidity, τ_0, of a solution of a single substance in a solvent is given by

$$\tau_0=\tau'+HRT\bar{V}_0C/[\partial(P\bar{V}_0)/\partial C], \qquad (1)$$

where τ' is the background scattering due to bulk density fluctuations given by the Smoluchowski-Einstein calculation, R, T, $\bar{V}_0$, C, and P are the gas constant, absolute temperature, partial molar volume of solvent, concentration in g/cc, and osmotic pressure respectively. H is the usual light scattering constant given by

$$H=(32\pi^3/3)(\bar{\mu}^2/N\lambda^4)(\partial\bar{\mu}/\partial C)^2,*$$

* The work reported in this paper was done in connection with the Government Research Program on Synthetic Rubber under contract with the Office of Rubber Reserve, Reconstruction Finance Corporation.

** Present address: General Electric Research Laboratory, Schenectady, New York.

[1] P. Debye, J. Phys. Colloid Chem. **51**, 18 (1947).

[2] G. Oster, Chem. Rev. **43**, 319 (1948).

[3] A. Einstein, Ann. d. Physik **33**, 1275 (1910).

* Instead of the quantity $\bar{\mu}^2(\partial\bar{\mu}/\partial C)^2$ the formula should in its exact form contain $(\frac{1}{4})(\partial\epsilon/\partial C)^2$ where ϵ is the dielectric constant of the solution. The quantity ϵ at 1.5 Mc has been measured in this laboratory up to concentrations of polymer of over 25 percent for this system and found to be linear and extrapolates to the value for the pure polymer. (See P. Debye and F. J. Bueche,

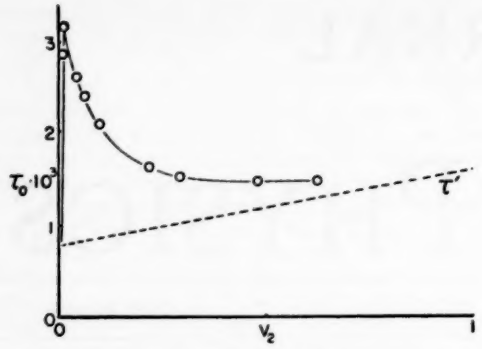

FIG. 1. Turbidity of polystyrene in benzene (τ_0) *vs.* volume fraction of polymer (circles).

where $\bar{\mu}$ is the refractive index of the solution, λ the wave-length of the light in vacuum and N is Avogadro's number. Writing C in terms of the volume fraction of polymer as $C=v_2d_2$ (d_2 was found to be 1.09 for this system at 30°C from measurements in the dilute solution range) and using Flory's[4] expression for the osmotic pressure assuming both $\bar{V}_0$ and d_2 to be independent of C the excess turbidity due to concentration fluctuations can be written as

$$\tau=\tau_0-\tau'=HMC\Big/\left[1-nv_2\left(\frac{1}{1-v_2}-2\mu\right)\right]$$

or

$$\tau=\frac{HMd_2}{n}\Big/\left(\frac{1+(n-1)v_2}{nv_2(1-v_2)}-2\mu\right),$$

where μ is the constant in the van Laar expression for the heat of mixing, n is the ratio of the molecular volumes of polymer and solvent, or the number of links in the polymer chain in the Flory-Huggins sense, and

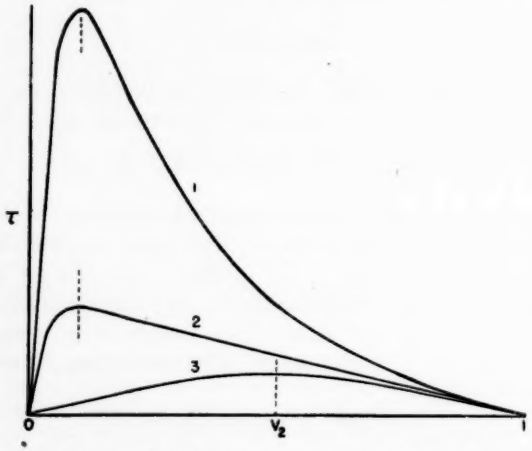

FIG. 2. Calculated turbidities of polymers. Curve 1, $n=100$, $\mu=0.45$; Curve 2, $n=100$, $\mu=0$; Curve 3, $n=1$, $\mu=0.45$. Vertical dashed lines indicate position of $(v_2)_m$.

M is the molecular weight of the polymer molecule. In the case of a molecular weight distribution of the polymer, H. C. Brinkman and J. J. Hermans[5] have shown by means of a formula developed in 1915 by Zernike that n must be replaced by the quotient formed by dividing the weight average molecular volume of the polymer by the molecular volume of the solvent. The quantity M is then the weight average molecular weight of the polymer. Thus the turbidity curve depends on only the weight average molecular weight rather than some combination of averages. This will always be true provided the free energy has the general form given in Eq. (18) of the article by Brinkman and Hermans. The Flory-Huggins formula is of this form.

From Eq. (2) it is evident that a maximum of the turbidity will occur where the term preceding 2μ in the denominator goes through a minimum. This means that the position of the maximum on the concentration axis will be *independent* of the interaction constant μ.

By differentiation of Eq. (2) with respect to v_2 it can be shown that the turbidity τ should have a maximum when

$$v_2=(v_2)_m=1/(1+n^{\frac{1}{2}}).$$

In the case of polymers of high molecular weight this reduces to $(v_2)_m=n^{-\frac{1}{2}}$.

It is interesting to notice that, according to the theories, $(v_2)_m$ is independent of the value of μ. The position of the maximum, then, allows one to determine the quotient of the molecular volumes for polymer and solvent independent of solvent type. For a given system it is to be expected from the theories that this quotient will be proportional to the molecular weight of the polymer. Always assuming the theory to be absolutely correct we have determined the absolute value of the actual volume displaced by a polymer molecule in the solution. After calibration for a given polymer-solvent system finding the position of the maximum may afford a rapid means of estimating molecular weights in the absence of a scattering standard and with a minimum of computation.

If the position of the maximum is to be used for this purpose one would certainly like the maximum to be as high and as sharp as possible. These conditions can be met by choosing a solvent in which the refractive index increment is large and for which the μ value is as close to 0.5 as possible. If $\mu=0.5$ the theories predict the polymer will precipitate when $v_2=(v_2)_m$.

In Fig. 2 we have plotted several theoretical curves using Eq. (2). It can be seen that while $(v_2)_m$ is independent of μ (curves 1 and 2) the height of the maximum and the shape of the curve will depend on μ. The slopes of the curves near $v_2=1$ correspond to a solution of solvent in pure polymer and are proportional to the molecular weight of the solvent. A comparison of the

J. Phys. Colloid Chem., to be published.) Since we know of no theoretical reason why it should not be linear we assume that the optical dielectric constant behaves similarly.

[4] P. Flory, J. Chem. Phys. **10**, 51 (1942).

[5] H. Brinkman and J. Hermans, J. Chem. Phys. **17**, 574 (1949); see also J. Kirkwood and R. Goldberg, *ibid.* **18**, 54 (1950) and W. Stockmayer, *ibid.* **18**, 58 (1950).

experimental data with the theoretical curves should enable one to decide whether a single value of μ will represent the data over the range studied and thus check the current theories of polymer solutions.

To compare our data with the calculated curves it is necessary to know how τ' depends on v_2. It is given by[3]

$$\tau' = (8\pi^3/27)(RT/N\lambda^4)\beta[(\bar{\mu}^2-1)(\bar{\mu}^2+2)]^2,$$

where β is the isothermal compressibility. However, β is unknown for these solutions. We can estimate τ' in the following manner. In the region near $v_2=1$ the slope of the experimental curve must correspond to that which represents the excess scattering produced by the solution of benzene in pure polystyrene. One can then choose an approximate value of μ and adjust the theoretical curve to the data such that they fit at some point in the region of the maximum. The slope that the calculated curve makes with the axis of $\tau=0$ at high concentrations will not be far different from the slope the data should make with $\tau=0$ after subtraction of τ'. In the present work we have, for the time being, followed this procedure, assumed τ' to be linear with v_2 and have represented it by the dotted line in Fig. 1. We hesitate, however, to say that the great variation in τ' is caused by changes in compressibility alone. Any dust added with the polymer would have the same effect.

The adjusted data are compared in Fig. 3 with curves calculated from Eq. (2) using $\mu=0.45$ and 0.47 and $n=5.77\times10^3$. The data presented here are not sufficient to allow a calculation of a precise value of n. The value used is estimated from the position of the highest point. The molecular weight of the polymer is about 2.18×10^5 so that this value of n would lead to the conclusion that the effective volume of one styrene unit in the polymer chain is 2.76 times the volume of a benzene molecule. As will be seen the maxima fall approximately in the same place but neither curve fits the data exactly in the intermediate concentration range. The small discrepancies may be the result of the rough approximation for τ' or reflect the inadequacy of the thermodynamic theories for polymer solutions. A more complete investigation in which more data are obtained at low concentrations and in the region around the maximum would be interesting. Measurements at different temperatures may be carried out quite easily with the experimental arrangement used and would lead to estimates of the heats of solution enabling one to compute the entropies of mixing. Further work along these lines is in progress.

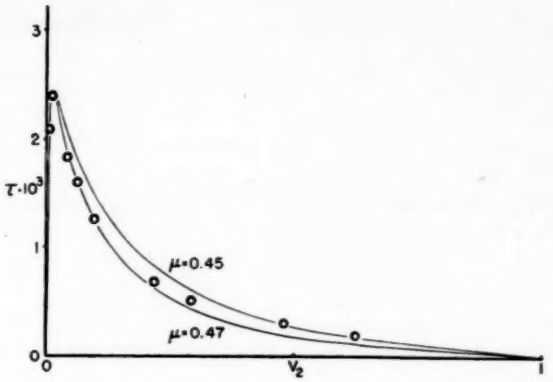

FIG. 3. Comparison of corrected turbidities for polystyrene in benzene with theory.

Originally this work was undertaken in order to approach the turbidity of the solid polymer from the side of its solution. Solutions of very high polymer concentrations are difficult to handle; however, the curve in Fig. 1 which goes to $v_2=0.62$ seems to indicate that a final value for the turbidity of an ideal solid polymer is already nearly reached at this point. This value still is definitely smaller than that found experimentally for any solid polystyrene so far investigated. Whether or not this difference is due to inhomogeneities which might be frozen in during the preparation of the solid polymer has not yet been decided.

THE JOURNAL OF CHEMICAL PHYSICS VOLUME 18, NUMBER 11 NOVEMBER, 1950

The Theory of Ionic Solutions

JOSEPH E. MAYER
Institute for Nuclear Studies, University of Chicago, Chicago, Illinois
(Received June 6, 1950)

The virial development for the osmotic pressure of a solution may be used, if the potentials of average force of the solute molecules at infinite dilution are known, to compute the deviations from perfect solution behavior. The expression for the logarithm of the activity coefficient can thus be obtained as a sum of coefficients multiplied by powers of the concentration. For an ionic solution, with $1/R^2$ forces, the series is only conditionally convergent. By summing certain additive terms occurring in the coefficients over all powers of concentration convergence can be attained.

The integrations necessary to obtain terms correct up to and including c^1 are performed. The results are given in terms of certain functions which can readily be computed.

I. INTRODUCTION

THE pressure of a gas may be expressed by the equation

$$P/kT+c-\sum_{n\geq 2}(n-1)B_n c^n, \tag{1}$$

where c is the concentration in molecules per unit volume of the gas and $-(n-1)B_n$ is the n'th virial coefficient. The quantity, B_n, may be expressed as an integral over the coordinates of n molecules of an integrand depending upon the potential energies of n and fewer molecules. In the particular case that the potential energy, U_n, of n molecules can be expressed as the sum of the potentials $u(R_{ij})$ between the pairs, i and j, of molecules:

$$U_n=\sum_{n\geq i>j\geq 1}\sum u(R_{ij}), \tag{2}$$

then the integrand of B_n is a sum of products of the functions:

$$f_{ij}^*=\{\exp[-u(R_{ij})/kT]\}-1. \tag{3}$$

The osmotic pressure, P, of a solution may likewise be expressed in the form of Eq. (1) with c the concentration of solute molecules expressed in the units of molecules per unit volume.

Let $W_n(x_1\cdots z_n)$ be the potential of average force of n solute molecules in the solution at the limit of infinite dilution. This potential of average force has the following meaning. Consider n solute molecules at the coordinate positions $x_1\cdots z_n$ in an infinitely dilute solution, so that no other solute molecules are in the neighborhood. There will be an average force $\bar{f}_{xi}(x_1\cdots, z_n)$ acting along any one of the coordinates, say the x coordinate of the i'th molecule. This average force on i will be additively composed of the direct force due to the other fixed solute molecules, and a fluctuating force due to the fact that the fixed solute molecules perturb the spherical symmetry of the solvent molecules around the i'th. This average force may be written as the derivative of a potential, $\bar{f}_{xi}(x_1, \cdots, z_n)=-\partial W_n(x_1, \cdots, z_n)/\partial x_i$.

It can be rigorously shown[1] that if W_n replaces U_n in the expression for B_n the coefficients in the osmotic pressure equation are given by the same formalism as in the pressure of the gas. If, corresponding to Eq. (2), one writes

$$W_n=\sum_{n\geq i>j=1} w(R_{ij}),$$

then the B_n's in the osmotic pressure equation have as an integrand a sum of products of functions

$$f_{ij}=\{\exp[-w(R_{ij})/kT]\}-1. \tag{4}$$

In the case that the solute consists of σ chemical species, $1, \cdots s, \cdots r, \cdots \sigma$ Eq. (1) may still be employed.[2] In this case one interprets $n=n_1, \cdots, n_\sigma$, to be a set of numbers of the molecules of the different species and $c=c_1, \cdots, c_\sigma$, to be a set of the concentrations. We use the symbolism

$$c^n=c_1^{n_1}c_2^{n_2}\cdots c^{n_\sigma}, \tag{5}$$

and

$$n!=n_1!n_2!\cdots n_\sigma!. \tag{6}$$

Equation (1) then takes the form:

$$P/kT=\sum_{s=1}^{s=\sigma} c_s-\sum_{n\geq 2}(\textstyle\sum n_s-1)B_n c^n. \tag{7}$$

Since by appropriate thermodynamic manipulation the osmotic pressure expression can be used to give the activity coefficients, γ_s of the different solute species, the calculation of the coefficients B_n permits the evaluation of all the thermodynamic properties of the solution.

Equation (7) has not frequently been used to calculate the properties of a solution since usually the potentials of average force W_n are not assumed to be known functions. Zimm[3] has used this expression to give the dependence upon molecular weight of the deviations from ideality of a solution of polymers. However, in the case of an ionic solute one has an obvious although not neces-

[1] J. E. Mayer, J. Chem. Phys. **10**, 629 (1942).
[2] W. G. McMillan, Jr., and J. E. Mayer, J. Chem. Phys. **13**, 276 (1945).
[3] B. H. Zimm, J. Chem. Phys. **14**, 164 (1946).

sarily exact expression to use for the potentials of average force. At large distances, R_{sr} between two ions, one of type s and one of type r, the potential of average force in the infinitely dilute solution will be given by the expression, $w(R_{sr})=z_s z_r \epsilon^2/DR_{sr}$ where ϵ is the electronic charge, D the dielectric constant of the solvent, and z_s, z_r are the integer charges of type s and r respectively. At sufficiently short distances the mutual potential of the pair of ions must be positive and extremely large due to their mutual repulsion when their electronic shells overlap. If we write

$$w(R_{sr})=(z_s z_r \epsilon^2/DR_{sr})+w^*(R_{sr}), \tag{8}$$

we may assume, as a first approximation, that:

$$\begin{aligned} w^*(R_{sr})&=\infty, \quad R_{sr}\leq a_s+a_r \\ &=0, \quad R_{sr}>a_s+a_r. \end{aligned} \tag{9}$$

This may be regarded as the equation for the potential of average force between a pair of "ideal" ions in an "idealized" solvent. For real ions in a real solvent Eq. (8) may still be used and w^* will differ from zero only for small values of the distance, although not having the simple form of Eq. (9). In the development that follows it is not essential to assume the simple form Eq. (9) for w^*, and if w^* were known its value could be used. This simple form is, however, actually assumed in the present lack of knowledge of a better form to use.

If Eq. (8) is used in (4) for f_{sr} one runs immediately into difficulties in the evaluation of the coefficients B_n. For large distances for which w is small the exponent in (4) can be expanded and

$$f_{sr}\cong(z_r z_s \epsilon^2/DkT)(1/R_{sr}).$$

The second virial coefficient B_{sr} giving the effect of the interaction of ions of type s with ions of type r is

$$B_{sr}=\frac{1}{1+\delta(s,r)}\int_0^\infty 4\pi R^2 f_{sr}(R)dR.$$

If the expansion for f_{sr} at large distances is substituted in this, the integral clearly diverges. The divergence in this case is not serious since the summation over all values of s and r leads to zero before integration due to the demand of electrical neutrality for the solution. However, the higher terms in the development of the exponent of f_{sr} lead to terms with the distance square in the denominator and with the square of the charges occurring. These integrals also diverge and since the square of the charges appear no summation helps us out of the difficulty.

An equation similar to (7) can be used to calculate the osmotic pressure in which the coefficients B_n are calculated from the potential of average force in a solution of any definite concentration of solute ions which need not necessarily be zero.[2] In this case we know from the Debye theory that the potential of average force at large distances involves an additional factor $e^{-\kappa R}$ where the Debye κ is proportional to the square root of the concentration of ions. If this factor is used all integrals necessarily converge and no difficulty is experienced in evaluating the coefficient B_n. However, a certain logical difficulty arises in the use of this method. The Debye theory gives only a first approximation to the potential of average force. If corrections of higher powers of the concentration occur in the equation for the potential these may radically affect the B_n for higher n values and, therefore, the osmotic pressure equation at higher concentrations. The method of calculation which is given below does not involve this difficulty. It is, however, formally identical to using the Debye equation with the potentials multiplied by the factor $e^{-\kappa R}$ in (8) and letting the initial concentration at which the B_n's are computed and, therefore, also κ, approach zero. If this procedure is followed the initial concentrations $c_s^{(0)}$ which enter the somewhat more complicated form of Eq. (7) and the Debye κ should logically approach zero with a definite relationship between them. It turns out, however, that the equations can be handled by letting κ and $c_s^{(0)}$ approach zero independently. This means that we can use a somewhat more logically elegant, but more formal, mathematical method to evaluate Eq. (7). The analogy with the use of the Debye κ is discussed here only to point out a physical significance to the mathematical method which we employ.

If one computes the properties of a solute containing particles s and r for which the mutual potential of pairs is given by the equation:

$$w(R_{sr})=(z_s z_r \epsilon^2/DR_{sr})e^{-\alpha R_{sr}}+w^*(R_{sr}), \tag{10}$$

no difficulty is encountered in evaluating the coefficient B_n since all integrals necessarily converge as long as α is finite and positive.

As has been stated the integrand of the integral B_n is a sum of products. Equation (7) is, therefore, really a multiple sum in which the order of summation has been implicitly specified, namely, that one sums over all products in the integrand of a specific B_n and *then* over all values of n. As long as the integrals converge it is, of course, equally legitimate to sum first over all values of n for some specified type of product in the integrand, and then later over all types of products. If this is done in a particular way the sum over n of certain types of products of the integrands can be seen to converge in the limit that α approaches zero. In this case we have then computed the properties of a solution for which the potentials of average force between solute molecules is of the form of Eq. (8).

II. METHOD

We treat a system composed of σ kinds of monatomic particles, the indices $1\leq r, s, t, u\leq\sigma$ being used to indicate the particle type. The potential, w_{sr}, between two particles of type s and r, as a function of the distance,

R, between them, is assumed to have the form of Eq. (10) where $w_{sr}^*(R)$ falls rapidly to zero as R becomes large. We shall later let α approach zero, and identify ϵ with the electronic charge, z_s, z_r with the charges in units of electronic charge of the ions s and r, and D the dielectric constant of the solvent.

The distribution function, F_{sr} is $\exp -w_{sr}/kT$, so that, if,

$$\lambda = 4\pi\epsilon^2/DkT, \tag{11}$$

$$g(R) = e^{-\alpha R}/4\pi R, \tag{12}$$

$$k_{sr}^{**}(R) = e^{-w_{sr}^*/kT} - 1, \tag{13}$$

then, by developing the exponential of g we find:

$$f_{sr} = F_{sr} - 1 = k_{sr}^{**}(R) + \sum_{n\geq 1} [-\lambda z_r z_s g(R)]^n [k_{sr}^{**}+1]/n!. \tag{14}$$

The short range potential $w_{sr}^*(R)$ is large and positive for very small values of R, so that $k_{sr}^{**} = -1$ for small R's, and since $w_{sr}^*(R) \to 0$ as $R \to \infty$ one has that $k_{sr}^{**} = 0$ for large values of R. We choose an arbitrary distance a_{sr} and write:

$$\begin{aligned} k_{sr}^{**}(R) &= e^{-u_{sr}^*/kT} - 1 = k_{sr}(R) + k_{sr}^*(R) \\ k_{sr}^*(R) &= -1, \quad \text{for} \quad 0 \leq R \leq a_{sr}, \\ k_{sr}^*(R) &= 0, \quad \text{for} \quad a_{sr} < R \leq \infty. \end{aligned} \tag{15}$$

The value of a_{sr} can be so chosen that, for any single ion pair, the integral of any given function times $k_{sr}(R)$ is zero.

Define the integral:

$$B_n = B_{n_1, n_2, \cdots, n_r, \cdots, n_\sigma} = [\prod_s n_s!]^{-1} \int\int \cdots \int \sum \prod (F_{sr} - 1) d\tau_{n-1}, \tag{16}$$

where the integration is extended over the coordinates of all but one of the particles, and the integrand is a sum of products of functions, $F_{sr} - 1$, of the distances between the constituent molecules of the set n. The summation runs over all products that form a more than singly connected graph[4] (except for $n = 2$ when the single term is $F_{sr} - 1$).

Let c_s be the concentration, in molecules per unit volume, of the species s, and let

$$c^n = {c_1}^{n_1} \cdots {c_s}^{n_s} \cdots {c_\sigma}^{n_\sigma}. \tag{17}$$

Define

$$S = \sum_n (\sum n_s \geq 2) B_n c^n. \tag{18}$$

Then if γ_s is the activity coefficient of species s, the equation*

$$-\ln \gamma_t = S_t = \partial S/\partial c_t, \tag{19}$$

permits the evaluation of this quantity in terms of the integrals of Eq. (16), and the osmotic pressure P is given by the equation

$$P/kT = \sum_{s=1}^{s=\sigma} c_s + S - \sum_{s\geq 1}^{s=\sigma} c_s \partial S/\partial c_s. \tag{19'}$$

Now the integrand of B_n is a sum of products. Rather than summing all products, integrating to find B_n, and then forming the sum S of (18), we may sum over n for some given type of product in the integrand and *then* sum all product types to form S. This rearrangement of the order of summation is necessary because of the divergence of the individual integrals as $\alpha \to 0$. The rearrangement has significance only if certain types of products occurring in the integrand of B_n, Eq. (16), are classified and described.

To classify the products in (16) it is convenient to draw a one to one correspondence between the product of functions $F_{sr} - 1$, and a graph, the n vertices of which represent the particles of the set n, $\nu = \sum n_s$, and the lines of which, connecting the vertices, represent the functions, $k_{sr}^{**}(R)$ or $-\lambda z_r z_s g(R)$ of the development (14) of $F_{sr} - 1$. When a function, $k_{sr}^{**}(R)$, of the distance between two particles is represented by a line in a graph we shall refer to this as a k-bond, and in the figures the line is drawn dotted, when a function $-\lambda z_r z_s g$ is represented, the line is solid in the figures, and is referred to as a g-bond. Two or more solid lines drawn between the same two vertices will represent the second or higher power of g, respectively, in the development (14).

For $\nu = 2$ there are two graphs, sr, l; and $sr, k0$; of Fig. 1, in which the two particles, one of type s, and one of type r, are connected by a single line, a g-bond or k-bond respectively. These are the only two graph types in which any particle is but singly connected to the other vertices of the graph.

In all graphs for $\nu > 2$ the particles must be more than singly connected, or the corresponding product does not occur in (16). This means that there are at least two paths of lines, not intersecting at any vertex, by which one can go between any two member vertices of the graph.

The graphs of all other types in Fig. 1 are graphs in which all particles are doubly, and no more than doubly, connected. In type c all bonds are g-bonds. Type c graphs will be referred to as cycles. Types $sr, k1$, differs from c in that a k-bond replaces a g-bond between two particles of the particular types s and r. Type srl,

[4] The meaning of more than singly connected becomes obvious in the later discussion of this section. It is also explained in J. Mayer and M. G. Mayer, *Statistical Mechanics* (John Wiley and Sons, Inc., New York, 1940), p. 288.

* This equation is derived immediately from (72) of reference 2 by setting z equal to the activity of solution in the limit of infinite dilution. Equation (19′) is (73) of reference 2 with the same substitution.

$k0$, 1, $k0$, has two k-bonds, as has type $srtu$, $k0$, 0110, $k0$. Further types with more k-bonds can readily be visualized.

In all other graphs there are some particles which are more than doubly connected with each other, the others being exactly doubly, and no more, connected to any other members of the graph. In Fig. 2 are shown some types in which two particles, one of type s, and one of type r, are triply or more connected.

In Fig. 3 are some examples of graphs in which more than two particles have the property of being more than doubly connected to each other, or at least to one of the others of the unique set.

The integral due to the term corresponding to the single graph type sr, l, multiplied by $c_s c_r$, and summed over all s, r lead to a zero contribution to the sum, S, of Eq. (9). The terms due to the cycles, type c of Fig. 1 lead to the Debye-Hückel limiting law.

The remaining graphs have been labelled, and classified into types according to the following system. There are some particles which are unique in that they are either connected together directly by k-bonds, or are more than doubly connected, whereas the remaining particles are in g-bond chains which connect members of the unique set. For a given type, t, m, the set m of the unique particles, and the structure by which they are connected by k-bonds, or by chains of g-bonds is fixed, but the number of members in the various g-bond chains is variable. Thus each type, t, m, is characterized by a prototype graph, Fig. 4, in which all g-bond chains are of zero length, i.e., all g-bond chains connect the members of the set m directly, and no particles other than those of the set m occur in the prototype graph.

There is one set of numbers, ν_s, $1 \leq s \leq \sigma$, for each prototype graph type, t, m, which is of importance. This number, ν_s, is the number of g-bond ends in the prototype (or g-bond chain ends in the graph type) which end in a particle of type s (of the set m). The total number, ν, of g-bonds in the prototype is then $\nu = \frac{1}{2}\sum \nu_s$, since each bond has two ends.

We now wish to use the fact that, except for the unique cases already discussed, the single bonded type l of two particles, of Fig. 1, and the cycles of g-bonds, type c of Fig. 1, all possible graphs of allowed products of Eq. (16) for B_n can be classified into a graph type, t, m, by the scheme outlined above. Thus to each graph there exists a prototype graph. Conversely, if in any graph there is either a direct g-bond between two particles which are either connected by k-bonds or are triply or more connected, or if there is a g-bond chain between these two particles, then there exist an infinite number of other graphs differing from the first only in the length, and constituent kinds of ions, of this g-bond chain.

We shall first sum (18) over the n for all members belonging to one prototype, and then over the prototypes.

Now we propose to demonstrate the following: Let

$$q(R) = e^{-\kappa R}/4\pi R, \tag{20}$$

where κ is the Debye-Hückel κ:

$$\kappa^2 = \lambda \sum_s z_s^2 c_s, \tag{21}$$

so that $q(R)$ differs from $g(R)$ only in the replacement of α in g by κ in q. Let $B_m^{(t)}$ be the integral of those products of (16) which correspond to the prototype graph of the type t, m, in which all g-bond chains between particles of the set m have no intermediate atoms, but in which the functions $-\lambda z_s z_r g(R)$ are replaced by $-\lambda z_s z_r q(R)$. Then the contribution, $S^{(t,m)}$, to the sum, S, Eq. (18), of all the terms:

$$B_{m+n}^{(tm)} c^{m+n}$$

summed over all sets n of the particles in the g-bond chains, for all products corresponding to the graph

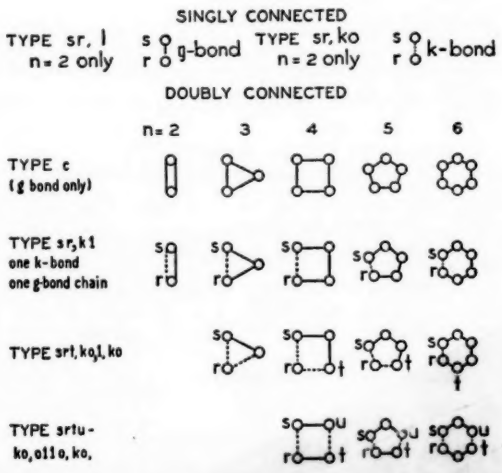

FIG. 1. Graphs representing products which are singly connected or doubly connected only. Solid lines represent g-bonds, dotted lines represent k-bonds.

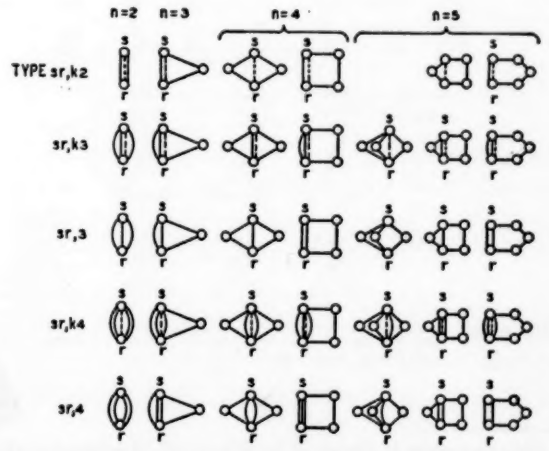

FIG. 2. Graphs representing products in which two molecules, one of type s and one of type r, are more than doubly connected. All other molecules are only doubly connected to all other members of the set.

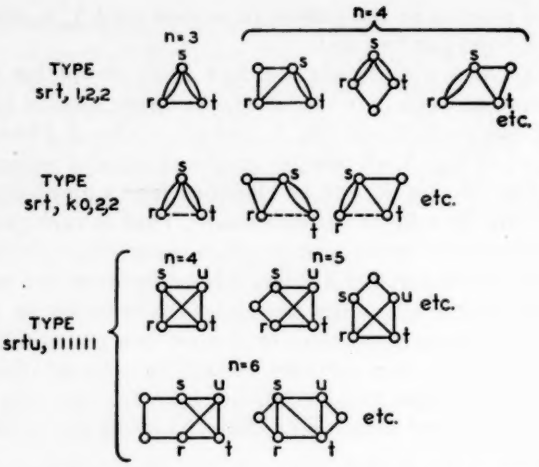

FIG. 3. Graphs representing products in which three molecules, one each of types s, r, t respectively, are more than doubly connected to each other. All other molecules are but doubly connected to all other members of the set.

type l, m, is

$$S^{(l,m)}=B_m^{(l)}c^m \tag{22}$$

in the limit, $\alpha\to 0$, where α is the exponential factor of Eq. (10).

To demonstrate this it is convenient to first define and evaluate an integral. Let

$$q_n(R_{ij})=\int\int\cdots\int g(R_{i1})g(R_{12})\cdots \times g(R_{n-1,n})g(R_{n,j})d\tau_n, \tag{23}$$

which is the integral over the intermediate particles of a chain of g-bonds having n intermediate vertices. If,[5]

$$G(l)=4\pi\int_0^\infty R^2g(R)\frac{\sin lR}{lR}dR.$$
$$g(R)=\frac{1}{2\pi^2}\int_0^\infty l^2G(l)\frac{\sin lR}{lR}dl, \tag{24}$$

and

$$Q_n(l)=G(l)^{n+1}, \tag{25}$$

then $q_n(R)$ and $Q_n(l)$ are related in the same way that $g(R)$ and $G(l)$ are related in Eq. (24).

Consequently, if

$$q(R)=\sum_{n\geq 0}(-\kappa^2)^nq_n(R), \tag{26}$$

then,

$$Q(l)=\sum(-\kappa^2)^nQ_n(l)$$
$$=\sum(-\kappa^2)^n[G(l)]^{n+1}$$
$$=\frac{1}{\kappa^2+[G(l)]^{-1}}, \tag{27}$$

is related to $q(R)$ by the same relation as (24).

Now using (12), that $g=e^{-\alpha R}/4\pi R$ one finds $G=(\alpha^2+l^2)^{-1}$, and*

$$Q(l)=(\kappa^2+\alpha^2+l^2)^{-1}.$$

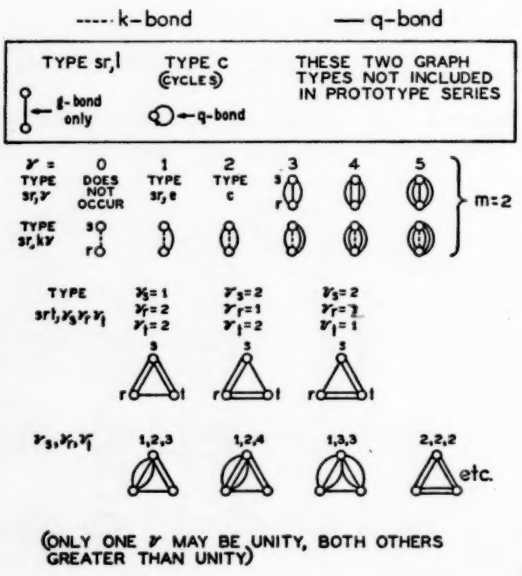

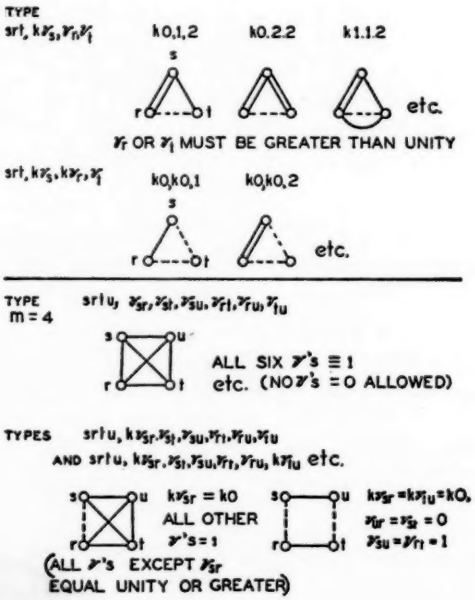

FIG. 4. Prototype graph types.

[5] This procedure is discussed by Elliott W. Montroll and J. E. Mayer, J. Chem. Phys. 9, 626 (1941).

* Onsager has pointed out to the author that the series only converges for $\alpha^2+l^2>\kappa^2$. The function $Q(\alpha,\kappa,l)=(\kappa^2+\alpha^2+l^2)^{-1}$ is thus determined for $\alpha^2+l^2>\kappa^2$.

The function $q(R)=(4\pi R)^{-1}\exp-(\kappa^2+\alpha^2)^{\frac{1}{2}}$ is thus directly determined for $\alpha^2>\kappa^2$. Its single analytical continuation becomes equal to the $q(R)$ of (29) as $\alpha\to 0$.

In the limit $\alpha \to 0$ this leads to

$$Q(t) = (\kappa^2 + t^2)^{-1}, \tag{28}$$

$$q(R) = e^{-\kappa R}/4\pi R. \tag{29}$$

Now consider a particular graph of type t, m. Such a graph has ν chains of g-bonds connecting the members of the set m. Number the g-bond chains consecutively from 1 to ν using the index i, $1 \leq i \leq \nu$. Let us suppose the graph chosen has the set n_i of intermediate particles in the i'th chain:

$$n = \sum_{i=1}^{i=\nu} n_i, \tag{30}$$

where it is to be noted that n and n_i are both sets of numbers: $n_i = n_{i1}, \cdots, n_{is}, \cdots, n_{i\gamma}$, etc. The integral of a single product corresponding to this graph will be:

$$(-\lambda)^\nu [\prod_s z_s^{\nu_s}] \{\prod_i \prod_s (-\lambda z_s^2)^{n_{is}}\} \times I_m^{(t,m)}(\nu_1, \cdots, \nu_i, \cdots), \tag{31}$$

where I is the integral of a single product of the prototype graph with $q_{ni}(R)$ of Eq. (23) replacing the i'th bond in the prototype.

Now we must multiply (31) by c^{n+m}, by the factor, $[\prod_s n_s!]^{-1}$, of Eq. (16) in the definition of B_n, and by the total number of products which lead to the integral (31).

Use the shorthand:

$$n! = n_1! n_2! \cdots, n_s!, \cdots n_\sigma!. \tag{32}$$

The total number of products leading to (31) may be represented as the product of three factors:

(1) The number of ways one may select the sets $m, n_1, \cdots, n_i, \cdots, n_\nu$ from the set $m+n$, which is

$$\frac{(m+n)!}{m! \prod_i n_i!}$$

(2) The product, for each chain, of the number of ways the particles composing the chain can be ordered, which is

$$\prod \nu_i!, \text{ where } \nu_i = \sum_s n_{is}.$$

(3) The number, A_{tm}, of products occurring in the prototype graph containing only the set m of vertices.

Multiplication of (31) by $c^{m+n}/(m+n)!$ times the three factors listed above yields:

$$(-\lambda)^\nu [\prod_s z_s^{\nu_s}] c^m \frac{A_{tm}}{m!} \times \left\{ \prod_i n_i! \prod \frac{(-\lambda z_s^2 c_s)^{n_{si}}}{n_s!} \right\} I_m^{(t,m)}(\nu_1, \cdots, \nu_i, \cdots).$$

Now for given numerical value of the number n_i sum over all values of n_{si}, $n_i = \sum_s n_{si}$, for each i, and one finds

$$(-\lambda)^\nu [\prod_s z_s^{\nu_s}] c^m \frac{A_{tm}}{m!} \prod_i (-\kappa^2)^{n_i} I_m^{(t,m)}(\nu_1, \cdots, \nu_i, \cdots)$$

where κ is given by (21). Then for each i sum over ν_i from zero to infinity. The integral, I, had q_{ni} in the i'th bond, so one replaces this by q, Eq. (26), by making the summation. After summing thus for all i one finds:

$$(-\lambda)^\nu [\prod_s z_s^{\nu_s}] c^m \frac{A_{tm}}{m!} I_m^{(t)},$$

where $I_m^{(t)}$ is the integral over a single product corresponding to the prototype graph t, m, with q-functions in place of each g-bond of the graph.

Since $B_m^{(t)}$ as defined for Eq. (22) is just

$$B_m^{(t)} = (-\lambda)^\nu [\prod_s z_s^{\nu_s}] \frac{A_{tm}}{m!} I_m^{(t)},$$

one arrives at (22).

We now demonstrate that the contribution to S, Eq. (18), of the terms corresponding to graph types l, Fig. 1, is zero. The value of $B_{sr}^{(l)}$ is simply

$$B_{sr}^{(l)} = 4\pi(-z_s z_r \lambda) \int_0^\infty R e^{-\alpha R} dR$$

$$= 4\pi(-z_s z_r \lambda)\alpha^{-2}.$$

Multiply by $c_s c_r$ and sum over all s, r:

$$S^{(l)} = \sum_{s=1}^{s=\sigma} \sum_{r=1}^{r=\sigma} B_{sr}^{(l)} c_s c_r$$

$$= -\frac{4\pi\lambda}{\alpha^2} (\sum z_s c_s)^2.$$

But

$$\sum z_s c_s = 0,$$

if the solution of ions in the solvent is electrically neutral, so $S^{(l)} \equiv 0$.

There remains the case of the simple cycles of g-bonds, type c of Fig. 1. A given product of a set n leads to the integral:

$$\prod_s (-\lambda z_s^2)^{n_s} q_{n-1}(R=0).$$

This must be multiplied by $c^n/n!$ and by the number, $\frac{1}{2}(\nu-1)!$, of ways that ν numbered objects can be arranged in a cycle. One thus finds,

$$\frac{1}{2\nu} \left\{ \nu! \prod_s \frac{(-\lambda z_s^2 c_s)^{n_s}}{n_s!} \right\} q_{\nu-1}(R=0),$$

which must be summed for all values of n_s, and of the

numbers $\sum n_s=n$ between 2 and ∞, to obtain the contribution $S^{(c)}$ to the sum S of Eq. (18). One finds using (21) for κ^2 that

$$S^{(c)}=\sum_{n\geq 2}\frac{1}{2n}(-\kappa^2)^n q_{n-1}(R=0), \tag{33}$$

and,

$$\frac{dS^{(c)}}{d(\kappa^2)}=-\tfrac{1}{2}\sum_{n\geq 1}(-\kappa^2)^n q_n(R=0)$$
$$=-\tfrac{1}{2}[q(R=0)-q_0(R=0)],$$

where the last expression was obtained by using (26) for q, and $q_0=g=e^{-\alpha R}/4\pi R$. With (29) for q, we have:

$$q(R=0)=\lim_{R\to 0}\left[\frac{1}{4\pi R}(1-\kappa R)\right],$$

$$q_0(R=0)=\lim_{R\to 0}\left[\frac{1}{4\pi R}(1-\alpha R)\right],$$

or, in the limit that $\alpha\to 0$,

$$\frac{dS^{(c)}}{d(\kappa^2)}=\frac{\kappa}{8\pi}.$$

Finally, integrating with respect to κ^2 one obtains:

$$S^{(c)}=\kappa^3/12\pi. \tag{34}$$

Since, from (21) for κ^2 one has that

$$\partial\kappa^2/\partial c_t=\lambda z_t^2, \tag{35}$$

and

$$\sum_s c_s\partial\kappa^2/\partial c_s=\kappa^2, \tag{35'}$$

one finds that the contributions of these cyclic integrals to $\ln\gamma_t$ and to the osmotic pressure, are, from (19) and (19′), given by,

$$\ln\gamma_t^{(c)}=-\lambda z_t^2\kappa/8\pi, \tag{36}$$

and,

$$P^{(c)}/kT=c-\kappa^3/24\pi, \tag{36'}$$

which are the expressions of the Debye-Hückel limiting law.

III. ESTIMATION OF ORDERS

We now return to the prototype graphs of Fig. 4, and their contributions, $S^{(t,m)}$, to the sum S of Eq. (9). The integral $B_m^{(t)}$ must be multiplied by c^m, so these contributions to $\ln\gamma_t=-\partial S/\partial c_t$, Eq. (19), are multiplied by the $(m-1)$'th power of the concentration. The integrand, however, is a function of κ, Eq. (21), which is proportional to the square root of the concentration. We may not assume, therefore, that each term is simply proportional to c^{m-1}. We wish to order these terms in the order of their importance at low concentrations, and to discard those proportional to higher powers than $c^{\frac{1}{2}}$.

We use the order appropriate to low concentrations:

$$0(c^{a-\epsilon})<0c^a(\ln c)^{b-\epsilon}<0c^a(\ln c)^b<0c^a,$$

where ϵ may have any small positive value.

If the integral, $B_m^{(t)}$, converges in the limit $c\to 0$, and $\kappa\sim c^{\frac{1}{2}}\to 0$, then $0(S_t^{(t,m)})=c^{m-1}$. If, however, as $\kappa\to 0$ we have $B_m^{(t)}\sim(\ln\kappa)^b\kappa^{-a}$ then $0(S_t^{(t,m)})=c^{m-1-\frac{1}{2}a}(\ln c)^b$.

Turn first to the prototype graphs of two vertices, $m=2$, of Fig. 4. Consider first types sr, $k0$; sr, $k1$; and sr, $k2$. The k-bond is short range, that is the function $k_{sr}{}^{**}(R)\to 0$ for large values of R. As $\kappa\to 0$ the function $k_{sr}{}^{**}$ is multiplied by R^2, R, R^0 respectively, so all three integrals converge as $\kappa\to 0$. We have, then:

$$0(S_t^{(sr,\,k0)})\geq c,$$
$$0(S_t^{(sr,\,k1)})\geq c,$$
$$0(S_t^{(sr,\,k2)})\geq c.$$

Add $S_t^{(sr,\,k\nu)}$ to $S_t^{(sr\nu)}$ for all $\nu\geq 3$. The integrand has $-\lambda z_r z_s q(R)$ raised to the power ν, times the sum $1+k_{sr}(R)+k_{sr}{}^*(R)$, from Eq. (15). The additive part, $k_{sr}(R)$, always leads to a convergent integral since k_{sr} is zero at $R=0$ and $R=\infty$. Since $1+k_{sr}{}^*(R)=0$ for $0\leq R\leq a_{sr}$, and $1+k_{sr}(R)=1$ for $R>a_{sr}$, one has the integral, from $a_{sr}<R\leq\infty$ of $(e^{-\kappa R}/R)^\nu$ times R^2dR, which converges for $\nu>3$ as $\kappa\to 0$, but is proportional to $\ln\kappa$ for $\nu=3$. We find:

$$0(S_t^{(sr,\,k3)}+S_t^{(sr,\,3)})\geq c\ln c,$$
$$0(S_t^{(sr,\,k4)}+S_t^{(sr,\,\nu)})\geq c,\quad \nu>3.$$

Consider now the cases in which $m=3$. Again any divergences of the integrals at the lower limit in which the distance, R, between any pair, is small, can be removed by adding the contribution of the corresponding type with an added k-bond. We must worry only about divergences at the limit $R\to\infty$ when $\kappa\to 0$.

If one integrates a simple cycle of three g-bonds one finds that the integral over the first particle, say t, results in a factor $\alpha-1$ and a function of order $1/R_{sr}$ (as $\alpha\to 0$) connecting the remaining two, which function now multiplies the direct function, $1/R_{sr}$ already connecting these two particles. In type srt, 122 (Fig. 4) particle t is connected to the other two by three bonds: $R_{st}{}^{-2}R_{rt}{}^{-1}\exp-\kappa(2R_{st}+R_{rt})$. Integration of this when R_{rs} is small leads to a factor $\ln\kappa$ and a function of order $1/R_{rs}$ as $\kappa\to 0$. This now multiplies the original double g-bond connecting r and s, and integration now leads to a second factor $\ln\kappa$. The result is:

$$0(S_t^{(srt,\,122)})\geq c^2(\ln c)^2.$$

Similarly we find:

$$0(S_t^{(srt,\,12\nu)})\geq c^2(\ln c),\quad(\nu\geq 3),$$
$$0(S_t^{(srt,\,222)})\geq c^2(\ln c),$$
$$0(S_t^{(srt,\,22\nu)})\geq c^2,\quad(\nu\geq 3),$$

where, in each case we assume the appropriate structure with k-bonds is added to remove any divergences at $R=0$.

Proceed now to the types with $m=3$ having k-bonds between some of the set s, r, t, and fewer q-bonds than required in the absence of k-bonds. In each case the k-bond prevents any divergence of the corresponding integral as $R\to 0$. One readily finds:

$$0(S^{(srt,\,k\nu,\,12)})\geq c^2\ln c, \quad (\nu\geq 0),$$
$$0(S^{(srt,\,k\nu,\,\nu\mu)})\geq c^2. \quad (\nu+\mu>3).$$

For $m=4$ the two cases with k-bonds represented in Fig. 4 are readily seen to lead to high orders. When $k\nu_{sr}=k0$ and all other k's are unity one may consider the integral when R_{sr} is extremely small. The graph is then like the case *stu* 122 which leads to $(\ln\kappa)^2$, or

$$0(S^{srtu,\,k0,\,11111})\geq c^3(\ln c)^2.$$

The integral of the case $k\nu_{sr}=k\nu_{tu}=k0$, and $\nu_{ur}=\nu_{st}=0$, $\nu_{su}=\nu_{rt}=1$ may be examined by considering that R_{sr} and R_{ut} must remain small or the factors $k_{sr}{}^{**}(R_{sr})$ and $k_{ut}{}^{**}(R_{ut})$ vanish. The integral is then of order κ^{-1}, or

$$0(S^{(srtu,\,k0,\,0110k0)})\geq c^{\frac{1}{2}}.$$

The case *srtu*, 111111, is more complicated. Integrate first over one particle, say u, with R_{sr}, R_{ur}, R_{su}, all small. One will obtain a factor $\ln\kappa$, and there remains an extra function connecting the three remaining particles. This function certainly has the property of being of order $R_{st}{}^{-1}$ as $\kappa\to 0$ and $R_{st}\to\infty$ if R_{sr} is very small, so that integration over t gives another factor $\ln\kappa$. Now particles sr are joined directly by the function $e^{-\kappa R}/R$, and the integration over t and u has presumably left a factor of order $R_{sr}{}^{-2}$ when $R_{sr}\to\infty$, $\kappa\to 0$. If this were true we would find:

$$0(S^{(srtu,\,111111)})\sim c^3(\ln c)^3.$$

The factor $R_{sr}{}^{-2}$ from integration over t and u is uncertain, since no analytical integration appears to be possible in this case. If the factor were of order R^{-1} one would have to reduce the order above to $c^{\frac{1}{2}}(\ln c)^2$. Even if the factor is of order R^0 one has:

$$0(S^{(srtu,\,111111)})\geq c^2(\ln c)^2.$$

This latter assignment appears safe, and is adequate to assure the correctness of neglecting this term in calculation up to order $c^{\frac{1}{2}}$.

We thus conclude that up to, and including terms of order $c^{\frac{1}{2}}$, we may write:

$$\ln\gamma_t=-z_t{}^2\frac{\lambda\kappa}{8\pi}-\frac{\partial}{\partial c_t}\sum_{r=1}^{r=\sigma}\sum_{s=1}^{s=\sigma}\{S^{(sr,\,k0)}+S^{(sr,\,k1)}+S^{(sr,\,k2)}+\sum_{\nu=3}[S^{(sr,\,k\nu)}+S^{(sr,\,\nu)}]\}+0(c\ln c)^2, \quad (37)$$

$$\frac{P}{kT}=\sum_{s=1}^{s=\sigma}c_s-\frac{\kappa^3}{24\pi}+\left[1-\sum_{s=1}^{s=\sigma}c_s\frac{\partial}{\partial c_s}\right]\sum_{r=1}^{r=\sigma}\sum_{s=1}^{s=\sigma}\{S^{(sr,\,k0)}+S^{(sr,\,k1)}+S^{(sr,\,k2)}+\sum_{\nu\geq 3}S^{(sr,\,k\nu)}+S^{(sr,\,\nu)}\}+0(c\ln c)^3. \quad (37')$$

IV. EVALUATION OF THE INTEGRALS

Write:

$$\begin{aligned}S_{sr}{}^{(0)}&=S^{(sr,\,k0)},\\ S_{sr}{}^{(1)}&=S^{(sr,\,k1)},\\ S_{sr}{}^{(2)}&=S^{(sr,\,k2)},\\ S_{sr}{}^{(\nu)}&=S^{(sr,\,k\nu)}+S^{(sr,\,\nu)}, \quad \nu\geq 3,\end{aligned} \quad (38)$$

$$S_{t,\,sr}{}^{(\nu)}=(\partial/\partial c_t)S_{sr}{}^{(\nu)}, \quad (39)$$

$$S_{sr}=\sum_{\nu\geq 0}S_{sr}{}^{(\nu)}, \quad (40)$$

$$S_{t,\,sr}=\sum_{\nu\geq 0}S_{t,\,sr}{}^{(\nu)}; \quad (41)$$

define the total ionic concentration as:

$$\rho=\sum_s c_s; \quad (42)$$

and the mol fraction x_s, of ions of species s in the solute as:

$$x_s=c_s/\rho. \quad (43)$$

With these definitions we have, from (37) and (37′),

$$\ln\gamma_t=-z_t{}^2\lambda\kappa/8\pi-\sum_{s=1}^{s=\sigma}\sum_{r=1}^{r=\sigma}S_{t,\,sr}, \quad (44)$$

$$P/ckT=1-(\kappa^3/24\pi c)+\sum_{s=1}^{s=\sigma}\sum_{r=1}^{r=\sigma}\left[\frac{1}{\rho}S_{sr}-\sum_t x_tS_{t,\,sr}\right]. \quad (44')$$

The quantity $S^{(sr,\,\nu)}$, of (38) is the integral of the function,

$$\tfrac{1}{2}c_sc_r(-\lambda z_sz_r/4\pi)^\nu(1/\nu!)e^{-\nu\kappa R}R^{-\nu}, \quad (45)$$

times $4\pi R^2dR$ between the limits zero and infinity. The quantity $S^{(sr,\,k\nu)}$ is the integral of $k_{sr}{}^{**}(R)$ times (45), and times $4\pi R^2dR$, from zero to infinity. The function $k_{sr}{}^{**}(R)$ is given by (15) as the sum of two terms, one, $k_{sr}{}^{*}(R)$, is minus unity from zero to a_{sr}, and the other, $k_{sr}(R)$, is essentially unknown, but is non zero only for a short range and is zero at both $R=0$ and $R=\infty$. The contribution of k_{sr} to the sum S_{sr} can be written as:

$$S_{sr}{}'=2\pi c_sc_r\int_0^\infty k_{sr}(R)R^2\left[\exp-\frac{\lambda z_sz_r}{4\pi R}e^{-\kappa R}\right]dR, \quad (46)$$

and this should be added to the expressions which follow.

However we make the assumption that a_{sr} can be so chosen that (46) is essentially zero for all concentrations. We thenceforth neglect (46) and write:

$$S_{sr}^{(\nu)}=2\pi c_s c_r\left(\frac{-\lambda z_s z_r}{4\pi}\right)^{\nu}\frac{1}{\nu!}\int_{a_{rs}}^{l_\nu} e^{-\nu\kappa R}R^{2-\nu}dR, \quad (47)$$

$$l_\nu=0 \text{ for } \nu\leq 2, \quad l_\nu=\infty \text{ for } \nu\geq 3.$$

Change the variable of integration to $y=R/a_{rs}$ so that the lower limit becomes unity, the upper limit of zero or infinity remaining unchanged. Define

$$\left.\begin{aligned} I_\nu(x)&=\int_1^{l_\nu} e^{-\nu x y}y^{2-\nu}dy\\ I_\nu'(x)&=\int_1^{l_\nu} e^{-\nu x y}y^{3-\nu}dy\end{aligned}\right\}, \quad (48)$$

$$l_\nu=0 \text{ for } \nu\leq 2, \quad l_\nu=\infty \text{ for } \nu\geq 3,$$

and, one has:

$$S_{sr}^{(\nu)}=2\pi c_s c_r a_{sr}^3\left(\frac{-\lambda z_s z_r}{4\pi a_{sr}}\right)^{\nu}\frac{1}{\nu!}I_\nu(\kappa a_{sr}). \quad (49)$$

From (48) we have that,

$$dI_\nu(x)/dx=-\nu I_\nu'(x). \quad (50)$$

From (21), that $\kappa^2=\lambda\sum c_s z_s^2$, we find:

$$\partial\kappa/\partial c_t=\lambda z_t^2/2\kappa. \quad (51)$$

Carrying out the differentiation, $\partial/\partial c_t$, on $S_{sr}^{(\nu)}$ one finds for $S_{t,sr}^{(\nu)}$ from (39), with (49), (50) and (51) that:

$$\begin{aligned} S_{t,sr}^{(\nu)}&=\tfrac{1}{2}[\delta(s,t)x_r+\delta(r,t)x_s]4\pi\rho a_{sr}^3\\ &\times\left(\frac{-\lambda z_s z_r}{4\pi a_{sr}}\right)^{\nu}\frac{1}{\nu!}I_\nu(\kappa a_{sr})\\ &+\tfrac{1}{2}z_t^2 4\pi\rho a_{sr}^3\left(\frac{c\lambda^2}{8\pi\kappa}\right)x_s z_s x_r z_r\\ &\times\left(\frac{-\lambda z_s z_r}{4\pi a_{sr}}\right)^{\nu-1}\frac{1}{(\nu-1)!}I_\nu'(\kappa a_{sr}). \end{aligned} \quad (52)$$

Introduce, with N_0 Avogadro's number,

$$\begin{aligned} C_0&=(1000)32\pi^2/N_0\lambda^3,\\ &=\frac{1000}{2\pi N_0}\left(\frac{DkT}{\epsilon^2}\right)^3. \end{aligned} \quad (53)$$

For water at 25°C we have $D=78.54$ and

$$C_0=0.7269 \text{ mols/liter } (H_2O, 25°C). \quad (53')$$

Define,

$$C_s=1000c_s/N_0=\text{conc. in mols liter},$$

then,

$$\begin{aligned} \lambda^3 c_s/32\pi^2&=C_s/C_0\\ &=1.3757C_s, \ (H_2O, 25°C). \end{aligned} \quad (54)$$

The total concentration of ions in mols per liter is

$$\sum_s C_s=C. \quad (55)$$

Introduce

$$\begin{aligned} A_{sr}&=4\pi a_{sr}/\lambda\\ &=(a_{sr} \text{ in A})/7.137 \text{ (for } H_2O, 25°C). \end{aligned} \quad (56)$$

so that A_{sr} is a number of order of magnitude unity. We also define

$$n_\nu=\sum_s z_s^\nu x_s, \quad (57)$$

so that $\frac{1}{2}n_2$ is the factor by which the concentration C must be multiplied to give the usually defined ionic strength. The quantity $n_0\equiv 1$ and $n_1\equiv 0$ due to the requirement of electrical neutrality. Finally define $\varphi_{sr}=\kappa a_{sr}$.

From (12) that $\kappa^2=\lambda\sum c_s z_s^2$, and (57) one finds:

$$\varphi_{sr}^2=\lambda\rho n_2 a_{sr}^2, \quad (58)$$

and with (54) and (56):

$$\varphi_{sr}=[2n_2 A_{sr}^2 C/C_0]^{\frac{1}{2}}, \quad (58')$$

which is of order of magnitude not far from unity for normal concentrations.

With these introductions we have:

$$\left.\begin{aligned} 4\pi\rho a_{sr}^3&=A_{sr}\varphi_{sr}^2/n_2,\\ \lambda z_s z_r/4\pi a_{sr}&=z_s z_r/A_{sr},\\ \rho\lambda^2/8\pi\kappa&=\varphi_{sr}/2n_2 A_{sr}.\end{aligned}\right\} \quad (59)$$

The quantity $S_{t,sr}^{(\nu)}$ given in (52), has two terms. One of these occurs only when either s or r is identical to t. The other term depends on t only by the factor z_t^2 and occurs for all s and r. We define:

$$\begin{aligned} Q_{ts}^{(\nu)}&=4\pi\rho a_{ts}^3\left(\frac{-\lambda z_t z_s}{4\pi a_{ts}}\right)^{\nu}\frac{1}{\nu!}\left[I_\nu(\kappa a_{ts})+\delta(\nu-2)\frac{1}{\kappa a_{ts}}\right]\\ &=\frac{A_{ts}}{n_2}\left(\frac{-z_t z_s}{A_{ts}}\right)^{\nu}\frac{1}{\nu!}[\varphi_{ts}^2 I_\nu(\varphi_{ts})+\delta(\nu-2)\varphi_{ts}], \end{aligned} \quad (60)$$

where the last form is obtained from the first by using (59), and:

$$\begin{aligned} K_{sr}^{(\nu=1)}&=-n_2 4\pi\rho a_{sr}^3\left(\frac{\rho\lambda^2}{8\pi\kappa}\right)z_s z_r\\ &\times\left(\frac{-\lambda z_s z_r}{4\pi a_{sr}}\right)\frac{1}{\nu!}I_{\nu+1}'(\kappa a_{sr})\\ &=\frac{A_{sr}}{n_2}\left(\frac{-z_s z_r}{A_{sr}}\right)^{\nu=1}\frac{1}{4\nu!}\varphi_{sr}^3 I_{\nu+1}'(\varphi_{sr}). \end{aligned} \quad (61)$$

Now define:

$$f_\nu(x)=\frac{x^2}{\nu!}I_\nu(x)+\delta(\nu-2)\frac{x}{2}$$

$$=\frac{x^2}{\nu!}\int_1^{l_\nu} e^{-\nu x y}y^{2-\nu}dy+\delta(\nu-2)\frac{x}{2}, \quad (62)$$

$$l_\nu=0 \text{ for } \nu\leq 2, \quad l_\nu=\infty \text{ for } \nu\geq 3,$$

$$g_\nu(x)=\frac{x^3}{4(\nu-1)!}I_s'(x)=\frac{x^3}{4(\nu-1)!}\int_1^{l_\nu} e^{-\nu x y}y^{3-\nu}dy. \quad (62')$$

One then has:

$$Q_{ts}^{(\nu)}=\frac{A_{ts}}{n_2}\left(\frac{-z_t z_s}{A_{ts}}\right)^\nu f_\nu(\varphi_{ts}), \quad (63)$$

$$K_{sr}^{(\nu)}=\frac{A_{sr}}{n_2}\left(\frac{-z_s z_r}{A_{sr}}\right)^\nu g_\nu(\varphi_{sr}). \quad (63')$$

Define

$$Q_{ts}=\sum_{\nu\geq 0} Q_{ts}^{(\nu)}, \quad (64)$$

$$K_{sr}=\sum_{\nu\geq 1} K_{sr}^{(\nu)}, \quad (64')$$

and from (44), (44'), (49), and (52) one obtains:

$$\ln\gamma_t=-\sum_{s=1}^{s=\sigma} x_s Q_{ts}+\frac{z_t^2}{n_2}\sum_{s=1}^{s=\sigma}\sum_{r=1}^{r=\sigma} x_s x_r K_{sr}, \quad (65)$$

$$P/\rho kT=1+\tfrac{1}{6}n_2^{\frac{1}{2}}(C/2C_0)^{\frac{1}{2}}$$

$$-\tfrac{1}{2}\sum_{s=1}^{s=\sigma}\sum_{r=1}^{r=\sigma} x_s x_r(Q_{sr}-2K_{sr}). \quad (65')$$

The quantity

$$\ln\gamma_\pm=\sum_{t=1}^{t=\sigma} x_t \ln\gamma_t, \quad (66)$$

is the average activity coefficient of the solute. From (66) this is seen to be:

$$\ln\gamma_\pm=-\sum_{s=1}^{s=\sigma}\sum_{r=1}^{r=\sigma} x_s x_r(Q_{sr}-K_{sr}). \quad (67)$$

In the particular case that it is possible to write,

$$A_{sr}=A, \quad (68)$$

for all pairs, sr, of ion types, so that:

$$\varphi_{sr}=\varphi=A(2n_2C/C_0)^{\frac{1}{2}}, \quad (69)$$

we may readily carry out the summations over the ionic types. One finds, using (57), and (63) to (69) inclusive, that:

$$\ln\gamma_t=-\frac{A}{n_2}\sum_{\nu\geq 0}\frac{(-)^\nu n_\nu^2}{A^\nu}\left[z_t^\nu f_\nu(\varphi)-\frac{z_t^2}{n_2}n_\nu g_\nu(\varphi)\right], \quad (70)$$

$$P/\rho kT=1-\frac{A}{2n_2}\sum_{\nu\geq 0}\frac{(-)^\nu n_\nu^2}{A^\nu}$$

$$\times\{f_\nu(\varphi)-2g_\nu(\varphi)-\delta(\nu-2)\tfrac{1}{6}\rho\}, \quad (71)$$

$$\ln\gamma_\pm=-\frac{A}{n_2}\sum_{\nu\geq 0}\frac{(-)^\nu n_\nu^2}{A^\nu}[f_\nu(\varphi)-g_\nu(\varphi)]. \quad (72)$$

V. CONCLUSION

Equations (65), (65'), and (67) or (70), (71), (72) may be used for the calculation of the activity coefficients and osmotic pressure of an ionic solution. If the functions $f_\nu(\varphi)$ and $g_\nu(\varphi)$ are expressed as a power series in φ the equations include all terms up to order φ^3, which is of order $c^{\frac{1}{2}}$.

However, numerical calculation shows that a development in powers of φ and $\ln\varphi$ gives a poor approximation to the functions f_ν and g_ν, even at comparatively low values of φ. For this reason it appears to be advisable to compute the functions f and g exactly, rather than to use a power series approximation. There is, of course, no rigorous argument to justify the use of the equations for such high values of φ that a power series development of f and g is inapplicable. One may, however, give a plausibility argument to this effect.

The extremely large deviations of ionic solutions from the laws of the perfect solution are due partly to the long range of the mutual electrostatic potentials, but also to the comparatively large value which these potentials have. The difference in energy of two oppositely charged ions at infinite distance, in the solvent, and at closest approach, is sufficient to cause very considerable pairing, or undissociated molecular formation, even at concentrations of 10^{-1} or 10^{-2} mols per liter in water. The terms represented in the equations (65) to (72) account for these interactions at short range of all pair types, sr, and the effects on this interaction due to the long range electrostatic potential of any third ion in the neighborhood. The terms which are neglected include the very close interaction of three ions. Now, at least for salts in which all ions have the same magnitude of charge, uni-univalent and di-divalent salts, one might expect that close interaction of triples of ions plays a comparatively small role, and should not become important until comparatively high concentrations, beyond $1M$, are reached. One may therefore hope that the equations displayed here would be moderately satisfactory even beyond the concentration where a power series development could be used.

In developing the equations it was deemed advisable to retain the fairly general form of using a "cut-off dis-

tance," a_{sr} which is different for every pair type, sr, of ions. In practical use one would attempt to assume that one can assign a "radius" a_s to every ion type s and write $a_{sr}=a_s+a_r$. This assumption, if it works empirically, would permit the calculation of activity coefficients for all combinations of ions, were the radius, a_s, of each species s, once determined.

In the Eqs. (70), (71), (72) the assumption has been made that $a_{sr}=a$ for all ion pairs. For a solute containing only one species of positive ions and one of negative ions, only the interaction between the positive and negative ions is important at short range; the repulsion between two positives or two negatives making close approach of two like species an unlikely event.

This is evident in the form of Eq. (46). If z_s and z_r of (46) have the same sign the quantity in the exponent is negative, and large in magnitude for small values of R_{sr}. The factor multiplying $k_{sr}(R)$ is thus small in the region of R for which k_{sr} differs appreciably from zero. By a similar argument one may see that the terms in (65), (65′), and (66) involving a_{sr} for two positive ions; or two negatives, are unimportant.

For this case, then, of a solute salt with only one positive and one negative ion species, one would expect Eqs. (70), (71), and (72) to be applicable with the single a having the significance of a_{sr} for the positive and negative ion pair.

The activity coefficients, γ, for which the equations are applicable are not identically those normally defined and measured at atmospheric pressure. A correction, due to the osmotic pressure, must be applied.

The activity coefficients to which the equations of this article apply are defined by the relation

$$\bar{F}_t(c, P+P_0)-F_t^{(0)}=RT\ln\gamma_t c_t \tag{73}$$

where $\bar{F}_t(c, P+P_0)$ is the partial molal free energy of species t at concentration c and pressure equal to the sum of the osmotic pressure, P, of the solution plus the standard pressure P_0 (presumably one atmosphere). The dielectric constant, D, of the solvent, entering the equations, is that of the pure solvent at P_0. The constant, $F_t^{(0)}$, is chosen in the usual manner so that γ_t approaches unity in the limit of infinite dilution.

The usual activity coefficient, γ_t', is defined by:

$$\bar{F}_t(c, P_0)-F_t^{(0)}=RT\ln\gamma_t' c_t, \tag{74}$$

and differs from γ_t by:

$$\ln\gamma_t'=\ln\gamma_t-\frac{1}{RT}\int_{P_0}^{P_0+P}\bar{V}_t dP$$

$$\cong\ln\gamma_t-v_t\frac{P}{kT}, \tag{75}$$

where $\bar{V}_t$ is the partial molal volume of the solute species t, and,

$$v_t=\bar{V}_t/N_0, \tag{76}$$

is the volume per molecule. Since, in first approximation, the osmotic pressure divided by kT is ρ, the correction becomes:

$$\ln\gamma_t'=\ln\gamma_t-10^{-3}(\bar{V}_t \text{ in } \mathrm{cm}^3)C(P/\rho kT), \tag{77}$$

where the use of the leading term, unity, in (65′) or (71) for $P/\rho kT$, will usually be of sufficient accuracy.

The Structure and Dipole Moment of Isothiocyanic Acid *

C. I. BEARD†
Research Laboratory of Electronics, Massachusetts Institute of Technology, Cambridge, Massachusetts
AND
B. P. DAILEY‡
Department of Chemistry, Harvard University, Cambridge, Massachusetts
(Received June 16, 1950)

"Thiocyanic acid" in the vapor state has been found to be at least 95 percent HNCS. From an analysis of the microwave rotational spectrum the following bond distances and bond angle were determined rH−N =1.01A (assumed), rN−C=1.218A, rC−S=1.557A, H−N−C angle 136°. Analysis of the Stark spectrum indicates that the component of dipole moment along the molecular figure axis is 1.72 *D*. Stark components from transitions forbidden in the zero-field spectrum have been observed.

I. INTRODUCTION

CONFLICTING physical evidence concerning the nature of the valence bonds in the thiocyanates and the ratio of the equilibrium concentration of the two tautomeric forms of thiocyanic acid have lent the problem of the structure of these compounds considerable interest. The study of the microwave spectrum of CH_3NCS, which is complicated by the presence of internal rotating groups in the molecule, has also made it desirable to know the detailed structure of the NCS group in order to expedite the spectral analysis. The study of the microwave spectrum of the thiocyanic acids and the Stark effect in that spectrum, reported in this paper, was undertaken to help settle these questions. The structures of the molecules having observable spectra were obtained and it was also found possible to determine a component of the dipole moment from a quantitative analysis of the Stark effect. The Stark patterns of the microwave spectra permit the application of the detailed Stark effect theory to the class of slightly asymmetric molecules.

II. PREPARATION OF THE ACID

Rück and Steinmetz[1] suggest two methods of preparation for "thiocyanic acid." Both methods were used to some extent in this investigation. In the first method potassium thiocyanate and $KHSO_4$ crystals were pulverized, dried under vacuum, mixed thoroughly, and heated gently to speed up the reaction and drive the acid vapor into the wave-guide absorption cell. A modification of the second method, although requiring a short drying tube, made possible a convenient synthesis of the deuterium derivatives. D_2O and P_2O_5 were mixed to give D_3PO_4 to which KSCN was added. The mixture was then gently warmed to liberate the "thiocyanic acid." $KSC^{13}N$ was prepared by fusing sulfur with KCN containing 17 percent of C^{13}. It was then used in the preparation of $HNC^{13}S$ and $DNC^{13}S$.

Thiocyanic acid, which is said in the literature to be a tautomeric mixture of HSCN and HNCS, is a crystalline solid stable below 0°C and polymerizing at ordinary temperatures to a yellow insoluble compound. At high temperatures organic thiocyanates rearrange to give isothiocyanates. Two points of chemical interest were noted in this investigation; first, only isothiocyanic acid seemed to be present in the dilute samples of vapor admitted to the wave-guide absorption cell and second, the polymerization could be reversed to some extent by strong heating to liberate monomeric HNCS.

III. OBSERVED SPECTRUM

The microwave absorption spectrum of the isothiocyanic acid vapor was observed over the frequency range from 20,000 to 25,000 Mc using a Stark modulation microwave spectrometer. Square-wave modulation was used with the lower voltage at zero volts and with the higher voltage set at values from 4 to 160 v. The electrode separation within the wave guide was such as to make these voltages correspond to fields of from 20 to 800 v/cm. The observed zero-field spectrum and Stark patterns at the highest value of the field and at one intermediate value are shown in Fig. 1. Qualitative

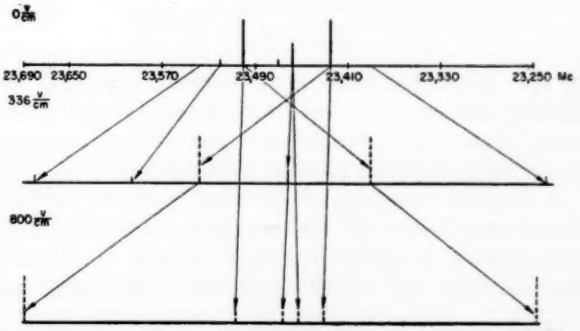

FIG. 1. Observed spectra.

* The research reported in this paper was made possible through support extended Harvard University by the Navy Department (ONR) under ONR Contract N5ori-76 and Massachusetts Institute of Technology under Joint Service Contract W-36-039sc-32037.

† Now with Applied Physics Laboratory, Johns Hopkins University, Silver Spring, Maryland.

‡ Now with Department of Chemistry, Columbia University, New York.

[1] V. Rück and H. Steinmetz, Zeits. f. Anorg. Chemie **77**, 51 (1912).

studies of the observed intensities and their variations with temperature seem to indicate that the two weakest lines in the zero-field spectrum correspond to rotational transitions of molecules in excited vibrational states. The remaining pattern, presumably due to rotational transitions of molecules in the ground state of vibration, consists of five lines, two of which could not actually be seen at zero field and whose frequencies have been fixed by extrapolation. Of the three visible zero-field lines two possessed both first-order and second-order Stark components while the center line possessed two second-order Stark components. These simple qualitative features of the Stark spectrum indicate immediately

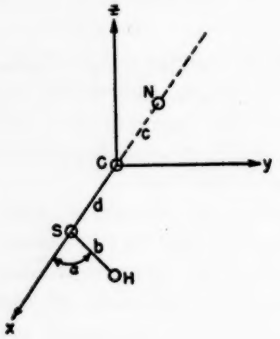

FIG. 2. HSCN coordinates.

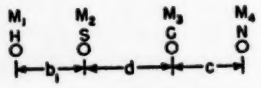

that the molecule is not linear (because of the presence of the first-order Stark components) but has nearly the structure of a symmetric rotor. Furthermore, the presence of two Stark components for each line (corresponding to $M^2=0$ and $M^2=1$) indicates that the transition involves $J=1$. The small asymmetry indicated for the molecule suggests that we are dealing with a linear NCS or SCN group[2] with the H bonded at an angle giving a close approach to a prolate symmetric-rotor. In such a case the transition would have to be $J=1 \rightarrow J=2$. For a slightly asymmetric rotor three $J=1 \rightarrow J=2$ transitions are possible

$$1_{1,1;0} \rightarrow 2_{1,2;-1}$$
$$1_{0,1;-1} \rightarrow 2_{0,2;-2}$$
$$1_{1,0;+1} \rightarrow 2_{1,1;0}.$$

In the symmetric-rotor approximation the first and third of these would possess both second-order and first-order Stark components while the second transition would have only second-order components.

A detailed discussion of the Stark patterns for these transitions, based on the accurate asymmetric-rotor treatment, is presented in another section. This discussion confirms the above qualitative conclusions and serves to determine a value for the dipole moment of the molecule.

[2] X-ray analysis in 1934 showed the $(SCN)^-$ ion was linear [M. Strada, Gazz. 64, 400 (1934)].

IV. ROTATIONAL CONSTANTS

From the observed frequencies of the three lines corresponding to the above transitions, values of two of the rotational constants for the molecule in the ground vibrational state may be obtained. These frequencies and the others given in Table I were measured to an accuracy of ± 1 Mc by the method of Good and Coles.[3]

From the observed frequencies for the $1_{1,1;0} \rightarrow 2_{1,2;-1}$ and $1_{1,0;+1} \rightarrow 2_{1,1;0}$ transitions it is possible to calculate values of the two nearly degenerate rotational constants B and C if the following approximation is made. Following Wang[4] the energy of a molecule which is nearly a prolate symmetric-rotor may be written

$$F(J,K)=\tfrac{1}{2}(B+C)J(J+1)+[A-\tfrac{1}{2}(B+C)]K^2,$$

so that for a $\Delta J=1$, $\Delta K=0$ transition the frequency would be

$$\nu=(B+C)(J+1)$$

where J is the lower of the two values of the principal rotational quantum number. This frequency would be approximately the average of the two observed frequencies. The average of the measured frequencies is 23,462 Mc and the corresponding value of $\frac{1}{2}(B+C)$ is 5865.5 Mc.

If the equation given by King, Hainer, and Cross[5] for the rotational energy levels of an asymmetric rotor,

$$E_T{}^J(a,b,c)=[\tfrac{1}{2}(a+c)]J(J+1)+[\tfrac{1}{2}(a-c)]E_\tau{}^J(K),$$

is used, together with the exact expressions for $E_\tau{}^J(K)$ tabulated in their paper the result may easily be derived that the difference in frequency of the two transitions $1_{1,1;0} \rightarrow 2_{1,2;-1}$ and $1_{1,0;+1} \rightarrow 2_{1,1;0}$ is equal to $(A-C)(K+1)$ or simply to $2(C-B)$. The observed frequency difference is 75 Mc so that $(C-B)$ is 37.5 Mc. The derived values of B and C together with the calculated moments of inertia are $B=5903$ Mc, $C=5728$ Mc, $I_B=142.1\times10^{-40}$ gcm², $I_C=143.96\times10^{-40}$ gcm². The

TABLE I. Observed spectrum of HNCS.

Transition	Molecule	νMc	
$1_{1,1;2} \rightarrow 2_{1,2;-1}$	HNCS	23,499.5	
$1_{1,0;+1} \rightarrow 2_{1,1;0}$	HNCS	23,424.5	
$1_{1,1;0} \rightarrow 2_{1,1;0}$	HNCS	23,537	(Extrapolated)
$1_{1,0;+1} \rightarrow 2_{1,2;-1}$	HNCS	23,387	(Extrapolated)
$1_{0,1;-1} \rightarrow 2_{0,2;-2}$	HNCS	23,458	
...	HNCS	23,475	(Weak)
...	HNCS	23,520	(Weak)
$\frac{1}{2}[\nu(1_0 \rightarrow 2_{-1})+\nu(1_{+1} \rightarrow 2_0)]$	$HNC^{33}S$	23,389	
$\frac{1}{2}[\nu(1_0 \rightarrow 2_{-1})+\nu(1_{+1} \rightarrow 2_0)]$	$HNCS^{34}$	22,915	
$\frac{1}{2}[\nu(1_0 \rightarrow 2_{-1})+\nu(1_{+1} \rightarrow 2_0)]$	DNCS	21,897	
$\frac{1}{2}[\nu(1_0 \rightarrow 2_{-1})+\nu(1_{+1} \rightarrow 2_0)]$	$DNC^{33}S$	21,839	

[3] W. E. Good and D. K. Coles, Phys. Rev. 71, 383 (1947).
[4] S. C. Wang, Phys. Rev. 34, 243 (1929).
[5] King, Hainer, and Cross, J. Chem. Phys. 11, 27–42 (1943).

most probable structure of thiocyanic acid is a planar one and for a rigid planar molecule the relation

$$I_C = I_A + I_B$$

must be satisfied. If the molecule is treated as a rigid one a value of $I_A = 1.83 \times 10^{-40}$ gcm^2 is obtained with $A = 459{,}000$ Mc. However, since the molecule was actually in the ground vibrational state and therefore not truly planar these last two values are merely rough approximations.

Less complete spectral patterns were obtained for the isotopic molecules so that only approximate values of $\frac{1}{2}(B+C)$ were obtained. The frequencies corresponding to these rotational constants were the superposition points of the two "non-forbidden" first-order Stark components. The identification of the majority of these lines as corresponding to the indicated isotopic molecule rests upon a very pronounced increase in intensity for samples of the acid vapor made from materials enriched in the appropriate isotopes. The line ascribed to $HNC^{12}S^{34}$, however, was observed in a non-enriched sample and its identification depends on the molecular structure derived from the other data, to some extent.

V. CALCULATION OF INTERNUCLEAR DISTANCES

The initial calculation of internuclear distances was based on the assumption that the molecule giving rise to the observed spectrum was HSCN, thiocyanic acid. This seemed reasonable since the acid was prepared from KSCN. Furthermore Sidgwick,[6] for example, states that of the two alternative structures H−S−C≡N and H−N=C=S, the former is the more probable.

If in calculating the internuclear distances and bond angles the molecule is treated as an asymmetric one, the method of Hirschfelder[7] may be used. Labeling the molecular coordinates as in Fig. 2 the following relations are obtained:

$$I_x = m_H b^2 \sin^2\alpha - (1/M)[m_H b \sin\alpha]^2$$
$$I_y = [m_S d^2 + m_N C^2 + m_H(d + b\cos\alpha)^2] - (1/M)[m_S d - m_N C + m_H(d + b\cos\alpha)]^2$$
$$I_z = [m_S d^2 + m_N C^2 + m_H(b^2 + d^2 + 2bd\cos\alpha)] - (1/M)[m_H b \sin\alpha]^2 - (1/M)[m_S d - m_N C + m_H(d + b\cos\alpha)]^2$$
$$I_{xy} = m_H(d + b\cos\alpha) b \sin\alpha - (1/M)[m_H b \sin\alpha][m_S d - m_N C + m_H(d + b\cos\alpha)]$$
$$I_{xz} = I_{yz} = 0.$$

From these quantities the three principal moments of inertia I_A, I_B, and I_C may be found using the equations:

$$I_A = \tfrac{1}{2}(I_x + I_y) - \tfrac{1}{2}[(I_x + I_y)^2 - 4(I_x I_y - I_{xy}^2)]^{\frac{1}{2}}$$
$$I_B = \tfrac{1}{2}(I_x + I_y) + \tfrac{1}{2}[(I_x + I_y)^2 - 4(I_x I_y - I_{xy}^2)]^{\frac{1}{2}}$$
$$I_C = I_z.$$

If complete sets of rotational constants were available for all of the isotopic molecules it would be formally possible to solve for the three interatomic distances and the one angle. In view of the obvious complications involved several simplifying approximations were made.

Since it is obvious from the observed spectrum that the effect of the H atom on the moments of inertia is small the molecule may be treated approximately as a linear molecule where the fictitious H−S distance along the SCN axis might be thought of as an "effective projection" of the actual H−S distance in space (Fig. 2). For a linear molecule the equation for I_C about an axis through the center of gravity can be written as:

$$I_C = (1/M)[m_1 m_2 l_{12}^2 + m_1 m_3 l_{13}^2 + m_1 m_4 l_{14}^2 + m_2 m_3 l_{23}^2 + m_2 m_4 l_{24}^2 + m_3 m_4 l_{34}^2]$$

where the l's are the distances between atoms of the same subscripts. When the l's are expressed in terms of b_1, d, and c with accurate values of atomic masses, four equations, one for each of the isotopic molecules, are obtained. The additional approximation is made that $\frac{1}{2}(B+C) \simeq C$ linear. A graphical solution of these equations resulted in the values

H−S=1.55A, C−N=1.33A, and S−C=1.47A.

The C−N and S−C distances are probably less in error than the H−S projection since they are less sensitive to changes in the symmetry of the molecule. If these two values are taken together with the value for the H−S distance, 1.35A, which is the observed distance in H_2S, it should be possible using the equations for I_C and the observed value of that quantity to calculate α, the bond angle. However, at this point it becomes obvious that no real solution to this equation is possible for the given set of constants. This suggests strongly that the assumed order of atoms in the molecule is incorrect. Furthermore, as is shown in Table II the S−C and C−N distances fall quite outside the limits set from an examination of the force-constant data by Goubeau and Gott[8] and Linnett and Thompson.[9] Goubeau and Gott, moreover, as a result of their

TABLE II.

Bond	HSCN calculated distances	Goubeau and Gott distances	Linnett and Thompson distances	HNCS calculated distances
A. Internuclear distances in the thiocyanates				
C−N	1.33A	1.21A	1.17–1.22A	
S−C	1.47	1.69	1.60–1.67	
N−C		1.21		1.21A
C−S		1.56		1.57
B. Bond distances calculated as sum of Pauling covalent radii				
C≡1X	C=N	C−N	H−N	
1.15A	1.27A	1.47A	1.00A	
S≡C	S=C	S−C	H−S	
1.47A	1.61A	1.81A	1.34A	

[6] N. V. Sidgwick, *The Organic Chemistry of Nitrogen* (Oxford University Press, London, 1937).
[7] J. O. Hirschfelder, J. Chem. Phys. **8**, 431L (1940).
[8] J. Goubeau and O. Gott, Ber. **73B**, 127 (1940).
[9] J. W. Linnett and H. W. Thompson, J. Chem. Soc. 1399–1403 (1937).

examination of the vibrational spectrum of thiocyanic acid and other thiocyanates conclude that HNCS is the predominant form of the acid. Gallais and Voight[10] from measurements of molecular magnetic rotations also conclude that the molecule is isothiocyanic acid.

If the above procedure is repeated for HNCS the results of the graphical solution of the four linear equations are: "H−N"=0.76A, N−C=1.21, and C−S =1.57. The accurate equation for I_C is

$$I_C=I_z=[m_s d^2+m_N C^2+m_H(b^2+c^2+2bc\cos\alpha)] -(1/M)[m_H b\sin\alpha]^2 -(1/M)[m_s d-m_N C-m_H(c+b\cos\alpha)]^2$$

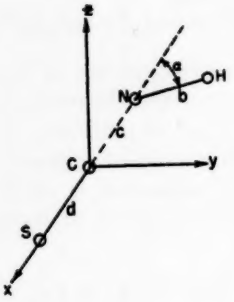

FIG. 3. HNCS coordinates. Structural parameters: $a=44°$, $b=1.01$A (assumed), $c=1.218$A, $d=1.557$A.

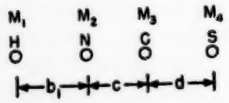

and for I_y

$$I_y=[m_s d^2+m_N C^2+m_H(c+b\cos\alpha)^2] -(1/M)[m_s d-m_N C-m_H(c+b\cos\alpha)]^2.$$

If the following equation is used, which is a somewhat better approximation than the linear one

$$\tfrac{1}{2}(I_y+I_z)\cong 2(J+1)(h/8\pi^2 c)/\nu \text{ cm}^{-1})$$

slightly more accurate values of the internuclear distances are obtained, namely: N−C=1.218A, C−S =1.557A. If these two distances together with the H−N distance 1.01A observed in the NH_3 molecule are substituted in the equation for I_z and the experimental value of that quantity is used, a value for the H−N−C angle of 136° results. While this value of the angle is only approximate, because of the lack of sensitivity of the observed moment, the resulting set of structural parameters gives an accurately calculated spectrum which agrees with the observed one to within the accuracy claimed for the structural data (±0.01A and ±5°). The final structure for isothiocyanic acid obtained in this investigation is shown in Fig. 3. The N−C and C−S distances are seen in Table II to be in good agreement with the data of Goubeau and Gott. Since only one set of spectral lines was observed it would appear as a result of this investigation that the equilibrium concentration of HSCN in a mixture of the two thiocyanic acids is less than five percent of the concentration of HNCS.

[10] F. Gallais and D. Voight, Comptes Rendus **210**, 104 (1940).

VI. STARK SPECTRUM AND DIPOLE MOMENT

The rotational energy levels of a rigid slightly asymmetric rotor in the presence of a homogeneous electric field have been treated by Penney.[11] The Stark effect calculations presented here have been carried out using the method of Golden and Wilson[12] and, though somewhat more elaborate, account for the observed Stark spectrum in greater detail.

The diagonal elements of the energy matrix H are given by

$$H_{J\tau M}=W_{J\tau}{}^0+E^2\sum_{J',\tau',g}{}' \frac{\mu_g{}^2[(\Phi_{Zg})_{J,\tau,M;J',\tau',M}]^2}{(W_{J\tau}{}^0-W_{J'\tau'}{}^0)},$$

neglecting polarization terms, or

$$H_{J\tau M}=W_{J\tau}{}^0+\sum_g[W_g{}^{(2)}]_{J\tau M},$$

where

$$W_{gJ\tau M}{}^{(2)}=\mu_g{}^2E^2\left[\frac{(J^2-M^2)}{4J^2(4J^2-1)}\sum_\tau{}'\left\{\frac{[(\Phi_{Zg})_{J,\tau;J-1,\tau'}]^2}{W_{J\tau}{}^0-W_{J-1,\tau'}{}^0}\right\}\right.$$
$$+\frac{M^2}{4J^2(J+1)^2}\sum_{\tau'\neq\tau}{}'\left\{\frac{[(\Phi_{Zg})_{J,\tau;J,\tau'}]^2}{W_{J\tau}{}^0-W_{J\tau'}{}^0}\right\}$$
$$\left.+\frac{(J+1)^2-M^2}{4(J+1)^2(2J+1)(2J+3)}\sum_\tau{}'\left\{\frac{[(\Phi_{Zg})_{J,\tau;J+1,\tau'}]^2}{W_{J\tau}{}^0-W_{J+1,\tau'}{}^0}\right\}\right].$$

Cross, Hainer, and King[13] have tabulated values of line strength λ defined as follows:

$$\lambda=\sum_{FMM'}|\Phi_{Fg}|^2{}_{J\tau M;J'\tau'M'}$$
$$=3|\Phi_{Zg}|^2{}_{J,J'}X|\Phi_{Zg}|^2{}_{J\tau;J'\tau'}X\sum_{M,M'}|\Phi_{Zg}|^2{}_{J,M;J'M'}.$$

The necessary values of $[(\Phi_{Zg})_{J,\tau;J'\tau'}]^2$ were therefore calculated from the tabulated values of λ. In order to determine the Stark energy levels for $1_{1,1;0}$ and $1_{1,0;+1}$

TABLE III. Stark effect of $J=1\rightarrow 2$ transition in HNCS.

$H1_{0;0}$	$=W1_0-2.16\times10^{-6}\mu_g{}^2E^2$ Mc
$H1_{0;1}$	$=W1_0-1.62\times10^{-6}\mu_g{}^2E^2$ Mc
$H1_{+1;0}$	$=W1_{+1}-2.155\times10^{-6}\mu_g{}^2E^2$ Mc
$H1_{+1;0}$	$=W1_{+1}-1.616\times10^{-6}\mu_g{}^2E^2$ Mc
$H1_{-1;0}$	$=W1_{-1}+4.324\times10^{-6}\mu_g{}^2E^2$ Mc
$H2_{0;0}$	$=W2_0+1.246\times10^{-6}\mu_g{}^2E^2$ Mc
$H2_{0;1}$	$=W2_0+0.814\times10^{-6}\mu_g{}^2E^2$ Mc
$H2_{-1;0}$	$=W2_{-1}+1.235\times10^{-6}\mu_g{}^2E^2$ Mc
$H2_{-1;1}$	$=W2_{-1}+0.930\times10^{-6}\mu_g{}^2E^2$ Mc
$H2_{-2;0}$	$=W2_{-2}+1.026\times10^{-6}\mu_g{}^2E^2$ Mc
$H1_{-1;1}$	$=W1_{-1}-2.881\times10^{-6}\mu_g{}^2E^2$ Mc
$H2_{-2;1}$	$=W2_{-2}+0.52\times10^{-6}\mu_g{}^2E^2$ Mc

[11] W. G. Penney, Phil. Mag. **11**, 602 (1931).
[12] S. Golden and E. B. Wilson, J. Chem. Phys. **16**, 669 (1948).
[13] Cross, Hainer, and King, J. Chem. Phys. **12**, 210 (1944).

TABLE IV. Stark spectrum of HNCS $\mu_0=1.72$ D.

Field volts cm	$\frac{1}{2}(\nu_{1_{+1}\to 2_0}+\nu_{1_0\to 2_{-1}})$ Calc.	Obs.	$\nu_{1_{+1}\to 2_0}$; $M^2=1$ Calc.	Obs.	$\nu_{1_0\to 2_{-1}}$; $M^2=1$ Calc.	Obs.	$\nu_{1_0\to 2_0}$; $M^2=1$ Calc.	Obs.
800	23,467	23,469	23,249	23,247.5	23,685	23,689		
600	23,464.7	23,464.5	23,308	23,307	23,622	23,622		
400	23,463	23,465	23,369	23,371	23,557	23,560		
336	23,463	23,463.5	23,390	23,390	23,536	23,537	23,684	23,680
270	23,462.5	23,462.5	23,412.5	23,411	23,512.5	23,514	23,649	23,654
200	23,462	23,462	23,436	23,436	23,488	23,488	23,614	23,618
156	23,462	23,462	23,449	23,451	23,475	23,473	23,589	23,596
120	23,462	23,462	23,463	23,462	23,461	23,462	23,573	23,581
40	23,462	23,462	23,497	23,488	23,427	23,437	23,539	23,551
18	23,462	23,462	23,498	23,496	23,426	23,428		

and for $2_{1,2;-1}$ and $2_{1,1;0}$ which are nearly degenerate pairs of levels it was necessary to solve secular equations. Their solutions had the form

$$W=\tfrac{1}{2}(H_{J\tau M}+H_{J'\tau' M}) \pm\tfrac{1}{2}\{[H_{J\tau M}-H_{J'\tau' M}]^2+4|\xi^2|E^2\}^{\frac{1}{2}}.$$

For these two cases $|\xi|^2$ had the form

$$|\xi|^2=(M^2/4J^2(J+1)^2)\mu_g{}^2|(\Phi_{Z_0})_{J\tau,J\tau_1}|^2.$$

The results of the Stark effect calculations for HNCS are given in Tables III and IV and are compared to the observed frequencies. A satisfactory fit of these data was obtained using a value of 1.72 debye units for the component of the permanent electric dipole moment along the I_A axis. The influence of the component of the dipole moment perpendicular to this axis was found to be negligible.

The originally puzzling anomaly of Stark components which did not originate in any of the lines observed in the zero-field spectrum is resolved by a consideration of the discussion of the intensity of Stark components given by Golden and Wilson.[12] A result of this discussion is the conclusion that if transitions are normally permitted between state m and state l but not between state m and state k, transitions between the latter become possible in the presence of an electric field if states k and l are degenerate. Figure 4 shows the normally permitted and forbidden transitions between the two pairs of nearly degenerate levels involved in this spectrum. The zero-field frequencies of lines A and D had to be obtained by extrapolation since the lines were completely forbidden in the absence of the field. To the accuracy of the extrapolation the theoretical relation between the frequency differences

$$B-C=[\tfrac{1}{2}(a-c)](2K+2)$$
$$A-D=[\tfrac{1}{2}(a-c)](4K+4)$$
$$A-D=2(B-C)$$

was obeyed. The intensity of the forbidden lines was a function of the electric field, being zero at zero field, building up to a maximum at intermediate values of the field, and then declining at higher fields. Since the line broadened at the same time (due to inhomogeneities in the field) it could not be observed at values of the field above 400 v/cm. Presumably the intensity of these lines goes to zero at some high value of the field.

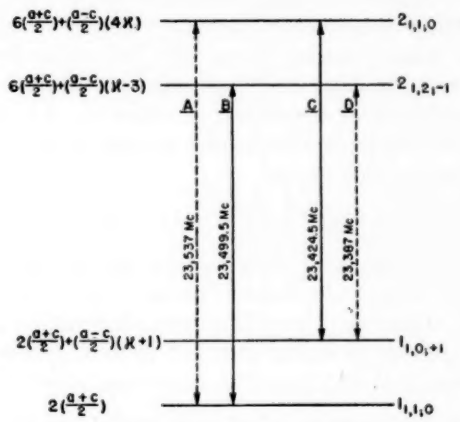

FIG. 4. Forbidden transitions.

Another point of interest in the Stark spectrum is the shift in the "center of gravity" of the first-order Stark components due the second-order terms in $H_{J\tau M}$. This shift amounted to some 6 Mc at 800 v/cm. The Stark effects for the first-order components of the forbidden and allowed transitions were simply related being the sum of terms for the former and the difference for the latter. The agreement of calculated and observed frequencies is quite good in all cases except two; the Stark effect for the first-order components of the forbidden lines and for the first-order components of the allowed lines, at the lowest values of the field. Both of these discrepancies may represent experimental error since the breadth and weakness of the components of the forbidden lines made accurate frequency measurements difficult and because "zero basing" and accurate measurement of the very low voltage square waves gave some trouble.

VII. OTHER LINES

Two other lines appeared in the observed spectrum having intensities very much less than for the lines so far identified. These probably represent transitions for molecules in excited vibrational states. It was not found possible to make accurate temperature coefficient measurements of intensity so that this hypothesis has not been adequately tested. The line at 23,520 Mc appeared to have a first-order Stark component while the line at 23,475 Mc had a purely second-order Stark effect.

Intermolecular Forces in Benzene and Ammonia

VERNON MYERS
The Pennsylvania State College, State College, Pennsylvania
(Received August 3, 1950)

The intermolecular forces between benzene molecules and between ammonia molecules are computed in a semi-empirical manner. The long-range attractive forces are calculated from optical dispersion data and dipole moments, and the short-range repulsive forces are estimated from second virial coefficients.

BENZENE

As benzene is a non-polar molecule, the only long-range interactions are the van der Waals' dispersion forces arising from the electronic motions. These may be computed from optical disperion data.[1] Measurements of the index of refraction for benzene vapor can be represented quite accurately by the one-level dispersion formula[2]

$$n-1=9.35987\cdot10^{27}/(6051.36\cdot10^{27}-\nu^2), \quad (1)$$

where n is the index of refraction referred to an ideal gas at 25°C and atmospheric pressure and ν is the frequency. These data yield a static polarizability of $10.0\cdot10^{-24}$ cm³, an oscillator strength of 9.62, and a resonance energy of 10.17 ev. The dispersion effect is

$$V=-(1270\cdot10^{-12}R^{-6}+4760\cdot10^{-12}R^{-8})\text{ergs}, \quad (2)$$

R is in angstroms.

The short-range repulsive forces arising from Coulombic repulsion and electron exchange represent too formidable a theoretical computation for molecules as complex as benzene; however, it is possible to fix the limits of the repulsive forces from second virial coefficients. The second virial coefficient is the coefficient of $1/v$ in the series expansion for the equation of state:

$$pv/RT=1+B(T)/v+C(T)/v^2+\cdots. \quad (3)$$

The classical expression for the second virial coefficient is

$$B(T)=2\pi N\int_0^\infty[1-\exp(-V/kT)]R^2dR. \quad (4)$$

The procedure used here is to compute $B(T)$ for a particular choice of repulsive force and compare with the experimental B. Measurements of the second virial coefficient for benzene vapor have been made recently by Lambert[3] and his co-workers in the temperature range 45 to 90°C.

The simplest model is the hard sphere approximation, and Table I shows the results with the potential

$$V=-(1270\cdot10^{-12}R^{-6}+4760\cdot10^{-12}R^{-8})\text{ ergs}, \quad R>4.52\text{A}$$
$$V=\infty,\ R<4.52\text{A}. \quad (5)$$

The depth at the potential minimum is −0.11 ev.

A more realistic model makes use of a repulsive force with a finite range. Investigations of the interactions of spherically symmetric atoms indicate that the repulsive forces may be represented by $A\exp(-R/b)$. Of course, the repulsive forces for non-spherical molecules like benzene would have an angular dependence, but this has not been taken into account for simplicity. A range b of 0.28A was chosen as Heller[4] has found this range represents satisfactorily the interactions in a large number of cases. The potential

$$V=5.60\cdot10^{-7}\exp(-R/0.28)-(1270\cdot10^{-12}R^{-6}+4760\cdot10^{-12}R^{-8})\text{ erg} \quad (6)$$

gave the best results. The potential minimum occurs at 4.45A and is −0.078 ev. Better agreement is obtained with experiment for the exponential repulsion model than for the hard sphere model as is evident in Table II.

The major uncertainty in the use of virial coefficients below the critical temperature (562°K for benzene) is the effect of dimerization, i.e., the formation of double molecules, $(C_6H_6)_2$. It is possible to show that[3]

$$B_{\text{true}}=B_{\text{exp}}+RT/K_p. \quad (7)$$

B_{true} is the "true" monomer coefficient and B_{exp} is the measured coefficient, K_p is the equilibrium constant for

TABLE I. A comparison of the experimental and theoretical second virial coefficients for benzene on the basis of the hard sphere model.

Temp. °K	Experimental virial cm³/mole	Theoretical virial cm³/mole	Percent difference
318	−1200	−1240	−3.3
338	−1060	−1060	0.0
358	− 935	− 905	3.2

Table II. A comparison of the experimental and theoretical second virial coefficients for benzene on the basis of the exponential repulsion.

Temp. °K	Experimental virial cm³/mole	Theoretical virial cm³/mole	Percent difference
318	−1200	−1220	−1.7
338	−1060	−1060	0.0
358	− 935	− 930	0.5

[1] H. Margenau, J. Chem. Phys. **6**, 896 (1938).
[2] K. L. Ramaswamy, Proc. Ind. Acad. Sci. **4A**, 675 (1936).
[3] Lambert, Roberts, Rowlinson, and Wilkinson, Proc. Roy. Soc. **196A**, 113 (1949).
[4] R. Heller, J. Chem. Phys. **9**, 154 (1941).

the reaction $X_2 \rightleftarrows 2X$. It might be expected that an appreciable amount of dimerization would be present in benzene; however, Lambert concludes that dimerization is not important in this case since Berthelot's equation of state with the constants chosen at the critical point yields a satisfactory fit to the second virial coefficient. This is not the case for highly associated vapors such as acetone or methyl alcohol.

The only quantum correction[5] of importance is caused by the quantum-mechanical partition function not being exactly proportional to $\exp(-V/kT)$. This contributes only about 2 to 4 cm³/mole for benzene and may be neglected.

AMMONIA

The long-range forces in polar molecules are of three types: (1) The attractions or repulsions between the permanent electric moments of the molecules. The Boltzmann factor makes alignment of the moments more probable than other orientations so the alignment effect is attractive. (2) Attractions caused by the induction of additional multipole moments by the fields of permanent moments—the induction effect. (3) The dispersion forces arising from the electronic motions.

The alignment effect has been considered in some detail for water molecules.[6] It was found that the effect of quadrupole and higher moments could not be neglected. The procedure adopted in the case of water was to augment the dipole-dipole term R^{-3} by a term in R^{-5} whose coefficient was chosen so that the mean square of this approximate alignment potential corresponded as nearly as possible to the mean square of the exact alignment potential based on dipole, quadrupole, and higher moments. The principal contribution to the R^{-5} term comes from the dipole-quadrupole interaction for this method. The author[7] has made some force calculations for ammonia using the same ratio of dipole-quadrupole term to dipole-dipole term as was used for water. In the present paper a few modifications have been made. The dipole moment is taken to be $1.44\cdot10^{-18}$ e.s.u. which is based on microwave determinations[8] rather than the previously accepted value of $1.48\cdot10^{-18}$ e.s.u.[9] In the absence of detailed information on the electrical structure of NH_3, the ratio of the dipole-quadrupole term to the dipole-dipole term is assumed to be $1/R^2$. For water this ratio is about $2.4/R^2$. Of course this procedure is a phenomenological approach and the value of the dipole-quadrupole term may be in error; however, the present choice would probably be an underestimate of the effect of higher moments and should be in better accord with the facts than the point dipole assumption of Stockmayer.[10]

The alignment effect is then

$$V=-(2.07\cdot10^{-12}R^{-3}+2.07\cdot10^{-12}R^{-5})f(\theta_1,\theta_2,\phi)\text{ erg}, \quad (8)$$

$f(\theta_1,\theta_2,\phi)=2\cos\theta_1\cos\theta_2-\sin\theta_1\sin\theta_2\cos\phi$. θ_1 and θ_2 being the polar angles between fixed lines in the molecules and R, ϕ the relative azimuth.

Wolf[11] and Herzfeld list the dispersion formula

$$n-1=2.9658\cdot10^{27}/(8135\cdot10^{27}-\nu^2). \quad (9)$$

This results in a static polarizability of $2.15\cdot10^{-24}$ cm³, an oscillator strength of 2.72, and a resonance energy of 11.8 ev. The induction effect is found by the method of reference 6:

$$V_{\text{ind}}=-(8.9\cdot10^{-12}R^{-6}+8.9\cdot10^{-12}R^{-8})\text{ erg}. \quad (10)$$

The dispersion effect is

$$V_{\text{dis}}=-(65.5\cdot10^{-12}R^{-6}+212\cdot10^{-12}R^{-8})\text{ erg}. \quad (11)$$

If the intermolecular forces are non-central as is the case for ammonia, the classical expression for B is

$$B_{\text{cl}}=2\pi N\int_0^\infty R^2dR\int_\Omega[1-\exp(-V/kT)]d\Omega/8\pi, \quad (12)$$

$d\Omega=d(\cos\theta_1)d(\cos\theta_2)d\phi$. For polar molecules there is a sizeable quantum correction[12] to the classical expression for the second virial coefficient due to the interactions of the translational and rotational motions of the molecules. This correction is

$$B_q=-2\pi N\int_0^\infty R^2dR[\exp(-a(R)/kT)]\times\int\exp(bf/kT)\chi d\Omega/8\pi,$$

$$\chi=(h^2/3(kT)^2)(Jb(R)\{-f+(1/4kT)b\times[1+(3/2)(\cos^2\theta_1\cos^2\theta_2-f^2]\}). \quad (13)$$

$b(R)$ is the alignment term $(2.07\cdot10^{-12}R^{-3}+2.07\cdot10^{-12}R^{-5})$. $a(R)$ = repulsion term $-(74.4\cdot10^{-12}R^{-6}+221\cdot10^{-12}R^{-8})$. J is the geometric mean moment of inertia about two axes normal to the dipole axis.

The first model used was the hard sphere case. Table III shows the results for the potential

$$V=-(2.07\cdot10^{-12}R^{-3}+2.07\cdot10^{-12}R^{-5})f(\theta_1,\theta_2,\phi)-(74.4\cdot10^{-12}R^{-6}+221\cdot10^{-12}R^{-8})\text{ erg}, \quad R>3.115\text{A}.$$

$$V=\infty,\ R<3.115\text{A}. \quad (14)$$

The measured values of B are those of Keyes.[13] Computations were made also with an exponential repulsion force with a range of 0.28A. The following potential

[5] G. E. Uhlenbeck and E. Beth, Physica **3**, 729 (1936).
[6] H. Margenau and V. Myers, Phys. Rev. **66**, 307 (1944).
[7] V. Myers, Phys. Rev. **75**, 1620 (1949).
[8] B. Bleaney and R. P. Penrose, Proc. Roy. Soc. **189A**, 358 (1947).
[9] Uhlig, Kirkwood, and Keyes, J. Chem. Phys. **1**, 155 (1933).
[10] W. H. Stockmayer, J. Chem. Phys. **9**, 398 (1941).
[11] K. L. Wolf and K. F. Herzfeld, *Handbuch der Physik* (1928).
[12] J. G. Kirkwood, J. Chem. Phys. **1**, 597 (1933).
[13] F. G. Keyes, J. Am. Chem. Soc. **60**, 1761 (1938).

TABLE III. A comparison of the experimental and theoretical second virial coefficients for ammonia on the basis of the hard sphere model.

Temp. °K	Classical virial cm³/mole	Quantum correction cm³/mole	Theoretical virial cm³/mole	Experimental virial cm³/mole	Percent difference
300	−282	6	−276	−270	−2.2
400	−119	1	−118	−119	−0.8
500	− 64.1	0.5	− 63.6	− 66.6	4.5
600	− 37.3	0.2	− 37.1	− 40.6	8.6

TABLE IV. A comparison of the experimental and theoretical second virial coefficients for ammonia on the basis of the exponential repulsion.

Temp. °K	Classical virial cm³/mole	Quantum correction cm³/mole	Theoretical virial cm³/mole	Experimental virial cm³/mole	Percent difference
300	−261	8	−253	−270	6.3
400	−122	2	−120	−119	0.8
500	− 72.8	0.8	− 72.0	− 66.6	− 8.1
600	− 46.0	0.4	− 45.6	− 40.6	−12.3

was used:

$$V=5.00\cdot10^{-9}\exp(-R/0.28)-(74.4\cdot10^{-12}R^{-6}+221\cdot10^{-12}R^{-8})-(2.07\cdot10^{-12}R^{-3}+2.07\cdot10^{-12}R^{-5})f(\theta_1,\theta_2,\phi)\text{ erg.}\quad(15)$$

It is seen in Table IV that the repulsion term counteracts the increasing effect of the polar forces at lower temperatures and reverses the trend of the calculated values given in Table III.

The critical temperature of NH_3 is 405°K so dimerization may occur below this temperature. The value of B at 300°K is therefore somewhat uncertain. The author wishes to thank Mr. Andrew Skumanich for performing most of the numerical work.

THE JOURNAL OF CHEMICAL PHYSICS VOLUME 18, NUMBER 11 NOVEMBER, 1950

Dodecahedral Octacovalent Bond Orbitals

GEORGE H. DUFFEY
Chemistry Department, South Dakota State College, Brookings, South Dakota
(Received June 30, 1950)

Dodecahedral octacovalent bond orbitals of D_{2d} symmetry are considered. The bond orbitals are divided into two groups which may differ widely in composition, the over-all composition remaining sp^3d^4. When the average orbital strength is greatest, it equals 2.981 and the orbitals of group one and group two differ in composition and strength. The concept of orbital strength does not allow us to exclude either the dodecahedral or the tetragonal antiprism structure in AB_8 when A employs the sp^3d^4 configuration.

IN a recent paper[1] the author considered hybrid orbitals of tetragonal antiprism symmetry. Since covalent molecules or ions of type AB_8 may also possess a dodecahedral arrangement (an arrangement which $Mo(CN)_8^{-4}$ can assume), it is of interest to consider hybrid orbitals of this symmetry. For a figure illustrating this structure see the paper of Hoard and Nordsieck.[2]

When eight spd hybrid orbitals of D_{2d} symmetry are set up, one obtains the following functions:

$$\psi_1=[(1/2)\cos\alpha]s+[(1/2)\cos\beta]p_z+[(1/\sqrt{2})\cos\gamma]p_x+[(1/2)\sin\alpha]d_z+[(1/2)\sin\beta]d_{xy}+[(1/\sqrt{2})\sin\gamma]d_{x+z},\quad(1)$$

$$\psi_2=[(1/2)\sin\alpha]s+[(1/2)\sin\beta]p_z+[(1/\sqrt{2})\sin\gamma]p_y-[(1/2)\cos\alpha]d_z-[(1/2)\cos\beta]d_{xy}+[(1/\sqrt{2})\cos\gamma]d_{y+z},\quad(2)$$

$$\psi_3=[(1/2)\cos\alpha]s+[(1/2)\cos\beta]p_z-[(1/\sqrt{2})\cos\gamma]p_x+[(1/2)\sin\alpha]d_z+[(1/2)\sin\beta]d_{xy}-[(1/\sqrt{2})\sin\gamma]d_{x+z},\quad(3)$$

$$\psi_4=[(1/2)\sin\alpha]s+[(1/2)\sin\beta]p_z-[(1/\sqrt{2})\sin\gamma]p_y-[(1/2)\cos\alpha]d_z-[(1/2)\cos\beta]d_{xy}-[(1/\sqrt{2})\cos\gamma]d_{y+z},\quad(4)$$

$$\psi_5=[(1/2)\sin\alpha]s-[(1/2)\sin\beta]p_z+[(1/\sqrt{2})\sin\gamma]p_x-[(1/2)\cos\alpha]d_z+[(1/2)\cos\beta]d_{xy}-[(1/\sqrt{2})\cos\gamma]d_{x+z},\quad(5)$$

$$\psi_6=[(1/2)\cos\alpha]s-[(1/2)\cos\beta]p_z+[(1/\sqrt{2})\cos\gamma]p_y+[(1/2)\sin\alpha]d_z-[(1/2)\sin\beta]d_{xy}-[(1/\sqrt{2})\sin\gamma]d_{y+z},\quad(6)$$

$$\psi_7=[(1/2)\sin\alpha]s-[(1/2)\sin\beta]p_z-[(1/\sqrt{2})\sin\gamma]p_x-[(1/2)\cos\alpha]d_z+[(1/2)\cos\beta]d_{xy}+[(1/\sqrt{2})\cos\gamma]d_{x+z},\quad(7)$$

$$\psi_8=[(1/2)\cos\alpha]s-[(1/2)\cos\beta]p_z-[(1/\sqrt{2})\cos\gamma]p_y+[(1/2)\sin\alpha]d_z-[(1/2)\sin\beta]d_{xy}+[(1/\sqrt{2})\sin\gamma]d_{y+z}.\quad(8)$$

The s, p, and d functions are defined in the same way as in previous papers[1] by the author. The z axis coincides with the fourfold rotation-reflection axis (S_4). The numbering of the bonds is the same as the numbering of the ψ_i. Thus bonds one, three, five, and seven

[1] G. H. Duffey, J. Chem. Phys. **18**, 746 (1950).
[2] J. L. Hoard and H. H. Nordsieck, J. Am. Chem. Soc. **61**, 2853 (1939).

lie in the xz plane, bonds two, four, six, and eight in the yz plane.

The eight orthogonal bond orbitals fall into two groups. Group one includes ψ_1, ψ_3, ψ_6, and ψ_8, which represent four equivalent bond orbitals with the over-all composition $s^n p^{3m} d^{4-n-3m}$. Group two includes ψ_2, ψ_4, ψ_5, and ψ_7, which represent four equivalent bond orbitals with the over-all composition $s^{1-n} p^{3-3m} d^{n+3m}$. The parameters n and m are related to the parameters α, β, and γ by the two equations

$$n=\cos^2\alpha, \tag{9}$$

$$m=\tfrac{1}{3}(\cos^2\beta+2\cos^2\gamma). \tag{10}$$

The tetrahedral orbitals and the tetragonal plane orbitals discussed by Kuhn[3] are special cases of group one and group two orbitals.

A function orthogonal to $\psi_1, \cdots \psi_8$ is given by

$$\psi_9=d_{x+y}. \tag{11}$$

Let ϑ_1 be the angle between the z axis and the maximum in ψ_1 (approximately the angle between the axis and bond one), and ϑ_2 the angle between the z axis and the maximum in ψ_2 (approximately the angle between the axis and bond two). Let the maximum value of ψ_1 be called S_1, and the maximum value of ψ_2, S_2. Assume the energy of each bond is given by Eq. (13) of "Hexacovalent bond orbitals III."[4] Assume that the sum of the W's and the sum of the R's over all bonds are independent of the variation of the parameters. This assumption is reasonable if the degrees of ionic character of all bonds are equal and constant. Then in dodecahedral AB_8 the values of the parameters giving the largest sum of the bond energies are found by maximizing $4S_1+4S_2$. The results are given in the second row of Table I.

The average strength of the best dodecahedral orbitals equals 2.981. The sp^3d^4 configuration may also yield the tetragonal antiprism structure where the strength of each orbital is[1] 2.979. Thus the concept of orbital strength does not allow us to exclude either structure when the sp^3d^4 configuration is used and one might expect that some molecules or ions of type AB_8 could be prepared in both the dodecahedral and the tetragonal antiprism forms. It is probable that a considerable potential barrier restricts the conversion of one form into the other.

TABLE I. Properties of three sets of dodecahedral octacovalent bond orbitals.

Function maximized	Cosα[a]	Cosβ[a]	Cosγ[a]	S_1[b]	ϑ_1[c]	S_2[d]	ϑ_2[e]
S_1	0.6760	0.9048	0.4827	2.999	35°46′	2.954	72°53′
S_1+S_2	0.6457	0.9422	0.5144	2.995	34°33′	2.968	72°47′
S_2	0.5990	0.9485	0.5962	2.979	34°5′	2.971	70°36′

[a] The orbitals of group one have the over-all composition $s^n p^{3m} d^{4-n-3m}$; the orbitals of group two $s^{1-n} p^{3-3m} d^{n+3m}$, where $n=\cos^2\alpha$, $m=\frac{1}{3}(\cos^2\beta+2\cos^2\gamma)$.
[b] Maximum value of an orbital of group one.
[c] Acute angle between the rotation-reflection axis and the maximum in an orbital of group one.
[d] Maximum value of an orbital of group two.
[e] Acute angle between the rotation-reflection axis and the maximum in an orbital of group two.

In the "best" dodecahedral structure the s content, the p content, and the d content of an orbital of group one equal 0.1042, 0.3542, and 0.5416, respectively; the s content, the p content, and the d content of an orbital of group two equal 0.1458, 0.3958, and 0.4584, respectively.

Consider dodecahedral $Mo(CN)_8^{-4}$. In molybdenum[5] the $4d$ orbitals are more stable than the $5s$ or $5p$ orbitals. However, the high $5s$ and $5p$ content and the low strength of an orbital of group two in the "best" structure are not extreme enough to make the energy of a bond in group two very much less than the energy of a bond in group one. Hence one would expect the Mo—C bonds of group two to be only slightly longer than the Mo—C bonds of group one. In the ideal structure postulated by Pauling[6] and Hoard and Nordsieck,[2] all bonds were taken of equal length, the angle between the z axis and bond one was set equal to 36°51′, and the angle between the z axis and bond two was set equal to 69°28′. The experimental data[2] do not seem accurate enough to distinguish between this ideal structure and the structure obtained here. One should note that the bond angles, and consequently the effective strength and the composition of the orbitals, may be altered by the repulsion between the attached groups and by the environment of the ion in the crystal state.

[3] H. Kuhn, J. Chem. Phys. **16**, 727 (1948).
[4] G. H. Duffey, J. Chem. Phys. **18**, 510 (1950).
[5] In Mo the state $4d^45s^2\ {}^5D_0$ is 31 kcal./mole less stable than the state $4d^55s\ {}^7S_3$. See F. R. Bichowsky and F. D. Rossini, *The Thermochemistry of the Chemical Substances* (Reinhold Publishing Corporation, New York, 1936).
[6] L. Pauling, *The Nature of the Chemical Bond* (Cornell University Press, Ithaca, 1940).

THE JOURNAL OF CHEMICAL PHYSICS VOLUME 18, NUMBER 11 NOVEMBER, 1950

Determination of Molecular Shape by Osmotic Measurement

A. ISIHARA
Department of Physics, Faculty of Science, University of Tokyo, Tokyo, Japan
(Received July 10, 1950)

The second coefficient A_2 of osmotic pressure π of high-polymer solutions is calculated in the case of the rigid ovaloid. A_2 is a function of the molecular shape and thus we can determine the shape of high polymers.

1. PRINCIPLE OF CALCULATION

RECENTLY Zimm[1] has calculated the second coefficient A_2 in the expansion of osmotic pressure π of high-polymer solutions:

$$\frac{\pi}{RTC}=\frac{1}{M_2}+A_2C+A_3C^2+\cdots, \tag{1}$$

and lately Kotani[2] has calculated the same quantity in the case of rigid ellipsoid of revolution in an approximate manner and has shown that the numerical factor f in the expression,

$$A_2=(4N_0v/M_2^2)f, \tag{2}$$

becomes larger than 1 when the solute molecules deviate from spherical shape. In this equation N_0 is Avogadro's number, v the volume of a solute molecule and M_2 is the molecular weight of a polymer. In this paper, we shall show that more general expression for A_2 can be given, which is rigorous in the case of the rigid ovaloid.

The integral for f is to be extended over all the positions of a molecule, say B, relative to another molecule A, in which A and B commute with each other. Such motions of B constitute a subset I in the group of motions G and the determination of f reduces to search for the volume of I. In order that the results do not depend on the choice of the standard position of B we are required to seek the Haar's measure $m(I)$ of I in G. This is obtained by integrating the characteristic function $f(x)$:

$$f(x)=\begin{cases}1; & x\epsilon I,\\ 0; & x\bar{\epsilon} I,\end{cases} \tag{3}$$

of I over whole G. This integration can be performed as:

$$m(I)=\int_{G/g}d\bar{x}\int_g f(x\xi)d\xi, \qquad f=(1/8v)m(I), \tag{4}$$

where ξ is the element of translation group g which is the normal subgroup of G and $\bar{x}$ is the element of G/g which is isomorphic to the three-dimensional rotation group in the case of rigid body model. The meaning of this integration is that we at first integrate $f(x)$ over the translation group, and then integrate the result over the group G/g, because the result of the former integration is a function of $\bar{x}$ only:

$$\int_g f(x\xi)d\xi=\int_g f(xa\eta)da\eta=\int_g f(xa\eta)d\eta=f(\bar{x}), \qquad (a\epsilon g) \tag{5}$$

if we remember $d\xi$ is the left invariant measure of g. Also, because $d\bar{x}$ is the left invariant measure of G/g,

$$\int_{G/g}f(\bar{b}\bar{x})d\bar{x}=\int_{G/g}\bar{f}(\bar{b}\bar{x})d(\bar{b}\bar{x})=\int_{G/g}f(\bar{y})d\bar{y}, \qquad b\epsilon G;\quad \bar{b}\epsilon G/g. \tag{6}$$

Hence,

$$m(bI)=\int_{G/g}d\bar{x}\int_g f(bx\xi)d\xi =\int_{G/g}d\bar{x}f(\bar{b}\bar{x})=\int f(\bar{x})d\bar{x}, \tag{7}$$

or

$$m(bI)=m(I), \tag{8}$$

which shows that $m(I)$ given by Eq. (3) does not depend on the standard position of B.

The infinitesimal Haar's measure of translation group g is nothing but the ordinal volume element in three dimensional Euclidian space and that of the rotation group G/g is given by

$$\frac{1}{8\pi^2}\sin\theta d\theta d\varphi d\tau=\frac{1}{8\pi^2}d\omega d\tau, \tag{9}$$

if we express its elements by

$$\begin{bmatrix}\sin\varphi\sin\tau+\cos\theta\cos\varphi\cos\tau, & -\cos\varphi\sin\tau+\cos\theta\sin\varphi\cos\tau, & -\cos\tau\sin\theta\\ -\sin\varphi\cos\tau+\cos\theta\cos\varphi\sin\tau, & \cos\varphi\cos\tau+\cos\theta\sin\varphi\sin\tau, & -\sin\theta\sin\tau\\ \sin\theta\cos\varphi, & \sin\theta\sin\varphi, & \cos\theta\end{bmatrix}. \tag{10}$$

[1] B. H. Zimm, J. Chem. Phys. 14, 164 (1946).
[2] M. Kotani read 1947 in the meeting of the Physical Society of Japan.

2. RIGID OVALOID

Let us consider two ovaloids A and B, A being fixed in space and B moves around it. $\tilde{f}(\bar{x})$ is nothing but the volume of C which is described by a point $0'$ fixed in B when B moves around A keeping its orientation and always in touch with A. It is easily shown that C is another ovaloid.

Next, let us consider a common contact plane of A and B and draw perpendiculars from a point 0 of A and $0'$ of B to the plane and designate respective lengths by $H(\theta, \varphi)$ and $K(\bar{x}; \theta, \varphi)$. Here (θ, φ) represents the direction of the perpendicular and $\bar{x}$ the rotation θ_1, φ_1 and τ_1 of B. Again we define the linear differential expression with respect to H or K of regular functions on the unit sphere:

$$(H, K)=\left(\frac{\partial^2 H}{\partial\theta^2}+H\right)\left(\frac{1}{\sin^2\theta}\frac{\partial^2 K}{\partial\varphi^2}+\frac{\cos\theta}{\sin\theta}\frac{\partial K}{\partial\theta}+K\right)$$
$$-2\frac{\partial}{\partial\theta}\left(\frac{1}{\sin\theta}\frac{\partial H}{\partial\varphi}\right)\cdot\frac{\partial}{\partial\theta}\left(\frac{1}{\sin\theta}\frac{\partial K}{\partial\varphi}\right)$$
$$+\left(\frac{1}{\sin^2\theta}\frac{\partial^2 H}{\partial\varphi^2}+\frac{\cos\theta}{\sin\theta}\frac{\partial H}{\partial\theta}+H\right)\left(\frac{\partial^2 K}{\partial\theta^2}+K\right). \quad (11)$$

Then the volume of C that is $\tilde{f}(\bar{x})$ is given by

$$f(\bar{x})=\frac{1}{6}\int (H+K(\bar{x}))(H+K(\bar{x}),\quad H+K(\bar{x}))d\omega. \quad (12)$$

This comes from the fact that on the one hand (H, H) is twice times the product of principal radii of the ovaloid corresponding to (θ, φ):

$$(H, H)=2R_1R_2, \quad (13)$$

and on the other the volume of an ovaloid is expressed as:

$$v=\frac{1}{3}\int HR_1R_2d\omega, \quad (14)$$

where $d\omega$ is the surface element on the unit sphere belonging to the direction (θ, φ), and the integration extends over whole surface of unit sphere.[3] Thus the Haar's measure $m(I)$ of Eq. (3) is expressed:

$$m(I)=\frac{1}{8\pi^2}\int \tilde{f}(\bar{x})d\omega_1 d\tau_1$$
$$=\frac{1}{48\pi^2}\int d\omega_1 d\tau_1 \int (H+K(\bar{x}))$$
$$\times(H+K(\bar{x}),\quad H+K(\bar{x}))d\omega. \quad (15)$$

To evaluate this we at first show that the above differential expression (11) is self-adjoint on the whole surface of unit sphere. That is, if $L(\theta, \varphi)$ is another one-valued function on the surface as is $H(\theta, \varphi)$ or $K(\theta, \varphi)$, we demonstrate the equality:

$$\int L(H, K)d\omega-\int H(L, K)d\omega=0. \quad (16)$$

For convenience we put:

$$L\frac{\partial H}{\partial\theta}-H\frac{\partial L}{\partial\theta}=P;\quad \frac{1}{\sin\theta}\frac{\partial H}{\partial\varphi}L-\frac{1}{\sin\theta}\frac{\partial L}{\partial\varphi}H=Q. \quad (17)$$

Then

$$\{L(H, K)-H(L, K)\}\sin\theta$$
$$=\frac{\partial P}{\partial\theta}\left(\frac{1}{\sin\theta}\frac{\partial^2 K}{\partial\varphi^2}+\cos\theta\frac{\partial K}{\partial\theta}+\sin\theta\cdot K\right)$$
$$+\left(\cos\theta\cdot Q-\frac{\partial P}{\partial\varphi}-\sin\theta\frac{\partial Q}{\partial\theta}\right)\cdot\frac{\partial}{\partial\theta}\left(\frac{1}{\sin\theta}\frac{\partial K}{\partial\varphi}\right)$$
$$+\left(\frac{\partial Q}{\partial\varphi}+\cos\theta\cdot P\right)\left(\frac{\partial^2 K}{\partial\theta^2}+K\right)$$
$$=\frac{\partial}{\partial\theta}\Big[\sin\theta\Big\{P\left(\frac{1}{\sin^2\theta}\frac{\partial^2 K}{\partial\varphi^2}+\frac{\cos\theta}{\sin\theta}\frac{\partial K}{\partial\theta}+K\right)$$
$$-Q\frac{\partial}{\partial\theta}\left(\frac{1}{\sin\theta}\frac{\partial K}{\partial\varphi}\right)\Big\}\Big]$$
$$-\frac{\partial}{\partial\varphi}\left\{P\frac{\partial}{\partial\theta}\left(\frac{1}{\sin\theta}\frac{\partial K}{\partial\varphi}\right)-Q\left(\frac{\partial^2 K}{\partial\theta^2}+K\right)\right\},$$

from which we can easily arrive at Eq. (16).

Now remembering Eq. (11) is linear with respect to H or K and using Eq. (16), we can rewrite Eq. (15) as follows:

$$m(I)=v_A+v_B$$
$$+\frac{1}{16\pi^2}\int H(K(\bar{x}),\quad K(\bar{x}))d\omega d\omega_1 d\tau_1$$
$$+\frac{1}{16\pi^2}\int K(\bar{x})(H, H)d\omega d\omega_1 d\tau_1. \quad (18)$$

The remaining two integrals in this equation can easily be shown to be separated with respect to $d\omega$, $d\omega_1$ and $d\tau_1$ owing to the self-adjoint character expressed by Eq. (16) and the fact that we can apply the constant rotation $\bar{b}$ to B:

$$\int K(\bar{x})d\bar{x}=\int K(\bar{b}\bar{x})d\bar{b}\bar{x}=\int K(\bar{b}\bar{x})d\bar{x},$$

[3] W. Blaschke, Kreis und Kugel, Jber. Deutsch. Math.-Vereinig. Band 24 (1915).

which rotates B from (θ, φ) to $(0, 0)$, and also the fact that because of Eq. (10) $K(\bar{x}; 0, 0)$ reduces to $K(\theta_1, \varphi_1)$:

$$K(\theta_1, \varphi_1, \tau_1; 0, 0) = K(\theta_1, \varphi_1). \tag{19}$$

On the other hand we utilize the formulas which express the surface F and mean of the mean radius of curvature $M/4\pi$ of ovaloid by the surface integration over unit sphere:

$$\left.\begin{aligned} F &= \int R_1 R_2 d\omega = \frac{1}{2}\int H(R_1+R_2)d\omega, \\ M &= \int H d\omega = \frac{1}{2}\int (R_1+R_2)d\omega. \end{aligned}\right\} \tag{20}$$

Then Eq. (18) reduces to

$$\begin{aligned} m(I) &= v_A + v_B + \frac{1}{8\pi}\int H d\omega \int (K, K)d\omega_1 \\ &\quad + \frac{1}{8\pi}\int K d\omega_1 \int (H, H)d\omega \\ &= v_A + v_B + \frac{1}{4\pi}(M_A F_B + M_B F_A). \end{aligned} \tag{21}$$

Therefore we obtain the final expression for f:

$$f = \frac{MF}{16\pi v} + \frac{1}{4}, \tag{22}$$

in the homogeneous case. When the solution is heterogeneous, we are only required to replace the three quantities M, F and v by their number averages.

3. SPECIAL FORMS OF f

(1) Ellipsoid of Revolution

First we consider the typical case of ellipsoid of revolution:

$$\left.\begin{aligned} x &= a\sin\theta\cos\varphi, \\ y &= a\sin\theta\sin\varphi, \\ z &= b\cos\theta, \end{aligned}\right\}. \tag{23}$$

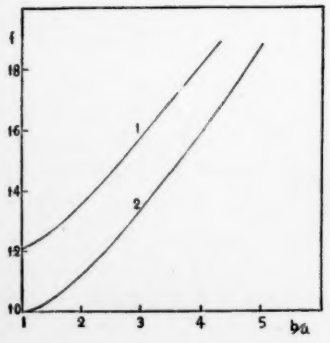

FIG. 1. f as a function of axial ratio. 1: Cylinder; 2: Ellipsoid of revolution. Curve 1 corresponds to the elongated form; the case of flat cylinder is not shown.

In this case $H(\theta, \varphi)$ is independent of H and is given by

$$H = (a^2\sin^2\theta + b^2\cos^2\theta)^{\frac{1}{2}}. \tag{24}$$

Thus, if we use the eccentricity:

$$\begin{aligned} \epsilon^2 &= \frac{a^2-b^2}{a^2}, \quad (a \geqslant b\text{: oblate}) \\ &= \frac{b^2-a^2}{b^2}. \quad (a \leqslant b\text{: prolate}) \end{aligned} \tag{25}$$

Then the mean of the mean radius of curvature $M/4\pi$ and the surface area F are given by

$$\begin{aligned} M &= 2\pi a\left\{(1-\epsilon^2)^{\frac{1}{2}} + \frac{\sin^{-1}\epsilon}{\epsilon}\right\}, \quad \text{(oblate)} \\ &= 2\pi b\left\{1 + \frac{1-\epsilon^2}{2\epsilon}\log\frac{1+\epsilon}{1-\epsilon}\right\}; \quad \text{(prolate)} \end{aligned} \tag{26}$$

$$\begin{aligned} F &= 2\pi a^2\left\{1 + \frac{1-\epsilon^2}{2\epsilon}\log\frac{1+\epsilon}{1-\epsilon}\right\}, \quad \text{(oblate)} \\ &= 2\pi ab\left\{(1-\epsilon^2)^{\frac{1}{2}} + \frac{\sin^{-1}\epsilon}{\epsilon}\right\}. \quad \text{(prolate)} \end{aligned} \tag{27}$$

Introducing these equations into Eq. (23), we arrive at the same expression for f regardless of both types of ellipsoids:

$$\begin{aligned} f = \frac{1}{4} + \frac{3}{16}&\left(1 + \frac{1}{(1-\epsilon^2)^{\frac{1}{2}}}\frac{\sin^{-1}\epsilon}{\epsilon}\right) \\ &\times\left(1 + \frac{1-\epsilon^2}{2\epsilon}\log\frac{1+\epsilon}{1-\epsilon}\right). \end{aligned} \tag{28}$$

When $\epsilon \ll 1$ this can be expanded as a power series of ϵ:

$$f = 1 + \frac{\epsilon^4}{15} + \frac{37}{60}\epsilon^6 + \cdots. \tag{29}$$

Figure 1, curve 2 shows the variation of f with axial ratio a/b. Comparing these theoretical values with the experimental data we can thus determine the axial ratio of solute molecules as ellipsoid of revolution. Actually, f for hemoglobin is 1.27 and for serum albumin 1.6.[1] Accordingly, we obtain $b/a = 2.5$ in the former case and 4 in the latter case. Considering elongated case,[4] the viscosity value for hemoglobin is 4.6 and for serum albumin is 5.6 whereas the diffusion values are 3.7 and 5.0 respectively.

(2) Cylinder

In this case the calculation is comparatively easy. Let us put the contact plane to the given cylinder of

[4] R. Simha, J. App. Phys. **13**, 147 (1942).

length $2b$ and radius a on the corner of the cylinder, then the perpendicular from the center of the cylinder that is $H(\theta, \varphi)$ is given by

$$H(\theta, \vartheta) = b\cos\theta + a\sin\theta. \tag{30}$$

Therefore, we can calculate f as follows (see Fig. 1, curve 1):

$$f = \frac{1}{4}\left\{1 + \frac{b}{a}\left(1 + \frac{a}{2b}\right)\left(1 + \frac{a\pi}{2b}\right)\right\}. \tag{31}$$

When $b \gg a$, A_2 thus evaluated reduces to the expression given by Zimm:

$$A_2 = \frac{4\pi N_0 a b^2}{M_2^2}. \quad (b \gg a) \tag{32}$$

Attention must be paid to the fact that whereas we have deduced Eq. (22) in the case of smooth ovaloid, circular cylinder considered here is not smooth. But from the physical point of view, we can consider that Eq. (22) is also true in this case. The above coincidence with the result of Zimm shows also this plausibility. Thus we can calculate the "second virial coefficient" in a wide range of shapes of molecules. At least the principle of calculation explained in Section 1 can be applied if the molecules are not ovaloid-shaped.

Another attention must be drawn to the general character that f is always larger than 1 when the molecules are not spherical. This is easily seen if we rewrite Eq. (22) as

$$f = 1 + \left(\frac{MF}{16\pi v} - \frac{3}{4}\right) \tag{33}$$

the quantity in the bracket is not negative owing to the inequality:

$$M^2 \geqslant 4\pi F; \quad F^3 \geqslant 36\pi v^2. \tag{34}$$

Here the equality is established only in the case of sphere.

THE JOURNAL OF CHEMICAL PHYSICS VOLUME 18, NUMBER 11 NOVEMBER, 1950

The Magnetic Anisotropy of $\alpha - NiSO_4 \cdot 6H_2O$ between 13 and 295°K. A Torsion Balance for Magnetic Anisotropy Measurements

J. W. Stout and Maurice Griffel*
Institute for the Study of Metals, University of Chicago, Chicago, Illinois
(Received July 13, 1950)

The magnetic anisotropy of single crystals of $\alpha - NiSO_4 \cdot 6H_2O$ has been measured at temperatures between 13 and 295°K. Two crystals of different origin gave concordant results. The difference in magnetic susceptibility between directions parallel and perpendicular to the tetragonal crystallographic axis is given by $\chi_\perp - \chi_\parallel = 1.37\times10^{-5} + 1.502\times10^{-2}/T + 1.686/T^2$. The susceptibility difference was independent of field strength up to 10,000 gauss over the temperature range investigated. The results are discussed in connection with the theoretical treatment of the susceptibility of nickel salts by Schlapp and Penney. A torsion balance for the magnetic anisotropy measurements is described.

INTRODUCTION

THE theory of the splitting of the ground states of paramagnetic ions by the electrical fields present in crystalline solids has been developed by Van Vleck and co-workers. In particular, Schlapp and Penney[1] have calculated the case of Ni^{++} ion in a crystalline field of predominantly cubic symmetry with a superimposed smaller field of rhombic symmetry. The ground state which is triply degenerate in the cubic field is split by the combined action of the rhombic field and the spin-orbit coupling. This splitting produces an anisotropy in the magnetic susceptibility.

The anisotropy of $NiSO_4 \cdot 6H_2O$ has been measured by Krishnan and co-workers[2] over the temperature range 90 to 300°K. From these measurements and the theory they deduced a value for the spin-orbit coupling constant in good agreement with that obtained from spectroscopic measurement of gaseous nickel ion. The present paper presents more accurate measurements of the magnetic anisotropy and extends the range of the measurements to liquid hydrogen temperatures. The torsion balance used for this and other crystals is also described.

APPARATUS

Torsion Balance

The magnetic anisotropy was measured with the torsion balance whose construction is shown in Fig. 1. The single crystal sample, $T8$, which is symmetrically located between the poles of the electromagnet, H, is cemented with thin collodion to a 2-mm diameter quartz rod, $T7$, which is flared and ground flat on the bottom. The quartz rod is fastened to a 3.2-mm diameter phosphor bronze rod, $T6$, on which are mounted the

* AEC Predoctoral Fellow 1948–49. Present address: Iowa State College, Ames, Iowa.

[1] R. Schlapp and W. G. Penney, Phys. Rev. **42**, 666 (1932).

[2] (a) Krishnan, Chakravorty, and Banerjee, Trans. Roy. Soc. **A232**, 107 (1934). (b) K. S. Krishnan and A. Bose, Nature **141**, 329 (1938). (c) Krishnan, Mookherji, and Bose, Trans. Roy. Soc. **A238**, 125 (1940).

oil damper *O* and the hexagonal mirror *M*. The whole assembly hangs from the beryllium-copper torsion fiber, *T*5. The upper end of the torsion fiber is fastened by a clamp to a spring assembly made from a sylphon bellows which permits vertical motion but is rigid to rotation. The rod *T*1 leads through a gas-tight rubber seal and is rigidly attached to the spindle *T*2 and the circular scale *T*3. The whole upper torsion assembly rotates in the ball bearing *B*1. The position of this assembly is adjusted by means of a shaft and gear system so placed that the adjustment may be made by the operator who is simultaneously observing through a telescope the angular position of the mirror *M*. The circular scale *T*3 is divided into 1000 units and its position may be read with the vernier *T*4 to 0.05 unit.

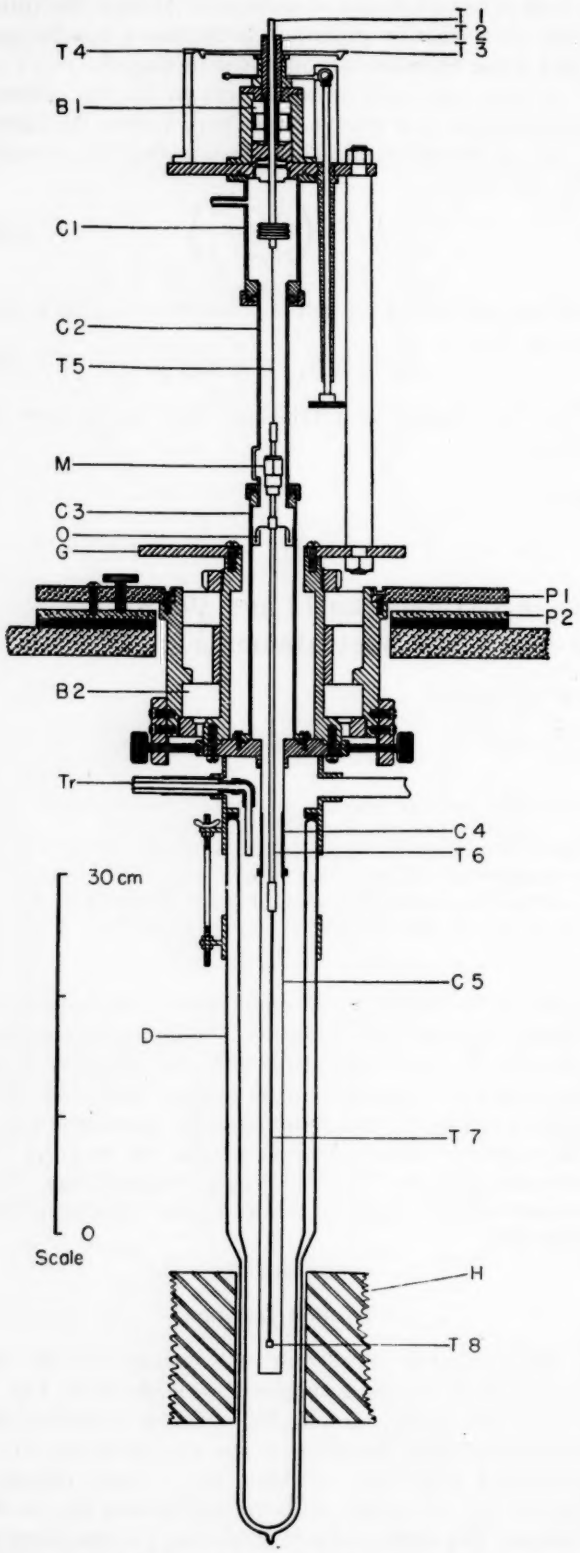

FIG. 1. Torsion balance for magnetic anisotropy measurements.

The torsion assembly is surrounded by the gas-tight chamber *C*1 to *C*5. During measurements, this chamber is filled with helium gas at slightly above atmospheric pressure. The joints at room temperature are made with rubber gaskets. The lower brass can, *C*5, is 19 mm o.d. and 0.9 mm wall. It telescopes into the brass tube *C*4 and a vacuum-tight connection is made with a cup filled with Rose metal. *C*5 is removed for mounting and centering the crystal in the magnet. *C*2 is a glass tube sealed with rubber O-rings. It has a plane glass window through which the image of an illuminated scale seen in the mirror *M* may be viewed in a telescope. The oil damping cup, *O*, was filled with Silicone D.C. 703. In order to prevent frothing of the oil when the chamber *C* was evacuated prior to filling with helium, it was necessary to degas the damping fluid by heating under vacuum. The glass tube *C*2 was slid up and the degassed damping oil added to the cup with a medical syringe. The chamber is then closed, evacuated, and filled with helium. When the Dewar is cooled by adding refrigerant, additional helium is added to the chamber *C*. The pressure of He is kept at about 4 cm above atmospheric by means of a mercury bubbler.

The Pyrex Dewar, *D*, of capacity one liter, presses against a rubber ring in the brass Dewar cap and is sealed with adhesive tape. The liquid refrigerants are introduced through the transfer tube *Tr* which is an L-shaped double-walled evacuated monel tube 1.27 cm o.d. and 0.56 cm i.d. The longer leg (not shown) extends to the bottom of the storage Dewar and ends in a valve operated from the outside. The shorter leg slips within a brass sleeve soldered into one of the bosses of the Dewar cap and ends in a brass male taper which fits in a female taper permanently mounted by thermal insulating supports inside the Dewar cap. This arrangement allows convenient assembly and the evaporation of the refrigerant during transfer was quite small. Two other tubes soldered into bosses in the Dewar cap served for the thermocouples and for gas outlet.

The entire balance including the Dewar could be rotated on the ball bearings *B*2 and clamped in position. The ball-bearing housing was mounted on an aluminum plate *P*1 provided with leveling and clamping screws attached to a rubber mounted aluminum plate *P*2. The whole assembly was mounted on a carriage which permitted the balance to be rolled from between the pole

pieces of the magnet for assembly and then accurately returned to its original position.

Temperature Measurement and Control

Temperatures were measured by means of copper-constantan thermocouples soldered to the outside of the brass can *C*5 at various heights. The thermocouples were calibrated at the transition point of $Na_2SO_4 \cdot 10H_2O$, the sublimation point of CO_2, and against vapor pressures and triple points of nitrogen and hydrogen. For interpolation purposes the ratio between the observed e.m.f. and that calculated from the temperature using the table of Giauque, Buffington, and Schulze[3] was plotted against the observed e.m.f. The ratio varied smoothly from 1.1530 at 312°K to 1.1585 at 12°K and the curve could be used for determining intermediate temperatures between the calibration points. During the measurements at hydrogen temperatures, the vapor pressure of the bath was read with a mercury manometer and the temperature calculated directly from the vapor pressure.

Since it was not possible to attach a thermocouple directly to the sample during a measurement of magnetic anisotropy, a series of experiments was performed to prove that the temperature equilibrium between the outside of the brass tube and the sample, maintained by the helium in the chamber, was sufficiently good so that a thermocouple soldered directly opposite the sample indicated the sample temperature. The temperatures of two thermocouples, previously compared against one another while mounted in the same apparatus, were compared when one thermocouple was soldered outside the brass tube and the other was soldered to a brass block cemented to the end of the quartz rod in the position usually occupied by the sample. There was no systematic difference between the temperature at the sample position and on the brass tube and the difference was always less than 0.05°. We estimate that the reported sample temperatures are correct to ±0.05°.

The refrigerants used were ethane, oxygen, nitrogen, and hydrogen. For temperatures below the normal boiling point, the pressure was kept constant with a solenoid valve controlled by a mercury manometer. A 150-liter ballast tank served to smooth out the surges caused by opening and closing of the valve. By means of manual valves connected in series and parallel with the solenoid valve the surges were further reduced. With the above device, difficulty was encountered in controlling the temperature of liquid nitrogen because of superheating and bumping of the liquid at the bottom of the Dewar which caused temperature fluctuations of several tenths of a degree. This difficulty was eliminated by introducing a slow stream of gaseous nitrogen through a small plastic tube that led to the bottom of the Dewar.

[3] Giauque, Buffington, and Schulze, J. Am. Chem. Soc. **49**, 2343 (1927).

Magnetic Field Measurement and Control

The magnetic field was produced with the electromagnet described by Kay.[4] It was provided with plane pole pieces 5 in. in diameter adjusted to a 2-in. gap. Under these conditions a field of about 10,000 gauss is produced by a current of 25 amp. The homogeneity of the field was checked with a search coil and a sensitive galvanometer. Within a spherical region of 2-cm radius from the geometrical center of the gap, the field was uniform to 0.02 percent. The sample was always in this volume.

The magnet current was adjusted and controlled by means of an electronic controller acting on the field current of the generator. By means of the controller, the current could be regulated to give magnetic fields between 1500 and 10,000 gauss. The current was maintained constant by the controller to within 0.1 percent.

The magnetic field was measured with a search coil and a General Electric light beam fluxmeter. Since the magnetic field at a given magnet current was not reproducible to the accuracy desired, we adopted the procedure of measuring the field strength during each anisotropy measurement. A search coil mounted in a Lucite holder which located it in a definite position was placed against one pole piece of the magnet. The magnetic field strength could be measured by removing this search coil from its position next to a pole piece to one of negligible field while the center of the magnet gap was occupied by the sample and Dewar vessel. The search coil was made of 0.25-mm diameter manganin wire. In order to obtain the full sensitivity of the fluxmeter a series of shunts of manganin wire was constructed so that by use of the appropriate shunt a full-scale deflection of the fluxmeter could be obtained at fields from 1500 to 10,000 gauss. The shunts were placed directly across the search coil leads. Since both coil and shunts were made of manganin wire, their resistance was independent of the room temperature and the correction factor for the shunt could be calculated from the accurately measured resistance of the shunt and the coil. The observed fluxmeter deflections are multiplied by a "shunt factor," $[R(\text{shunt})+R(\text{coil})]/R(\text{shunt})$, to give the deflection corresponding to the unshunted coil. The validity of this expression for the fluxmeter and coil used was experimentally verified within the limit of accuracy of the fluxmeter. In separate experiments with the sample and Dewar removed, the fluxmeter deflections produced by a standard search coil of accurately known turn area placed at the center of the magnet were compared with those produced by the working coil in its usual position against a pole piece. This calibration was made at various field strengths. The field at the center of the magnet was lower than that at the coil position by amounts ranging from 0.45 to 0.65 percent depending on the field strength. The

[4] W. B. Kay, Doctoral dissertation, University of Chicago (1926).

fluxmeter was calibrated at frequent intervals during the measurements using a standard mutual inductance and a current measured with a White potentiometer. It is estimated that the over-all accuracy of the field determination is about 0.5 percent.

Torsion Fibers

The torsion fibers were made of two percent beryllium-copper (Berylco No. 25) wire. This material was quite satisfactory and much more convenient to use than quartz suspensions which are very easily broken. The suspensions were made a uniform length (16.8 cm over-all) with the ends of the wire soldered into bronze tips, 0.79 cm long and 0.16 cm diameter, which fitted into clamps in the torsion assembly so that the wire with its attached tips could be easily removed for calibration. The torsion constant of the suspensions was determined by measuring the period of oscillation of an aluminum cylinder of known moment of inertia and of mass (68.6 g) approximating that carried by the suspension during the anisotropy measurements. The temperature coefficient of the torsion constant of the beryllium-copper wire was found to be about -0.03 percent per °C, so accurate control of the suspension temperature during the anisotropy measurements was not necessary. The suspensions were calibrated frequently during the measurements and no significant changes with time were observed. Three sizes of torsion suspension were used, of wire 0.003, 0.005, and 0.010 in. diameter. These had torsion constants of 8.66, 61.0, and 1082 dyne cm radian^{-1} in the 16.8-cm length suspensions used.

EXPERIMENTAL PROCEDURES

Preparation of Samples

Two crystals of tetragonal $\alpha-NiSO_4\cdot 6H_2O$ were used in the measurements. Crystal A was selected from a batch of crystals grown by slow evaporation at about 35°C of a saturated solution of Mallinckrodt's low cobalt analytical reagent nickel sulfate. These crystals had well developed natural faces and it was found that they cleaved readily with a razor blade along the 001 plane. The cleaved surfaces were smooth, showed specular reflection of light, and were suitable for use as reference planes for the orientation of the crystal in the magnetic apparatus. The selected crystal was mounted with paraffin in a machined brass block and surfaces perpendicular to the 001 plane and to one another were made by rubbing on a sheet of 2/0 flint paper on a flat surface. The finished crystal was a rectangular prism weighing 0.3821 g. The magnetic anisotropy measurements on crystal A gave results appreciably lower than previously reported, so check measurements were made on another crystal of tetragonal $\alpha-NiSO_4\cdot 6H_2O$ from a different source. This specimen, called crystal B, was prepared from a large crystal kindly supplied by Mr. A. N. Holden of the Bell Telephone Laboratories. It weighed 0.3449 g. The orientation and perfection of both crystals were checked by mounting them on a universal stage between crossed polaroids and noting the extinction of polarized light. These measurements confirmed the tetragonal symmetry of the crystals and the accuracy of orientation of the cleavage planes normal to the c axis within an experimental error of about 1°.

Mounting of the Samples

The crystals were mounted in the torsion balance with the c axis in a plane normal to the axis of rotation of the suspension. The magnetic field direction lies in this plane. A plane surface of the crystal specimen which had been accurately sanded so as to contain the direction of the c axis was glued with collodion cement to the ground surface of the quartz specimen holder ($T7$ in Fig. 1). The suspension was then allowed to hang freely between the pole pieces of the magnet and the orientation of the crystal relative to the pole pieces of the magnet checked by observations with a telescope. If the c axis of the crystal is not exactly perpendicular to the axis of the suspension, the observed anisotropies must be divided by the square of the cosine of the angle of deviation from 90°. This correction was very small, less than 0.01 percent for crystal A and 0.28 percent for crystal B.

Method of Measurement

The couple acting on an anisotropic magnetic body in a homogeneous magnetic field is given by

$$C=(m/2M)\mathbf{H}^2(\chi_1-\chi_2)\sin 2\theta \qquad (1)$$

where m is the mass, $\mathbf{H}$ the magnetic field strength, M the molecular weight, χ_1 and χ_2 the two principal molal susceptibilities in the plane of rotation, and θ the angle of rotation. There are, therefore, four positions, $\theta=0$, 90°, 100° and 270°, where no couple is exerted by the magnetic field. Of these positions, two are at a minimum in potential energy corresponding to the alignment of the principal axis of greater magnetic susceptibility with the field direction and are stable zeros. The other two are unstable. When the crystal is mounted in the torsion balance the angular reading of the torsion head corresponding to an alignment of the c axis of the crystal in the direction of the field is noted. This position will correspond to one of the zeros for a crystal of tetragonal symmetry. The position of the four zeros can be found more accurately by noting the positions of zero deflection upon application of a magnetic field, and the preliminary orientation during assembly is used only to identify the zeros with the crystallographic directions. Upon the application of a field, the suspension turns toward the stable zeros and away from the unstable ones so one can readily determine if the axis of greater susceptibility is parallel or perpendicular to the c axis. Once the position of the zeros is deter-

mined, the torsion head is set at a chosen position, usually taken as one of the four positions where the couple is a maximum, and the reading of the scale in the telescope noted. The field is then applied and the torsion head rotated to bring the scale reading in the telescope back to its original value. The magnetic field and bath temperature are then measured. Equation (1) was experimentally checked at various values of θ and found to be valid for the $NiSO_4 \cdot 6H_2O$ crystals within the experimental error. The deflection of the suspension and the collodion was measured with the crystal removed and although measurable deflections were found, they were less than 0.1 percent of that produced by the $NiSO_4 \cdot 6H_2O$ crystals at room temperature. The overall accuracy of the anisotropy measurements is estimated at about one percent. The principal error is in the measurement of the field strength.

EXPERIMENTAL RESULTS

Krishnan, Mookherji, and Bose[2c] noted that $NiSO_4 \cdot 6H_2O$ tends to dehydrate when cooled to low temperatures and then warmed up. We found that no measurable loss of weight or change in appearance of a crystal of $NiSO_4 \cdot 6H_2O$ occurred when it was subjected to a vacuum at room temperature. However, to follow the extent of any possible dehydration, the room temperature anisotropy was first measured before the crystal was cooled and then remeasured after each subsequent cooling. The room temperature measurements were corrected to a common temperature using our observed curve for the temperature dependence of the magnetic anisotropy. No change was observed in crystal *A* after it was cooled to liquid nitrogen temperature and rewarmed to room temperature. After the measurements at liquid hydrogen temperatures had been made, the magnetic anisotropy at room temperature was found to be 1.8 percent smaller than before and remained at this value for the room temperature measurements after the series at liquid ethane and oxygen temperatures. We believe that the change was due to partial dehydration of the crystal which occurred while the crystal was slowly warming from liquid hydrogen temperatures to room temperature and have multiplied all readings since the liquid hydrogen measurements by the factor 1.018 to put them on the basis of the original crystal. After the conclusion of the measurements, the crystal was removed and it was found that the surface was covered with a thin yellowish film and the weight had decreased by 0.0010 g. This loss of weight together with the change in magnetic anisotropy at room temperature would correspond to a dehydration of 1.8 percent of the original crystal to a tetrahydrate. A similar correction, the factor being 1.0148, was made to the measurements on crystal *B* which lost 0.0007 g during the measurements.

The results of the anisotropy measurements are presented in Table I and represented graphically in Fig. 2. At all temperatures the molal susceptibility in the direction of the tetragonal crystallographic axis, $\chi_{\parallel}$, is less than the susceptibility, $\chi_{\perp}$, in a direction perpendicular to this axis. Because of the tetragonal symmetry, the susceptibility is independent of direction in the plane perpendicular to the tetragonal axis. The values at fields in the neighborhood of 9800 gauss represent the mean of several measurements taken at the same temperature. The values at lower field strengths are individual measurements taken to check the validity of Eq. (1). Any ferromagnetic impurity which saturates at low fields would give an apparent decrease in the susceptibility difference at larger field strengths. The measurements at the smaller fields are less accurate because the measured couple is smaller and the measurement of field strength is somewhat less precise. Within the accuracy of the measurements, Eq. (1) is obeyed, and there is no evidence for ferromagnetic impurities. The measurements at liquid hydrogen temperatures were made with a 0.010-in. suspension and the remainder with a 0.003-in. suspension. A check reading, not included in the table, was taken at the boiling point of nitrogen with the 0.010-in. suspension. The value obtained agreed with that from the 0.003-in. suspension within two percent which is as closely as the small deflection with the heavier suspension could be read, and is evidence of the consistency of the suspension calibrations.

The data are represented by the equation

$$(\chi_{\perp}-\chi_{\parallel})T^2=1.686+1.502\times10^{-2}T+13.7\times10^{-5}T^2 \quad (2)$$

which was obtained from a least-squares treatment of the measurements in Table I taken at fields near 9800 gauss. The anisotropy calculated from this equation is

TABLE I. Molal magnetic anisotropy of $\alpha-NiSO_4 \cdot 6H_2O$. (Molecular weight 262.85.)

Crystal	T, °K	H, gauss	$(\chi_{\perp}-\chi_{\parallel})\times10^6$ Obs.	Calc. Eq. (2)
B	293.69	9815	84.2	84.4
A	291.81	9800	85.2	85.0
A	291.87	7855	85.0	85.0
A	291.93	5865	84.8	84.9
A	291.99	3918	84.7	84.9
A	185.14	9840	143.6	144.0
A	122.25	9830	248.6	249.4
A	90.51	9835	385.9	385.4
A	90.51	6130	385.1	385.4
B	77.58	9820	490	487
B	77.57	6160	488	488
A	77.39	9810	492	489
A	77.39	6010	488	489
A	77.39	3930	484	489
A	59.40	9835	743	744
A	20.37	9800	4870	4815
A	20.37	5965	4880	4815
A	20.37	3910	4820	4815
A	16.00	9830	7440	7540
A	15.73	9830	7700	7780
A	13.96	9830	9640	9740
A	13.92	5995	9730	9759
A	13.92	3930	9710	9795

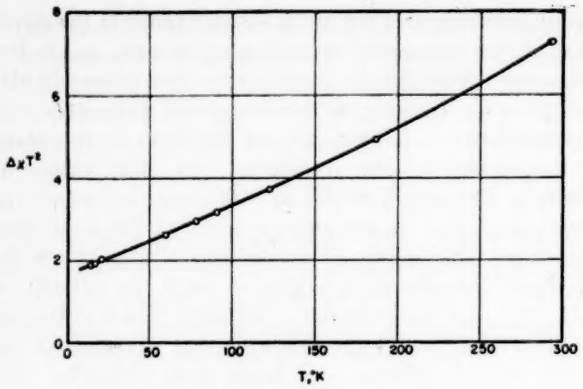

FIG. 2. Molal magnetic anisotropy of $\alpha-NiSO_4\cdot 6H_2O\cdot\Delta\chi=\chi_\perp-\chi_{\parallel}$.

listed in the last column of Table I. The temperature measurements at 15.73 and 16.00°K were less reliable than the other points, so these points were weighted lightly in the least-squares treatment. Within the expected accuracy, the equation represents the data over the temperature range from 14 to 295°K.

Krishnan, Mookherji, and Bose[2c] have obtained a value of $\chi_\perp-\chi_{\parallel}$ of 112×10^{-6} at 21°C, compared with 83.9×10^{-6} given by Eq. (2), and Krishnan, Chakravorty, and Banerjee[2a] report a value of 109×10^{-6} at 30°C where we obtain 81.6×10^{-6}. The discrepancy is well outside the experimental error so the measurements reported above on crystal *B* were made and confirmed our anisotropy values with a completely different sample. Krishnan and Bose[2b] have also reported a value of 4.86 for the ratio of the magnetic anisotropy at −183°C to that at 23°C. Our results give 4.65 for this ratio.

DISCUSSION

If one assumes that all the magnetic ions in a crystal of $NiSO_4\cdot 6H_2O$ are acted on by electrostatic fields having the tetragonal symmetry of the crystal, then the formulas derived by Schlapp and Penney[1] for a cubic plus rhombic field when adapted to the tetragonal case become

$$(\chi_\perp-\chi_{\parallel})T^2=8N\beta^2\Delta\alpha(-2\lambda^2/3k^2+8\lambda T/3k-T^2). \quad (3)$$

Here N is Avogadro's number, β the Bohr magneton, k Boltzmann's constant, λ the spin-orbit coupling constant, T the absolute temperature, and $\Delta\alpha$ is the difference between the tetragonal field parameters perpendicular and parallel to the tetragonal axis. This equation has the same form as Eq. (2) and the parameters $\Delta\alpha$ and λ can be evaluated from that equation. The ground state of the Ni^{++} ion in the crystal is split into two levels, one single and one doubly degenerate, which are separated in energy by $\delta=-4\lambda^2\Delta\alpha$. Because of thermal expansion effects and diamagnetic anisotropy, one would not expect an exact correspondence between Eqs. (2) and (3). However, these effects will both become of negligible importance at the lower temperatures which are of principal importance in determining the first two terms of Eq. (2). By equating the first term in Eqs. (2) and (3), one obtains $\delta=2.34$ cm^{-1} and from the ratios of the first two terms in each equation, $\lambda=-312$ cm^{-1} and $\Delta\alpha=-6.01\times10^{-6}$ cm. The value $\lambda=-355$ cm^{-1} has been deduced by Laporte[5] from the over-all multiplet width of gaseous Ni^{++}. The agreement is as good as one would expect from the approximations in the theory. If one takes λ as independent of temperature and equal to -312 cm^{-1}, then the value of $\Delta\alpha$ necessary to satisfy Eqs. (2) and (3) varies only from -6.01×10^{-6} cm at 15°K to -6.10×10^{-6} at 300°K. Such a small change is quite reasonable and is evidence that the theoretical picture of Schlapp and Penney is substantially correct.

The crystal structure of $\alpha-NiSO_4\cdot 6H_2O$ determined by Beevers and Lipson[6] has four nickel ions, each surrounded by an octahedron of water molecules, per unit cell. The local electric field acting on the ions does not necessarily have the symmetry of the unit cell and the principal axes of susceptibility of the four ions in a unit cell may be oriented in different directions. In such a case the energy splitting δ, would be greater than that deduced from Eq. (3) assuming all the ions to be equivalent. It is of interest to note that low temperature heat capacity measurements of Stout and Giauque[7] on orthorhombic $NiSO_4\cdot 7H_2O$ show energy separations of about 2.6 cm^{-1} between the three energy levels. Similar measurements on $NiSO_4\cdot 6H_2O$ would yield values of δ to compare with the value 2.34 cm^{-1} obtained assuming the ions to be magnetically equivalent.

We are indebted to Mr. Joseph Getzholtz and to Mr. R. A. Wentzel for their excellent machine work in constructing the torsion balance.

[5] O. Laporte, Zeits. f. Physik **47**, 761 (1928).
[6] C. A. Beevers and H. Lipson, Zeits. f. Krist. **83**, 123 (1932).
[7] J. W. Stout and W. F. Giauque, J. Am. Chem. Soc. **63**, 714 (1941).

The Magnetic Anisotropy of Manganous Fluoride between 12 and 295°K

MAURICE GRIFFEL* AND J. W. STOUT
Institute for the Study of Metals, University of Chicago, Chicago, Illinois

(Received July 13, 1950)

The magnetic anisotropy of single crystals of MnF_2, a typical antiferromagnetic substance, has been measured over the temperature range 12 to 295°K. At temperatures above 100°K the anisotropy is of the order of 0.1 percent of the susceptibility and the greater susceptibility is in the direction of the c axis of the tetragonal crystal. Below 70°K the anisotropy becomes extraordinarily large and the susceptibility in the direction of the c axis is smaller than that perpendicular to this axis. Within the limit of experimental error, the anisotropy was independent of field strength up to 10,000 gauss. From the present measurements, combined with those of previous investigators on the powder susceptibility, the directional susceptibilities parallel and perpendicular to the c axis have been calculated. As the temperature is lowered from 70 to 14°K, the perpendicular susceptibility increases by about 12 percent and the parallel susceptibility approaches zero at zero temperature. These results are discussed in connection with the theory of antiferromagnetism proposed by Van Vleck.

INTRODUCTION

MANGANOUS fluoride is an example of that class of paramagnetic substances which are called antiferromagnetic. In ferromagnetic materials the exchange forces between neighboring paramagnetic ions favor a parallel alignment of the electronic spins and the ordered arrangement stable at low temperatures has a permanent magnetic moment within each domain consisting of many atoms. In antiferromagnetic materials the exchange forces favor an antiparallel alignment of the spins and the low temperature ordered arrangement has no permanent moment and a magnetic susceptibility less than would be obtained if there were no interaction between the magnetic ions. The magnetic susceptibility of powdered MnF_2 as measured by Bizette and Tsai[1] and de Haas, Schultz, and Koolhaas[2] has a maximum in the neighborhood of 70°K and decreases at lower temperatures, reaching at 15°K a value roughly three-fourths of the maximum. The heat capacity measurements of Stout and Adams[3] show a sharp maximum at 66.5°K. About 34 percent of the total magnetic entropy of k ln 6 per Mn^{++} ion, corresponding to the change from a completely ordered state to one of complete randomness of the spins, was found in that portion of the heat capacity curve which was clearly anomalously high. The remainder of the magnetic entropy is presumably gradually acquired at higher temperatures in such a fashion that the corresponding heat capacity could not be distinguished from the ordinary vibrational heat capacity.

Van Vleck[4] has derived a theory of antiferromagnetism which is formally similar to the Weiss-Heisenberg theory of ferromagnetism. In Van Vleck's theory the magnetic ions are divided into two subclasses, each of which is acted on by an internal field proportional to the magnetic moment of the other. Since the two subclasses have opposite orientations, there is no net magnetic moment. As in the Weiss theory, there is a Curie temperature at which long-range order appears. Below the Curie temperature the magnetic susceptibility parallel to the direction of alignment of the spins decreases to zero as the temperature is lowered to 0°K while that perpendicular to this direction remains constant. Van Vleck did not consider the identification of these susceptibilities with any crystallographic directions but by averaging calculated that the powder susceptibility at 0°K should be two-thirds its value at the Curie temperature.

Recent accurate measurements of Corliss, Delabarre, and Elliott[5] on the powder susceptibility of MnF_2 at temperatures above 180°K may be represented by the Curie-Weiss formula, $\chi=C/(T+\Delta)$, with the Curie constant equal to that calculated for the ^6S state of gaseous Mn^{++} ion and a Δ of 97°K. The large value of Δ is presumably associated with the exchange coupling between the magnetic ions. The energy associated with the exchange forces depends only on the relative orientations of the spins of the interacting ions and is independent of the orientations of the spins with respect to the crystallographic directions.[6] MnF_2 has the tetragonal rutile crystal structure[7,8] with each Mn^{++} ion surrounded by two nearest neighbors at a distance of 3.3103A in the direction of the c axis, eight neighbors at a distance of 3.8229A in the 111 directions and four at a distance of 4.8734A in the ab plane. Although the exchange forces, which are primarily responsible for the ordering that begins near 70°K, cannot directly produce a magnetic anisotropy, it was conceivable that this ordering could affect the small anisotropy expected from other causes. Our measurements show that in the ordered state the anisotropy becomes extraordinarily

* AEC Predoctoral Fellow 1948–49. Present address: Iowa State College, Ames, Iowa.

[1] H. Bizette and B. Tsai, Comptes Rendus **209**, 205 (1939).

[2] de Haas, Schultz, and Koolhaus, Physica **7**, 57 (1940).

[3] J. W. Stout and H. E. Adams, J. Am. Chem. Soc. **64**, 1535 (1942).

[4] J. H. Van Vleck, J. Chem. Phys. **9**, 85 (1941).

[5] Corliss, Delabarre, and Elliott, J. Chem. Phys. **18**, 1256 (1950).

[6] See J. H. Van Vleck, Phys. Rev. **52**, 1178 (1937).

[7] P. P. Ewald and C. Hermann, *Strukturbericht* (Leipzig, 1931), Vol. I, p. 192.

[8] M. Griffel and J. W. Stout, J. Am. Chem. Soc. (to be published).

large. The measurements and the interpretation will be discussed below. A preliminary account of them has been published.[9]

EXPERIMENTAL

The magnetic anisotropy was determined with a torsion balance which measured the couple on an oriented single crystal in a homogeneous magnetic field. The apparatus and method of measurement have been described previously.[10] The preparation and properties of the single crystals of MnF_2 used have also been described.[8] Two crystals, designated as A and B, were used for the measurements. Crystal A was in the form of a right circular cylinder 0.9 cm tall and 0.9 cm in diameter, and weighed 2.224 g. The boule from the single crystal furnace was first oriented approximately by observation through crossed polaroids. It was then attached to the goniometer head of a Laue back reflection x-ray camera and adjusted until the c axis coincided with the direction of the incident x-rays. An accurately milled miter box was then placed around the crystal and lined up with respect to the camera. The crystal was cemented to the miter box with a beeswax-rosin mixture. The miter box was then rotated on the bed of the camera by 180° and an x-ray picture taken of the opposite side of the crystal. The perfect agreement of the two pictures as well as the uniform extinction of polarized light proved that the crystal was indeed single.

TABLE I. Couple produced at various angular positions. The angular position, θ, is measured from a position of zero torque. The couple produced by the magnetic field is proportional to the rotation, Δ, of the torsion head needed to bring the crystal in the magnetic field back to its position, θ, in zero field. $\Delta=1000$ corresponds to one complete rotation. All measurements are on crystal A.

	θ	Δ	Average
$T=295.7$°K	45°	41.05	40.14
0.005-in. suspension	225°	39.23	
9845 gauss	135°	40.19	40.65
	315°	41.11	
$T=90.15$°K	45°	85.15	84.73
0.005-in. suspension	225°	84.30	
9860 gauss	135°	87.55	84.53
	315°	81.50	
$T=20.34$°K	45°	163.85	163.95
0.010-in. suspension	225°	164.05	
2045 gauss	135°	163.70	164.10
	315°	164.50	

The miter box was then mounted on the cross feed of a lathe and the ends of the crystal ground down parallel to the ends of the box against a rotating flat sanding plate. These faces contained the c axis of the crystal and were used as reference planes in the further machining operations. The crystal was next cut with a jeweler's saw, the selected half removed from the miter box and the reference surface cemented to a flat-surfaced brass piece held in the collet of the lathe. The crystal was then ground with sandpaper into the form of a right circular cylinder with the c axis lying in the basal plane. The orientation was confirmed to within 1° by an x-ray picture taken perpendicular to the c axis. The crystal was etched in HCl solution to remove any possible ferromagnetic impurities on the surface and was mounted in the torsion balance with the c axis accurately perpendicular to the axis of the suspension and the direction of the c axis in the basal plane known roughly by a mark on the crystal. The exact angular orientation of the c axis was determined from the positions of zero torque.

Crystal B, prepared from another boule, was a small square plate approximately 0.6 cm along an edge and 0.15 cm thick. It was similarly oriented by x-rays to within 1° and weighed 0.2054 g.

Before the measurements were made it was expected that the magnetic anisotropy of MnF_2 might be quite small and so some pains were taken to grow a large crystal and to form it into a geometrical shape with circular symmetry about the axis of rotation of the balance suspension. There is a torque on a magnetically isotropic crystal of non-symmetrical shape in a uniform magnetic field because of demagnetization effects.[11] Thus an isotropic paramagnetic needle tends to align itself with the direction of the magnetic field. This effect is not important for moderately anisotropic paramagnetic salts, as was the case, for example, with our measurements on $NiSO_4\cdot 6H_2O$, but in the case of MnF_2, when the anisotropy is small and the susceptibility relatively large, it can be of importance unless care is taken to have a symmetrical sample. After the measurements on crystal A had shown the anisotropy at hydrogen temperatures to be very large, we prepared crystal B, which has square symmetry, for the measurements at these temperatures.

When the anisotropy is small there is another effect that is of importance. The quartz rod to which the crystal is attached is neither perfectly straight, nor perfectly centered, nor is the field absolutely uniform. Consequently, if the field exerts a slight lateral force on the paramagnetic sample or the quartz rod, because of the lack of perfect alignment and centering of the suspension, rod and sample, a torque on the suspension is observed. To a good approximation this torque varies as $\sin\theta$ where θ is the angular position of the suspension. It was found experimentally that this effect could be minimized by selecting straight rods and by careful alignment. The total couple measured in an arbitrary position is then

$$C=C_1\sin(\theta+\alpha)+C_2\sin 2(\theta+\psi). \quad (1)$$

[9] J. W. Stout and M. Griffel, Phys. Rev. **76**, 144 (1949).
[10] J. W. Stout and M. Griffel, J. Chem. Phys. **18**, 1449 (1950).
[11] E. C. Stoner, *Magnetism and Matter* (Methuen and Company, Ltd., London, 1934), p. 40.

TABLE II. Molal magnetic anisotropy of MnF_2. (Molecular weight 92.93.)

Crystal	T, °K	H, gauss	$(\chi_{\parallel}-\chi_{\perp})\times10^{3}$
A	295.7	9845	0.0133
A	185.1	9850	0.0248
A	158.8	9840	0.0290
A	131.7	9850	0.0334
A	90.15	9860	0.0279
A	90.15	6040	0.0282
A	90.15	3910	0.0282
A	77.30	9870	0.0009
A	77.27	6030	0.0012
A	73.42	9920	− 0.0237
A	70.38	9840	− 0.0603
B	68.70	9790	− 0.1109
A	68.4±0.1	9870	− 0.114
A	67.34	9890	− 0.184
B	66.19	9815	− 0.884
B	62.98	9800	− 2.76
B	62.35	9850	− 3.10
B	59.80	9820	− 4.46
B	58.00	9830	− 5.32
B	54.76	9820	− 6.87
B	20.37	9806	−21.8
B	20.37	7755	−21.8
B	20.37	6040	−21.7
B	20.37	3955	−21.7
B	20.37	2075	−21.8
A	20.34	4015	−21.5
A	20.34	2045	−21.5
A	20.34	1010	−21.3
A	16.40	2040	−23.0
B	16.24	9820	−23.2
A	13.92	2040	−23.7
B	13.92	9820	−23.9
B	11.9	9815	−24.4

α and ψ are phase angles which in general are not equal and $C_2=\frac{1}{2}(m/M)\mathbf{H}^2(\chi_1-\chi_2)$ where the notation is the same as used in the previous paper.[10] The validity of Eq. (1) was checked by several series of measurements at ten to twenty equally spaced intervals around a complete circle and treating the data by Fourier analysis. Only the coefficients of the "1θ"- and "2θ"-terms were found to be appreciable. It is sometimes difficult to keep the temperature constant for the time required to take a large number of readings. Since generally $C_2\gg C_1$ and since the torque at the maximum is not sensitive to small changes in angle a simpler procedure of eliminating the "1θ"-terms was adopted. A zero torque position is found; the torsion head is rotated 45° to the position of maximum torque and a reading taken. The torsion head is then rotated by 180° and another observation made. The average of these two readings is the correct one since the "1θ"-terms cancel. As a check two further readings were often taken at the two remaining maxima. In Table I are presented some typical data. It is evident that at room temperature and at the boiling point of oxygen where the anisotropy is small the "1θ"-correction is important whereas at the boiling point of hydrogen it is smaller than the experimental error. At the boiling point of nitrogen, which is very near the temperature where the anisotropy passes through zero, the "1θ"- and "2θ"-deflections were comparable in magnitude and it was necessary to take a complete set of readings and make the Fourier analysis.

The results of the measurements are presented in Table II. The results are believed to be accurate to one percent or to an absolute value of 0.3×10^{-6} susceptibility difference per mole, whichever is larger. In the region near 66°K, where the anisotropy is changing very rapidly with temperature, the principal uncertainty is introduced by the temperature measurement which was accurate to 0.05° unless otherwise indicated. The results of the anisotropy measurements below 100°K are shown in Fig. 1. In order to investigate the region between 20 and 55°K where no refrigerant bath was available a warming curve of one-hour duration was taken over this temperature range. Measurements of temperature and anisotropy were made throughout the warming time and the curve in Fig. 1 has been drawn through these points which are indicated by crosses. Since the uncertainty in the temperature of the specimen when there may be appreciable thermal gradients in the apparatus makes the warming curve points considerably less reliable than the ones taken with a refrigerant bath, we have not presented these data in tabular form. However, they show the general nature of the variation of the anisotropy over the temperature range 20 to 55°K.

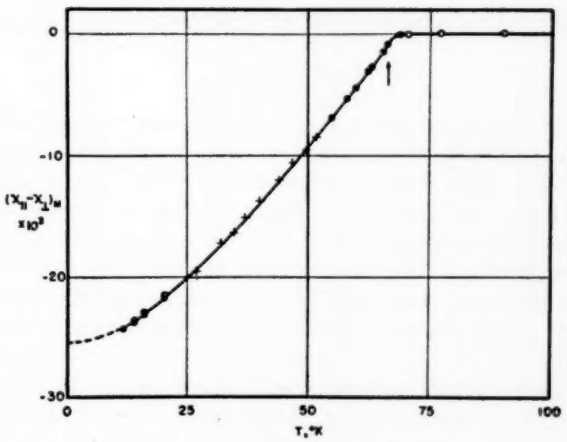

FIG. 1. Molal magnetic anisotropy of MnF_2. The arrow indicates the temperature of the heat capacity maximum.

At high temperatures the susceptibility parallel to the c axis, $\chi_{\parallel}$, is greater than the perpendicular susceptibility, $\chi_{\perp}$, and the anisotropy, $\chi_{\parallel}-\chi_{\perp}$, is of the order of 0.1 percent of the susceptibility. As the temperature is lowered, the anisotropy rises, reaching a maximum at about 120°K and then falls rapidly. The anisotropy passes through zero at about 77°K and as the temperature is lowered becomes large and negative until at the temperatures of liquid hydrogen it is greater than the susceptibility of powdered specimens. The susceptibility of a randomly oriented powder specimen is given by $\chi_{Av}=\frac{1}{3}\chi_{\parallel}+\frac{2}{3}\chi_{\perp}$. By combining our measurements with those of de Haas, Schultz, and

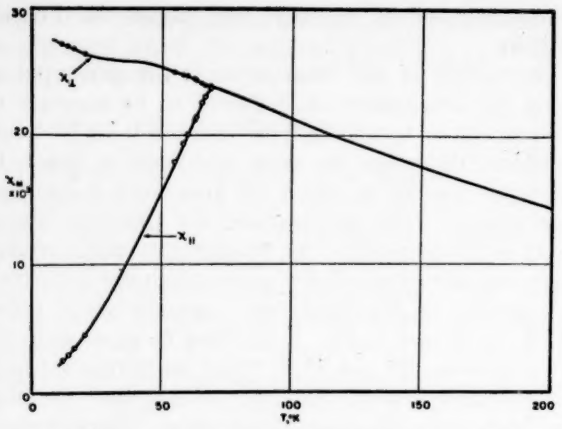

FIG. 2. Molal magnetic susceptibility of MnF_2 parallel and perpendicular to c axis of crystal.

Koolhaas[2] on a powder specimen we have calculated the individual values of $\chi_\parallel$ and $\chi_\perp$ which are illustrated in Fig. 2. Within the accuracy of the powder susceptibility data, $\chi_\parallel$ approaches zero at zero temperature. The use of the powder susceptibility measurements of Bizette and Tsai[1] combined with our data would extrapolate to a negative value of $\chi_\parallel$ at 0°K. As is seen from the data in Table II, we found no significant variation of the anisotropy with field strength at the lowest temperatures and at fields up to 10,000 gauss.

DISCUSSION

The small magnetic anisotropy at room temperature is comparable to that observed[12] in more dilute manganous salts which, according to Van Vleck and Penney,[13] is caused by a slight splitting of the sixfold degenerate ground level of Mn^{++} ion by the crystalline electrostatic fields. Since at high temperatures the susceptibility of MnF_2 parallel to the c axis is greater than that perpendicular, the states corresponding to the alignment of the spins in the direction of the c axis will be energetically more favored than the others by a few tenths of a wave number. If this effect of the crystalline electric fields were the only one, the anisotropy would be always of the same sign and vary inversely as T^2. However, the heat capacity anomaly near 66.5°K and the large Δ of 97° in the Curie-Weiss formula that represents the powder susceptibility measurements[5] above 180°K are indications of much stronger forces acting on the magnetic ions. These are presumably exchange forces which couple together the spins of the Mn^{++} ions. In the neighborhood of 70°K this coupling begins to produce a long-range order and, as the temperature is lowered, the magnetic ions approach a completely ordered arrangement with no net magnetic moment.

The exchange forces cannot in themselves produce any anisotropy. However, once the magnetic ions are coupled together by the exchange forces in ordered groups the energy needed to turn the spins with respect to the crystal lattice is the energy of a few tenths of a wave number for each individual ion times the effective number in a group. Below the Curie temperature of around 70°K the size of the group rapidly increases. With this addition, Van Vleck's theory[4] of antiferromagnetism is in good qualitative agreement with the results we have observed on MnF_2. At high temperature, where there is no long-range order, there is a small tendency favoring alignment of the spins parallel to the c axis of the crystal and consequently a slightly greater susceptibility in this direction. Below the Curie temperature, where long-range order sets in, the spins become largely lined up in the direction of the c axis and the susceptibility in this direction becomes small because of an effect analogous to the saturation of a paramagnetic substance in a very large magnetic field.

The magnetic dipole-dipole coupling between neighboring ions in MnF_2 could also produce an alignment of the spins with respect to the crystal lattice since the dipole energy contains a term dependent on the orientation of the spins relative to the radius vector between them. For two Mn^{++} ions at the nearest neighbor distance of 3.310A, which are coupled together by strong forces in an antiparallel fashion, the dipole energy would be 0.9 cm^{-1} lower for an alignment of the dipoles perpendicular to the c axis than for alignment with this axis. Taking the nearest and next nearest neighbors into consideration the dipole forces would favor alignment of the spins perpendicular to the c axis provided that the nearest neighbors are coupled together in an antiparallel fashion. This is not in agreement with the alignment of the spins in the direction of the c axis deduced from our measurements. However, if the chains of nearest neighbors running in the c direction are coupled together by the exchange forces in a parallel (ferromagnetic) sense, and if the chains are coupled to one another by antiferromagnetic interaction between the next-nearest neighbors, then the dipole forces would favor the alignment of the spins along the c axis and since the chains are coupled antiparallel the crystal as a whole would be antiferromagnetic.

[12] K. S. Krishnan and S. Banerjee, Trans. Roy. Soc. **A235**, 343 (1936).
[13] J. H. Van Vleck and W. G. Penney, Phil. Mag. **17**, 961 (1934).

Raman Spectra of Hydrocarbons. V. *n*-Hexane, *n*-Heptane, 2-Methylpentane, 3-Methylpentane, 2,4-Dimethylpentane, and 2,3-Dimethylbutane*

FORREST F. CLEVELAND AND PASQUALE PORCELLI†
Spectroscopy Laboratory, Department of Physics, Illinois Institute of Technology, Chicago 16, Illinois

(Received July 21, 1950)

Raman displacements, semiquantitative relative intensities, and quantitative depolarization factors are given for the above named hydrocarbons in the liquid state. The relative intensities and depolarization factors were obtained by use of a Gaertner microdensitometer. The depolarization factors were determined by a well-tested, single-exposure method. The previous data have been collected, tabulated, and compared with the present results, and probable values and average deviations are listed.

THE hydrocarbons used in this work were prepared under the direction of Professor C. E. Boord of the Department of Chemistry of the Ohio State University as part of the American Petroleum Institute Hydrocarbon Research Project in the Industrial Research Foundation of the University. The Raman spectral data were obtained by previously described[1] apparatus and methods.

n-HEXANE, $CH_3-CH_2-CH_2-CH_2-CH_2-CH_3$

Raman displacements and estimated relative intensities for *n*-hexane have been obtained in 12 investigations,[2–13] but polarization data (largely qualitative) were obtained in only one of these.[12]

TABLE I. Raman spectral data for liquid *n*-hexane (C_6H_{14}).*

I PR	Δν PR	ρ PR	ρ HKW	*N*	Δν PV	*AD*	*I* PR	Δν PR	ρ PR	ρ HKW	*N*	Δν PV	*AD*
vw	148			1	148		69	1082	0.85	0.86	8	1080	1.5
vw	169			1	169		54	1140	0.46	0.57	9	1138	2.2
vw	189			1	189		19	1167	0.00		6	1166	1.0
51	±309	0.78	*P*?	7	311	1.9	*vw*	1196			4	1218	11.2
45	±335	0.37	*P*?	6	333	1.8	40	1287			4	1271	13.8
83	±371	0.09	*P*?	9	368	2.6	95	1304	0.78	0.80	9	1302	1.8
56	±400	0.69	*P*?	9	400	1.1	*vw*	1340			3	1340	2.0
24	455	0.40		7	453	3.9	*vw*	1366			3	1364	2.6
20	484			3	493	6.3	220	1440	0.85	0.86	7	1439	1.6
				3	729	0.7	280	1459			7	1457	2.6
				3	745	1.7	*vw*	1485			1	1485	
				1	760		7	2667			4	2668	2.2
				1	794		11	2700			2	2701	1.5
14	807	0.67	*P*	6	810	1.3	26	2730	0.30		8	2732	1.2
50	823	0.59		8	825	2.0	840	2850	0.27		8	2851	1.9
56	867	0.42	*P*	9	868	1.3	1000	2868					
110	895	0.43	0.49	13	894	2.3				*P*	5	2863	1.2
				4	899	1.0					5	2876	1.0
10	949			7	951	2.1					4	2899	2.5
12	975			7	973	3.6	750	2906	0.22	*P*	4	2914	4.0
18	1006	0.00	*P*	9	1007	1.6	720	2937	0.19		9	2938	1.6
54	1039	0.38	0.58	11	1039	1.3	450	2960	0.74		8	2963	1.4
49	1065			6	1064	1.2							

* *I*=relative intensity; Δν=Raman displacement in cm^{-1}; ρ=depolarization factor; *PR*=present results; *HKW*=Herz, Kahovec, and Wagner (reference 12); *N*=number of times the line has been observed in apparently reliable independent investigations, including the present one; *PV*=probable value (mean of the *N* values); *AD*=average deviation of the *N* values from the mean; ± indicates lines that were observed both as Stoke's and anti-Stoke's lines; *P*=polarized; *vw*=very weak; and the braces join lines that were unresolved on the polarization spectrograms.

The present results, the previous polarization data, and the probable values of the Raman displacements are given in Table I. The probable values were obtained by taking a mean of all those values for a given line which seemed to be within the normal limits of experimental error. Some of the weak lines reported by only a few observers may result from impurities in the

TABLE II. Raman spectral data for liquid *n*-heptane (C_7H_{16}).*

I PR	Δν PR	ρ PR	ρ HKW	*N*	Δν PV	*AD*	*I* PR	Δν PR	ρ PR	ρ HKW	*N*	Δν PV	*AD*
				2	150	3.5	12	1027	0.87		7	1023	2.6
				2	203	4.5	48	1047	0.69		8	1046	0.6
				1	223						2	1058	2.0
45	±281	0.23	*P*	6	282	1.5					1	1069	
130	±310			11	310	1.2	68	1080	0.88	0.85	11	1081	2.2
13	358			6	356	1.0	52	1136	0.54	0.56	11	1136	1.6
38	±395	0.83	*D*	11	395	1.2	18	1163	0.79		10	1161	1.0
				1	405						5	1206	1.7
vw	454			7	451	3.0					5	1243	4.2
				1	483						6	1265	3.3
vw	498			7	497	2.7					1	1281	
				2	505	0.5	110	1305	0.87	0.89	12	1302	1.8
				4	543	2.7					1	1310	
				1	696						5	1345	2.2
				4	722	2.7					5	1365	2.4
vw	740			6	741	2.5	320	1442	0.94	0.86	9	1438	2.4
9	775	0.83		11	775	3.4		1459			9	1457	2.1
											1	1654	
				1	805						1	2523	
				1	826						1	2610	
62	835	0.61	0.59	10	836	1.8					3	2666	5.7
40	853	0.92		6	853	0.7					2	2708	1.5
				1	868						7	2732	0.8
vw	881			6	886	2.0	24	2730	0.45		7	2732	0.8
69	902	0.40	*PP*	12	901	1.9	870	2851	0.11	*P*	9	2852	2.7
				2	907	0.0	1000	2870	0.10		9	2873	2.0
vw	933			6	934	3.0	950	2903	0.16		6	2903	1.7
				1	949					*P*	2	2918	2.0
760	2932	0.07									11	2936	3.0
9	954	*D*		10	957	4.0	320	2958	0.87		10	2962	1.7
				1	988						1	2994	

* *D*=depolarized; *PP*=partly polarized; other symbols have the same meaning as in Table I.

* Presented in part at the Pittsburgh meeting of the American Physical Society, April 1944; abstract in Phys. Rev. **65**, 350 (1944).

† Present address: Department of Mathematics, University of Texas, Austin, Texas.

[1] F. F. Cleveland, J. Chem. Phys. **11**, 1, 227 (1943); **13**, 101 (1945).

[2] A. Petrikaln and J. Hochberg, Zeits. f. physik. Chemie **B3**, 217, 405 (1929).

[3] J. Okubo and H. Hamada, Science Reports Tôhoku Univ. **18**, 601 (1929).

[4] Godchot, Canals, and Cauquil, Comptes Rendus **194**, 176 (1932).

[5] Andant, Lambert, and Lecomte, Comptes Rendus **198**, 1316 (1934).

[6] K. W. F. Kohlrausch and F. Köppl, Zeits. f. physik. Chemie **B26**, 209 (1934).

[7] G. B. Bonino and R. Manzoni-Ansidei, Proc. Ind. Acad. Sci. **8A**, 405 (1938).

[8] Rosenbaum, Grosse, and Jacobson, J. Am. Chem. Soc. **61**, 689 (1939).

[9] H. Okazaki, J. Chem. Soc. Japan **60**, 559, 1269 (1939).

[10] Mizushima, Morino, and Takeda, Sci. Papers Inst. Phys. and Chem. Research (Tokyo) **38**, 437 (1941).

[11] Bazhulin, Plate, Sololova, and Kazanskii, Bull. Acad. Sci. URSS, sér. chim. (Russ) No. 1, 13 (1941).

[12] Herz, Kahovec, and Wagner, Monatshefte f. Chemie **76**, 100 (1946).

[13] N. Sheppard and G. J. Szasz, J. Chem. Phys. **17**, 86 (1949).

TABLE III. Raman spectral data for liquid 2-methylpentane (C_6H_{14}).

I PR	$\Delta\nu$ PR	ρ PR	N	$\Delta\nu$ PV	AD	I PR	$\Delta\nu$ PR	ρ PR	N	$\Delta\nu$ PV	AD
vw	182		1	182		3	1072		2	1071	1.0
14	328		3	323	3.0	1	1108		1	1108	
8	361		2	371	10.0	13	1149	0.91	3	1149	1.0
6	393		2	394	1.0	14	1175	0.73	2	1173	2.0
30	447	0.37	2	446	0.5	1	1240		2	1240	0.0
4	499		1	499		8	1301	0.90	2	1299	1.5
5	732		2	733	1.0	9	1340	0.93	2	1339	1.0
2	785		2	783	1.5	60	1443	0.91	2	1444	0.5
40	814	0.32	2	814	0.0	60	1463		2	1462	0.5
1	857		2	857	0.0	8	2722	0.93	1	2722	
9	890		3	890	0.0	30	2848		2	2847	0.5
4	936		1	936		1000	2875	0.42	2	2873	2.0
10	961	0.91	1	961		450	2910		2	2913	2.5
1	1016		1	1016		450	2934		2	2934	0.0
12	1039	0.92	2	1038	1.0	500	2963	0.69	2	2962	0.5

TABLE IV. Raman spectral data for liquid 3-methylpentane (C_6H_{14}).

I PR	$\Delta\nu$ PR	ρ PR	N	$\Delta\nu$ PV	AD	I PR	$\Delta\nu$ PR	ρ PR	N	$\Delta\nu$ PV	AD
21	393		2	390	3.0	36	1155		3	1157	1.0
43	443		2	444	1.0	23	1176		2	1175	1.0
			1	470		15	1281		2	1279	1.5
22	615		1	615		8	1316		2	1319	3.0
			1	736		18	1350	0.92	2	1352	2.0
50	745	0.58	3	747	1.0	2	1380		2	1379	0.5
			1	754		190	1446	0.93	2	1447	0.5
6	765		2	766	1.0	190	1460		2	1460	0.0
35	816	0.80	2	817	0.5	11	2735		1	2735	
22	876		3	877	1.7	650	2856		2	2856	0.0
24	954		3	957	6.3	900	2874	0.17	2	2876	2.0
25	977		2	983	5.0	700	2898		2	2899	0.5
34	1019	0.38	3	1017	2.0		2913		2	2913	0.0
			1	1038		1000	2934	0.21	2	2936	1.5
54	1042		1	1050		550	2961	0.56	2	2963	1.5

samples used. The 311 cm^{-1} line was resolved into the doublet 305, 317 in one investigation.[11] Measurement of depolarization factors in the 2900 cm^{-1} region was difficult because the lines were broad and overlapped each other.

n-HEPTANE, $CH_3-CH_2-CH_2-CH_2-CH_2-CH_2-CH_3$

Likewise, Raman displacements and estimated relative intensities for n-heptane have been obtained in 13 investigations,[6–18] but polarization data (again largely qualitative) were obtained in only one of these.[12]

The present results, the previous polarization data, and the probable values of the Raman displacements are given in Table II. Of the 16 lines observed in only a single investigation, 11 were reported by Okazaki[9] and 3 by Narayanaswamy.[18] Until verified with other carefully purified samples, these lines must be accepted with caution. The 1023 cm^{-1} line was resolved into the doublet 1021, 1031 by Okazaki.[9]

2-METHYLPENTANE, $CH_3-\underset{\displaystyle CH_3}{\underset{|}{CH}}-CH_2-CH_2-CH_3$

Raman displacements and estimated relative intensities for 2-methylpentane have been obtained in only two investigations,[5,8] and no polarization data have been reported.[19]

The present results and the probable values of the Raman displacements are given in Table III. The doublet 936, 961 was reported as a single line in the previous work.[5,8] Because of overlapping lines, depolarization factors for some of the lines in the 2900 cm^{-1} region could not be obtained.

3-METHYLPENTANE, $CH_3-CH_2-\underset{\displaystyle CH_3}{\underset{|}{CH}}-CH_2-CH_3$

Likewise, no polarization data have been reported for 3-methylpentane and Raman displacements and estimated relative intensities have been obtained in only two investigations.[5,8] The present results are given in Table IV.

TABLE V. Raman spectral data for liquid 2,4-dimethylpentane (C_7H_{16}).

I PR	$\Delta\nu$ PR	ρ PR	N	$\Delta\nu$ PV	AD	I PR	$\Delta\nu$ PR	ρ PR	N	$\Delta\nu$ PV	AD
			1	137		7	985		3	985	0.0
			1	149					1	996	
			1	169		5	1035		3	1035	1.3
12	183		2	181	2.0	3	1075		2	1076	1.0
40	308	0.59	3	308	0.3				1	1109	
4	329		2	333	3.5	60	1157	0.71	2	1157	0.0
			1	353		50	1169		2	1171	2.0
8	396		2	388	8.0	10	1232		2	1248	2.0
			1	419			1253				
14	446		1	446					1	1300	
50	470	0.06	3	469	0.3	33	1321	0.49	3	1320	1.0
			1	497		50	1348	0.66	3	1345	3.0
			1	687		100	1449	0.69	2	1449	0.0
			1	714		100	1461		2	1464	3.0
			1	728		23	2711		2	2714	3.0
200	808	0.00	3	807	0.3	70	2843		3	2842	1.0
10	866		3	869	1.7	1000	2872	0.07	3	2872	0.7
36	923	0.14	3	920	2.3	400	2883		1	2883	
			1	925		350	2914		3	2917	2.7
50	959	0.77	2	957	2.0	400	2934		3	2936	1.0
						800	2961	0.62	3	2964	2.7

TABLE VI. Raman spectral data for liquid 2,3-dimethylbutane (C_6H_{14}).

I PR	$\Delta\nu$ PR	ρ PR	N	$\Delta\nu$ PV	AD	I PR	$\Delta\nu$ PR	ρ PR	N	$\Delta\nu$ PV	AD
			1	96		22	1161	0.79	3	1160	1.0
			1	220		13	1196	0.69	3	1197	1.0
7	271		1	271					1	1263	
9	289		3	291	1.0	15	1301	0.91	3	1300	0.7
11	346		3	346	0.0				1	1321	
11	388		1	378		11	1345		3	1345	0.7
			1	397		1	1381		2	1384	3.5
11	439		2	436	3.5	64	1447	0.80	2	1447	0.0
21	475		3	477	1.3	66	1468	0.80	2	1468	0.0
23	506		3	505	0.7				1	1478	
			1	629					1	2670	
100	728	0.01	3	728	0.0	4	2717		3	2718	1.0
30	753	0.08	3	755	1.0				1	2735	
2	819		2	817	2.0	3	2763		3	2760	2.3
			1	847					1	2774	
11	868	0.82	3	869	0.3	320	2857	0.06	3	2857	1.7
53	936	0.49	3	932	2.3	1000	2874	0.48	3	2873	1.3
50	946		4	943	2.2	760	2884		1	2884	
vw	955		3	955	0.3	560	2903		3	2903	0.0
11	1033	0.82	3	1033	0.3	830	2938		3	2936	1.0
2	1106		1	1106		850	2963		3	2963	1.3
5	1150		2	1150	0.0	400	2977		3	2980	1.7

[14] A. S. Ganesan and S. Venkateswaran, Ind. J. Phys. **4**, 195 (1929).
[15] G. B. Bonino and L. Brüll, Gazz. chim. Ital. **59**, 660 (1929).
[16] G. Collins, Phys. Rev. **40**, 829 (1932).
[17] S. C. Sirkar, Ind. J. Phys. **7**, 61, 257 (1932).
[18] P. K. Narayanaswamy, Proc. Ind. Acad. Sci. **26A**, 121 (1947).

[19] *Note added in proof:* In their literature search, the authors overlooked a paper by Fenske, Braun, Wiegand, Quiggle, McCormick, and Rank, Anal. Chem. **19**, 700 (1947), in which are given Raman displacements and approximate depolarization factors for some of the principal lines of each of the six compounds.

2,4-DIMETHYLPENTANE, $CH_3-\underset{\displaystyle CH_3}{\underset{|}{CH}}-CH_2-\underset{\displaystyle CH_3}{\underset{|}{CH}}-CH_3$

No polarization data have been reported for 2,4-dimethylpentane, but Raman displacements and estimated relative intensities have been reported twice.[7,8] The present results are given in Table V.

2,3-DIMETHYLBUTANE, $CH_3-\underset{\displaystyle CH_3}{\underset{|}{CH}}-\underset{\displaystyle CH_3}{\underset{|}{CH}}-CH_3$

Raman displacements and estimated relative intensities have been reported three times[5,8,9] but no polarization data have been obtained. The present results are given in Table VI. The 1033 cm^{-1} line was resolved into the doublet 1029, 1039 by Okazaki.[9]

ACKNOWLEDGMENTS

The Hilger E-518 spectrograph used in this investigation was obtained in part with a grant from the Permanent Science Fund of the American Academy of Arts and Sciences. Most of the measurements for *n*-hexane and *n*-heptane were made by Mr. Donald E. Lee in 1944 and by Sisters Miriam Michael Stimson and Mary Agnita Reuter of Siena Heights College, Adrian, Michigan, during the summer of 1945. The authors are grateful for this assistance, and to Professor C. E. Boord and the American Petroleum Institute for furnishing the compounds.

THE JOURNAL OF CHEMICAL PHYSICS VOLUME 18, NUMBER 11 NOVEMBER, 1950

Asymmetry of Inner Electron Distributions in Homonuclear Diatomic Molecules

HOWARD REISS AND HOWARD SALTSBURG

Department of Chemistry, Boston University, Boston, Massachusetts

(Received July 17, 1950)

Disturbances in the distributions of inner shell electrons due to bond formation in homonuclear diatomic molecules have been investigated using a Fermi-Thomas type statistics. In the majority of molecules examined the disturbance seems to penetrate only to the shell directly beneath the valence shell.

Plots of the *number of electrons disturbed versus* atomic number are periodic, the disturbance being less for the alkali molecules than for the halogens. In any one group, these plots are remarkably linear. This behavior has permitted us to calculate the bond distance in Rb_2. It is found to be 4.28A. This value is to be compared with the distance 4.32A between nearest neighbors in the metal.

I. INTRODUCTION

THE role of inner shell electrons in chemical binding has always been a source of concern. James[1] has demonstrated that serious error can be introduced by ignoring their presence in Li_2. Van Vleck and Sherman[2] have appropriately referred to the phenomenon as the "Inner Shell Nightmare."

The participation of inner shells in bond formation should be observable in the distribution of electrons about the nucleus of a bound atom. Near the nucleus the distribution should be spherically symmetric; identical with that of an isolated atom. At points further removed from the nucleus (especially on the bond axis) elements of asymmetry should begin to appear. At one point this asymmetry will become so pronounced that by no stretch of the imagination will it be possible to regard the distribution as spherically symmetric. The fraction of electrons corresponding to the distribution beyond this point may be *defined* as *disturbed by the presence of the bond*, and may be used, as a measure of the depth of the disturbance caused by the binding process.

In this paper, an attempt will be made to establish a criterion by means of which the asymmetric point, mentioned above, can be located. This criterion will be used to estimate the number of electrons disturbed by the bonds in the homonuclear diatomic molecules of the halogen and alkali groups.

II. DESCRIPTION OF THE CRITERION

Electronic distributions will be determined through use of the Fermi-Thomas statistical method.[3-5] The problem of the isolated atom has been thoroughly

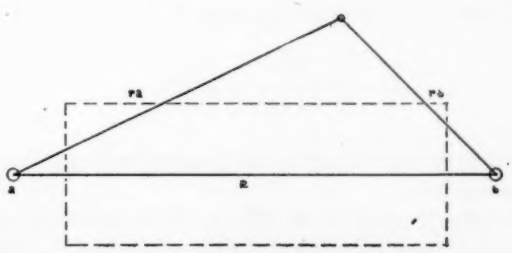

FIG. 1. Coordinate system.

[1] James, J. Chem. Phys. **2**, 794 (1934); Phys. Rev. **43**, 589 (1933).

[2] Van Vleck and Sherman, Rev. Mod. Phys. **7**, 168 (1935).

[3] Thomas, Proc. Camb. Phil. Soc. **23**, 542 (1927).

[4] Fermi, Zeits. f. Physik. **48**, 73 (1928).

[5] Fermi, Zeits. f. Physik. **49**, 550 (1928).

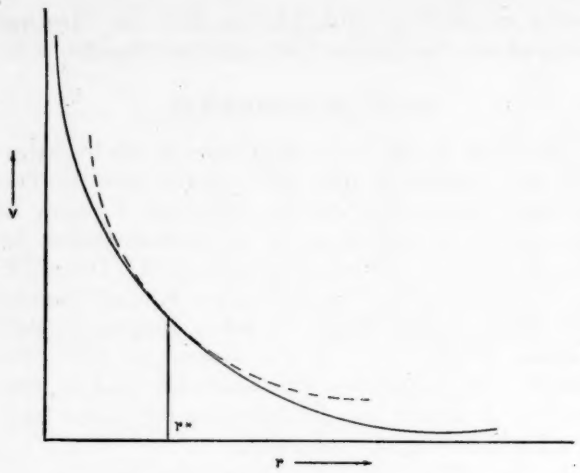

FIG. 2. Particular solutions.

solved,[3–5] and in what follows we shall avail ourselves of these results.

At the outset, a word of qualification is in order. It is recognized that the substitution of statistical methods for the normal procedures of quantum mechanics is more valid in the treatment of heavier rather than lighter atoms. Nevertheless, if an *absolutely* quantitative result is not required, useful information can still be obtained concerning systems with relatively few electrons. An example of this is found in Fermi's computation of the numbers of electrons which can be accommodated in the various momentum shells of an atom.

In a completely degenerate[6] electron gas the number density, n, of electrons[4] at a point of configuration space where the potential is V is given by

$$n=\frac{2^{9/2}\pi(me)^{3/2}}{3h^3}V^{3/2}, \tag{1}$$

where m=mass of the electron; $-e$=charge on the electron; h=Planck's constant. In view of (1), Poisson's equation[7] for the potential, V, can be written in the form

$$\nabla^2V=\frac{2^{13/2}\pi^2m^{3/2}e^{3/2}}{3h^3}V^{3/2}=\alpha V^{3/2}. \tag{2}$$

Applied to the spherically symmetric case of the isolated atom, (2) assumes the form

$$\frac{d^2V}{dr^2}+\frac{2}{r}\frac{dV}{dr}=\alpha V^{3/2}, \tag{3}$$

where r is the magnitude of the radius vector originating at the nucleus.

For the treatment of homonuclear diatomic molecules it is more convenient to use a coordinate system in which the coordinate surfaces are ellipsoids and hyperboloids of revolution, having foci at the two nuclei, separated by distance, R.

The ellipses (s=constant) are specified (Fig. 1) by

$$s=(r_a+r_b)/R \tag{4}$$

and the hyperbolas (t=constant) by

$$t=(r_a-r_b)/R. \tag{5}$$

ϑ is the angle of revolution. r_a and r_b are the distances from nuclei a and b, respectively. Taking account of axial symmetry Eq. (2), in this coordinate system, assumes the form.

$$\frac{4}{R^2(s^2-t^2)}\left[(s^2-1)\frac{\partial^2V}{\partial s^2}+2s\frac{\partial V}{\partial s}+(1-t^2)\frac{\partial^2V}{\partial t^2}-2t\frac{\partial V}{\partial t}\right]=\alpha V^{3/2}. \tag{6}$$

The ranges of the variables s and t are

$$1\leqq s\leqq\infty$$
$$-1\leqq t\leqq 1. \tag{7}$$

Consider the region within the broken line rectangle of Fig. 1. In this region

$$s\approx 1$$
$$|t|<1. \tag{8}$$

In view of the axial symmetry

$$\partial V/\partial s=0, \quad \text{when} \quad s=1, \tag{9}$$

or else the potential gradient across the line of centers will be discontinuous. Because of (8) and (9), the first two terms in (6) may be considered to be zero within the rectangular region. Since the potential passes to limit

$$V\rightarrow Ze/r_a \quad \text{or} \quad Ze/r_b \tag{10}$$

at either nucleus, where Z is the charge on the nucleus,

$$\partial^2V/\partial s^2\rightarrow\infty \tag{11}$$

at the nuclei. This renders it invalid to ignore the first term in (6). The restriction, $|t|<1$, represented by the vertical sides of the rectangle, is based upon this fact. Inside the rectangle (6) reduces to the ordinary differential equation

$$\frac{4}{R^2}\left[\frac{d^2V}{dt^2}-\frac{2t}{1-t^2}\frac{dV}{dt}\right]=\alpha V^{3/2}. \tag{12}$$

How long the rectangle may be, consistent with the reasonably valid application of (12) is a matter for conjecture. If it is very thin so that s lies very close to unity its sides may approach a and b rather closely. In what follows we shall assume that the rectangle approaches the limit of infinite thinness, and confine our

[6] Mayer and Mayer, *Statistical Mechanics* (John Wiley and Sons, Inc., New York, 1940), Chapter 16.

[7] Slater and Frank, *Introduction to Theoretical Physics* (McGraw-Hill Book Company, Inc., New York, 1933), p. 212.

TABLE I. Data and results.

Element	Atomic no.	R(A)	$\mu\times10^{9}$	L	x^*	N
Na_2	11	3.08[a]	2.142	14.38	2.18	5.73
Cl_2	17	1.98[a]	1.846	9.30	1.40	10.95
K_2	19	3.91[a]	1.779	21.98	2.84	8.49
Br_2	35	2.28[a]	1.451	15.71	2.35	17.54
I_2	53	2.66[a]	1.264	21.04	2.78	24.12
Cs_2	55	4.55[b]	1.248	36.46	3.36	22.22

[a] Sponer, *Molekulspektren I* (Julius Springer, Berlin, 1935).
[b] Finkelnberg and Hahn, Physik Zeits. **39**, 98 (1939).

attention to the immediate neighborhood of the line of centers.

In this neighborhood

$$r_b=R-r_a \tag{13}$$

so that according to (5)

$$r_a=R(1+t)/2. \tag{14}$$

There is a plane of symmetry normal to and bisecting the molecular axis. Consequently it is only necessary to investigate the region to one side of this plane. If the left side is chosen r_a can be identified with r, and the insertion of the transformation (14) into (12) yields the equation

$$\frac{d^2V}{dr^2}+\left(\frac{1}{r}-\frac{1}{R-r}\right)\frac{dV}{dr}=\alpha V^{3/2}. \tag{15}$$

Near the nucleus, the spherically symmetric Eq. (3) is valid. Further from the nucleus (15) is valid. In an intermediate region the accuracy of (3), as an approximation, decreases with increasing r, while the accuracy of (15) increases. This is a mathematical statement of the onset of the asymmetry discussed in Section I.

The asymmetric point mentioned in Section I will be defined as that value of r, r^*, at which (15) becomes a better approximation than (3). This choice is reasonable because r^* is the point at which another physically significant approximation, Eq. (15), is to be preferred over (3). Since, both (3) and (15) become better and worse approximations monotonously, in the same direction, it follows that they are equal in accuracy at r^*, and that, at this point, the solutions of (3) and (15) match most closely in shape.

III. THE DETERMINATION OF r^*

Denote particular solutions of (3) and (15) by V_1 and V_2, respectively. The particular solutions which correspond to the distribution of electrons are determined by the application of initial conditions at $r=0$, and $r=R/2$, to (3) and (15) respectively, since at these points the two equations are respectively most valid. The resulting curves might resemble the plots in Fig. 2. In Fig. 2 the curves have been drawn tangent, at r^*, the point of best match. Even though it is probable that the regions in which V_1 and V_2 are good approximations are not mutually exclusive but, rather, overlap, it does not follow that the curves must be tangent at r^*. The plot in Fig. 2 must be regarded as an ideal limit in our considerations. Although the curves may be close at r^*, they may not actually touch. Nevertheless, the argument which follows will be limitingly valid even when the two curves are not tangent to each other, but only close, for the particular solution of a differential equation varies continuously with the choice of initial conditions, provided that these conditions are not specified at a singular point.[8]

At the point of best match not only will the values of V_1 and V_2 as well as those of their slopes be equal or similar, but also their curvatures will be most similar. The *fractional* difference, Ω, in their curvatures, should therefore pass through a minimum at r^*. This difference is given by[9]

$$\Omega=1-\frac{d^2V_2/dr^2}{[1+(dV_2/dr)^2]^{3/2}}\frac{[1+(dV_1/dr)^2]^{3/2}}{d^2V_1/dr^2}. \tag{16}$$

Now, the particular solution, V_2, cannot actually be plotted because the correct initial conditions applicable at $r=R/2$ are unknown. For this reason, instead of (16), the function obtained from it by making the substitution

$$V_2=V_1, \quad dV_2/dr=dV_1/dr \tag{17}$$

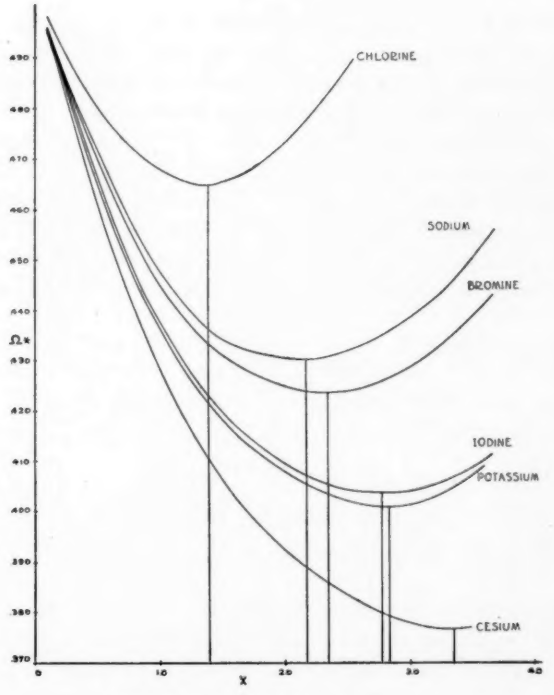

FIG. 3. Determination of minima.

[8] Ford, *Differential Equations* (McGraw-Hill Book Company Inc., New York, 1933), p. 91.
[9] Granville, Smith, and Longley, *Elements of Differential and Integral Calculus* (Ginn and Company, New York, 1929), p. 152.

will be considered. If this function is further simplified by using (3) and (15) to express the second derivatives in terms of V_1 and dV_1/dr, the result is

$$\Omega^*=\frac{[1/r+1/(R-r)]}{[2/r-(\alpha V_1^{3/2}/dV_1/dr)]}. \tag{18}$$

The conditions (17) are only valid or almost valid at r^*. Consequently it cannot be expected that Ω^* will resemble Ω except in some small interval surrounding r^* in which the curves tend to become parallel and equal. Ω^*, like Ω, will have a minimum in this interval, but since its behavior cannot be accounted for in regions outside of the interval, the minimum may not be unique, and other minima may exist in other regions. If this were so the utility of Ω^* would be severely reduced since the location of its minimum could not be used to determine r^* unambiguously. Fortunately, as it will be shown, plots of (18) yield only a single minimum, which appears at a very reasonable value of r, so that (18) can be used to determine r^*.

In closing it should be indicated that (3) and (15) are equations for the potential, V. The r^* determined through their use is therefore the asymmetric point for the potential. We are interested, however, in the distribution of electrons, n. If the transition to asymmetry were discontinuous at r^*, then since

$$V=\beta n^{\frac{1}{3}} \tag{19}$$

where β is a constant (see (1)), r^* would also be the asymmetric point for n. Since the transition is not discontinuous it is necessary to see if the use of r^* determined by (18) leads to an appreciable error.

Employing (19), both (3) and (15) can be written as differential equations for n. Next (16) and (17) are written with n replacing V. The differential equations for n together with the new versions of (16) and (17) can be used to develop a new Ω^* for n. Finally (19) can be used to partially reinsert V into this new Ω^*. The

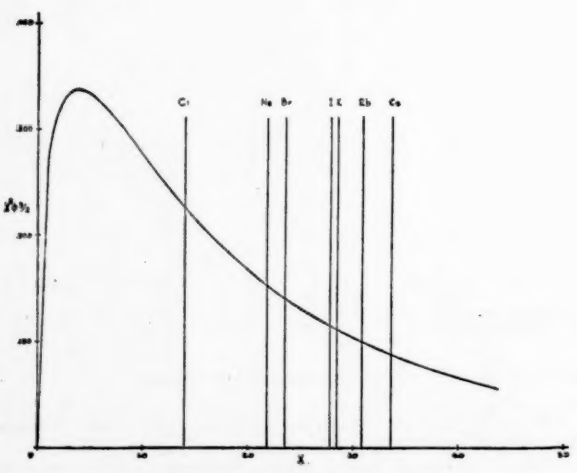

FIG. 4. Distribution for isolated atom.

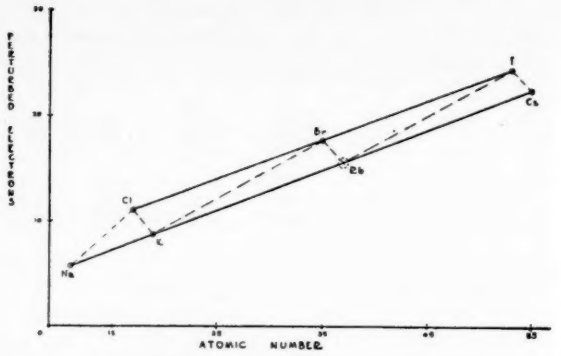

FIG. 5. Dependence of N on atomic number.

result is

$$\Omega^*=\frac{[1/r+1/(R-r)]}{[2/r-1/3n_1-(\alpha V_1^{3/2}/dV_1/dr)]}. \tag{20}$$

The only difference between (18) and (20) is the term $1/3n_1$. The magnitude of $2/r$ is about 10^8 while that of $1/3n_1$ is about 10^{-24}; utterly negligible. Consequently (20) and (18) are really identical so that the r^* determined by (18) is the asymmetric point for the electron distribution as well as for the potential.

IV. CALCULATIONS

The values of V_1 and dV_1/dr necessary for the evaluation of (18) are tabulated conveniently in Baker's[10] paper on distributions in positive ions. Actually Baker tabulates the functions $\psi(x)$ and $d\psi/dx$ where

$$\begin{aligned}\gamma\psi&=xV_1\\ \mu x&=r,\end{aligned} \tag{21}$$

where

$$\gamma=\frac{2^{13/3}\pi^{4/3}me^3z^{4/3}}{3^{2/3}\hbar^2} \tag{22}$$

$$\mu=\frac{3^{2/3}\hbar^2}{2^{13/3}\pi^{4/3}me^2z^{1/3}} \tag{23}$$

and

$$\alpha\gamma^{\frac{1}{3}}=1/\mu^2. \tag{24}$$

The choice of these functions permits the problem to be set up in dimensionless form so that one solution will suffice for the treatment of all atoms.

Introducing the relations

$$\begin{aligned}V_1&=\gamma\varphi\\ r&=\mu x\\ R&=\mu L\end{aligned} \tag{25}$$

into (18) yields the result

$$\Omega^*=\frac{[1/x+1/(L-x)]}{[2/x-(\varphi^{3/2}/d\varphi/dx)]}. \tag{26}$$

[10] Baker, Phys. Rev. **36**, 632 (1930).

This formulation is easiest to use in connection with Baker's tables. The relations,

$$\varphi=\psi/x$$
$$d\varphi/dx=1/x(d\psi/dx)-4/x^2 \tag{27}$$

are fulfilled.

Using (26), φ^* has been plotted for sodium, potassium, cesium, chlorine, bromine, and iodine. The curves appear in Fig. 3. The values of R (or L) necessary for the evaluation of Ω^* have been selected from various sources and are listed in Table I. It is gratifying to note that each curve in Fig. 3 does go through a unique minimum ($x=x^*$), and that the value of x^* is larger for heavier atoms in any one family.

According to Fermi-Thomas statistics the average fraction of electrons contained within a spherical surface of radius, x^*, is given by the integral

$$\int_0^{x^*} x^2\varphi^{3/2}dx. \tag{28}$$

The fraction of electrons corresponding to the distribution beyond x^* is then given by

$$1-\int_0^{x^*} x^2\varphi^{3/2}dx. \tag{29}$$

According to the discussion in Section I this fraction will be used as the average fraction of electrons disturbed by the presence of the bond. Of course, since the transition from symmetry to asymmetry is not discontinuous, some electrons below x^* will be partially disturbed. x^* is the point at which the disturbance becomes severe. Multiplication of (29) by Z the atomic number will give the average *number*, N, of electrons disturbed.‡

In Fig. 4, the density function $x^2\varphi^{\frac{3}{2}}$ is plotted. The areas under this curve out to the various values of x^* have been measured in order to evaluate (29), and consequently, N. The values of x^* and N are also listed in Table I.

It is interesting to note that in the cases of Na_2, K_2, Cl_2, Br_2, I_2, the disturbance (measured on this basis) penetrates only as far as the shell directly beneath the valence shell. For the halogens, the number of electrons disturbed in the subshell is given by $(N-7)$, while for the alkalis it is given by $(N-1)$. In the case of Cs, the disturbance penetrates somewhat beyond the first subshell.

When, N, is plotted against the atomic number, the periodic, dotted curve shown in Fig. 5 is obtained. It will be noticed that the disturbances are less for the alkali group than for the halogen group. This agrees with our concept of greater stability for an alkali kernel than for a halogen kernel.

Closer scrutiny of Fig. 5 brings to light a curious fact, which the authors are at a loss to explain. The plot of N *versus* atomic number seems to be an excellent straight line for any one group. These lines are drawn as the two, almost parallel, full curves in Fig. 5. If we denote the atomic number by Z, the analytical expressions for the curves, determined by a least square procedure, are

$$\text{Halogens} \qquad N=4.73+0.366Z, \tag{30}$$

$$\text{Alkalis} \qquad N=1.47+0.377Z. \tag{31}$$

No data are available for the internuclear distance in Rb_2. The distances between nearest neighbors in the solid metallic elements Na, K, Rb, Cs are, however, available. These are given in Table II.

TABLE II. Internuclear distances.*

	Distance measured in diatomic molecule	Distance between neighbors in metal
Na_2	3.08A	3.14A
K_2	3.91	4.06
Rb_2		4.32
Cs_2	4.55	4.70

* Sidgewick, *Chemical Elements and Their Compounds* (Oxford University Press, London, 1950), I, p. 66.

The distances measured in the diatomic molecules are all slightly less than those for the solids.

Now Eq. (31) can be used to calculate R for Rubidium. Inserting the atomic number, 37, for Z, one calculates N, and from this one calculates x^*. A glance at (26) reveals that to each value of x^*, there corresponds a value of L or, what is the same thing, of R. We have calculated R for Rb_2 in this manner. The result is

$$R=4.28\text{A}. \tag{33}$$

This result is to be compared with the value 4.32A in Table II. Notice that it is somewhat lower than this value.

In the absence of any explanation for the extreme linearity of the curves in Fig. 5, the expressions (30) and (31) must be regarded, simply, as useful interpolation formulas.

‡ Although we use the term "number of disturbed electrons," N, we do not really imply that we can calculate this quantity. It is felt that the point of disturbance, x^*, would not have immediate meaning to the chemist if it were specified in units of x. Instead, it is measured in terms of N which corresponds to the number of electrons in the shells beyond x^*. The value of N, therefore, permits one to immediately locate the shell to whose depth the disturbance extends, in force. For the lack of a better name we have called N the "number of disturbed electrons." Notice that N is *defined* as the number of disturbed electrons.

Kinetics of OH Radicals from Flame Emission Spectra. II. Rotational and Vibrational Distribution Functions and Temperature Determinations in the $^2\Sigma^+-{}^2\Pi$ Transition of OH

K. E. SHULER*
Applied Physics Laboratory,† The Johns Hopkins University, Silver Spring, Maryland

(Received July 17, 1950)

Rotational and vibrational distribution functions for a rotating oscillator are developed for a steady state with non-equipartition of energy such as might be found for electronically excited species in a flame. Methods are described for the separate spectrocsopic determination of rotational and vibrational equilibria and "temperatures" for the case of thermal equilibrium and for the case of a non-equipartition distribution of energy. These methods are applied to the study of electronically excited OH radicals in an equimolar oxy-natural gas (88 percent CH_4) flame. Rotation-vibration equilibrium with a rotation-vibration temperature of ~2550°K was found. Analysis of the data indicates that the vibrational transition probabilities for the $^2\Sigma^+-{}^2\Pi$ transition calculated in Part I of this paper are accurate to about the 10 percent claimed in that communication.

I. INTRODUCTION

In Part I of this series[1] the vibrational transition probabilities for the $^2\Sigma^+-{}^2\Pi$ transition of OH were calculated and applied to some spectroscopic data of Dieke and Crosswhite[2,3] on the outer cone of an oxy-acetylene flame. It was found for this case that while there was vibrational and rotational equilibrium, there was apparently a lack of equipartition between these two internal degrees of freedom, with a vibrational "temperature" of ~3750°K compared to a rotational "temperature" of ~3000°K. The question then arose whether this 25 percent difference in the "temperatures" was really due to a lack of equipartition or whether it was due to the various approximations in the calculation of both rotational and vibrational transition probabilities. To obtain additional information on this point, vibrational and rotational distribution functions have been formulated for a steady state non-equipartition distribution which will permit the separate determination of vibrational and rotational equilibria and temperatures. The measurements have been extended to the outer cone of an oxygen-natural gas flame (88 percent CH_4) where it appears, from the data of other workers,[4–6] that thermal equilibrium obtains. The data obtained for this expected equilibrium distribution in the flame can then be used to test the accuracy of the calculated vibrational transition probabilities of OH.

II. ROTATIONAL AND VIBRATIONAL DISTRIBUTION FUNCTIONS

Recent theoretical work on the application of quantum mechanics to chemical kinetics[7] and on the influence of activation energy and heat of reaction on the energy distribution of chemically reacting species[8] has shown that there may be a considerable perturbation of the original Maxwell-Boltzmann distribution of the reactants and products during a chemical reaction. It seems possible that the energy released by the type of exothermic reaction responsible for the formation of electronically excited radicals in flames will go preferentially into specific degrees of freedom of both products and reactants, and that by inelastic collisions the separate degrees of freedom may then be brought into an equilibrium type distribution without equipartition of energy among all the degrees of freedom. Something of this sort was noted by Golden and Peiser[7] who found for the reaction $H_2+Br\rightarrow HBr+H$ that the vibration-rotation distribution of products can be represented by a Boltzmann-like expression which is differentiated from a thermal equilibrium distribution by having different values of the distribution modulus β for the different degrees of freedom. Such a distribution may conceivably arise if the transfer of rotational and vibrational energy is governed by a resonance principle similar to that for "collisions of the second kind" for atoms[9] and molecules,[10] so that vibration-vibration and rotation-rotation energy exchange take place much more readily than vibration-rotation transfers.[11] In the case of a flow system such as that of a flame this type of non-equipartition distribution of excited species may

* This research was conducted while the author was an AEC Post-Doctoral Fellow of the National Research Council.
† The work described in this paper was supported in part by the Bureau of Ordnance, U. S. Navy under Contract NOrd-7386.

[1] K. E. Shuler, J. Chem. Phys. **18**, 1221 (1950).
[2] G. H. Dieke and H. M. Crosswhite, *The Ultraviolet Bands of OH, Fundamental Data*, Bumblebee Series, Report No. 87, November 1948, The Johns Hopkins University.
[3] G. H. Dieke and H. M. Crosswhite, Quarterly Report, NOrd-8036, JHB-3 Problem A. Oct. 1–Dec. 31, 1949, The Johns Hopkins University.
[4] H. H. Lurie and G. W. Sherman, Ind. Eng. Chem. **25**, 404 (1933).
[5] S. Silverman, J. Opt. Soc. Am. **39**, 275 (1949).
[6] G. H. Dieke and H. M. Crosswhite, Quarterly Report, NOrd 8036, JHB-3, Problem A. Jan. 1–March 31, 1950, The Johns Hopkins University.
[7] S. Golden and A. M. Peiser, J. Chem. Phys. **17**, 620, 630 (1949).
[8] I. Prigogine and E. Xhrouet, Physica **15**, 913 (1949). I. Prigogine and M. Mahieu, Physica **16**, 51 (1950). I. Prigogine, "Symposium on Anomalies in Reaction Kinetics," Minneapolis, 1950.
[9] G. Herzberg, *Atomic Spectra and Atomic Structure* (Dover Publications, New York, 1944), p. 231.
[10] K. J. Laidler, J. Chem. Phys. **15**, 712 (1947).
[11] This type of energy transfer has been discussed in detail by O. Oldenberg and A. A. Frost, Chem. Rev. **20**, 99 (1937).

under certain conditions be maintained as a steady-state distribution, and it is advisable to take account of this possibility in kinetic flame spectroscopy.

For a non-equipartition distribution resulting from such a resonance type transfer of vibrational and rotational energy one can formulate rotation-vibration distribution functions by considering the system of electronically excited rotating oscillators formed in a non-equilibrium distribution by a chemical reaction as an "inhibited idealized system."[12] The system is idealized in that it is a system of independent mass points so that the multiplicative law of independent probabilities will be applicable. The system is inhibited in that the rate of flow of energy between the rotational and vibrational quantum states is so slow that this type of energy transfer may be neglected in calculating the statistical properties of the system. The distribution function for such a system is

$$\frac{n_{K,v}}{N}=\frac{n_K}{N_K}\cdot\frac{n_v}{N_v}=\frac{g_K\exp(-\beta_1\epsilon_K)}{\sum_K g_K\exp(-\beta_1\epsilon_K)}\cdot\frac{g_v\exp(-\beta_2\epsilon_v)}{\sum_v g_v\exp(-\beta_2\epsilon_v)}, \quad (1)$$

where g_K and g_v are the statistical weights of the rotational and vibrational states, ϵ_K and ϵ_v are the rotational and vibrational energies of states K and v, and $n_{K,v}/N$ is the probability of finding the system of N rotators and vibrators in the state K,v. In analogy with the case of complete thermal equilibrium one can then define a rotational and a vibrational "temperature," T_r and T_v, by

$$\beta_1\equiv 1/kT_r, \quad \beta_2\equiv 1/kT_v, \quad (2)$$

where, for the non-equipartition distribution discussed here, $T_r\neq T_v$. If the rate of rotation-vibration energy interchange is rapid enough, the system will be found in an equilibrium, equipartition distribution and Eq. (1) reduces to

$$\frac{n_{K,v}}{N}=\frac{n_K}{N_K}\cdot\frac{n_v}{N_v}=g_Kg_v\frac{\exp[-\beta(\epsilon_K+\epsilon_v)]}{\sum_{K,v} g_Kg_v\exp[-\beta(\epsilon_K+\epsilon_v)]} \quad (3)$$

with $T_r=T_v$.[13] For the intermediate case when the rate of transfer of energy among the various degrees of freedom is of the same order of magnitude as the rate with which the experimental observations can be made, the properties of the system can no longer be described by the methods of statistical mechanics.

The application of these concepts to the spectroscopic study of flames is straightforward. Within the approximation of treating the rotational and vibrational transition probabilities A_K' and A_v' as separable and independent,[1] the intensity of a line $I_{K,v}$ is given by

$$I_{K,v}=C'A_K'A_v'n_{K,v}h\nu_{K,v} \quad (4)$$

where C' contains the electronic transition probability. Substitution of Eqs. (1) and (2) into (4) leads to

$$I_{K,v}=CA_KA_vh\nu_{K,v}\exp(-\epsilon_K/kT_r)\exp(-\epsilon_v/kT_v) \quad (5)$$

where the statistical weight factors have been taken into the transition probabilities and C contains the factors $N/\sum_\sigma g_\sigma\exp(-\beta_i\epsilon_\sigma)$. If an analysis of the spectrum shows that Eq. (5) is satisfied with $T_r\neq T_v$ one is dealing with the type of non-equipartition distribution discussed above. If Eq. (5) is satisfied with $T_v=T_r$ one has an equilibrium, equipartition distribution. If Eq. (5) is not satisfied for either the rotational or the vibrational states or both, one is faced with a type of non-equilibrium distribution where the concept of vibrational and rotational "temperatures" no longer has any meaning.

III. EXPERIMENTAL

A 50-50 oxygen-natural gas flame was burned off a hand torch at atmospheric pressure. The natural gas contained ~88 percent CH_4, the other constituents being higher saturated hydrocarbons and about one percent N_2. The spectra were taken in the second order of a 3 meter concave grating (15,000 lines/inch) in a Wadsworth mounting with a linear dispersion of 5.5A/mm using a 15 micron slit. The exposure times using Eastman 103-0 film were 5 minutes for the (0,0) band of OH used for the rotational equilibrium and temperature determination and 2 hours for the (0,0), (2,1), (1,0) and (1,1) bands of OH used for the vibrational equilibrium and temperature determination. Intensity measurements were made with a Leeds and Northrop recording photoelectric microdensitometer. In order to examine a region of the flame where there was the best possibility of finding thermal equilibrium, the spectra were taken in the outer cone of the flame about 3 inches above the tip of the inner cone reaction zone. Several exposures were taken of this flame and the results for the rotational and vibrational temperatures agreed to within 100°K in each case.

IV. ROTATIONAL EQUILIBRIUM AND TEMPERATURE

For an analysis of the rotational energy and intensity distribution within one vibrational transition, a knowledge of the energy distribution among the various vibrational bands is not necessary, and it is immaterial whether vibrational equilibrium exists. For the case of rotational equilibrium, the intensity of a transition $n\rightarrow m$ is given by

$$I_{nm}=CA_{nm}h\nu_{nm}\exp(-E_n/kT_r) \quad (6)$$

where C is a constant for the particular electronic and vibrational transition under consideration. In the case of rotational equilibrium, a plot of $\ln I_{n_m}-\ln(A_{n_m}\nu_{n_m})$

[12] J. E. Mayer and M. G. Mayer, *Statistical Mechanics* (John Wiley and Sons, Inc., New York, 1940) pp. 83–85.

[13] Only when the rotations and vibrations are in energetic equilibrium with all the other degrees of freedom and chemical equilibrium obtains for all the species engaged in the reaction can β be connected with the equilibrium temperature T by $\beta=1/kT$.

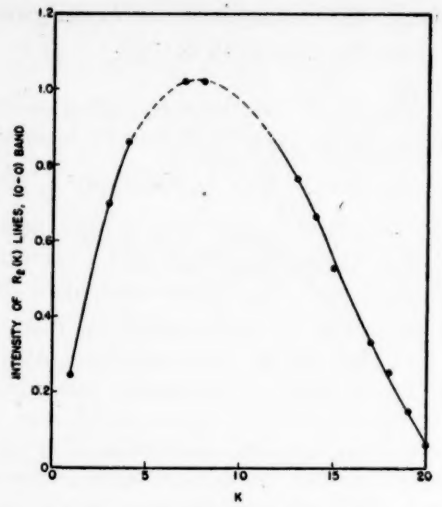

FIG. 1. Intensity distribution in the R_2 branch of the (0,0) band of OH($^2\Sigma^+ - {}^2\Pi$) in the outer cone of a 50-50 oxy-natural gas (88 percent CH_4) flame.

vs. E_n will then give a straight line with a slope of $-1/kT_r$ from which the rotational temperature T_r can be determined. This method, which has been applied extensively to flame spectra by Gaydon and Wolfhard,[14] has the disadvantage that both plate standardization, i.e., wave-length response of the plate, and plate calibration, i.e., intensity response of the plate are necessary for accurate measurements of line intensities.

This plate calibration and standardization, which unless done with great care will seriously affect the accuracy of the intensity measurements, can be avoided by using an iso-intensity, iso-frequency method developed by Dieke and Crosswhite[2] in their studies on flame temperatures.[15] The intensity distribution [16] for the R_2 branch of the (0,0) band of OH in the outer cone of an oxygen-natural gas flame is shown in Fig. 1. If one takes the intensity to be a smooth and continuous function of the rotational quantum number K it is possible to chose points of equal density, and thus equal intensity, on the ascending and descending branches of the curve corresponding to the values K' and K, where $K'<K$ and where the K and K' are not necessarily integers. This iso-intensity aspect of the method makes plate calibration unnecessary. By choosing a head forming branch such as the R_2 branch in the (0,0) band of OH it is possible to select lines K and K' of *equal* intensity with such a small wave-length difference ($\Delta\lambda \leq 5$A) that it is unnecessary to standardize the plate for change of sensitivity with wave-length. As pointed out by Dieke and Crosswhite,[2] the R_2 lines from $K=1$ to $K=20$ in the (0,0) band of OH are most suitable for these measurements. These lines are not accompanied by satellites, and since for ordinary flame temperatures (2000°K–3000°K) the maximum intensity is near the head of the band ($K=9$ to $K=11$) it is possible to chose a number of lines of equal intensity with a small $\Delta\lambda$. Furthermore, the effect of self-reversal can be minimized by avoiding strong lines, and for lines of equal intensity the effect will cancel out in first order approximation since the self-absorption parameter is proportional to I_0, the intensity of the line with no absorption.[17]

From Eq. (6) it follows that for lines of equal intensity

$$I_K = CA_K h\nu_K \exp(-E_K/kT_r) = I_{K'} = CA_{K'} h\nu_{K'} \exp(-E_{K'}/kT_r) \quad (7)$$

so that

$$A_{K'}/A_K = \exp[(E_{K'} - E_K)/kT_r] \quad (8)$$

with $\nu_{K'}/\nu_K \sim 1$ since $\Delta\lambda$ is very small. The rotational transition probabilities $A_K, A_{K'}$ with the statistical weight factor included have been derived for the $^2\Sigma^+ - {}^2\Pi$ transition of OH by Hill and Van Vleck[18] and Earls[19] and have been calculated and tabulated for OH by Dieke and Crosswhite,[2] who have also measured and tabulated the energy levels needed in the evaluation of Eq. (8). A plot of $\log A_{K'} - \log A_K$ *vs.* $E_{K'} - E_K$ for the R_2 branch of the (0,0) band of OH in the outer cone of an oxygen-natural gas flame is shown in Fig. 2. The majority of the pairs of K, K' values used in the construction of Fig. 2 are on the solid part of the intensity curve of Fig. 1, i.e., between $K(1)$ to $K(4)$ and $K(11)$ to $K(20)$ where the curve is better defined due to the greater number of experimental points corresponding to lines which could be clearly resolved by our spectrograph. Two of the points of Fig. 2 were obtained from the dotted part of the intensity curve. From plots of E_K *vs.* K and A_K *vs.* K, where E_K and A_K are considered to be smooth and continuous functions of K, values of E_K and A_K corresponding to these iso-intensity values of K and K' are obtained. Substitution of these energies and transition probabilities into Eq. (8) gives the points shown in Fig. 2. The rather good straight line which can be drawn through these points indicates that the electronically excited OH radicals do have an equilibrium rotational distribution and the slope, as determined by a least square calculation, gives a rotational "temperature" T_r of ~ 2600°K.

V. VIBRATIONAL EQUILIBRIUM AND TEMPERATURE

In the determination of vibrational equilibrium and "temperature" it is not possible to avoid plate calibration or standardization entirely. However, once the presence of rotational equilibrium has been established

[14] H. G. Wolfhard, Zeits. f. Physik **112**, 107 (1939). A. G. Gaydon and H. G. Wolfhard, Proc. Roy. Soc. **194A**, 169 (1948); **199A**, 89 (1949); **201A**, 561 (1950).

[15] This method is related to the intensity coincidence method of H. P. Knauss and M. S. McCay, Phys. Rev. **52**, 1143 (1937).

[16] This is really a plot of photographic density $D \propto \log I_k$ *vs.* K. This type of plot, however, is all that is necessary in the application of the iso-intensity method.

[17] R. D. Cowan and G. H. Dieke, Rev. Mod. Phys. **20**, 418 (1948).

[18] E. L. Hill and J. H. Van Vleck, Phys. Rev. **32**, 250 (1928).

[19] L. T. Earls, Phys. Rev. **48**, 423 (1935).

and a rotational "temperature" calculated by the method described in Section IV, it is possible to use the band spectrum itself to calibrate and standardize the plate. The relative intensities I_K of all lines in a given vibrational transition can be calculated by Eq. (6) and the photographic densities D corresponding to these intensities can be read off the densitometer record. The plate is then calibrated by plotting D *vs.* $\log I_K$ for wave-length regions $\leq$20A. If necessary, the plate can be standardized by repeating this procedure at 20A intervals across the whole spectrum and plotting the results in the usual three-dimensional D *vs.* $\log I$ *vs.* λ plot. It is important in this method to avoid all strong lines so that self-reversal, which is particularly pronounced in the OH spectrum, will not adversely affect the results. If one finds that the particular spectrum being analyzed does not show rotational equilibrium, the above method of plate calibration can still be used by using a line spectrum with known rotational equilibrium as an auxiliary comparison spectrum.

Vibrational equilibrium and temperature determinations have usually been made using either integrated intensities of unresolved bands or peak intensities of band heads.[20] There are several disadvantages in using these unresolved band intensities and it is preferable to use well resolved individual lines for the determination of vibrational equilibrium and "temperatures." This is particularly true in the case of overlapping band systems where it is not possible to measure the integrated band intensity of the various bands. In the OH band system, the (0,0) and (1,1) bands overlap without interference from other OH bands between about 3110A and 3185A and the (1,0) and (2,1) bands overlap without interference from other OH bands between about 2855A and 2945A. In these two regions it is possible to pick out several pairs of lines from the two different bands which are free from blends and satellites, weak enough not to be affected seriously by self-reversal, and which lie so close together ($\Delta\lambda \leq 5$A) that their intensity ratios can be measured from the calibration curves without prior standardization for change of plate sensitivity with wave-length. All that is necessary therefore in the case of such overlapping band systems is to calibrate some narrow overlap region for change of plate response with intensity.

Taking account of the rotation-vibration interaction and rotational distortion of the OH radicals by adding the small correction terms E_{Kv} to the rigid rotator energy E_K, Eq. (5) can be written as

$$I_{K,v}=CA_KA_v h\nu_{K,v}\exp[-(E_K+E_{Kv})/kT_r]\exp(-E_v/kT_v). \quad (9)$$

The ratio of intensities of two rotational lines K_a and K_b (with $\Delta\lambda \leq 5$A) in the (1,1) and (0,0) bands is given by

$$\frac{I_{(1,1),K_a}}{I_{(0,0),K_b}}=\frac{|M_{(1,1)}|^2}{|M_{(0,0)}|^2}\frac{|M_{K_a}|^2}{|M_{K_b}|^2}\exp\{[(E_{K_b}+E_{K_bv})-(E_{K_a}+E_{K_av})]/kT_r\}\exp[(E_0-E_1)/kT_v] \quad (10)$$

where, because of the small $\Delta\lambda$, the transition probabilities can be replaced by the squares of the dipole matrix moments $|M|^2$ and the frequency ratios cancel. The first exponential term in Eq. (10) refers to the rotational energies and the second exponential term refers to the vibrational energies. An identical equation can be written for the intensity ratios in the (1,0) and (2,1) overlap region. The vibrational "temperature," T_v, can be calculated from Eq. (10), all other quantities in this equation being known. The intensity ratios are measured from the spectra, the rotational[18,19] and vibrational[1] transition probabilities for the $^2\Sigma^+-{}^2\Pi$ transition of OH have been calculated, the rotational and vibrational energy levels have been measured accurately by Dieke and Crosswhite[2] and the rotational "temperature," T_r, can be determined by the method of Section IV.

This procedure has been applied to the spectra of the outer cone of the oxygen-natural gas flame for which the rotational temperature had been determined previously (Section IV). Five pairs of appropriate lines in the (0,0), (1,1) and (1,0), (2,1) overlap regions were

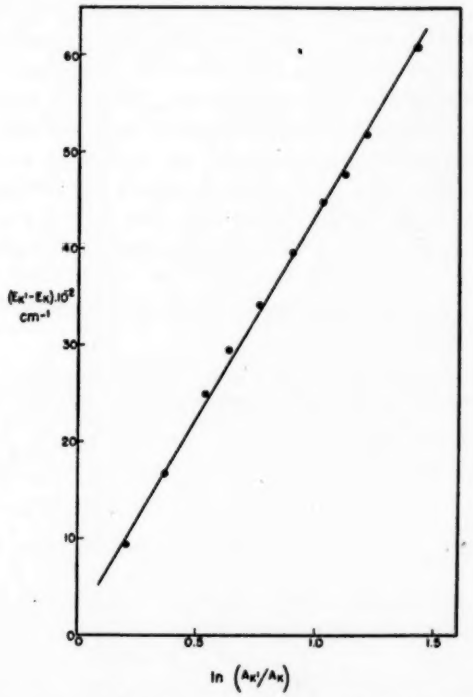

FIG. 2. A plot of $E_{K'}-E_K$ *vs.* $\ln(A_{K'}/A_K)$ for the R_2 branch of the (0,0) band of OH($^2\Sigma^+-{}^2\Pi$) in the outer cone of a 50-50 oxy-natural gas (88 percent CH_4) flame. The slope gives a rotational "temperature," T_r, of 2600°K.

[20] For references on these methods see G. H. Herzberg, *Molecular Spectra and Molecular Structure. I. Spectra of Diatomic Molecules*, 2nd Edition (D. Van Nostrand Company, Inc., New York, 1950), p. 466.

analyzed; the results are shown in Table I. The rather good agreement of T_v in the (1,1), (0,0) with T_v in the (2,1), (1,0) bands indicates vibrational equilibrium with a vibrational "temperature" T_v of $\sim$2540°K.

VI. DISCUSSION OF RESULTS

The agreement of the vibrational "temperatures" T_v for the levels $v'=0$ and 1 and $v'=1$ and 2 is within the experimental error;[21] it indicates that the vibrational distribution function (Eq. 9) is of the right form and that vibrational equilibrium exists in the flame.

TABLE I. Vibrational temperature of OH radicals in the outer cone of a 50-50 oxy-natural gas flame at atmospheric pressure.

Spectral lines (0,0)	(1,1)	Δλ(A)	$I_{(1,1)}/I_{(0,0)}$	T_v(°K)
$P_1(14)$[a]	$Q_1(10)$	1.7	0.372	2400
$P_1(13)$	$Q_1(9)$	2.2	0.343	2410
$Q_1(19)$	$Q_2(5)$	5.4	0.720	2490
$P_2(14)$	$P_1(6)$	1.1	0.296	2470
$P_1(17)$	$P_1(10)$	5.0	0.550	2620
			T_v(av.)	2480°K
(1,0)	(2,1)		$I_{(2,1)}/I_{(1,0)}$	
$Q_1(18)$	$Q_1(7)$	5.3	1.637	2700
$Q_1(19)$	$Q_1(8)$	0.8	1.856	2470
$P_1(16)$	$P_1(8)$	4.2	0.918	2590
$P_1(15)$	$P_1(5)$	4.1	0.718	2680
$P_1(16)$	$Q_2(12)$	6.7	1.010	2570
			T_v(av.)	2600°K

[a] The rotational quantum numbers refer to the final state.

It would, of course, be preferable if this constancy of T_v could be checked over more than just the first three energy levels, $v'=0$, 1, and 2. In the case of the transitions of OH there is the possibility of extending this treatment to the $v'=3$ level since the (3,3) band overlaps some of the lower transitions. This will, however, be quite difficult since the (3,3) band is rather weak and because the overlapping bands are so many, i.e., (0,0), (1,1), (2,2), and (3,3) that it might be difficult to separate a sufficient number of lines for an analysis. In any case, for most of the species appearing in flames, it will not be possible to extend the vibrational measurements to as many energy levels as are available for the rotational analysis.

[21] The five percent difference in the average vibrational "temperatures" T_v in Table I corresponds to about a 10 percent uncertainty in the values of the calculated vibrational transition probabilities of OH.

The good agreement between the vibrational "temperature" ($T_v\sim$2540°K) and the rotational "temperature" ($T_r\sim$2600°K) indicates equipartition of energy among these two degrees of freedom. The vibration-rotation "temperature" of $\sim$2550°K is in good agreement with the findings of other workers on the temperature of the oxy-methane or oxy-natural gas ($\sim$90 percent CH_4) flame. The temperature of the oxy-natural gas flame has been measured by Lurie and Sherman[4] by the Na line reversal method. Their measurements just above the tip of the inner cone gave $T\sim$2900°K for the 50-50 mixture used in our investigation. The results of Henning and Tingwaldt[22] show that flame temperatures decrease very rapidly away from the reaction zone, the decrease being about 25 percent in 7 cm. The rotational-vibrational "temperature" of $\sim$2550°K determined about 3 cm above the tip of the inner cone is in reasonably good agreement with these results. Silverman,[5] who determined the temperature of hydrocarbon flames using the infra-red radiation of the CO_2 band at 4.4 $m\mu$ as a brightness thermometer, found a temperature of between 2300°K to 2500°K for an oxy-methane flame. Since temperatures determined by the infra-red brightness technique are generally somewhat lower than the calculated equilibrium values,[5] the agreement between Silverman's values and the result of this investigation is satisfactory. Dieke and Crosswhite[6] found a rotational "temperature" of $\sim$2650°K for an oxy-methane flame in good agreement with our rotational "temperature" of $\sim$2600°K.

The good agreement and internal consistency obtained in all these investigations indicates that the vibrational transition probabilities of OH calculated in Part I[1] are substantially correct and will give reasonably accurate values for the vibrational temperature of OH.

VII. ACKNOWLEDGMENTS

The author wishes to express his thanks to Dr. F. T. McClure and Dr. R. C. Herman of this laboratory and to Dr. H. M. Hulburt of Catholic University for several stimulating discussions in the course of this investigation.

[22] F. Henning and C. Tingwaldt, Zeits. f. Physik 48, 805 (1928).

Infra-Red and Raman Spectra of Fluorinated Ethanes II: 1,1,1-Trifluoroethane*

J. Rud Nielsen and Howard H. Claassen
Department of Physics, University of Oklahoma, Norman, Oklahoma

and

D. C. Smith
Naval Research Laboratory, Washington, D. C.

(Received July 21, 1950)

The infra-red absorption spectrum of gaseous 1,1,1-trifluoroethane between 2 and 23μ has been investigated with a prism spectrometer of high resolution. The Raman spectrum of CF_3-CH_3 in the gaseous state has been photographed with a three-prism glass spectrograph of linear dispersion 15A/mm at 4358A. The 12 fundamental frequencies have been assigned, and the spectra have been interpreted in detail. Thermodynamic functions have been calculated. A value of 3290 cal./mole has been obtained for the potential barrier opposing internal rotation.

INTRODUCTION

THE Raman spectrum of CF_3-CH_3 in the liquid state at $-75°C$ has been studied by Hatcher and Yost.[1] Some corrections to their data were given by Russell, Golding and Yost.[2] The infra-red spectrum of CF_3-CH_3 has been studied by Thompson and Temple.[3] Attempts at the assignment of fundamentals have been made by Kohlrausch,[4] Russell, Golding and Yost,[2] Thompson and Temple,[3] and Herzberg.* There is wide divergence among the assignments proposed by these workers, and none has attempted to determine the twisting frequency. Recently, Daily, Minden and Shulman,[5] have derived a value for the twisting frequency from the relative intensities at different temperatures of certain microwave absorption lines.

EXPERIMENTAL

The sample of 1,1,1-trifluoroethane was prepared and purified in the Jackson Laboratory of E. I. du Pont de Nemours and Company. No information was available about its purity. However, some of the very weak infra-red bands observed appear to be caused by impurities.

The infra-red absorption spectrum of gaseous CF_3-CH_3 was measured over the range from 2 to 23μ by means of a prism spectrometer of high resolution.[6] The Raman spectrum of the compound in the gaseous state was photographed by means of a three-prism glass spectrograph of linear dispersion 15A/mm at 4358A. This instrument and the irradiation apparatus used have been briefly described elsewhere.[7]

RESULTS

The infra-red absorption of CF_3-CH_3 gas between 2 and 23μ is shown in Fig. 1. The wave numbers of the observed absorption maxima are given in the first column of Table I. In the second column relative intensities are indicated and for some bands unusual sharpness. The observed Raman shifts for gaseous CF_3-CH_3 are listed in the first column of Table II. In the second column are given rough estimates of the relative intensities of the bands, as well as indication about unusual sharpness or diffuseness. The following abbreviations are used in both tables: *vs* very strong, *s* strong, *m* medium, *w* weak, etc., *sh* sharp, *d* diffuse.

A comparison of the infra-red data with those of Thompson and Temple[3] is made difficult by the great difference in resolution. It shows, however, that the bands observed by them at 684 and 900 cm^{-1} must have been caused by impurities. All of the Raman bands observed by Hatcher and Yost in liquid CF_3-CH_3 were here in the gas, most of the bands being shifted a few cm^{-1} toward greater wave numbers. One new Raman band at 1232 cm^{-1} was observed and also rotational branches of two bands.

ASSIGNMENT OF FUNDAMENTALS

Electron diffraction work of Brockway and Livingston[8] has given the C−C distance $=1.45\pm0.05$A, C−F distance 1.33 ± 0.03A, FCF angle $=108\frac{1}{2}\pm2°$. Assuming a C−H distance of 1.09A and tetrahedral angles for the methyl group, the following moments of inertia were calculated

$$I_A=I_B=155\times10^{-40}, \quad I_C=152\times10^{-40} \text{ g cm}^2.$$

Thus, the molecule is very nearly spherical and the parallel and perpendicular bands may be expected to have similar contours.

The CF_3-CH_3 molecule undoubtedly has the symmetry C_{3v}, the fluorine atoms being either "eclipsed"

* This work has been supported by the ONR under Contract N7onr-398, Task Order I.

[1] J. B. Hatcher and D. M. Yost, J. Chem. Phys. **5**, 992 (1937).
[2] Russell, Golding, and Yost, J. Am. Chem. Soc. **66**, 16 (1944).
[3] H. W. Thompson and R. B. Temple, J. Chem. Soc. **90**, 1428 (1948).
[4] K. W. F. Kohlrausch, *Ramanspektren* (Akademische Verlagsgesellschaft Becker & Erler, Leipzig, 1943), p. 173.
* Private communication to J. Rud Nielsen.
[5] Dailey, Minden, and Shulman, Phys. Rev. **75**, 1319 (1949).
[6] Nielsen, Crawford, and Smith, J. Opt. Soc. Am. **37**, 296 (1947).
[7] Smith, Nielsen, and Claassen, J. Chem. Phys. **18**, 326 (1950).
[8] L. O. Brockway and R. L. Livingston, Abstracts, Am. Chem. Soc. Meeting, Buffalo, New York, 1942.

or "staggered" with respect to the hydrogen atoms. In either case, the normal vibrations divide into symmetry species in the following manner: $5A_1+1A_2+6E$. The fundamentals of species A_1 and E are active both in infra-red absorption and in the Raman effect. The torsional oscillation of species A_2, on the other hand, is inactive both in the infra-red and in the Raman effect.

Since the mass of a methyl group is not much smaller than that of a fluorine atom, the problem of assigning the fundamental vibration frequencies for CF_3-CH_3 may be conveniently attacked by taking the vibration spectrum of CF_4 as a starting point. This spectrum consists[9] of a doubly degenerate fundamental at 437 cm^{-1}, a triply degenerate at 635, a totally symmetrical at 904, and a triply degenerate fundamental near 1265 cm^{-1}. Consideration of the correlations between CF_4 and molecules of type XCF_3 leads to the conclusion that the "skeletal vibrations" of CF_3-CH_3 consist of a doubly degenerate fundamental near 400 cm^{-1}, a fundamental of species E and another of species A_1 in the neighborhood of 900 cm^{-1}, and E and A_1 fundamentals near 1250 cm^{-1}.

The Raman band at 365 cm^{-1}, which has the diffuse appearance typical of doubly degenerate bands, must be the lowest E fundamental. It may be roughly characterized as a rocking of the methyl group. Of the next two skeletal frequencies the totally symmetrical is lower for both $ClCF_3$ and Cl_3CF, according to Kahovec

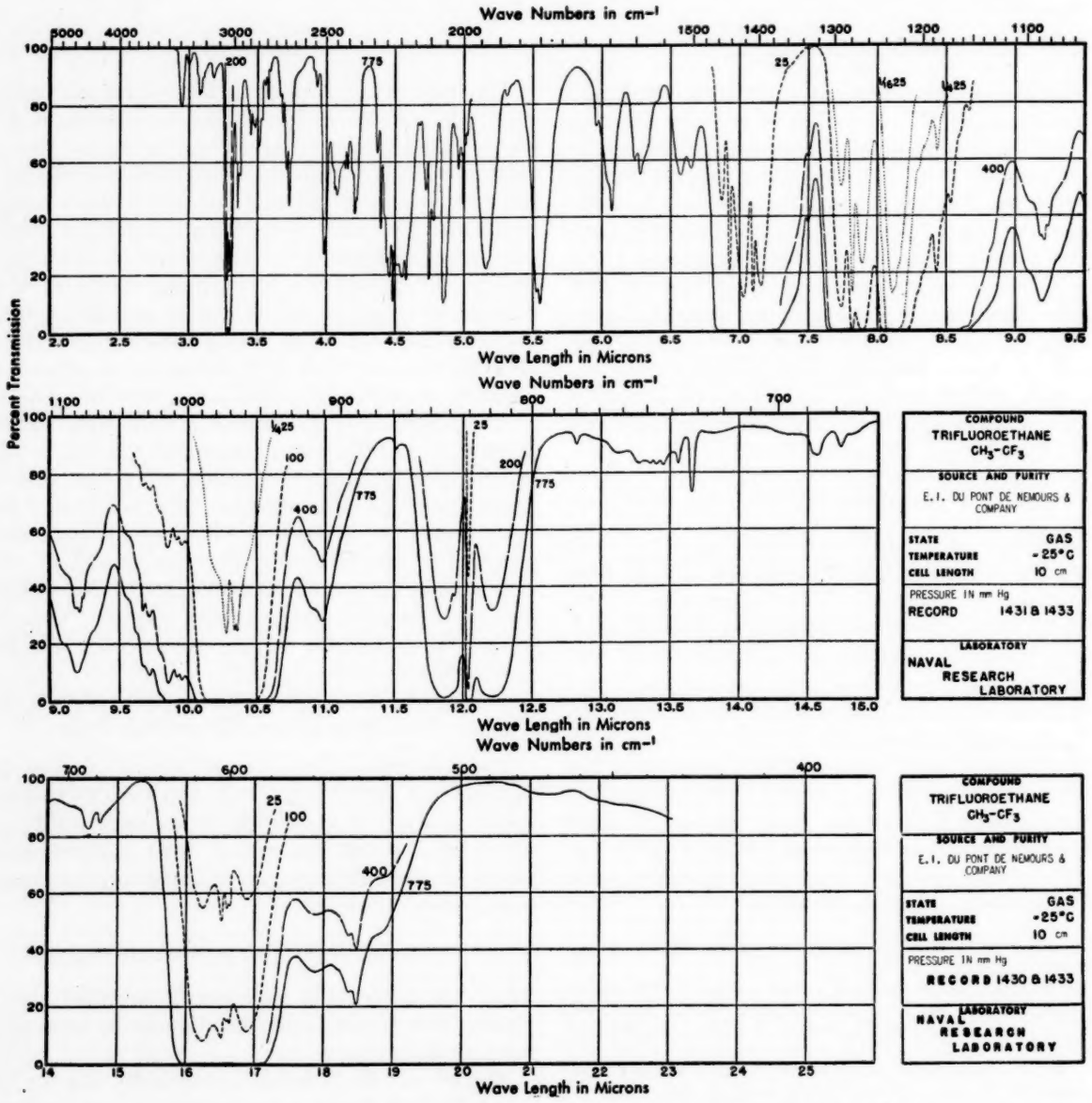

FIG. 1. Infra-red absorption spectrum of gaseous 1,1,1-trifluoroethane.

[9] See reference 4, p. 151.

TABLE I. Infra-red spectrum of $CF_3 \cdot CH_3$ (gas).

Wave number	Description	Interpretation
~ 470 cm^{-1}	*vvw*	2×238=476 (A_1); 830−365=465 (E)
530	*w*	
541	*m sh*	E fundamental
546	*m*	
560	*w*	
594	*s*	
600	*s*	
602	*s*	238+365=603 (E)
605	*s sh*	A_1 fundamental
616	*s*	
678	*vvw*	1280−604=676 (A_1), or impurity
~ 686	*vw*	1233−541=692 (A_1+A_2+E), or impurity
732	*w sh*	2×365=730 (A_1+E), or impurity
737	*vw sh*	1280−541=739 (E)
743	*vw*	
746	*vw*	
749	*vw*	
~ 754	*vw*	
762	*vw*	
780	*vvw*	238+541=779 (E)
~ 818	*s*	
831	*s sh*	A_1 fundamental
838	*w*	1443−604=839 (E)
~ 842	*s*	
869	*vvw*	Impurity
911	*m*	365+541=906 (A_1+A_2+E)
918	*w*	1280−365=915 (E)
965	*vs sh*	
967	*vs sh*	365+604=969 (E)
973	*vs sh*	E fundamental
1005	*m*	
1008	*m*	Impurity (C_3F_8)
1015	*m*	
1029	*m*	
1034	*m*	604+970−541=1033 (A_1+A_2+E)
~1045	*w*	1408−365=1043 (E)
~1070	*w*	
1082	*m*	1443−365=1078 (A_1+A_2+E)
1086	*m sh*	2×541=1082 (A_1+E)
1089	*m*	
~1100	*w*	
1155		Impurity
1172	*w sh*	365+830=1195 (E)
1186	*m sh*	2×604=1208 (A_1); 238+970=1208 (E)
1208		1443−238=1205 (E)
1233	*vs*	E fundamental
1267		
1280	*vs sh*	A_1 fundamental
1292		
1333	*vw*	365+970=1335 (A_1+A_2+E)
1397	*s*	
1408	*s sh*	A_1 fundamental
1422	*s*	
1443	*s sh*	E fundamental
1456	*s*	
1504	*w*	541+970=1511 (A_1+A_2+E)
1522	*w*	830+1233−541=1522 (A_1+A_2+E)

TABLE I.—(*Continued*)

Wave number	Description	Interpretation
~1570	*vvw*	604+970=1574 (E)
1592	*w*	365+1233=1598 (A_1+A_2+E)
1603	*vw*	
1647	*m*	365+1280=1645 (E)
~1660	*w*	2×830=1660 (A_1)
1678	*w*	238+1443=1681 (E)
1802	*s*	830+970=1800 (E)
1808	*s*	365+1443=1808 (A_1+A_2+E)
1883	*vvw*	604+1280=1884 (A_1)
1938	*m*	2×970=1940 (A_1+E)
1992	*vw*	541+1443=1984 (A_1+A_2+E)?
1997	*vw*	Impurity?
2002	*w sh*	Impurity?
2006	*vw*	2×365+1280=2010 (A_1+E)
2015	*vw*	604+1408=2012 (A_1)
2061	*m*	830+1233=2063 (E)
2093	*m*	
2106	*m sh*	830+1280=2110 (A_1)
2117	*m*	
2137	*vvw*	
2183	*m sh*	365+541+1280=2186 (A_1+A_2+E)
2197	*m*	970+1233=2203 (A_1+A_2+E)
2215	*m*	
2231	*m sh*	830+1408=2238 (A_1)
2242	*m*	
2251	*w*	970+1280=2250 (E)
2273	*m sh*	830+1443=2273 (E)
2286	*w sh*	
2369	*w*	
2376	*w sh*	970+1408=2378 (E)
~2386	*w*	
2406	*vw*	970+1443=2413 (A_1+A_2+E)
2415	*vw*	
2451	*w sh*	2×1233=2466 (A_1+E)
2460	*w*	
2509	*w sh*	1233+1280=2513 (E)
2542	*vvw*	2×1280=2560 (A_1)
2615	*vvw*	2975−365=2610 (E)
2630	*vvw*	1233+1408=2641 (E)
2681	*w sh*	1233+1443=2676 (A_1+A_2+E)
2694	*vw*	1280+1408=2688 (A_1)
2714	*vw*	604+830+1280=2714 (A_1)
2725	*vvw*	1280+1443=2723 (E)
2784	*vvw*	
2794	*vvw sh*	3035−238=2797 (E)
2807	*vvw*	2×1408=2816 (A_1)
2833	*vvw*	604+830+1408=2842 (A_1)
2849	*w sh*	1408+1443=2851 (E)
2860	*vw*	
2874	*vw*	604+830+1443=2877 (E)
2882	*vw*	2×1443=2886 (A_1+E)
2897	*w sh*	3×970=2910 (A_1+A_2+E)
2910	*vvw*	365+2×1280=2925 (E)
2967	*vw*	
2978	*w sh*	A_1 fundamental
2987	*vw*	

TABLE I.—*Continued*

Wave number	Description	Interpretation
3025	*m*	
3036	*m sh*	*E* fundamental
3049	*m*	
3143	*vw*	541+2975−365=3151 (A_1+A_2+E)
3234	*vw*	
3249	*vw*	238+3035=3273 (E)
3336	*vvw*	365+2975=3340 (E)
3397	*vw*	365+3035=3400 (A_1+A_2+E)

and Wagner,[10] but in neither case is the difference in frequency great. For CCl_3-CH_3 Wagner,[11] on the basis of a valence force model and considering the methyl group as a mass point, calculated almost equal values for these two frequencies but found from polarization measurements that the E fundamental lies somewhat lower than the A_1 fundamental. In the case of CF_3-CH_1 the frequencies in question are undoubtedly 541 and 602 cm^{-1}, of which the former has medium and the latter high intensity in the infra-red. The Raman band at 541 cm^{-1} is diffuse, whereas the Raman band at 602 cm^{-1} is sharp. Thus, there can be little doubt that 541 cm^{-1} is an E and 602 cm^{-1} an A_1 fundamental. These skeletal fundamentals may be characterized roughly as CF_3 deformations.

The frequency at 830 cm^{-1}, which is observed as an intense infra-red absorption band and as a strong and sharp Raman band, must be the skeletal fundamental of species A_1 corresponding to the "breathing vibration" of CF_4. It may be designated very roughly as largely a C−C stretching frequency.

The very intense infra-red bands at 1233 and 1280 cm^{-1} must represent the remaining two skeletal fundamentals. Both of them may be roughly characterized as C−F stretching modes. According to Kahovec and Wagner,[10] the E fundamental lies lower than the A_1 fundamental for the Cl_3CF, whereas the A_1 fundamental is the lower for $ClCF_3$. For CF_3-CF_3 the average value of the highest frequencies belonging to species A_{1g} and A_{2u} is higher than the average of the corresponding frequencies belonging to E_g and E_u.[12] The infra-red band at 1280 cm^{-1} has a typical *PQR*-structure, while the stronger band at 1233 has less regular appearance and resembles the E fundamental at 541 cm^{-1}, and also the perpendicular band at 1250 cm^{-1} in CF_3-CF_3.[12] In the Raman spectrum of CF_3-CH_3 both bands are very faint. However, the band of lower frequency is diffuse, whereas the other appears to be sharp. For these reasons it seems most probable that the band at 1233 cm^{-1} is an E fundamental and the band at 1280 cm^{-1} an A_1 fundamental. This conclusion could be tested by polarization measurements. However, because of the very low intensities of the Raman bands at 1233 and 1280 cm^{-1}, and their proximity to 2975 and 3035 cm^{-1} excited by the 4047A mercury line, such measurements would be extremely difficult with gaseous CF_3-CH_3. Since this was the only assignment problem requiring polarization data, no such measurements were made.

To the skeletal vibrations must be added an A_1 and an E C−H stretching frequency near 3000 cm^{-1}, an A_1 and an E methyl deformation frequency in the region 1400 to 1460 cm^{-1}, a doubly degenerate CH_3 rocking frequency near 1000 cm^{-1}, and finally the low twisting frequency of species A_2. The order of these frequencies follows uniquely from Wagner's work[13] on molecules of type XCH_3.

Thus, the very strong infra-red band at 966 cm^{-1} is evidently the methyl rocking frequency of species E. It is observed as a medium diffuse band in the Raman effect. The two strong infra-red bands at 1408 and 1443 cm^{-1} must be the A_1 and E methyl deformation frequencies, respectively. The former was not observed in the Raman effect, as is commonly the case for compounds containing methyl groups. The E methyl deformation was observed in the Raman effect as a very diffuse band with a broad maximum near 1450 cm^{-1}. The band at 2975 cm^{-1}, which is very strong and sharp in the Raman effect, must be the totally symmetric C−H stretching frequency. The band at 3035 cm^{-1} must be the corresponding fundamental of species E.

There remains the torsional frequency of species A_2 which is inactive as well in the infra-red as in the Raman effect. The first attempt to determine this fundamental from infra-red combination bands led to a value, 180 cm^{-1}, which agreed within the experimental error with the frequency, 165±25 cm^{-1}, obtained by Dailey, Minden, and Shulman[5] from intensity measurements at different temperatures in the microwave absorption spectrum of CF_3-CH_3.

TABLE II. Raman spectrum of $CF_3 \cdot CH_3$ (gas).

Wave number	Description	Interpretation
365	*w d*	*E* fundamental
541	*w d*	*E* fundamental
603	*m sh*	A_1 fundamental
830.3	*vs sh*	A_1 fundamental
969	*m vd*	*E* fundamental
1232	*vw d*	*E* fundamental
1278	*vw*	A_1 fundamental
~1450	*m vd*	*E* fundamental
2796	*vw*	2×1408=2816 (A_1); 3035−238=2797 (E)
2833	*vvw*	604+830+1408=2842 (A_1)?
2890	*vvw d*	2×1443=2886 (A_1+E)
2965	*vw d*	*P*, *O* branches
2974.6	*vs*	A_1 fundamental
3022	*vw d*	*P*, *O* branches
3035	*m*	*E* fundamental
3049	*vwd*	*R*, *S* branches

[10] L. Kahovec and J. Wagner, Zeits. f. physik. Chemie **B48**, 188 (1940).
[11] J. Wagner, Zeits. f. physik. Chemie **B45**, 341 (1940).
[12] Nielsen, Richards, and McMurry, J. Chem. Phys. **16**, 67 (1948).
[13] J. Wagner, Zeits. f. physik. Chemie **B40**, 36 (1938).

The evidence for this value, however, was not very strong. Moreover, when thermodynamic properties were calculated and compared with the calorimetric data of Russell, Golding, and Yost[2] it became fairly clear that the torsional fundamental must lie somewhat higher. A renewed study was made of the infra-red spectrum and the value, 238 cm^{-1}, was obtained for the A_2 fundamental.* As may be judged from Table I and Fig. 1, the spectroscopic evidence for this value, while stronger than the evidence for the previously assumed value, can hardly be regarded as conclusive. It will be shown below, however, that the value 238 cm^{-1} for the torsional frequency, in conjunction with the values assigned for the active fundamentals, gives good agreement between calculated and observed thermodynamic properties.

The assigned fundamental vibration frequencies for CF_3-CH_3 are listed in Table III. The characterizations of the various vibration modes given in the second column are fairly meaningful for the vibrations involving primarily the atoms of the methyl group. For the skeletal vibrations they have only rough significance.

The assignment of fundamentals given here differs greatly from those made by Russell, Golding, and Yost[2] and by Thompson and Temple.[3] The former workers assigned the Raman bands observed at 368 and 968 cm^{-1} to A_1 and 1279 cm^{-1} to E. Assuming that a Raman band, here ascribed to excitation by the mercury line 4047A, is caused by Hg 4358A, they obtained a frequency, 1025 cm^{-1}, which they regarded as an E fundamental. They did not have the frequency 1233 cm^{-1}, which had not been observed in the Raman effect by Hatcher and Yost,[1] and assigned six fundamentals to A_1 and five to E, rather than the opposite. Thompson and Temple[3] assigned 541 to A_1 and 606, as well as both 1412 and 1450 cm^{-1}, to E. They took 1135 cm^{-1}, which was undoubtedly caused by an impurity in their sample, to be an A_1 fundamental.

The assignment given here confirms Kohlrausch's assignment[4] of nine of the fundamentals and agrees with an assignment of the active fundamentals by Herzberg,† except for an interchange of 1233 and 1280 cm^{-1}.

INTERPRETATION OF THE SPECTRA

On the basis of the fundamental vibration frequencies listed in Table III it has been possible to interpret all of the Raman bands and all but about a dozen of the 120 infra-red absorption maxima observed. The interpretations of the bands are given in the third columns of Tables I and II.

Some of the intense infra-red bands interpreted as fundamentals have extra zero branches and abnormal contours. In some cases this seems caused by overlapping combination bands, listed in Table I. The interpretation of the infra-red bands is on the whole satisfactory. Except for bands that are masked by stronger bands or lie outside the range of observation, all active binary sum bands have been observed, as well as a few binary difference bands. In several cases two interpretations appear equally plausible. A few bands, mostly of very low intensity, are interpreted as ternary combination bands. Because of the large number of such active combinations, there are many cases, especially at high wave numbers, in which alternative interpretations can be made. No attempt has been made to indicate all such alternatives in the table.

TABLE III. Fundamental vibration frequencies for $CF_3 \cdot CH_3$.

Species	Approximate character*	Wave number
A_1	CH stretching	2975 cm^{-1}
A_1	CH_3 deformation	1408
A_1	CF stretching	1280
A_1	C−C stretching	830
A_1	CH_3 deformation	604
A_2	Twisting	238
E	CH stretching	3035
E	CH_3 deformation	1443
E	CF stretching	1233
E	CH_3 rocking	970
E	CF_3 deformation	541
E	CF_3 rocking	365

* The designations in this column have only very rough meaning, especially for vibration involving the CF_3 group.

Certain peculiarities and difficulties should be pointed out. The infra-red band at 541 cm^{-1}, interpreted as an E fundamental, has an irregular contour and an intensity that is somewhat lower than that of what appears to be its overtone at 1086 cm^{-1}. The absorption maxima at 600 and 602 cm^{-1}, ascribed in Table I to a combination band of species E, may also be interpreted as zero branches of upper-stage bands corresponding to the A_1 fundamental at 605 cm^{-1}. The very strong absorption maxima at 965, 967, and 937 cm^{-1} appear to arise from coupling of the combination 365+604 of species E with an E fundamental, the frequency of which has been assumed to be 970 cm^{-1}. The difference between calculated and observed frequencies is rather large for the infra-red bands at 1172 and 1186 cm^{-1}. This may be caused by their proximity to the fundamental at 1233 cm^{-1}.

The interpretation of the Raman bands given in Table II is satisfactory, although for the very faint bands at 2796 and 2833 cm^{-1} the difference between the observed and calculated wave numbers is rather high. The diffuse maxima at 2965, 3022, and 3049 cm^{-1} apparently are rotational branches belonging to the fundamentals at 2975 and 3035 cm^{-1}.

IMPURITIES

It has not been possible to find plausible interpretations for all of the faint absorption maxima around 750 cm^{-1}. They are probably caused by impurities. In

* After completion of the present paper, it has been reported by R. Karplus and R. S. Halford (J. Chem. Phys. **18**, 912 (1950)) that a new microwave study by Dailey and Minden has given the value 230±40 cm^{-1}.

† Private communication to J. Rud Nielsen.

TABLE IV. Calculated thermodynamic functions for CF_3-CH_3 at one atmos. (in cal./deg. mole).

	T	$C_p°$	$S°$	$-(F°-H_0°)/T$	$(H°-H_0°)/T$
250°K	Translational	4.97	38.34	33.36	4.97
	Rotational	2.98	22.32	19.41	2.91
	Vibrational	6.67	2.98	0.80	2.18
	Torsional	2.01	1.27	0.21	1.06
	Total	16.63	64.91	53.78	11.12
298	Translational	4.97	39.21	34.23	4.97
	Rotational	2.98	22.84	19.93	2.91
	Vibrational	8.68	4.32	1.26	3.06
	Torsional	2.12	2.10	0.87	1.23
	Total	18.75	68.47	56.29	12.17
400	Translational	4.97	40.67	35.69	4.97
	Rotational	2.98	23.72	20.81	2.91
	Vibrational	12.65	7.46	2.44	5.02
	Torsional	2.18	2.75	1.34	1.41
	Total	22.78	74.60	60.28	14.31
600	Translational	4.97	42.69	37.71	4.97
	Rotational	2.98	24.93	22.02	2.91
	Vibrational	18.53	13.77	5.17	8.61
	Torsional	1.96	2.58	0.91	1.67
	Total	28.44	83.97	65.81	18.16

particular, the sharp band at 732 cm^{-1}, and also the weaker maxima or shoulders at 780, 1008, 1155, 1200, and 1205, and near 1350 cm^{-1}, all correspond to positions of strong $CF_3-CF_2-CF_3$ absorption and are undoubtedly caused by the presence of a small amount of this compound (b.p.$=-38°$ *vs.* -47.5°C for CF_3-CH_3). Likewise, the very weak band at 869 cm^{-1} and the weak absorption at 1155 and near 470 cm^{-1} are probably caused by a small amount of contamination with CF_2H-CH_3 (b.p.$=-24.7$°C). The bands at 678 and 686 cm^{-1} are considerably weaker than those observed by Thompson and Temple[3] in this region and may be caused by an impurity, although they can be interpreted satisfactorily as difference bands. The absorption maximum at 1997 cm^{-1} has been left uninterpreted, and the interpretations of some of the neighboring maxima are not very plausible. Since similar absorption maxima occur at these wave numbers in $CF_2=CH_2$, and in part in C_2F_4, they too are probably caused by impurities.

CALCULATED THERMODYNAMIC FUNCTIONS

From the known molecular dimensions[8] and the fundamental frequencies listed in Table III the heat capacity, entropy, free energy function, and heat content function, have been calculated for gaseous CF_3-CH_3 at one atmosphere and temperatures 250 (b.p.), 298, 400, and 600°K. The translational, rotational, vibrational and torsional (hindered rotational) contributions are listed separately in Table IV. The potential barrier V_0 opposing the rotation of the methyl group relatively to the CF_3 group was calculated from the formula[14] $\nu=(\sigma_i/2\pi)(V_0/2I_r)^{\frac{1}{2}}$, where ν is the torsional frequency, $\sigma_i=3$ the internal symmetry number, and I_r the reduced moment of inertia, and the value 3290 cal./mole was obtained. For the remaining calculations the equations and tables given by Hougen and Watson[15] were used. The molecular symmetry number was taken to be three.

Russell, Golding, and Yost[2] have made calorimetric measurements on CF_3-CH_3 and have obtained the value 63.95 ± 0.10 cal./deg. mole for the entropy of the ideal gas at 224.40°K and 0.9330 atmos. Calculation on the basis of the present spectroscopic data gives 63.77 cal./deg. mole, in good agreement with the calorimetric value.

ACKNOWLEDGMENT

The writers wish to acknowledge their indebtedness to E. I. du Pont de Nemours and Company for the gift of the sample.

[14] See S. Glasstone, *Theoretical Chemistry* (D. Van Nostrand Company, Inc., New York, 1944), p. 421.

[15] O. A. Hougen and K. M. Watson, *Chemical Process Principles* (John Wiley and Sons, Inc., New York, 1947), Part II, Chapter XVII.

The Interpretation of the Dependence of Luminescent Efficiency on Activator Concentration

PETER D. JOHNSON AND FERD E. WILLIAMS
General Electric Research Laboratory, Schenectady, New York

(Received July 21, 1950)

The previously published analysis (see reference 1) of the dependence of efficiency of substitutionally activated inorganic phosphors on activator concentration is generalized to include a wide variety of inorganic phosphors under various types of excitation. In addition to the optical excitation of the activator, the creation of conduction electrons and excitons, and the transfer of their energy to the luminescent and non-luminescent activator ions and to other impurities and lattice defects are included in the formulation. The dependence of efficiency on activator concentration of ZnF_2:Mn under c.r., x-ray, vacuum u.v. and near u.v. has been measured and interpreted on the basis of the theory. Preliminary photo-conductivity measurements clarify the role of the conduction band in the luminescence of ZnF_2:Mn. Also the dependence of the efficiency *vs.* activator concentration of both ZnF_2:Mn and KCl:Tl on temperature has been measured and interpreted on the basis of the variation in activation energy for competing radiationless processes with distance between activator ions. In addition, other efficiency *vs.* activator concentration data previously published by other authors (see reference 8) on a variety of phosphors and at various temperatures can be correlated and explained with the general theory.

INTRODUCTION

IN a previously published paper[1] an approach to a theory relating luminescent efficiency of phosphors to their activator concentration was outlined. Magnetic measurements, which have been confirmed by N. Elliott,[2] were adduced to show that in ZnF_2:Mn there is a random distribution of activator ions among the cation sites of the host lattice. On the basis of a random distribution of activators and, recognizing that only activators not adjacent to other activators are capable of luminescence, the efficiency of the phosphor can be quantitatively related to the activator concentration and to the capture cross sections for the exciting energy of luminescent and non-luminescent activators and of the host lattice. The mechanism of excitation of the luminescent activators was considered to be direct optical excitation by the u.v. radiation. This mechanism is probably an important contributing factor in excitation of this and many other phosphors by near u.v. radiation. However, for luminescence excited by x-rays or cathode rays the assumption of direct excitation is untenable. In this paper the theory is extended to include excitation by x-rays, c.r., and vacuum u.v. In addition, the temperature dependence of efficiency *vs.* activator concentration is considered.

THEORETICAL

In order to extend the formulation of efficiency as a function of activator concentration to a wide variety of phosphors excited by all known means including c.r., x-rays, and vacuum and near u.v., it is necessary to consider in detail the processes which occur upon absorption of energy in phosphors. There are three alternative primary steps which can occur: (1) excitation of electrons from the filled band or impurity levels to the conduction band; (2) excitation of electrons from impurity levels to excited levels of the impurity; and (3) formation of excitons. The excited impurities may produce luminescence directly, whereas for the conduction electrons and excitons a second step is prerequisite to impurity luminescence. The conduction electrons and excitons may be annihilated by direct recombination, by interaction with non-luminescent activators and other impurities, and finally by interaction with the luminescent activators. Therefore, it is necessary to consider the capture cross sections of the activators and other impurities for excitons and conduction electrons in addition to those for the incident photons. The transfer of energy from non-luminescent impurities to luminescent activators, as in sensitized phosphors, is not considered here. The efficiency of excitation of luminescent activators, following absorption of the incident energy by the exciton or conduction band processes, or the efficiency of direct optical excitation of the luminescent activators is:

$$\eta=\frac{\sigma' x'}{\sum_\nu \sigma^\nu x^\nu}, \tag{1}$$

where the σ^ν and x^ν are the capture cross sections and the mole fractions respectively of the ν different types of sites capable of capturing energy in the form of conduction electrons, excitons or photons. The primes refer to the luminescent activators. Superscripts refer to the type of site in question and subscripts to the mechanism of excitation. When no subscript is used, the formulation includes any one of the three excitation mechanisms. In general the summation over ν includes as many terms as can be recognized from the constitution and method of preparation of the phosphor.

If all three processes are active, then the over-all efficiency is a linear combination of the efficiencies

[1] P. D. Johnson and F. E. Williams, J. Chem. Phys. **18**, 323 (1950).
[2] N. Elliott, Bull. Am. Phys. Soc. **25**, No. 1, 37 (1950).

obtained with each mechanism:

$$\eta=(1-f_{ex}-f_c)\eta_{op}+f_{ex}\eta_{ex}+f_c\eta_c, \tag{2}$$

where η_{op}, η_{ex} and η_c are respectively the efficiencies of the optical, exciton and conduction electron mechanisms, and f_{ex} and f_c are the fractions of the incident energy going into exciton and conduction electron formation, respectively:

$$f_{ex}=\frac{\rho_{ex}c_{ex}}{\rho_{ex}c_{ex}+\rho_c c_c+\sum_\nu \sigma_{op}{}^\nu x^\nu} \tag{3}$$

$$f_c=\frac{\rho_c c_c}{\rho_{ex}c_{ex}+\rho_c c_c+\sum_\nu \sigma_{op}{}^\nu x^\nu} \tag{4}$$

where ρ_{ex} is the capture cross section for incident energy resulting in exciton formation; c_{ex} is the mole fraction of sites where excitons can be formed; ρ_c and c_c are the corresponding quantities for exciting electrons to the conduction band. The term $\sum_\nu \sigma_{op}{}^\nu x^\nu$ in (3) and (4) is concentration dependent, which means that if direct optical excitation contributes appreciably to luminescence f_{ex} and f_c are concentration dependent. The quantities $\rho_{ex}c_{ex}$ and $\rho_c c_c$ are probably not strongly dependent on activator concentration.

If (1) and (3) and (4) are substituted in (2):

$$\eta=\frac{x'}{\rho_{ex}c_{ex}+\rho_c c_c+\sum \sigma_{op}{}^\nu x^\nu}\times\left[\sigma_{op}{}'+\frac{\rho_{ex}c_{ex}}{\sum_\nu \sigma_{ex}{}^\nu x^\nu}\sigma_{ex}{}'+\frac{\rho_c c_c}{\sum_\nu \sigma_c{}^\nu x^\nu}\sigma_c{}'\right] \tag{5}$$

where the σ_{ex}'s and the σ_c's are the capture cross sections of activators and other species present for excitons and conduction electrons, respectively. Defining the parameters a and b:

$$a=\frac{\rho_{ex}c_{ex}}{\sum_\nu \sigma_{ex}{}^\nu x^\nu} \tag{6a}$$

$$b=\frac{\rho_c c_c}{\sum_\nu \sigma_c{}^\nu x^\nu}. \tag{6b}$$

(5) reduces to:

$$\eta=\frac{(\sigma_{op}{}'+a\sigma_{ex}{}'+b\sigma_c{}')x'}{\sum_\nu(\sigma_{op}{}^\nu+a\sigma_{ex}{}^\nu+b\sigma_c{}^\nu)x^\nu}=\frac{\sigma_m{}'x'}{\sum_\nu \sigma_m{}^\nu x^\nu}, \tag{7}$$

where $\sigma_m{}^\nu$ are the weighted mean cross sections. It is obvious from (2) and (7) that for a given phosphor the relative contribution of each mechanism depends on the values of a and b, which vary with the type of excitation. Therefore, the efficiency as a function of activator concentration would be expected to vary with the type of excitation. This is indeed observed experimentally.

Initially, the fraction of activators not adjacent to any other activator and therefore capable of luminescence was calculated on the basis of the geometry of the crystal. The parameter z was taken as the number of nearest neighbor cation sites in the lattice. However in most crystals the perturbing effect of the impurity extends over a distance of several identity periods. Therefore, it is apparent that activators farther than the closest possible distance from a given activator may interact with this activator in such a way as to quench luminescence. Hence z is defined in general as the number of lattice positions (substitutional or interstitial, or both) surrounding a given activator such that if any one of these sites is occupied by another activator, luminescence is quenched. Theoretical considerations and the absorption data of Parkinson and Williams[3] on ZnF_2:Mn and its components indicate that approximately the same capture cross sections for incident photons be assigned to adjacent and non-adjacent activator ions. Utilizing the random distribution of activator ions over lattice sites to evaluate x' and assuming that x^ν for non-activators is $(1-c)$, (1) may be reduced to:

$$\eta=\frac{c(1-c)^z}{c+(\sigma/\sigma')(1-c)}, \tag{8}$$

where c is the total mole fraction of activator and σ is the capture cross section of non-activators. The ratio σ/σ' remains as an adjustable parameter except where it can be determined experimentally from optical absorption data for phosphors in which direct excitation to emission is solely responsible for luminescence. Another adjustable parameter has been produced in relinquishing the simple definition of z as the number of nearest cation neighbors; however, as will be seen from the following, the applicability of the formulation has been increased to cover all types of phosphors at all temperatures. Under certain conditions, indeed, z does have as a lower limit the number of nearest cation neighbors.

Since data is available on the efficiency *vs.* activator concentration of a number of phosphors at different temperatures, it is desirable to extend the formulation to include the effect of temperature. The transition probability for the emitting process is A. The rate constant, k', determines the rate at which de-excitation occurs by concentration dependent radiationless processes resulting from interaction with neighboring activator ions separated by a distance, r. Clearly k' is a function of r. Defining ϵ_0 as the height of the barrier for the radiationless process with infinite dilution of activator, ϵ the height of the barrier for activator ions separated by the finite distance r will be less than ϵ_0 by an amount approximately proportional to the over-

[3] W. W. Parkinson and F. E. Williams, J. Chem. Phys. 18, 534 (1950).

lap integral for the wave functions of the interacting activator ions. As r approaches zero, ϵ also will approach zero. The overlap integral varies exponentially with r, therefore k' is:

$$k' = se^{-\epsilon/kT} \cong s \exp[-\epsilon_0(1-e^{-ar})/kT] \tag{9}$$

where s is approximately the frequency of lattice vibrations. Clearly, increasing temperature will increase k' for all values of r. However, the radiationless processes for small r will dominate at low temperatures. For a given r the efficiency is:

$$n \propto \frac{A}{A+k'} = \frac{1}{1+\frac{s}{A}\exp(-\epsilon/kT)} \tag{10}$$

combining with (1):

$$\eta = \frac{\sigma' c}{\sum_\nu \sigma^\nu x^\nu} \sum_{i=1}^{\infty} \sum_{j=2}^{(z_i - z_{i-1})} \frac{\frac{(z_i - z_{i-1})!}{(j-1)!(z_i - z_{i-1} - j + 1)!}(1-c)^{(z_i - j + 1)} c^{(j-1)}}{1 + (s_{ij}/A)e^{-\epsilon_{ij}/kT}} \tag{11}$$

where the $z_2 - z_{i-1}$'s and ϵ_{ij}'s are the appropriate values for activators situated at positions in the lattice at successively greater distances, r_i, from the given activator. The expression in the numerator of the double summation gives the fraction of total activators which have $j-1$ activators in the ith shell surrounding the given activator and no activators in the sphere up to the ith shell. The frequency factor s_{ij} is obviously proportional to the number of activators in the ith shell, i.e., $s_{ij} = s_i(j-1)$. The number of activators in the ith shell would be expected to affect ϵ_{ij} only slightly. Also ϵ_{ij} is dependent on r_i as expressed by (9). The quantity z is the sum of the weighted $(z_i - z_{i-1})$'s in expression (11) up to the term, where $(s_{ij}/A)e^{-\epsilon_{ij}/kT}$ becomes negligible. Since at large z_i, ϵ_{ij}, does not change rapidly with a change in z_i, any term of the double summation is more dependent on the value of T than on the value of z_i. This means that z in expression (8) is dependent on temperature, being larger at higher temperature. The effect of temperature on the ratios of capture cross sections is small compared to the effect on z.

It was noted in the preliminary formulation that some disagreement was encountered between the theory and experimental data at high activator concentrations, e.g., 7 or 8 mole percent. The physical dimensions of the lattice are obviously affected by high activator concentrations. Accordingly, the relative positions of the filled and empty bands and impurity levels are affected so that luminescence competes with more active radiationless processes.

The absolute quantum efficiency is given by (1) only for the case where one incident photon can excite at best only one activator to luminescence. However (1) may be made general by introducing a factor which is the energy efficiency of the individual excitation process. The absolute energy efficiency, η', of a phosphor is then:

$$\eta' = \gamma\eta. \tag{12}$$

For direct optical excitation γ is the ratio of energy of an emitted quantum to absorbed quantum. Since the exciton and conduction band mechanisms are two-step excitation processes, γ also is a function of the quantities f_{ex} and f_e in (3) and (4).

EXPERIMENTAL

For measurement of the efficiency *vs.* activator concentration of ZnF_2:Mn in the near and vacuum ultraviolet a low voltage hydrogen discharge lamp with a "stocking" cathode, cylindrical nickel anode and LiF window was used for excitation. Operated at 3 or 4 amp. and 40 volts, the lamp provides an exceptionally steady source of u.v. The separation of near and vacuum u.v. was accomplished by use of a quartz plate whose transmission at 1849A was 64 percent. The vacuum u.v. includes wave-lengths transmitted by LiF but not transmitted by the quartz plate. Near u.v. is defined as light transmitted by quartz but not by a standard microscope slide. The powdered phosphor samples were placed in depressions of standard diameter in copper disks which were placed in a rigidly mounted holder to ensure constant geometry. A stream of dry nitrogen was passed through the apparatus during all measurements. A barrier layer photo-cell in conjunction with a galvanometer was used to measure the emission. Reflected light, emission excited by near u.v., and emission due to vacuum u.v. are determined by obtaining readings of the light from the phosphor with the glass slide, quartz plate and without filter between source and sample, and making appropriate subtractions.

The efficiency *vs.* activator concentration of KCl:Tl at 298°K and 80°K was measured by obtaining spectral emission curves of the phosphor at these temperatures and comparing the heights of the individual peaks. The relative efficiencies of ZnF_2:Mn at 80°K were also obtained in this manner. Excitation for these measurements was a 15-watt quartz mercury low pressure lamp. The spectroradiometer used for these measurements was designed by F. J. Studer.

For the measurements of relative efficiency under x-ray excitation the same geometry as for near and vacuum u.v. excitation was maintained using the same samples. An RCA 5819 photo-multiplier was used to

measure the emitted light. Cr $K\alpha$ radiation was used for excitation.

Approximate measurements on ZnF_2:Mn under cathode-ray excitation were made at 6 kv and 1μa/cm^2 on settled screens of the phosphor mounted in a demountable tube. The screen thickness was approximately 3 mg/cm^2.

The transmission of powdered samples of the ZnF_2:Mn phosphors and pure ZnF_2 0.2 and 2.0 mm thick for light of the wave-length of peak emission was measured and found to be substantially identical in all cases.

Optical absorption measurements have been made on several KCl:Tl crystals prepared by the Bridgman[4] method using a furnace similar to that described by Strong.[5] The spectroradiometer was used for the measurements.

Preliminary measurements have been made of photoconductivity of ZnF_2:Mn crystals. The two electrodes in contact with the phosphor crystal are Pt. A cylindrical Pt electrode completely surrounding the sample except for a 1×2 mm opening to admit the excitation is maintained positive with respect to both of the other electrodes to collect photo-emitted electrons. The apparatus could be evacuated or filled with any gas, although the photo-currents were found to be independent of the surrounding atmosphere. The first stage of the current measuring circuit is a Victoreen electrometer tube which enables currents less than 10^{-12} amp. to be detected. The samples consisted of clear crystals of ZnF_2:Mn about 1×1×2 mm.[6] Ordinary microcrystalline fused samples of ZnF_2:Mn have such large dark currents that photo-conductivity measurements are impractical. The low voltage hydrogen source, a G.E. 4-watt germicidal lamp and a G.E. BH-4 lamp were the sources used and were focused on the sample using a crystal quartz lens.

It should be pointed out that all efficiency *vs.* activator concentration data are relative measurements. For this reason all curves are normalized. All efficiency data are taken by viewing the phosphor from the same side as the excitation.

RESULTS AND DISCUSSION

Among the factors which can affect efficiency *vs.* activator concentration is absorption of its own emission by the phosphor. This effect has been discussed by numerous authors,[7] and can be accounted for adequately on the basis of existing theory when necessary. Both reflectance and transmission measurements on powdered ZnF_2:Mn and on KCl:Tl indicate that in these phosphors, absorption is not present at the wave-lengths of emission. This conclusion is substantiated by the fact that clear colorless crystals of these phosphors can be prepared. In inorganic phosphors in general, except for the negligible anti-Stokes overlap, self-absorption is usually unimportant except when the sample is thick and is viewed from the side opposite to the excitation. This effect may account for disagreement in the literature.[8,9]

Emission spectra of ZnF_2:Mn at various activator concentrations at both room and liquid air temperatures show that there is only one emission band with peak at 5860A in all cases at 298°K and 5950A at 80°K. The peak does not shift with activator concentration, so the data on this phosphor are not complicated by the presence of more than one emission process.

It is obviously important to determine what role, if any, photo-conductivity plays in the luminescence process. The photo-conductivity data on several crystalline samples of ZnF_2:0.038 Mn (which was the only composition, within 0.01 Mn, which gave samples of high enough resistivity in the dark to measure photo-conductivity), indicated photo-currents of the order of 10^{-9} amp. with 45 volt applied potential using the output of the hydrogen lamp at wave-lengths longer than 1850A. In the range from 1850 to 2500A capable of exciting luminescence there is estimated to be approximately 2×10^{14} quanta per sec. The intensity at longer wave-length is greater. Indeed, it has been found possible to observe photo-conductivity of the same order of magnitude as that indicated above by irradiation with light of wave-lengths too long to excite luminescence. On irradiating the same samples with a 4-watt "germicidal" lamp which gives mainly 2537A u.v. and only weakly excites the phosphor, the photo-current was approximately 6×10^{-10} amp. By irradiating with predominantly 3650A from a BH-4 lamp the photo-current was about 1×10^{-10} amp. The phosphor is not excited by 3650A. Without the quartz lens, the photo-current due to wave-lengths from the hydrogen source shorter than 1850A was found by subtraction to be as much as five times that due to wave-lengths longer than 1850A. Only the orders of magnitude of the photo-currents are significant since the actual amount of radiation falling on the sample in each case has not been measured.

Since as has been shown previously,[1] there is a significant amount of metallic or monovalent zinc in the phosphor, the photo-conductivity in the near u.v. is probably due to excitation to the conduction band from these impurities. The long wave-length "tail" in the absorption spectra of ZnF_2 and ZnF_2:Mn reported by Parkinson and Williams[3] is probably due to the presence of this zinc as in the case of the long wave-length tail in the absorption of ZnO:Zn. Theoretical considerations[3] demonstrate that the ground state of the Mn^{++} in ZnF_2:Mn is too far below the conduction

[4] P. Bridgman, Proc. Am. Acad. **60**, 305 (1925).
[5] J. Strong, Phys. Rev. **36**, 1663 (1930).
[6] P. D. Johnson and F. E. Williams, J. Chem. Phys. **17**, 583 (1949).
[7] J. Perrin, Comptes Rendus **177**, 469 (1923). E. Merritt, J. Opt. Soc. Am. **12**, 613 (1926). M. L. Brüninghaus, Comptes Rendus **149**, 1375 (1909).
[8] D. Pearlman, N. R. Nail and F. Urbach, paper No. 21, "Solid Luminescent Materials," Wiley, 1948. F. A. Kroger, "Some Aspects of the Luminescence of Solids," Elsevier, New York, 1948.
[9] J. W. Marden, Chem. and Met. Eng. 80–8 (August, 1941).

band to permit photo-conductivity by activator excitation in the u.v. above 1800A. Therefore, it is concluded that photo-conductivity occurs in ZnF_2:Mn independently of the luminescence process under near u.v. excitation.

The results of the efficiency *vs.* activator concentration measurements on ZnF_2:Mn at room temperature are shown in Figs. 1 and 2 along with calculated curves. It will be noticed that the falling-off of efficiency occurs over the same range of activator concentrations for all types of excitation, suggesting that the same mechanism extinguishes luminescence in all cases. The concentration for peak efficiency shifts from about 4.5 mole percent of activator for near u.v. to about 2 mole percent for cathode-ray excitation. The higher energy excitation causes the peak efficiency to occur at lower activator concentration.

At the long wave-length u.v. most of the excitation

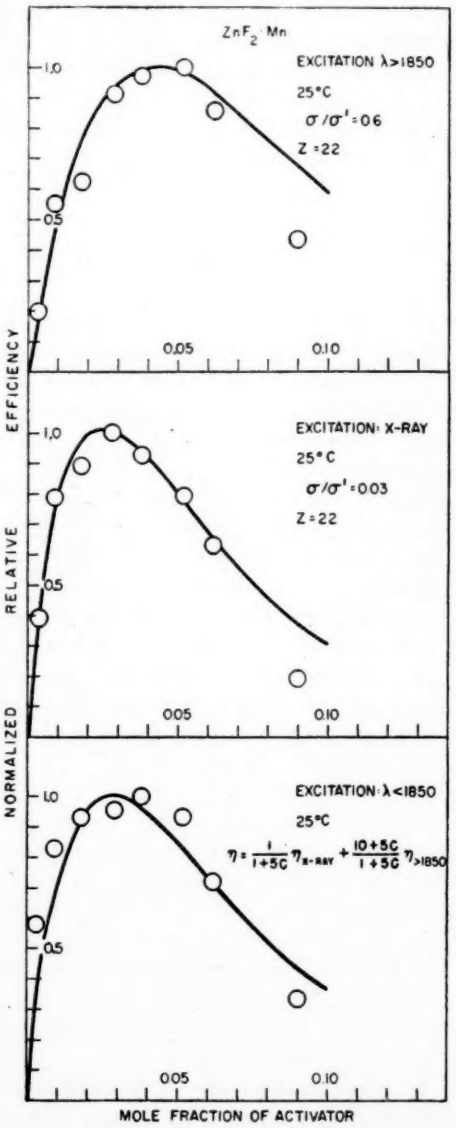

FIG. 1. Efficiency *vs.* activator concentration of ZnF_2:Mn as a function of excitation.

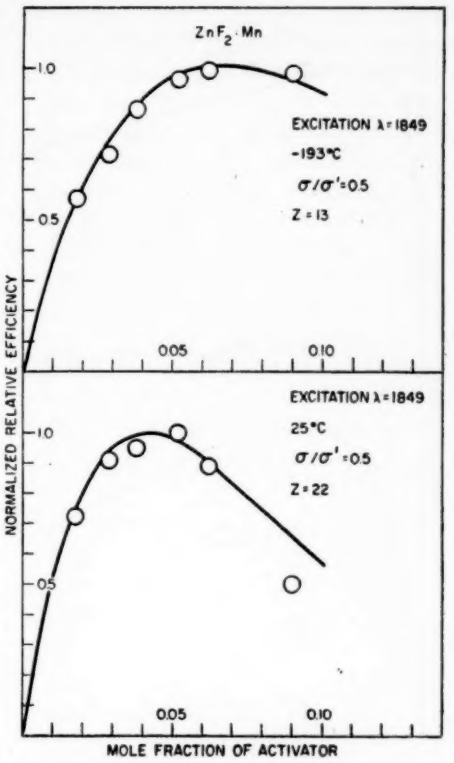

FIG. 2. Efficiency *vs.* activator concentration of ZnF_2:Mn as a function of temperature.

in this phosphor would be expected to occur by direct excitation to levels within the activator so that the capture cross sections in (1) are those for capture of incident photons. The values of z and σ/σ' which fit the data are 22 and 0.6, respectively. The latter value is in qualitative agreement with the absorption data of Parkinson and Williams.[3] The successively greater values of z which would normally be expected in the rutile lattice are 2, 10, 14, 22, and 26; these are the numbers of cations included in successively larger spheres surrounding a given cation site up to the point where one begins to include two primitive identity periods. Once the values of the ratio of capture cross section of adjacent to non-adjacent activators are set, z and σ/σ' are uniquely determined by the data. In spite of the remarkable fact that the z which fits the data agrees with one of the possible z's obtained from the geometry of the crystal, it is believed that this agreement is fortuitous since cations at successively greater distances from the activator would be expected to have a continually decreasing effect on the activator as indicated by (11). Naturally, at a given temperature z must be independent of the type of excitation, and the fact that the data obtained with different types of excitation at room temperature are accounted for using the same z is encouraging confirmation of the formulation.

In the case of c.r. or x-ray excitation very little direct excitation of the activator would be expected. Practically all excitation must take place through the conduction band or through the formation of excitons. With

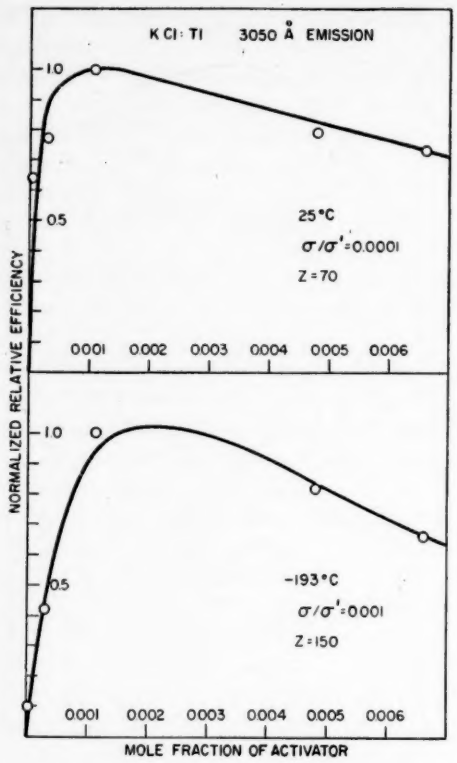

FIG. 3. Efficiency *vs.* activator concentration of 3050A emission of KCl:Tl as a function of temperature.

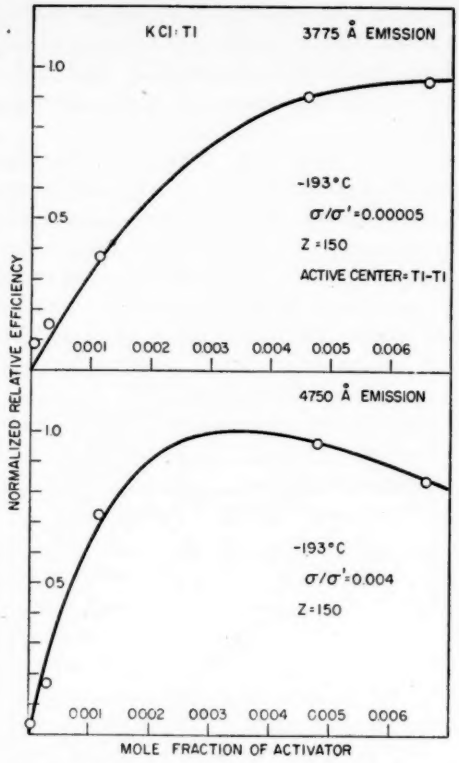

FIG. 4. Efficiency *vs.* activator concentration of low temperature emission of KCl:Tl.

these types of excitation neither mechanism can be completely eliminated from consideration and each must contribute to the excitation to a different extent in the two cases. From (7) the efficiency is:

$$\eta=\frac{(a\sigma_{ex}'+b\sigma_c')c(1-c)^z}{(a\sigma_{ex}'+b\sigma_c')c+(a\sigma_{ex}+b\sigma_c)(1-c)}. \qquad (13)$$

The simple ratio of capture cross sections used is then actually the ratio $(a\sigma_{ex}+b\sigma_c)/(a\sigma_{ex}'+b\sigma_c')$.

Compared to x-ray excitation, the efficiency *vs.* activator concentration under vacuum ultraviolet would be expected to have a larger component due to direct excitation, and this is indeed found to be the case upon examination of the ratios of capture cross sections in Table I. The occurrence of pronounced photo-conductivity with vacuum u.v. excitation suggests that the conduction band mechanism contributes to the luminescence. Equations (2)(3)(4) have been applied in Fig. 1 in the case of the vacuum u.v. excitation to demonstrate that the combination of individual efficiencies may be used to correlate the data. In Table I the ratio of capture cross sections given for this excitation is the weighted mean value in (7).

Figure 2 gives the efficiency *vs.* activator concentration of ZnF_2:Mn under 1849A excitation at room and liquid air temperatures. σ/σ' would not be expected to change by a significant amount on changing temperature, however, as (11) would lead us to expect, z does change to a lower value. The fact that the z which describes the data does not coincide precisely with any of the simple z values for the rutile lattice indicates that the contribution to quenching of luminescence by adjacent species is not a sharply discontinuous function of the interactivator distance. This conclusion is again in agreement with (11).

The efficiency *vs.* activator concentration of KCl:Tl is complicated by the existence of three different emission peaks which compete with each other for the exciting radiation. Since absolute absorption data are available on KCl and KCl:Tl, it would seem possible in this case as with ZnF_2:Mn to predict what σ/σ' should be. Unfortunately, however, the processes which result in the longer wave emission peaks are present to such an extent under all possible conditions that they completely overshadow the very weak absorption of pure KCl at 2537A. The σ in the equation for each peak is then due mainly to the competing emitting processes rather than to the absorption by the host lattice and extraneous impurities. It is interesting to note that although the short wave-length peak (3050A) in the emission is due to transitions occurring within the Tl^+ ion,[10] other activators within about 2.5 nearest neighbor distances (since $z=70$) can quench luminescence in this band. This is in agreement with the calculations of Williams[11] on KCl:Tl.

At 80°K emission bands, hardly observable at 298°K, with peaks at 3775A and 4750A appear. The competi-

[10] F. Seitz, J. Chem. Phys. **6**, 150 (1938).
[11] F. E. Williams, (to be published).

TABLE I.

Phosphor	Emission peak	Excitation	−193°C z	−193°C σ/σ'	25°C z	25°C σ/σ'
ZnF_2:Mn		>1850A			22	0.6
ZnF_2:Mn		<1850A			22	0.1
ZnF_2:Mn		x-ray			22	0.03
ZnF_2:Mn		c.r.			22	0.007
ZnF_2:Mn		1850A	13	0.5	22	0.5
KCl:Tl	3050A	1850+2537	150	0.001	70	0.0001
KCl:Tl	3775A	1850+2537	70(150)	0.005		
KCl:Tl	4750A	1850+2537	150	0.004		
ZnS:Cu					4000	5×10^{-5}
$ZnSiO_4$:Mn	Green		4	0.006	10	0.008
(Zn.15Be)SiO_4:Mn	Red		4	0.3	12	0.4
(Zn.15Be)SiO_4:Mn	Green		20	0.003	30	0.005

tion of these bands with the 3050A emission is greater at lower temperature. This fact in addition to the concentration dependence of the competing processes would be expected to exert an effect on z in opposition to that of the radiationless recombinations considered in the derivation of (11). There is an increase in z from 70 at 298°K to 150 at 80°K for the 3050A peak, demonstrating that in fact the low temperature emission bands are a more important factor in the temperature dependence of efficiency *vs.* activator concentration of KCl:Tl than are the radiationless processes. The effect of the competing radiation processes on the 3050A peak at 80°K is also noticeable in the higher value of σ/σ' found at this temperature. These effects are shown on Fig. 3.

It is of interest that the absolute total quantum efficiency as calculated on the basis of the z's and σ/σ''s given for KCl:Tl at 80°K equals almost unity over the range from about 0.002 to 0.0055 Tl. In addition, the maximum efficiency of the 3050A peak at 298°K is calculated to be 0.85, in good agreement with the known high efficiency of these phosphors.[12] These considerations are in accord with the idea that radiationless recombinations are less important in this phosphor than competing radiation processes.

The 3775A emission is most significant at high activator concentration. If the activator responsible for this emission at 80°K is considered to be a non-adjacent (in the sense defined in this paper) activator, the value of z is approximately one-half that for the other two peaks at this temperature. On calculating the concentration of activators having just one other activator in the nearest 150 cation positions[1] as a function of gross activator concentration and considering this grouping of activators as responsible for the 3775A emission, it is found that z is 150 as in the case of the other peaks. It is not to be inferred that the 3775A emission is due to an electron transfer between adjacent activators. On the contrary, the fact that z is 150 for this peak suggests that, as is probably the case with the 3050A and the 4750A peak, emission is due to a transition within the activator, however an adjacent activator is necessary to break down the selection rules sufficiently so that the 3775A optical transition can occur. The experimental data and computed curves are shown in Fig. 4.

Figure 5 shows some experimental points taken from data published by Pearlman *et al.*[8] on ZnS:Cu and the calculated curve which is in accord with this data. Since the precise mechanism of the luminescence of this phosphor is not completely understood there is no experimental confirmation of the value of σ/σ'. The value which one obtains for z is most interesting since it corresponds to interaction of activators to quench luminescence over distances of up to 10 identity periods. This indicates that the extension of the activator through the lattice is large, which is not unreasonable in view of the high dielectric constant of ZnS and the probably interstitial position of the activator.[13] Additional support for an extensive radial charge density for the activators in sulfide phosphors is provided by the fact that Roberts and Williams[14] have deduced by other methods that the emitting state of the activator in ZnS:Ag is only 0.17 ev below the conduction band.

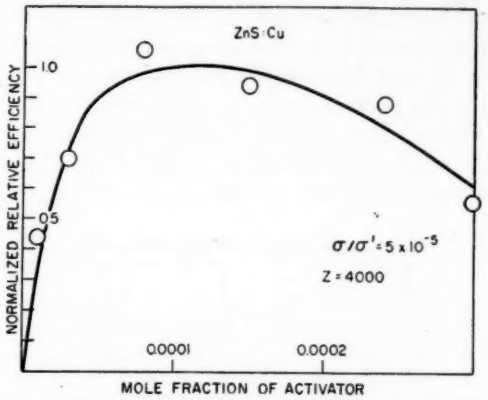

FIG. 5. Efficiency *vs.* activator concentration of ZnS:Cu (experimental points from Pearlman, *et al.*).

In Table I are included the σ/σ' and z for the willemite and zinc beryllium silicate phosphors activated with manganese which fit the data on these phosphors given by Kroger. It is interesting to note that at the lower temperature in two cases z becomes the actual number of nearest neighbor cation positions in the lattice. In addition, it is probably significant that the cross-section ratios, rather than the z values, are the same for the green band in both phosphors.

CONCLUSIONS

The theory of efficiency *vs.* activator concentration has been extended to apply to a wide variety of phosphors under various conditions of temperature and excitation. Experimental results on ZnF_2:Mn, KCl:Tl and other phosphors are discussed in connection with the theory. It is found that in all cases the theory adequately correlates and describes the available data.

ACKNOWLEDGMENTS

We wish to express our appreciation to Dr. F. J. Studer for making optical measurements involving the spectroradiometer and for advice in designing the hydrogen discharge lamp. We are also indebted to Dr. E. W. Balis and Mr. L. B. Bronk for phosphor analyses. Finally, we wish to thank Dr. M. Hebb for helpful criticism during the preparation of this manuscript.

[12] W. Bunger, Zeits. f. Physik **66**, 311 (1930).

[13] J. H. Simpson, Proc. Roy. Soc. **A197**, 269 (1949).

[14] S. Roberts and F. E. Williams, **40**, 516 (1950).

Lennard-Jones and Devonshire Equation of State of Compressed Gases and Liquids*

R. H. WENTORF, JR., R. J. BUEHLER, J. O. HIRSCHFELDER, AND C. F. CURTISS
University of Wisconsin Naval Research Laboratory, Department of Chemistry, Madison, Wisconsin
(Received July 24, 1950)

The reduced equation of state for compressed gases and liquids is computed according to the theory of Lennard-Jones and Devonshire for a large number of temperatures and densities. The corrections due to gas imperfection of internal energy, specific heat, and entropy as well as the compressibility factor (pv/RT) are expressed in terms of reduced variables. The calculations were made by punched-card methods. A comparison is made between experiment and theory. It is shown that the theory of Lennard-Jones and Devonshire is unsatisfactory at densities near the critical point and lower but improves at higher densities becoming better for normal liquids. Such results were to be expected from the nature of the cell or free-volume method.

THE Lennard-Jones and Devonshire (LJD)[1-6] equation of state for dense gases and liquids is the best practical equation of the "free-volume" type. In this treatment it is assumed that all of the molecules are held in their mean lattice positions except one which roams in the potential energy cage formed by its neighbors. For the sake of mathematical expediency, the potential energy is smeared to obtain radial symmetry within the cage. Such a model is clearly restricted to densities somewhat greater than the critical density where the molecules are in reality nearly always in the central portion of their cells and seldom escape due to the high potential barriers.

Eventually we can look forward to a more accurate type of equation of state based on the analysis of coordinated motion and the presence of holes. However, this will require the solution of a set of integral equations which are difficult according to present standards but

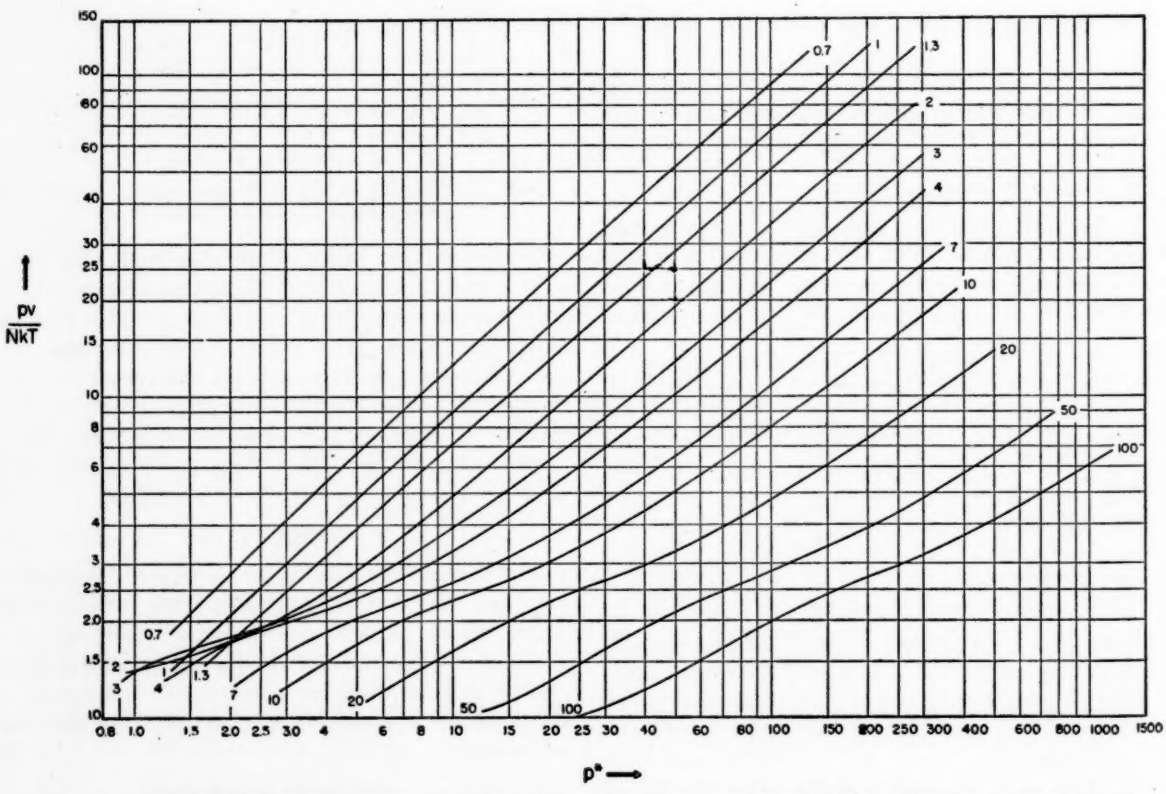

FIG. 1. Compressibility *vs.* reduced pressure, $p^* = p(\text{atmos.})/p_1$, where $p_1 = 136.23(\epsilon_m/k)/r_0^3$. The curves are isotherms and are labeled with the values of the reduced temperature, kT/ϵ_m.

* This work was carried out under Contract NOrd 9938 with the Navy Bureau of Ordnance.
[1] J. E. Lennard-Jones and A. F. Devonshire, Proc. Roy. Soc. **163A**, 53 (1937).
[2] J. E. Lennard-Jones and A. F. Devonshire, Proc. Roy. Soc. **165A**, 1 (1938).
[3] J. E. Lennard-Jones and A. F. Devonshire, Proc. Roy. Soc. **169A**, 317 (1939).
[4] J. E. Lennard-Jones and A. F. Devonshire, Proc. Roy. Soc. **170A**, 469 (1939).
[5] A. F. Devonshire, Proc. Roy. Soc. **174A**, 102 (1940).
[6] J. Corner and J. E. Lennard-Jones, Proc. Roy. Soc. **178A**, 401 (1941).

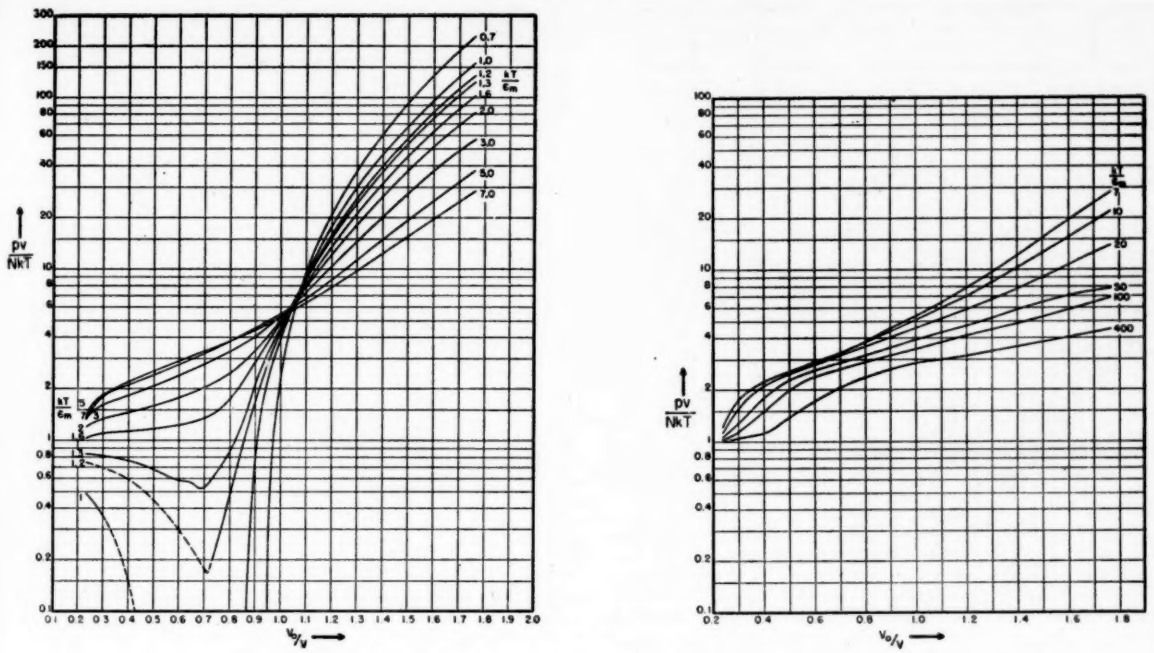

(a) (b)

FIG. 2. Compressibility *vs.* reduced density, $v_0/v = Nr_0^3/v$. The curves are isotherms and are labeled with the values of the reduced temperature, kT/ϵ_m.

which should be tractable with the help of high speed computing devices. Kirkwood[7] has shown that the LJD treatment represents the first approximation to these equations, and, as such, warrants careful consideration. From the utilitarian viewpoint, the LJD treatment provides the best estimates of PVT properties for gases and liquids at very high pressure (and even at high temperatures) where accurate experimental data are hard to obtain.

To facilitate the application of this theory we have prepared a rather complete table of the reduced equation of state together with tables of all the pertinent thermodynamic properties. Comparisons with experimental results are unsatisfactory in the critical region but improve at high densities. The numerical integrations were carried out by Mrs. Marjòrie S. Herrick with the use of the International Business Machines Corporation's 602-A unit and auxiliary equipment.

The equation of state of gases and liquids is completely determined by the law of force between the molecules. For spherical non-polar molecules it has been shown that the energy of interaction between a pair of molecules can be represented satisfactorily by the Lennard-Jones type potential:

$$\epsilon(r) = 4\epsilon_m[(r_0/r)^{12} - (r_0/r)^6]. \qquad (1)$$

Here ϵ_m is the maximum energy of interaction, and r_0 is the low temperature collision diameter, i.e., that value of r for which $\epsilon(r) = 0$. Experimentally it appears that hydrogen and helium molecules are somewhat more compressible than would be indicated by a repulsion energy varying as the inverse twelfth power of the separation. But with these exceptions, the Lennard-Jones potential seems to apply to all molecules which are reasonably non-polar and spherical. The equation of state under all conditions can then be

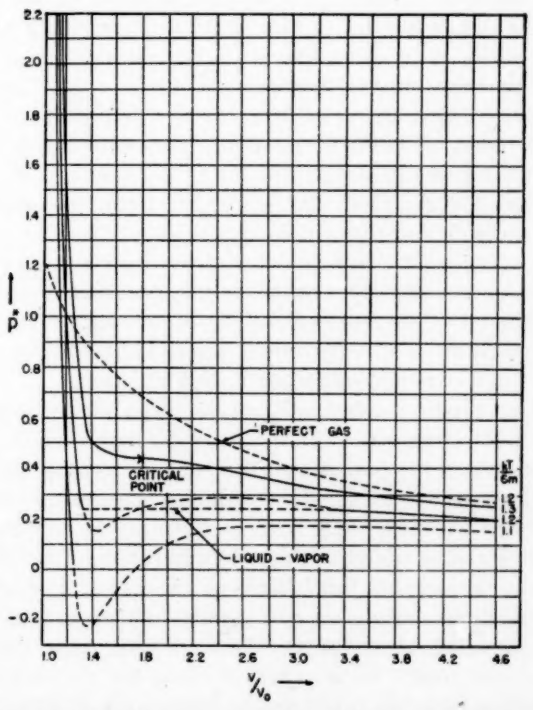

FIG. 3. Reduced pressure *vs.* reduced volume. The curves are isotherms and are labeled with the values of the reduced temperature kT/ϵ_m.

[7] J. G. Kirkwood, J. Chem. Phys. 18, 380 (1950).

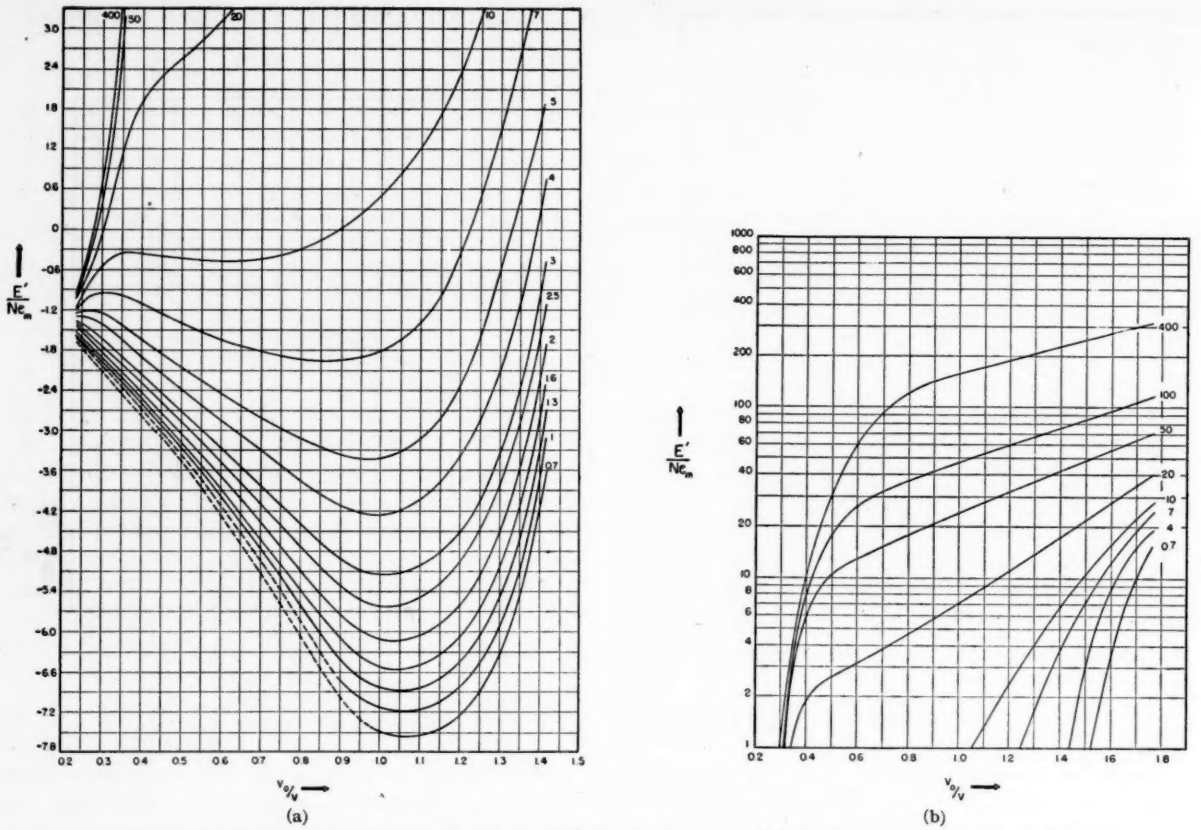

FIG. 4. Reduced internal energy of gas imperfection, $E'/N\epsilon_m$, *vs.* reduced density. The curves are isotherms and are labeled with the values of the reduced temperature, kT/ϵ_m.

expressed in terms of the two parameters ϵ_m and r_0. From the properties of the classical phase integral it can easily be shown that an intermolecular potential of this form implies that pv/NkT for any gas can be expressed as a universal function of v/Nr_0^3 and kT/ϵ_m. The theory of Lennard-Jones and Devonshire provides a method of calculating this universal function in the region of dense gases and liquids. In order to compare the numerical results obtained with experimental values it is necessary to have values of the two force constants. These constants have recently been obtained from experimentally determined values of viscosity.[8] In the comparisons with experiment discussed below we use the force constants obtained in this manner.

Two minor improvements have been made here in the LJD treatment: (1) In the original treatment the variation of the potential with distance from the center of the cage was assumed to be due entirely to the molecules in the first shell, i.e., to the nearest neighbors. Here we have added to the potential function the effect of the second and third shells of molecules. The additional shells contain six and twenty-four molecules and are situated at distances $\sqrt{2}a$ and $\sqrt{3}a$, respectively, from the center of the cage, a being the distance between nearest neighbors in the lattice. (2) In obtaining the partition function it is necessary to carry out an integration over a cell. Lennard-Jones and Devonshire arbitrarily took this cell to be a sphere of radius $0.5a$. Actually the range of integration should be a cell whose

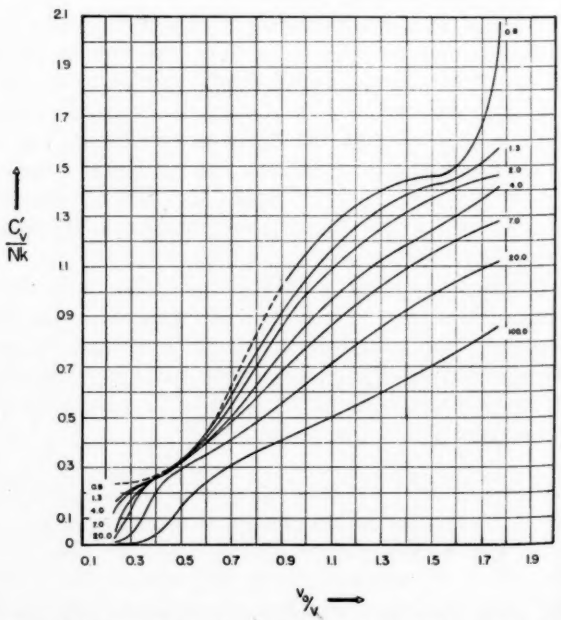

FIG. 5. Reduced specific heat of gas imperfection, c_v'/Nk, *vs.* reduced density. The curves are isotherms and are labeled with the value of the reduced temperature, kT/ϵ_m.

[8] Hirschfelder, Bird, and Spotz, Chem. Rev. 44, 205 (1949).

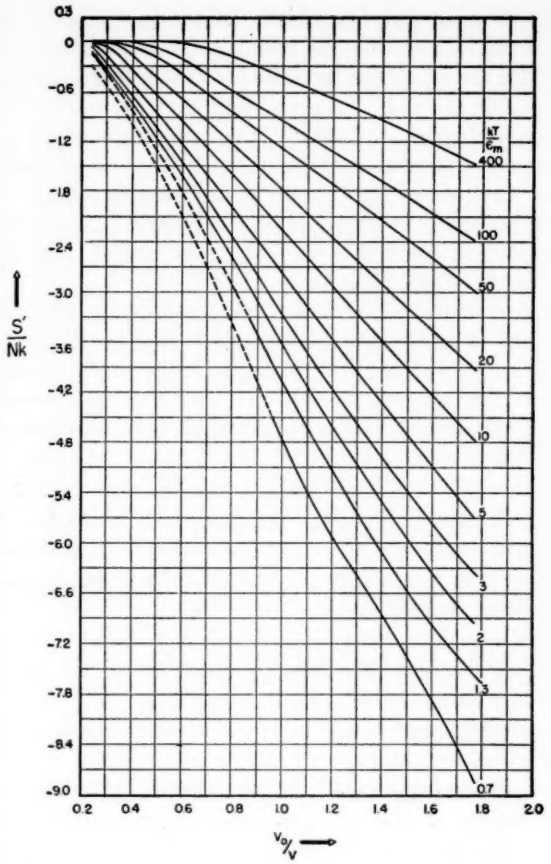

FIG. 6. Reduced entropy of gas imperfection, S'/Nk, *vs.* reduced density. The curves are isotherms and are labeled with the value of the reduced temperature, kT/ϵ_m.

volume is equal to the specific volume of the liquid. This gives us a sphere of radius $0.55267a$. Since throughout most of the region involved in the present tables the potential is effectively infinite at $0.5a$, this extension of the size of the cell does not affect the numerical results more than a few percent.

Corresponding to Eq. (50) of reference 1, we have† [9]

$$pv/NkT=\{1-(12\epsilon_m/kT)[2.4090(v_0/v)^2 -2.0219(v_0/v)^4]-(48\epsilon_m/kT)[(v_0/v)^2(g_M/G) -(v_0/v)^4(g_L/G)]\}. \quad (2)$$

Here ϵ_m is the parameter corresponding to the Λ of LJD,

$$\Lambda=12\epsilon_m, \quad (3)$$

while v_0 is related to the other parameter of the potential function by

$$v_0=Nr_0^3. \quad (4)$$

It is convenient to express r in terms of the dimensionless parameter, $y=(r/a)^2$. The functions G, g_L, and g_M were obtained by numerical integration from the following formulas:

$$G=\int_0^{0.30544} y^{\frac{1}{2}}e^{-[\psi(r)-\psi(0)]/kT}dy \quad (5)$$

$$g_L=\int_0^{0.30544} y^{\frac{1}{2}}L(y)e^{-[\psi(r)-\psi(0)]/kT}dy \quad (6)$$

$$g_M=\int_0^{0.30544} y^{\frac{1}{2}}M(y)e^{-[\psi(r)-\psi(0)]/kT}dy \quad (7)$$

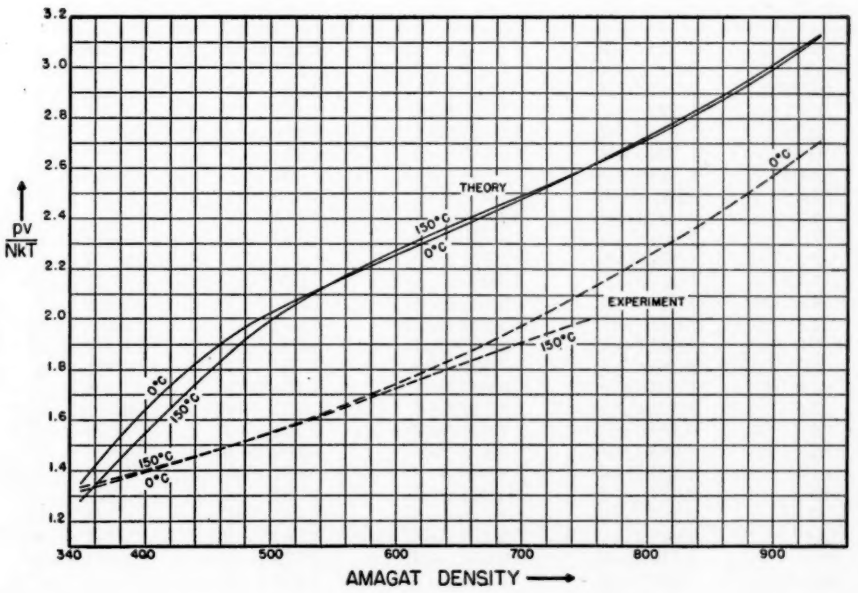

FIG. 7. Calculated and experimental values of the compressibility of hydrogen. Values of the compressibility, pv/NkT, are plotted *vs.* the density in Amagat units (ratio of the given density to the density of the same gas at 0°C and 1 atmos.). The solid lines are theoretical isotherms interpolated from Table V, and the dashed lines are isotherms taken directly from the experimental data of Michels and Goudeket (see reference 15).

† The numbers 2.4090 and 2.0219 appearing in the brackets were used rather than the rounded values of 2.4 and 2 used by LJD. These numbers were obtained from Lennard-Jones and Ingham (see reference 9).

[9] J. E. Lennard-Jones and A. E. Ingham, Proc. Roy. Soc. **107A**, 636 (1925).

TABLE I. Parameter values for which the integrands of g_L and g_M are large at the boundary of the cage.

v/v_0	kT/ϵ_m	v/v_0	kT/ϵ_m	v/v_0	kT/ϵ_m
4.2426	All entries	1.9799	$\geq$ 50	1.4142	$\geq$400
3.5355	$\geq$ 1.8	1.8385	$\geq$ 50	1.2728	$\geq$400
2.8284	$\geq$ 4	1.7678	$\geq$ 50	1.1314	$\geq$400
2.4749	$\geq$ 7	1.6971	$\geq$ 50	1.0607	$\geq$400
2.1213	$\geq$20	1.5556	$\geq$100	0.9899	$\geq$400

where

$$\psi(r)-\psi(0)=12\epsilon_m[(v_0/v)^4L(y)-2(v_0/v)^2M(y)] \quad (8)$$

$$L(y)=l(y)+(1/128)l(y/2)+(2/729)l(y/3) \quad (9)$$

$$M(y)=m(y)+(1/16)m(y/2)+(2/27)m(y/3) \quad (10)$$

$$l(y)=(1+12y+25.2y^2+12y^3+y^4)(1-y)^{-10}-1 \quad (11)$$

$$m(y)=(1+y)(1-y)^{-4}-1. \quad (12)$$

In their original treatment Lennard-Jones and Devonshire considered only the first shell of neighboring molecules. Thus they neglected the second and third terms of Eqs. (9) and (10) which result from taking the second and third shells into consideration. As a result, they used l and m in place of L and M in Eqs. (6) to (8), and obtained the integrals g, g_l, and g_m corresponding to our G, g_L, and g_M.

Simpson's rule was used in evaluating the integrals; the interval being divided into a sufficient number of strips so as to give from 15 to 30 non-negligible values of the integrand. Special treatment was required near $y=0$ for the integral G because here the integrand varies as $y^{\frac{1}{2}}$. For the high values of temperature and volume which are given in Table I, the integrands of g_L and g_M are of appreciable magnitude for $y>0.30544$. Under these conditions the "cage" or free-volume model for the equation of state is likely to become a bad approximation. The quantities G, g_L, g_M, and pv/NkT are presented in Tables II to V.

Values of the one shell integrals g, g_l, and g_m as evaluated by Prigogine and Garikian[10] and by Hill[11] are given in Table VI. For Λ/kT equal to 9 and 10 Lennard-Jones and Devonshire[1] made calculations for the same specific volumes, and their results were in agreement with the results of Prigogine and Garikian. A comparison is made in Table VII of selected values of the integrals calculated by Prigogine and Garikian, by Lennard-Jones and Devonshire, and our calculations. The excellent agreement serves as a check on our computational accuracy.

For certain values of the reduced variables, particularly for high densities, the inclusion of the second and third shells of neighboring molecules in the calculation of the integrals has an effect which is by no means negligible. Our three shell integrals are compared with the one shell integrals in Tables VII and VIII. Although the values of the one-shell and three-shell integrals differ considerably, the thermodynamic properties (ex-

TABLE II. A tabulation of G.

kT/ϵ_m \ v/v_0 \ $(v/v_0)^2$	0.5657 \ 0.320	0.6364 \ 0.405	0.7071 \ 0.5	0.8485 \ 0.72	0.9899 \ 0.98	1.0607 \ 1.125
0.70	4.820 (−6)	1.043 (−5)	2.187 (−5)	7.924 (−5)	2.406 (−4)	4.022 (−4)
0.75	5.371 (−6)	1.164 (−5)	2.422 (−5)	8.600 (−5)	2.635 (−4)	4.550 (−4)
0.80	5.942 (−6)	1.288 (−5)	2.665 (−5)	9.440 (−5)	2.868 (−4)	4.922 (−4)
0.85	6.530 (−6)	1.416 (−5)	2.715 (−5)	1.030 (−4)	3.103 (−4)	5.296 (−4)
0.90	7.129 (−6)	1.540 (−5)	3.171 (−5)	1.117 (−4)	3.341 (−4)	5.671 (−4)
0.95	7.746 (−6)	1.680 (−5)	3.435 (−5)	1.206 (−4)	3.581 (−4)	6.048 (−4)
1.00	8.375 (−6)	1.816 (−5)	3.704 (−5)	1.296 (−4)	3.824 (−4)	6.425 (−4)
1.05	9.019 (−6)	1.956 (−5)	3.980 (−5)	1.388 (−4)	4.228 (−4)	6.804 (−4)
1.1	9.677 (−6)	2.098 (−5)	4.262 (−5)	1.480 (−4)	4.480 (−4)	7.183 (−4)
1.2	1.104 (−5)	2.396 (−5)	4.843 (−5)	1.670 (−4)	4.987 (−4)	7.944 (−4)
1.3	1.244 (−5)	2.694 (−5)	5.444 (−5)	1.864 (−4)	5.498 (−4)	8.706 (−4)
1.4	1.391 (−5)	3.008 (−5)	6.066 (−5)	2.062 (−4)	6.013 (−4)	9.468 (−4)
1.6	1.696 (−5)	3.665 (−5)	7.364 (−5)	2.468 (−4)	7.052 (−4)	1.099 (−3)
1.8	2.021 (−5)	4.359 (−5)	8.649 (−5)	2.888 (−4)	8.098 (−4)	1.251 (−3)
2.0	2.362 (−5)	5.087 (−5)	1.007 (−4)	3.318 (−4)	9.150 (−4)	1.402 (−3)
2.5	3.289 (−5)	7.039 (−5)	1.384 (−4)	4.595 (−4)	1.178 (−3)	1.774 (−3)
3.0	4.302 (−5)	9.083 (−5)	1.784 (−4)	5.768 (−4)	1.441 (−3)	2.138 (−3)
3.5	5.396 (−5)	1.134 (−4)	2.204 (−4)	6.963 (−4)	1.701 (−3)	2.493 (−3)
4	6.559 (−5)	1.371 (−4)	2.641 (−4)	8.174 (−4)	1.952 (−3)	2.839 (−3)
5	8.983 (−5)	1.872 (−4)	3.699 (−4)	1.063 (−3)	2.460 (−3)	3.504 (−3)
7	1.454 (−4)	2.960 (−4)	5.681 (−4)	1.555 (−3)	3.418 (−3)	4.703 (−3)
10	2.384 (−4)	4.904 (−4)	8.794 (−4)	2.283 (−3)	4.705 (−3)	6.363 (−3)
20	6.162 (−4)	1.146 (−3)	1.947 (−3)	4.485 (−3)	8.400 (−3)	1.081 (−2)
50	1.823 (−3)	3.138 (−3)	4.882 (−3)	9.771 (−3)	1.609 (−2)	1.964 (−2)
100	3.750 (−3)	6.052 (−3)	8.923 (−3)	1.604 (−2)	2.437 (−2)	2.879 (−2)
400	1.251 (−2)	1.768 (−2)	2.333 (−2)	3.535 (−2)	4.759 (−2)	5.362 (−2)

Note.—The number in parentheses is the power of 10 by which the corresponding entry is to be multiplied.

[10] I. Prigogine and G. Garikian, J. Chim. Physique **45**, 273 (1948).
[11] T. L. Hill, J. Phys. and Colloid Chem. **51**, 1219 (1947).

TABLE II.—(*Continued*)

$(v/v_0)^2$ / v/v_0 / kT/ϵ_m	1.28 1.1314	1.62 1.2728	2 1.4142	2.42 1.5556	2.88 1.6971	3.125 1.7678
0.70	6.748 (−4)	1.635 (−3)	3.602 (−3)	7.198 (−3)	1.303 (−2)	1.698 (−2)
0.75	7.301 (−4)	1.744 (−3)	3.780 (−3)	7.415 (−3)	1.318 (−2)	1.703 (−2)
0.80	7.855 (−4)	1.853 (−3)	3.953 (−3)	7.626 (−3)	1.334 (−2)	1.710 (−2)
0.85	8.408 (−4)	1.960 (−3)	4.122 (−3)	7.832 (−3)	1.350 (−2)	1.719 (−2)
0.90	8.961 (−4)	2.066 (−3)	4.286 (−3)	8.033 (−3)	1.366 (−2)	1.729 (−2)
0.95	9.514 (−4)	2.170 (−3)	4.447 (−3)	8.229 (−3)	1.382 (−2)	1.740 (−2)
1.00	1.007 (−3)	2.273 (−3)	4.605 (−3)	8.420 (−3)	1.399 (−2)	1.751 (−2)
1.05	1.061 (−3)	2.374 (−3)	4.759 (−3)	8.608 (−3)	1.415 (−2)	1.763 (−2)
1.1	1.116 (−3)	2.475 (−3)	4.911 (−3)	8.752 (−3)	1.432 (−2)	1.776 (−2)
1.2	1.226 (−3)	2.672 (−3)	5.205 (−3)	9.108 (−3)	1.465 (−2)	1.802 (−2)
1.3	1.334 (−3)	2.865 (−3)	5.488 (−3)	9.450 (−3)	1.497 (−2)	1.830 (−2)
1.4	1.443 (−3)	3.054 (−3)	5.763 (−3)	9.781 (−3)	1.529 (−2)	1.857 (−2)
1.6	1.656 (−3)	3.419 (−3)	6.287 (−3)	1.041 (−2)	1.591 (−2)	1.913 (−2)
1.8	1.866 (−3)	3.771 (−3)	6.742 (−3)	1.100 (−2)	1.650 (−2)	1.968 (−2)
2.0	2.073 (−3)	4.110 (−3)	7.212 (−3)	1.156 (−2)	1.707 (−2)	2.022 (−2)
2.5	2.575 (−3)	4.908 (−3)	8.298 (−3)	1.284 (−2)	1.841 (−2)	2.152 (−2)
3.0	3.056 (−3)	5.611 (−3)	9.282 (−3)	1.400 (−2)	1.962 (−2)	2.272 (−2)
3.5	3.518 (−3)	6.303 (−3)	1.019 (−2)	1.506 (−2)	2.075 (−2)	2.384 (−2)
4	3.963 (−3)	6.955 (−3)	1.103 (−2)	1.603 (−2)	2.179 (−2)	2.489 (−2)
5	4.768 (−3)	8.160 (−3)	1.255 (−2)	1.779 (−2)	2.368 (−2)	2.680 (−2)
7	6.296 (−3)	1.027 (−2)	1.516 (−2)	2.077 (−2)	2.689 (−2)	3.008 (−2)
10	8.299 (−3)	1.292 (−2)	1.837 (−2)	2.439 (−2)	3.079 (−2)	3.407 (−2)
20	1.349 (−2)	1.945 (−2)	2.600 (−2)	3.287 (−2)	3.988 (−2)	4.339 (−2)
50	2.336 (−2)	3.115 (−2)	3.915 (−2)	4.717 (−2)	5.506 (−2)	5.892 (−2)
100	3.331 (−2)	4.243 (−2)	5.149 (−2)	6.030 (−2)	6.871 (−2)	7.269 (−2)
400	5.952 (−2)	7.065 (−2)	8.038 (−2)	8.833 (−2)	9.449 (−2)	9.698 (−2)

TABLE II.—(*Continued*)

$(v/v_0)^2$ / v/v_0 / kT/ϵ_m	3.38 1.8385	3.92 1.9799	4.50 2.1213	6.125 2.4749	8 2.8284	12.5 3.5355	18 4.2426
0.70	2.167 (−2)	3.331 (−2)	4.785 (−2)	9.401 (−2)	1.466 (−1)	2.421 (−1)	3.081 (−1)
0.75	2.156 (−2)	3.265 (−2)	4.630 (−2)	8.883 (−2)	1.366 (−1)	2.226 (−1)	2.829 (−1)
0.80	2.149 (−2)	3.212 (−2)	4.503 (−2)	8.463 (−2)	1.285 (−1)	2.072 (−1)	2.628 (−1)
0.85	2.146 (−2)	3.169 (−2)	4.400 (−2)	8.116 (−2)	1.218 (−1)	1.946 (−1)	2.465 (−1)
0.90	2.145 (−2)	3.135 (−2)	4.314 (−2)	7.827 (−2)	1.163 (−1)	1.842 (−1)	2.330 (−1)
0.95	2.147 (−2)	3.108 (−2)	4.242 (−2)	7.583 (−2)	1.117 (−1)	1.755 (−1)	2.217 (−1)
1.00	2.151 (−2)	3.087 (−2)	4.181 (−2)	7.375 (−2)	1.078 (−1)	1.681 (−1)	2.121 (−1)
1.05	2.156 (−2)	3.070 (−2)	4.130 (−2)	7.196 (−2)	1.044 (−1)	1.618 (−1)	2.039 (−1)
1.1	2.163 (−2)	3.057 (−2)	4.087 (−2)	7.041 (−2)	1.014 (−1)	1.563 (−1)	1.968 (−1)
1.2	2.179 (−2)	3.040 (−2)	4.020 (−2)	6.788 (−2)	9.662 (−2)	1.474 (−1)	1.851 (−1)
1.3	2.198 (−2)	3.032 (−2)	3.971 (−2)	6.592 (−2)	9.287 (−2)	1.404 (−1)	1.760 (−1)
1.4	2.219 (−2)	3.030 (−2)	3.937 (−2)	6.438 (−2)	8.989 (−2)	1.348 (−1)	1.687 (−1)
1.6	2.264 (−2)	3.041 (−2)	3.897 (−2)	6.216 (−2)	8.551 (−2)	1.266 (−1)	1.578 (−1)
1.8	2.312 (−2)	3.064 (−2)	3.882 (−2)	6.071 (−2)	8.252 (−2)	1.208 (−1)	1.502 (−1)
2.0	2.360 (−2)	3.094 (−2)	3.884 (−2)	5.975 (−2)	8.041 (−2)	1.167 (−1)	1.445 (−1)
2.5	2.481 (−2)	3.184 (−2)	3.928 (−2)	5.856 (−2)	7.736 (−2)	1.104 (−1)	1.354 (−1)
3.0	2.597 (−2)	3.282 (−2)	3.998 (−2)	5.830 (−2)	7.599 (−2)	1.070 (−1)	1.300 (−1)
3.5	2.707 (−2)	3.381 (−2)	4.080 (−2)	5.848 (−2)	7.544 (−2)	1.051 (−1)	1.266 (−1)
4	2.810 (−2)	3.478 (−2)	4.165 (−2)	5.890 (−2)	7.535 (−2)	1.040 (−1)	1.242 (−1)
5	3.002 (−2)	3.662 (−2)	4.335 (−2)	6.006 (−2)	7.587 (−2)	1.031 (−1)	1.211 (−1)
7	3.332 (−2)	3.991 (−2)	4.653 (−2)	6.275 (−2)	7.794 (−2)	1.032 (−1)	1.180 (−1)
10	3.738 (−2)	4.403 (−2)	5.064 (−2)	6.663 (−2)	8.140 (−2)	1.043 (−1)	1.161 (−1)
20	4.689 (−2)	5.382 (−2)	6.060 (−2)	7.653 (−2)	9.010 (−2)	1.072 (−1)	1.141 (−1)
50	6.272 (−2)	7.006 (−2)	7.693 (−2)	9.115 (−2)	1.007 (−1)	1.100 (−1)	1.131 (−1)
100	7.648 (−2)	8.338 (−2)	8.930 (−2)	9.992 (−2)	1.060 (−1)	1.112 (−1)	1.128 (−1)
400	9.913 (−2)	1.026 (−1)	1.051 (−1)	1.089 (−1)	1.108 (−1)	1.122 (−1)	1.126 (−1)

TABLE III. A tabulation of g_L.

$(v/v_0)^2$ / v/v_0 / kT/ϵ_m	0.32 0.5657	0.405 0.6364	0.50 0.7071	0.72 0.8485	0.98 0.9899	1.125 1.0607
0.70	4.21 (−8)	1.91 (−7)	6.283 (−7)	5.135 (−6)	3.204 (−5)	7.421 (−5)
0.75	5.29 (−8)	2.277 (−7)	7.437 (−7)	6.075 (−6)	3.723 (−5)	8.762 (−5)
0.80	6.48 (−8)	2.681 (−7)	8.706 (−7)	7.052 (−6)	4.281 (−5)	9.985 (−5)
0.85	7.79 (−8)	3.121 (−7)	1.009 (−6)	8.108 (−6)	4.879 (−5)	1.128 (−4)
0.90	9.21 (−8)	3.598 (−7)	1.160 (−6)	9.246 (−6)	5.517 (−5)	1.265 (−4)
0.95	1.07 (−7)	4.112 (−7)	1.323 (−6)	1.046 (−5)	6.192 (−5)	1.410 (−4)
1.00	1.24 (−7)	4.665 (−7)	1.499 (−6)	1.177 (−5)	6.904 (−5)	1.561 (−4)
1.05	1.41 (−7)	5.260 (−7)	1.687 (−6)	1.315 (−5)	7.848 (−5)	1.719 (−4)
1.1	1,60 (−7)	5.896 (−7)	1.888 (−6)	1.461 (−5)	8.640 (−5)	1.884 (−4)
1.2	2.01 (−7)	7.296 (−7)	2.330 (−6)	1.780 (−5)	1.033 (−4)	2.234 (−4)
1.3	2.460 (−7)	8.871 (−7)	2.825 (−6)	2.131 (−5)	1.217 (−4)	2.610 (−4)
1.4	2.965 (−7)	1.063 (−6)	3.374 (−6)	2.517 (−5)	1.415 (−4)	3.010 (−4)
1.6	4.131 (−7)	1.472 (−6)	4.637 (−6)	3.389 (−5)	1.852 (−4)	3.883 (−4)
1.8	5.521 (−7)	1.959 (−6)	6.163 (−6)	4.397 (−5)	2.342 (−4)	4.845 (−4)
2.0	7.148 (−7)	2.527 (−6)	7.874 (−6)	5.539 (−5)	2.882 (−4)	5.892 (−4)
2.5	1.233 (−6)	4.315 (−6)	1.318 (−5)	9.174 (−5)	4.442 (−4)	8.845 (−4)
3.0	1.922 (−6)	6.681 (−6)	1.999 (−5)	1.344 (−4)	6.275 (−4)	1.223 (−3)
3.5	2.791 (−6)	9.561 (−6)	2.834 (−5)	1.849 (−4)	8.357 (−4)	1.599 (−3)
4	3.846 (−6)	1.302 (−5)	3.826 (−5)	2.428 (−4)	1.067 (−3)	2.010 (−3)
5	6.574 (−6)	2.171 (−5)	6.460 (−5)	3.802 (−4)	1.589 (−3)	2.919 (−3)
7	1.436 (−5)	4.640 (−5)	1.326 (−4)	7.331 (−4)	2.840 (−3)	5.028 (−3)
10	3.246 (−5)	1.039 (−4)	2.790 (−4)	1.430 (−3)	5.120 (−3)	8.742 (−3)
20	1.526 (−4)	4.420 (−4)	1.103 (−3)	4.825 (−3)	1.499 (−2)	2.407 (−2)
50	9.931 (−4)	2.571 (−3)	5.733 (−3)	2.059 (−2)	5.483 (−2)	8.275 (−2)
100	3.619 (−3)	8.556 (−3)	1.762 (−2)	5.577 (−2)	1.358 (−1)	1.980 (−1)
400	3.468 (−2)	7.029 (−2)	1.278 (−1)	3.371 (−1)	7.268 (−1)	1.011 (0)

Note.—The number in parentheses is the power of 10 by which the entry is to be multiplied.

TABLE III.—(*Continued*)

$(v/v_0)^2$ / v/v_0 / kT/ϵ_m	1.28 1.1314	1.62 1.2728	2 1.4142	2.42 1.5556	2.88 1.6971	3.125 1.7678
0.70	1.666 (−4)	7.067 (−4)	2.527 (−3)	7.652 (−3)	1.989 (−2)	3.046 (−2)
0.75	1.902 (−4)	7.906 (−4)	2.760 (−3)	8.154 (−3)	2.071 (−2)	3.138 (−2)
0.80	2.152 (−4)	8.777 (−4)	2.998 (−3)	8.658 (−3)	2.154 (−2)	3.234 (−2)
0.85	2.415 (−4)	9.675 (−4)	3.237 (−3)	9.165 (−3)	2.238 (−2)	3.331 (−2)
0.90	2.691 (−4)	1.060 (−3)	3.481 (−3)	9.673 (−3)	2.323 (−2)	3.431 (−2)
0.95	2.979 (−4)	1.155 (−3)	3.727 (−3)	1.018 (−2)	2.408 (−2)	3.531 (−2)
1.00	3.278 (−4)	1.252 (−3)	3.975 (−3)	1.070 (−2)	2.493 (−2)	3.634 (−2)
1.05	3.589 (−4)	1,352 (−3)	4.227 (−3)	1.121 (−2)	2.579 (−2)	3.737 (−2)
1.1	3.912 (−4)	1.454 (−3)	4.481 (−3)	1.172 (−2)	2.665 (−2)	3.840 (−2)
1.2	4.589 (−4)	1.663 (−3)	4.998 (−3)	1.276 (−2)	2.838 (−2)	4.050 (−2)
1.3	5.307 (−4)	1.881 (−3)	5.525 (−3)	1.380 (−2)	3.012 (−2)	4.262 (−2)
1.4	6.065 (−4)	2.106 (−3)	6.058 (−3)	1.485 (−2)	3.187 (−2)	4.476 (−2)
1.6	7.693 (−4)	2.576 (−3)	7.150 (−3)	1.696 (−2)	3.538 (−2)	4.908 (−2)
1.8	9.458 (−4)	3.070 (−3)	8.267 (−3)	1.909 (−2)	3.891 (−2)	5.342 (−2)
2.0	1.135 (−3)	3.585 (−3)	9.408 (−3)	2.124 (−2)	4.246 (−2)	5.780 (−2)
2.5	1.657 (−3)	4.953 (−3)	1.236 (−2)	2.668 (−2)	5.137 (−2)	6.880 (−2)
3.0	2.241 (−3)	6.418 (−3)	1.541 (−2)	3.221 (−2)	6.035 (−2)	7.988 (−2)
3.5	2.879 (−3)	7.964 (−3)	1.855 (−2)	3.781 (−2)	6.937 (−2)	9.100 (−2)
4	3.562 (−3)	9.578 (−3)	2.177 (−2)	4.347 (−2)	7.844 (−2)	1.022 (−1)
5	5.048 (−3)	1.298 (−2)	2.841 (−2)	5.497 (−2)	9.670 (−2)	1.246 (−1)
7	8.399 (−3)	2.031 (−2)	4.225 (−2)	7.848 (−2)	1.336 (−1)	1.698 (−1)
10	1.412 (−2)	3.225 (−2)	6.407 (−2)	1.147 (−1)	1.897 (−1)	2.382 (−1)
20	3.683 (−2)	7.676 (−2)	1.421 (−1)	2.407 (−1)	3.813 (−1)	4.702 (−1)
50	1.200 (−1)	2.293 (−1)	3.977 (−1)	6.412 (−1)	9.769 (−1)	1.184 (−1)
100	2.788 (−1)	5.089 (−1)	8.524 (−1)	1.333 (0)	1.948 (0)	2.295 (0)
400	1.361 (0)	2.231 (0)	3.208 (0)	4.135 (0)	4.923 (0)	5.257 (0)

TABLE III.—(*Continued*)

$(v/v_0)^2$ / kT/ϵ_m	3.38	3.92	4.5	6.125	8	12.5	18
v/v_0	1.8385	1.9799	2.1213	2.4749	2.8284	3.5355	4.2426
0.70	4.523 (−2)	9.180 (−2)	1.693 (−1)	5.674 (−1)	1.377	4.640	10.42
0.75	4.615 (−2)	9.202 (−2)	1.672 (−1)	5.453 (−1)	1.302	4.323	9.684
0.80	4.713 (−2)	9.252 (−2)	1.659 (−1)	5.282 (−1)	1.243	4.075	9.104
0.85	4.817 (−2)	9.324 (−2)	1.652 (−1)	5.149 (−1)	1.196	3.877	8.640
0.90	4.925 (−2)	9.414 (−2)	1.651 (−1)	5.046 (−1)	1.159	3.717	8.265
0.95	5.037 (−2)	9.518 (−2)	1.653 (−1)	4.966 (−1)	1.129	3.587	7.958
1.00	5.152 (−2)	9.633 (−2)	1.658 (−1)	4.904 (−1)	1.104	3.480	7.703
1.05	5.270 (−2)	9.758 (−2)	1.666 (−1)	4.857 (−1)	1.084	3.391	7.490
1.1	5.389 (−2)	9.891 (−2)	1.677 (−1)	4.823 (−1)	1.068	3.317	7.311
1.2	5.633 (−2)	1.018 (−1)	1.703 (−1)	4.784 (−1)	1.045	3.205	7.032
1.3	5.882 (−2)	1.048 (−1)	1.734 (−1)	4.775 (−1)	1.030	3.127	6.828
1.4	6.135 (−2)	1.080 (−1)	1.769 (−1)	4.787 (−1)	1.022	3.073	6.678
1.6	6.649 (−2)	1.148 (−1)	1.849 (−1)	4.857 (−1)	1.019	3.017	6.483
1.8	7.171 (−2)	1.218 (−1)	1.936 (−1)	4.967 (−1)	1.028	3.005	6.377
2.0	7.698 (−2)	1.290 (−1)	2.028 (−1)	5.104 (−1)	1.044	3.021	6.322
2.5	9.029 (−2)	1.475 (−1)	2.271 (−1)	5.510 (−1)	1.103	3.125	6.299
3.0	1.037 (−1)	1.663 (−1)	2.524 (−1)	5.966 (−1)	1.176	3.275	6.343
3.5	1.172 (−1)	1.854 (−1)	2.781 (−1)	6.447 (−1)	1.257	3.440	6.407
4	1.307 (−1)	2.045 (−1)	3.041 (−1)	6.942 (−1)	1.341	3.608	6.476
5	1.579 (−1)	2.430 (−1)	3.565 (−1)	7.954 (−1)	1.515	3.931	6.604
7	2.125 (−1)	3.202 (−1)	4.619 (−1)	1.001	1.871	4.478	6.802
10	2.949 (−1)	4.363 (−1)	6.204 (−1)	1.310	2.383	5.075	6.991
20	5.730 (−1)	8.254 (−1)	1.148	2.283	3.710	6.079	7.261
50	1.418	1.961	2.581	4.183	5.480	6.910	7.452
100	2.658	3.395	4.099	5.512	6.406	7.237	7.521
400	5.552	6.037	6.406	6.978	7.267	7.501	7.574

TABLE IV. A tabulation of g_M.

(v/v_0) / kT/ϵ_m	0.32	0.405	0.5	0.72	0.98	1.125
v/v_0	0.5657	0.6364	0.7071	0.8485	0.9899	1.0607
0.70	1.0 (−8)	4.50 (−8)	1.48 (−7)	1.19 (−6)	7.235 (−6)	1.644 (−5)
0.75	1.2 (−8)	5.37 (−8)	1.75 (−7)	1.41 (−6)	8.381 (−6)	1.936 (−5)
0.80	1.5 (−8)	6.33 (−8)	2.05 (−7)	1.63 (−6)	9.608 (−6)	2.198 (−5)
0.85	1.8 (−8)	7.37 (−8)	2.373 (−7)	1.87 (−6)	1.092 (−5)	2.474 (−5)
0.90	2.17 (−8)	8.50 (−8)	2.725 (−7)	2.129 (−6)	1.230 (−5)	2.765 (−5)
0.95	2.54 (−8)	9.71 (−8)	3.104 (−7)	2.406 (−6)	1.377 (−5)	3.069 (−5)
1.00	2.92 (−8)	1.10 (−7)	3.515 (−7)	2.702 (−6)	1.531 (−5)	3.386 (−5)
1.05	3.33 (−8)	1.24 (−7)	3.952 (−7)	3.015 (−6)	1.738 (−5)	3.717 (−5)
1.1	3.77 (−8)	1.39 (−7)	4.419 (−7)	3.344 (−6)	1.908 (−5)	4.060 (−5)
1.2	4.75 (−8)	1.72 (−7)	5.444 (−7)	4.060 (−6)	2.270 (−5)	4.783 (−5)
1.3	5.81 (−8)	2.087 (−7)	6.590 (−7)	4.846 (−6)	2.660 (−5)	5.553 (−5)
1.4	7.00 (−8)	2.498 (−7)	7.858 (−7)	5.706 (−6)	3.076 (−5)	6.368 (−5)
1.6	9.75 (−8)	3.450 (−7)	1.077 (−6)	7.637 (−6)	3.988 (−5)	8.121 (−5)
1.8	1.30 (−7)	4.583 (−7)	1.427 (−6)	9.850 (−6)	4.997 (−5)	1.003 (−4)
2.0	1.68 (−7)	5.900 (−7)	1.818 (−6)	1.234 (−5)	6.099 (−5)	1.207 (−4)
2.5	2.896 (−7)	1.002 (−6)	3.020 (−6)	2.019 (−5)	9.215 (−5)	1.772 (−4)
3.0	4.498 (−7)	1.545 (−6)	4.549 (−6)	2.922 (−5)	1.279 (−4)	2.401 (−4)
3.5	6.510 (−7)	2.201 (−6)	6.407 (−6)	3.973 (−5)	1.676 (−4)	3.084 (−4)
4	8.948 (−7)	2.984 (−6)	8.593 (−6)	5.163 (−5)	2.108 (−4)	3.811 (−4)
5	1.521 (−6)	4.932 (−6)	1.435 (−5)	7.926 (−5)	3.058 (−4)	5.372 (−4)
7	3.286 (−6)	1.037 (−5)	2.881 (−5)	1.477 (−4)	5.224 (−4)	8.805 (−4)
10	7.315 (−6)	2.276 (−5)	5.889 (−5)	2.761 (−4)	8.921 (−4)	1.442 (−3)
20	3.297 (−5)	9.123 (−5)	2.161 (−4)	8.412 (−4)	2.302 (−3)	3.465 (−3)
50	1.956 (−4)	4.724 (−4)	9.783 (−4)	3.005 (−3)	6.827 (−3)	9.523 (−3)
100	6.446 (−4)	1.394 (−3)	2.618 (−3)	6.880 (−3)	1.395 (−2)	1.860 (−2)
400	4.621 (−3)	8.233 (−3)	1.318 (−2)	2.724 (−2)	4.671 (−2)	5.834 (−2)

Note.—The number in parentheses is the power of 10 by which the corresponding entry is to be multiplied.

TABLE IV.—(*Continued*)

$(v/v_0)^2$ / v/v_0 / kT/ϵ_m	1.28 1.1314	1.62 1.2728	2.0 1.4148	2.42 1.5556	2.88 1.6971	3.125 1.7678
0.70	3.610 (−5)	1.449 (−4)	4.848 (−4)	1.364 (−3)	3.280 (−3)	4.828 (−3)
0.75	4.104 (−5)	1.611 (−4)	5.258 (−4)	1.442 (−3)	3.388 (−3)	4.934 (−3)
0.80	4.623 (−5)	1.778 (−4)	5.671 (−4)	1.520 (−3)	3.496 (−3)	5.043 (−3)
0.85	5.165 (−5)	1.949 (−4)	6.085 (−4)	1.598 (−3)	3.605 (−3)	5.155 (−3)
0.90	5.729 (−5)	2.124 (−4)	6.502 (−4)	1.675 (−3)	3.714 (−3)	5.269 (−3)
0.95	6.315 (−5)	2.302 (−4)	6.921 (−4)	1.752 (−3)	3.823 (−3)	5.385 (−3)
1.00	6.921 (−5)	2.484 (−4)	7.342 (−4)	1.828 (−3)	3.932 (−3)	5.502 (−3)
1.05	7.548 (−5)	2.668 (−4)	7.762 (−4)	1.904 (−3)	4.041 (−3)	5.620 (−3)
1.1	8.196 (−5)	2.855 (−4)	8.185 (−4)	1.979 (−3)	4.149 (−3)	5.739 (−3)
1.2	9.544 (−5)	3.238 (−4)	9.033 (−4)	2.130 (−3)	4.365 (−3)	5.977 (−3)
1.3	1.096 (−4)	3.630 (−4)	9.883 (−4)	2.279 (−3)	4.579 (−3)	6.215 (−3)
1.4	1.244 (−4)	4.031 (−4)	1.074 (−3)	2.426 (−3)	4.791 (−3)	6.453 (−3)
1.6	1.558 (−4)	4.854 (−4)	1.245 (−3)	2.718 (−3)	5.210 (−3)	6.926 (−3)
1.8	1.892 (−4)	5.702 (−4)	1.416 (−3)	3.006 (−3)	5.622 (−3)	7.393 (−3)
2.0	2.246 (−4)	6.571 (−4)	1.588 (−3)	3.290 (−3)	6.027 (−3)	7.854 (−3)
2.5	3.198 (−4)	8.811 (−4)	2.016 (−3)	3.982 (−3)	7.010 (−3)	8.977 (−3)
3.0	4.229 (−4)	1.112 (−3)	2.441 (−3)	4.655 (−3)	7.956 (−3)	1.006 (−2)
3.5	5.323 (−4)	1.348 (−3)	2.863 (−3)	5.310 (−3)	8.870 (−3)	1.110 (−2)
4	6.467 (−4)	1.587 (−3)	3.281 (−3)	5.950 (−3)	9.756 (−3)	1.212 (−2)
5	8.870 (−4)	2.071 (−3)	4.104 (−3)	7.188 (−3)	1.145 (−2)	1.405 (−2)
7	1.398 (−3)	3.045 (−3)	5.700 (−3)	9.529 (−3)	1.462 (−2)	1.765 (−2)
10	2.204 (−3)	4.496 (−3)	7.980 (−3)	1.278 (−2)	1.895 (−2)	2.255 (−2)
20	4.968 (−3)	9.096 (−3)	1.482 (−2)	2.219 (−2)	3.117 (−2)	3.625 (−2)
50	1.277 (−2)	2.097 (−2)	3.141 (−2)	4.400 (−2)	5.862 (−2)	6.663 (−2)
100	2.401 (−2)	3.701 (−2)	5.281 (−2)	7.113 (−2)	9.129 (−2)	1.017 (−1)
400	7.106 (−2)	9.849 (−2)	1.257 (−1)	1.496 (−1)	1.692 (−1)	1.772 (−1)

TABLE IV.—(*Continued*)

(v/v_0) / v/v_0 / kT/ϵ_m	3.38 1.8385	3.92 1.9799	4.5 2.1213	6.125 2.4749	8 2.8284	12.5 3.5355	18 4.2426
0.70	6.889 (−3)	1.291 (−2)	2.199 (−2)	6.075 (−2)	1.229 (−1)	2.969 (−1)	4.979 (−1)
0.75	6.970 (−3)	1.283 (−2)	2.152 (−2)	5.785 (−2)	1.150 (−1)	2.739 (−1)	4.577 (−1)
0.80	7.060 (−3)	1.279 (−2)	2.117 (−2)	5.553 (−2)	1.088 (−1)	2.556 (−1)	4.259 (−1)
0.85	7.160 (−3)	1.278 (−2)	2.091 (−2)	5.367 (−2)	1.038 (−1)	2.409 (−1)	4.002 (−1)
0.90	7.265 (−3)	1.281 (−2)	2.072 (−2)	5.214 (−2)	9.964 (−2)	2.288 (−1)	3.791 (−1)
0.95	7.376 (−3)	1.285 (−2)	2.059 (−2)	5.089 (−2)	9.621 (−2)	2.187 (−1)	3.615 (−1)
1.00	7.490 (−3)	1.291 (−2)	2.050 (−2)	4.986 (−2)	9.333 (−2)	2.103 (−1)	3.467 (−1)
1.05	7.608 (−3)	1.298 (−2)	2.045 (−2)	4.900 (−2)	9.090 (−2)	2.031 (−1)	3.342 (−1)
1.1	7.728 (−3)	1.307 (−2)	2.043 (−2)	4.829 (−2)	8.884 (−2)	1.970 (−1)	3.234 (−1)
1.2	7.975 (−3)	1.327 (−2)	2.046 (−2)	4.720 (−2)	8.556 (−2)	1.871 (−1)	3.059 (−1)
1.3	8.226 (−3)	1.349 (−2)	2.056 (−2)	4.645 (−2)	8.313 (−2)	1.797 (−1)	2.925 (−1)
1.4	8.480 (−3)	1.374 (−2)	2.072 (−2)	4.594 (−2)	8.131 (−2)	1.739 (−1)	2.820 (−1)
1.6	8.993 (−3)	1.427 (−2)	2.115 (−2)	4.545 (−2)	7.894 (−2)	1.659 (−1)	2.667 (−1)
1.8	9.506 (−3)	1.482 (−2)	2.167 (−2)	4.540 (−2)	7.766 (−2)	1.608 (−1)	2.564 (−1)
2.0	1.002 (−2)	1.540 (−2)	2.224 (−2)	4.564 (−2)	7.706 (−2)	1.576 (−1)	2.492 (−1)
2.5	1.127 (−2)	1.685 (−2)	2.380 (−2)	4.691 (−2)	7.728 (−2)	1.542 (−1)	2.385 (−1)
3.0	1.248 (−2)	1.830 (−2)	2.542 (−2)	4.866 (−2)	7.874 (−2)	1.541 (−1)	2.330 (−1)
3.5	1.365 (−2)	1.971 (−2)	2.704 (−2)	5.061 (−2)	8.077 (−2)	1.555 (−1)	2.301 (−1)
4	1.479 (−2)	2.109 (−2)	2.864 (−2)	5.265 (−2)	8.309 (−2)	1.576 (−1)	2.283 (−1)
5	1.697 (−2)	2.374 (−2)	3.175 (−2)	5.677 (−2)	8.806 (−2)	1.625 (−1)	2.267 (−1)
7	2.101 (−2)	2.867 (−2)	3.757 (−2)	6.476 (−2)	9.809 (−2)	1.719 (−1)	2.261 (−1)
10	2.648 (−2)	3.534 (−2)	4.545 (−2)	7.577 (−2)	1.118 (−1)	1.829 (−1)	2.265 (−1)
20	4.171 (−2)	5.371 (−2)	6.709 (−2)	1.052 (−1)	1.446 (−1)	2.020 (−1)	2.281 (−1)
50	7.505 (−2)	9.283 (−2)	1.112 (−1)	1.536 (−1)	1.851 (−1)	2.179 (−1)	2.297 (−1)
100	1.121 (−1)	1.321 (−1)	1.502 (−1)	1.846 (−1)	2.055 (−1)	2.242 (−1)	2.303 (−1)
400	1.843 (−1)	1.958 (−1)	2.044 (−1)	2.175 (−1)	2.241 (−1)	2.293 (−1)	2.309 (−1)

TABLE V. The compressibility factor pv/NkT.

kT/ϵ_m \ $(v/v_0)^2$	0.32	0.405	0.5	0.72	0.98	1.125	1.28	1.62	2	2.42
kT/ϵ_m \ v/v_0	0.5657	0.6364	0.7071	0.8485	0.9899	1.0607	1.1314	1.2728	1.4142	1.5556
0.70	215.9	117.27	64.01	17.650	2.358	−0.8136	−2.642	−3.738	−3.566	−3.066
0.75	202.2	109.97	60.26	17.142	2.695	−0.3818	−1.999	−3.059	−2.948	−2.528
0.80	190.2	103.57	56.97	16.528	2.987	+0.0812	−1.442	−2.472	−2.413	−2.062
0.85	179.6	97.92	54.07	15.984	3.240	0.4862	−0.955	−1.960	−1.947	−1.654
0.90	170.13	92.92	51.49	15.500	3.462	0.8429	−0.5276	−1.511	−1.537	−1.296
0.95	161.66	88.40	49.18	15.065	3.657	1.1593	−0.1491	−1.113	−1.1743	−0.9789
1.00	154.02	84.35	47.10	14.672	3.830	1.4411	+0.1881	−0.759	−0.8515	−0.6961
1.05	147.10	80.68	45.21	14.316	3.886	1.6935	0.4897	−0.443	−0.5627	−0.4427
1.1	140.80	77.355	43.50	13.991	4.018	1.9205	0.7608	−0.1585	−0.3030	−0.191
1.2	129.74	71.525	40.50	13.419	4.245	2.311	1.2272	+0.3309	+0.1444	+0.203
1.3	120.38	66.593	37.953	12.932	4.432	2.634	1.6128	0.7357	0.5151	0.528
1.4	111.33	62.365	35.768	12.510	4.587	2.904	1.9355	1.0750	0.8262	0.803
1.6	99.23	55.492	32.205	11.816	4.826	3.326	2.4417	1.6086	1.3168	1.234
1.8	89.03	50.142	28.521	11.266	4.998	3.636	2.8163	2.0054	1.7135	1.557
2.0	80.866	45.856	27.258	10.817	5.123	3.870	3.1010	2.3090	1.9919	1.807
2.5	66.149	38.120	22.172	9.885	5.310	4.248	3.570	2.816	2.460	2.230
3.0	56.330	33.020	20.435	9.284	5.395	4.458	3.841	3.149	2.741	2.486
3.5	49.300	29.262	18.468	8.838	5.427	4.579	4.006	3.336	2.922	2.653
4	44.015	26.438	16.982	8.488	5.430	4.648	4.110	3.457	3.043	2.766
5	36.676	22.471	14.809	7.963	5.393	4.705	4.253	3.595	3.185	2.901
7	28.074	17.897	12.312	7.281	5.259	4.720	4.283	3.684	3.290	3.009
10	21.584	14.307	10.373	6.659	5.087	4.591	4.212	3.673	3.305	3.035
20	13.735	9.998	7.866	5.688	4.576	4.211	3.920	3.486	3.175	2.942
50	8.717	6.969	5.910	4.624	3.905	3.652	3.444	3.122	2.885	2.702
100	6.733	5.630	4.902	4.000	3.462	3.267	3.104	2.849	2.657	2.499
400	4.476	3.962	3.592	3.096	2.777	2.655	2.543	2.319	2.082	1.856

TABLE V.—(*Continued*)

kT/ϵ_m \ $(v/v_0)^2$	2.88	3.125	3.38	3.92	4.50	6.125	8	12.5	18
kT/ϵ_m \ v/v_0	1.6971	1.7678	1.8385	1.9799	2.1213	2.4749	2.8284	3.5355	4.2426
0.70	−2.535	−2.310	−2.107	−1.760	−1.486	−1.0215	−0.7382	−0.399	−0.1841
0.75	−2.070	−1.877	−1.701	−1.402	−1.165	−0.7626	−0.5168	−0.221	−0.0329
0.80	−1.667	−1.501	−1.349	−1.091	−0.885	−0.5366	−0.3234	−0.0661	+0.0990
0.85	−1.315	−1.172	−1.0407	−0.817	−0.6395	−0.3376	−0.1531	+0.0708	0.2149
0.90	−1.004	−0.8808	−0.7681	−0.575	−0.4219	−0.1613	−0.0021	0.1924	0.3173
0.95	−0.729	−0.6232	−0.5265	−0.360	−0.2282	−0.0040	+0.1329	0.3009	0.4084
1.00	−0.483	−0.3932	−0.3105	−0.168	−0.0547	+0.1371	0.2541	0.3985	0.4897
1.05	−0.2624	−0.1865	−0.1162	+0.005	+0.1015	0.2645	0.3634	0.4865	0.5676
1.1	−0.0634	+0.0002	+0.0590	0.161	0.2427	0.3798	0.4626	0.5664	0.6282
1.2	+0.2803	0.3222	0.3623	0.432	0.4880	0.5804	0.6353	0.7057	0.7411
1.3	0.5663	0.5908	0.6151	0.659	0.6933	0.7489	0.7806	0.8230	0.8340
1.4	0.8067	0.8173	0.8287	0.850	0.8673	0.8922	0.9044	0.9230	0.9113
1.6	1.1887	1.177	1.1684	1.156	1.1453	1.122	1.1035	1.084	1.030
1.8	1.476	1.448	1.425	1.387	1.357	1.297	1.256	1.207	1.115
2.0	1.698	1.658	1.624	1.568	1.522	1.435	1.376	1.304	1.761
2.5	2.077	2.017	1.965	1.878	1.806	1.675	1.586	1.471	1.266
3.0	2.310	2.238	2.176	2.070	1.985	1.826	1.719	1.571	1.305
3.5	2.461	2.383	2.314	2.198	2.104	1.928	1.810	1.633	1.321
4	2.565	2.483	2.410	2.287	2.187	2.001	1.874	1.670	1.323
5	2.691	2.605	2.529	2.398	2.291	2.093	1.957	1.700	1.311
7	2.797	2.708	2.630	2.495	2.385	2.178	2.031	1.682	1.271
10	2.829	2.743	2.666	2.534	2.424	2.217	2.048	1.606	1.219
20	2.760	2.683	2.614	2.494	2.394	2.166	1.901	1.402	1.128
50	2.556	2.492	2.431	2.308	2.178	1.829	1.531	1.191	1.056
100	2.348	2.270	2.188	2.020	1.856	1.520	1.305	1.101	1.029
400	1.661	1.579	1.506	1.387	1.296	1.156	1.085	1.026	1.007

TABLE VI. One shell integrals obtained by Hill and by Prigogine and Garikian.

	Hill*	Prigogine and Garikian**						
Λ/kT	6	7	9	10	12	14	17	20
v/v_0 \ kT/ϵ_m	2	1.714	1.333	1.200	1.00	.857	.706	.600
				Tabulation of g				
1.195	0.00262	0.00208	0.00166	0.00152	0.00122	0.00088	0.00081	0.00060
1.291	0.00395	0.00350	0.00272	0.00247	0.00202	0.00178	0.00162	0.00134
1.414	0.00659	0.00583	0.00513	0.00453	0.00390	0.00348	0.00306	0.00273
1.581	0.0115	0.01070	0.00952	0.00833	0.00820	0.00745	0.00666	0.00672
1.826	0.0213	0.02052	0.01880	0.01880	0.01790	0.01770	0.01790	0.01770
2.236	0.0425	0.04400	0.04350	0.04430	0.04610	0.04820	0.05260	0.05730
2.575	0.0615	0.06290	0.06600	0.06960	0.07440	0.08040	0.09230	0.10670
3.162	0.0930	0.09620	0.10600	0.11200	0.12500	0.14000	0.16800	0.21300
				Tabulation of g_l				
1.195	0.00182	0.00140	0.00100	0.00074	0.00056	0.00042	0.00031	0.00022
1.291	0.00380	0.00278	0.00202	0.00174	0.00130	0.00104	0.00074	0.00058
1.414	0.00865	0.00698	0.00518	0.00457	0.00353	0.00288	0.00216	0.00174
1.581	0.0222	0.01870	0.01480	0.01330	0.01080	0.00940	0.00800	0.00678
1.826	0.0667	0.05980	0.05020	0.04750	0.04170	0.03860	0.03570	0.03330
2.236	0.257	0.24300	0.22500	0.21500	0.21000	0.21000	0.21500	0.22700
2.575	0.583	0.55600	0.53400	0.53800	0.54000	0.56000	0.60800	0.67300
3.162	1.693	1.60000	1.64000	1.67000	1.77000	1.90500	2.18000	2.55000
				Tabulation of g_m				
1.195	0.000333	0.00057	0.000176	0.000156	0.000109	0.0000816	0.0000520	0.0000407
1.291	0.000662	0.00056	0.000379	0.000324	0.000252	0.000194	0.000149	0.000112
1.414	0.00140	0.00120	0.000882	0.000762	0.000639	0.000510	0.000399	0.000335
1.581	0.00325	0.00280	0.00233	0.00213	0.00173	0.00159	0.00134	0.00114
1.826	0.00843	0.00788	0.00614	0.00640	0.00600	0.00530	0.00523	0.00492
2.236	0.0255	0.02570	0.02400	0.02370	0.02380	0.02380	0.02530	0.02700
2.575	0.0478	0.04710	0.04730	0.04860	0.05100	0.05400	0.06040	0.06800
3.162	0.1021	0.10200	0.10800	0.11300	0.12400	0.13700	0.16200	0.19200

* See reference 11.
** See reference 10.

cept entropy) calculated from them do not show correspondingly large differences.

It is convenient to express the pressure in reduced form,

$$p^* = p(\text{atmos.})/p_1 = (pv/NkT)(kT/\epsilon_m)(v_0/v).$$

Here p_1 is the characteristic pressure of the substance defined as

$$p_1 = 136.23(\epsilon_m/k)/r_0^3 \text{ atmos.}$$

Here 136.23 is just the value of the gas constant in units consistent with taking ϵ_m/k in °K and r_0 in angstroms. Figure 1 shows the compressibility factor, pv/NkT, expressed as a function of the reduced pressure for different values of the reduced temperature, $T/(\epsilon_m/k)$. The variation of the compressibility factor with reduced density, $v_0/v = Nr_0^3/v$ for different reduced temperatures is shown in Figs. 2a and 2b.

The critical point is defined as the point at which both $(\partial p/\partial v)_T$ and $(\partial^2 p/\partial v^2)_T$ vanish. By a series of interpolations of the tabular values the critical constants were found to be

$$T_c = 1.30\epsilon_m/k, \tag{13}$$

$$v_c = 1.768v_0 = 0.84(\tfrac{2}{3}\pi N r_0^3), \tag{14}$$

$$p_c = 0.434N\epsilon_m/v_0, \tag{15}$$

$$p_c v_c/NkT_c = 0.591. \tag{16}$$

TABLE VII. Comparison of various calculated values of the integrals g, g_l, g_m.

$kT/\epsilon_m = 1.2$; $\Lambda/kT = 10$						
	LJD* (one shell)			Prigogine and Garikian** (one shell)		
v/v_0	g	g_l	g_m	g	g_l	g_m
1.195	0.00161	0.000747	0.000139	0.00152	0.00074	0.000156
1.414	0.00478	0.00441	0.000762	0.00453	0.00457	0.000762
3.162	0.1125	1.667	0.1126	0.1120	1.670	0.1130
	Calculated by the methods of this report (one shell)			This report (three shells)		
v/v_0	g	g_l	g_m	G	g_L	g_M
1.195	0.001635	0.0007638	0.0001475	0.001878	0.001002	0.000198
1.414	0.004765	0.004455	0.0007688	0.005205	0.004998	0.0009033
3.162	0.11238	1.6734	0.11296	0.12062	2.064	0.1335

* See reference 1.
** See reference 10.

TABLE VIII. Effect of the second and third shells of neighboring molecules on the basic integrals.

			Punched-card calculation (three shells)			Prigogine and Garikian* (one shell)		
v/v_0	Λ/kT	kT/ϵ_m	G	g_L	g_M	g	g_l	g_m
1.195	17	0.706	0.0011159	0.000416	0.0000862	0.00081	0.00031	0.0000520
	12	1.000	0.001576	0.000744	0.000150	0.00122	0.00056	0.000109
	7	1.714	0.002605	0.00276	0.000336	0.00208	0.00140	0.00057
1.414	17	0.706	0.003623	0.00255	0.000490	0.00306	0.00216	0.000399
	12	1.000	0.004605	0.003975	0.000734	0.00390	0.00353	0.000639
	7	1.714	0.006547	0.00779	0.00134	0.00583	0.00698	0.00120
3.162	17	0.706	0.18995	2.894	0.2032	0.1680	2.18	0.162
	12	1.000	0.13624	2.225	0.1485	0.1250	1.77	0.124
	7	1.714	0.10244	1.961	0.1182	0.0962	1.60	0.102

* See reference 10.

TABLE IX. Reduced values of the critical constants.

Gas	Force constants from viscosity data* ϵ_m/k, °K	r_0, A	kT_c/ϵ_m	v_c/v_0	$p_cv_0/N\epsilon_m$	p_cv_c/NkT_c
H_2	33.3	2.968	1.00	4.13	0.074	0.305
He	6.03	2.70	0.87	4.87	0.054	0.302
N_2	91.46	3.680	1.38	3.00	0.134	0.292
A	124.0	3.418	1.22	3.13	0.113	0.291
Ne	35.7	2.80	1.24	3.15	0.117	0.296
Theoretical			1.30	1.768	0.434	0.591

* See reference 9.

TABLE X.

kT/ϵ_m	Volume of saturated liquid v_l/v_0	Volume of saturated vapor v_g/v_0	Reduced vapor pressure p^*
0.70	1.04		
0.75	1.06		
0.80	1.08		
0.85	1.09	Greater than tabulated values	Vapor density too small to permit calculation with LJD
0.90	1.11		
0.95	1.13		
1.00	1.17		
1.05	1.22		
1.1	1.26		
1.2	1.36	3.5	0.240

Table IX gives a comparison of the theoretical and experimental values of T_c, v_c, p_c, and p_cv_c/NkT_c. The force constants used in the comparison were obtained from the experimental viscosity of the dilute gas so that no adjustable parameters were used. It is seen that the reduced temperatures agree quite well with the theoretical value although the volumes and the pressures do not agree. The experimental values of pv/NkT at the critical point are remarkably constant, indicating that a two-parameter intermolecular potential is correct; but the value is quite different from the theoretical value. This indicates that the critical density is not sufficiently dense for the LJD treatment to apply satisfactorily. These critical values are in substantial agreement with the findings of Lennard-Jones and Devonshire,[1] of Prigogine and Garikian,[10] and of Hill.[11] Prigogine and Garikian were able to show that the value of p_cv_c/NkT_c is relatively insensitive to the form of the potential function and hence that it is not likely that the LJD model can be made to give a satisfactory quantitative description of the critical point.

Below the critical temperature, there are two phases: liquid and gas. Correspondingly, there is a vapor pressure defined by the requirement that the free energy of the gas and the liquid are equal. The isotherms in the region of the critical temperature are of the van der Waals type, and are shown in Fig. 3. Thus the LJD equation of state represents a metastable state when the volume lies between the liquid volume and the vapor volume at the vapor pressure. Table X gives the vapor pressure and the liquid and vapor volumes. In all graphs, this metastable region is indicated by dashed curves.

From the general equation of state one can easily obtain the contribution of the intermolecular forces to the various thermodynamic functions. First we have the internal energy of gas imperfection per mole [Eq.

TABLE XI. The reduced internal energy of gas imperfection $E'/N\epsilon_m$.

$(v/v_0)^2$	.320	.405	.5	.72	.98	1.125	1.28	1.62	2	2.42
v/v_0 / kT/ϵ_m	.5657	.6364	.7071	.8485	.9899	1.0607	1.1314	1.2728	1.4142	1.5556
0.70	14.94	2.375	−3.590	−7.374	−7.505	−7.177	−6.785	−5.947	−5.220	−4.638
0.75	15.05	2.451	−3.517	−7.284	−7.446	−7.137	−6.735	−5.906	−5.189	−4.612
0.80	15.16	2.525	−3.444	−7.220	−7.387	−7.084	−6.686	−5.866	−5.157	−4.587
0.85	15.26	2.598	−3.372	−7.156	−7.329	−7.032	−6.637	−5.827	−5.126	−4.562
0.90	15.36	2.675	−3.300	−7.093	−7.271	−6.979	−6.509	−5.788	−5.095	−4.537
0.95	15.45	2.742	−3.228	−7.030	−7.214	−6.927	−6.541	−5.749	−5.064	−4.512
1.00	15.54	2.814	−3.157	−6.967	−7.157	−6.876	−6.494	−5.710	−5.033	−4.487
1.05	15.63	2.885	−3.086	−6.904	−7.120	−6.825	−6.447	−5.672	−5.002	−4.462
1.1	15.71	2.957	−3.015	−6.841	−7.066	−6.774	−6.400	−5.634	−4.972	−4.435
1.2	15.88	3.100	−2.874	−5.717	−6.958	−6.673	−6.308	−5.559	−4.912	−4.385
1.3	16.04	3.244	−2.734	−6.593	−6.851	−6.573	−6.217	−5.485	−4.852	−4.336
1.4	16.19	3.387	−2.596	−6.470	−6.745	−6.475	−6.127	−5.412	−4.792	−4.286
1.6	16.49	3.674	−2.323	−6.226	−6.536	−6.282	−5.951	−5.269	−4.675	−4.188
1.8	16.79	3.958	−2.015	−5.986	−6.331	−6.093	−5.779	−5.129	−4.553	−4.090
2.0	17.08	4.240	−1.758	−5.749	−6.129	−5.908	−5.611	−4.991	−4.438	−3.994
2.5	17.80	4.934	−1.120	−5.217	−5.638	−5.459	−5.204	−4.656	−4.158	−3.755
3.0	18.52	5.666	−0.4897	−4.668	−5.165	−5.028	−4.813	−4.317	−3.886	−3.520
3.5	19.23	6.310	+0.1330	−4.130	−4.707	−4.612	−4.434	−4.002	−3.618	−3.289
4	19.92	6.949	0.7476	−3.602	−4.262	−4.207	−4.066	−3.964	−3.356	−3.061
5	21.38	8.214	1.876	−2.576	−3.405	−3.428	−3.324	−3.097	−2.845	−2.613
7	23.95	10.687	4.124	−0.6285	−1.792	−1.912	−1.982	−1.961	−1.861	−1.745
10	27.73	14.05	7.372	+2.095	+0.5218	+0.1349	−0.1051	−0.3553	−0.4584	−0.4962
20	39.08	24.79	17.21	10.28	7.150	6.213	+5.503	+4.504	+3.841	+3.375
50	69.86	52.31	42.11	30.14	23.75	21.55	19.78	17.08	15.13	13.66
100	114.29	91.08	76.05	57.82	47.18	43.36	40.21	35.30	31.65	28.64
400	311.2	264.5	231.2	186.7	158.3	147.4	137.45	117.14	95.25	74.18

TABLE XI.—(*Continued*)

$(v/v_0)^2$ / v/v_0 / kT/ϵ_m	2.38	3.125	3.38	3.92	4.50	6.125	8	12.5	18
	1.6971	1.7678	1.8385	1.9799	2.1213	2.4749	2.8284	3.5355	4.2426
0.70	−4.177	−3.984	−3.810	−3.5129	−3.2666	−2.7997	−2.4644	−2.0005	−1.6861
0.75	−4.156	−3.964	−3.792	−3.4968	−3.2517	−2.7862	−2.4514	−1.9878	−1.6738
0.80	−4.135	−3.945	−3.774	−3.4807	−3.2368	−2.7729	−2.4386	−1.9756	−1.6620
0.85	−4.114	−3.926	−3.756	−3.4656	−3.2219	−2.7596	−2.4260	−1.9636	−1.6506
0.90	−4.093	−3.966	−3.738	−3.4484	−3.2070	−2.7464	−2.4136	−1.9519	−1.6396
0.95	−4.072	−3.887	−3.720	−3.4321	−3.1920	−2.7332	−2.4013	−1.9404	−1.6290
1.00	−4.051	−3.868	−3.702	−3.4158	−3.1770	−2.7201	−2.3891	−1.9292	−1.6188
1.05	−4.030	−3.848	−3.684	−3.3994	−3.162	−2.7070	−2.3770	−1.9181	−1.6088
1.1	−4.009	−3.828	−3.665	−3.3830	−3.1469	−2.6940	−2.3649	−1.9071	−1.5992
1.2	−3.967	−3.789	−3.629	−3.3501	−3.1168	−2.6679	−2.3410	−1.8856	−1.5807
1.3	−3.925	−3.750	−3.592	−3.3171	−3.0864	−2.6418	−2.3173	−1.8645	−1.5632
1.4	−3.883	−3.711	−3.555	−3.2840	−3.0561	−2.6158	−2.2937	−1.8436	−1.5466
1.6	−3.799	−3.632	−3.481	−3.2174	−2.9951	−2.5636	−2.2467	−1.8027	−1.5159
1.8	−3.715	−3.553	−3.407	−3.1505	−2.9338	−2.5113	−2.1998	−1.7623	−1.4882
2.0	−3.631	−3.475	−3.333	−3.0835	−2.8722	−2.4589	−2.1530	−1.7226	−1.4631
2.5	−3.423	−3.279	−3.147	−2.9155	−2.7177	−2.3270	−2.0359	−1.6255	−1.4099
3	−3.216	−3.084	−2.903	−2.7475	−2.5628	−2.1953	−1.9186	−1.5325	−1.3674
3.5	−3.012	−2.891	−2.779	−2.5799	−2.4078	−2.0630	−1.8010	−1.4446	−1.3330
4	−2.810	−2.699	−2.596	−2.4128	−2.2532	−1.9306	−1.6834	−1.3623	−1.3045
5	−2.411	−2.320	−2.235	−2.0808	−1.9451	−1.6660	−1.4485	−1.2153	−1.2606
7	−1.631	−1.577	−1.524	−1.4261	−1.3358	−1.1399	−0.9874	−0.9839	−1.2036
10	−0.5013	−0.4968	−0.489	−0.4670	−0.4396	−0.3641	−0.3456	−0.7479	−1.1556
20	+3.033	+2.895	+2.774	+2.5735	+2.4091	+1.9559	+1.1918	−0.3793	−1.0931
50	12.51	12.00	11.50	10.457	9.263	5.879	2.9761	−0.0967	−1.0520
100	25.66	24.06	22.36	18.81	15.321	8.208	3.804	+0.00948	−1.0376
400	56.17	48.57	41.88	30.99	22.834	10.470	4.5205	0.09335	−1.0266

TABLE XII. The reduced specific heat of gas imperfection c_v'/Nk.

$(v/v_0)^2$ / v/v_0 / kT/ϵ_m	.3200	.4050	.5	.720	.98	1.125	1.280	1.62	2	2.42
	.5657	.6364	.7071	.8485	.9899	1.0607	1.1314	1.2728	1.4142	1.5556
0.75	2.17	1.494	1.452	1.545	1.177	0.934	0.989	0.804	0.632	0.504
0.80	2.07	1.466	1.447	1.272	1.168	1.054	0.980	0.795	0.628	0.503
0.85	1.99	1.450	1.442	1.268	1.159	1.047	0.971	0.787	0.624	0.502
0.90	1.92	1.443	1.438	1.265	1.150	1.041	0.961	0.780	0.621	0.501
0.95	1.85	1.440	1.432	1.261	1.142	1.034	0.953	0.773	0.617	0.500
1.00	1.79	1.435	1.425	1.258	1.120	1.028	0.946	0.767	0.614	0.500
1.05	1.74	1.435	1.421	1.254	1.100	1.022	0.937	0.760	0.610	0.500
1.1	1.69	1.435	1.416	1.250	1.080	1.015	0.930	0.755	0.607	0.500
1.2	1.617	1.435	1.402	1.242	1.073	1.002	0.916	0.744	0.602	0.497
1.3	1.567	1.435	1.390	1.234	1.065	0.990	0.903	0.734	0.596	0.495
1.4	1.529	1.430	1.380	1.226	1.060	0.977	0.891	0.726	0.591	0.493
1.6	1.493	1.427	1.345	1.210	1.037	0.956	0.869	0.710	0.590	0.489
1.8	1.470	1.417	1.310	1.194	1.019	0.935	0.850	0.696	0.580	0.485
2.0	1.460	1.404	1.283	1.150	1.000	0.918	0.833	0.684	0.568	0.482
2.5	1.440	1.391	1.268	1.096	0.964	0.879	0.798	0.674	0.553	0.473
3.0	1.422	1.376	1.253	1.087	0.931	0.848	0.770	0.654	0.540	0.466
3.5	1.415	1.283	1.237	1.067	0.903	0.821	0.746	0.623	0.529	0.460
4	1.410	1.274	1.196	1.046	0.879	0.799	0.738	0.610	0.520	0.454
5	1.400	1.256	1.127	1.008	0.840	0.772	0.719	0.587	0.505	0.443
7	1.275	1.190	1.108	0.947	0.792	0.728	0.653	0.555	0.482	0.427
10	1.231	1.110	1.060	0.887	0.746	0.665	0.611	0.524	0.459	0.410
20	1.108	1.035	0.946	0.779	0.635	0.584	0.540	0.469	0.417	0.376
50	0.974	0.864	0.773	0.621	0.521	0.483	0.451	0.399	0.359	0.327
100	0.855	0.747	0.656	0.536	0.455	0.423	0.397	0.351	0.313	0.278

TABLE XII.—(*Continued*)

$(v/v_0)^2$	2.88	3.125	3.38	3.920	4.500	6.125	8	12.5	18
v/v_0	1.6971	1.7678	1.8385	1.9799	2.1213	2.4749	2.8204	5.5355	4.2426
kT/ϵ_m									
0.75	0.417	0.385	0.359	0.321	0.297	0.268	0.258	0.249	0.241
0.80	0.418	0.386	0.360	0.323	0.298	0.266	0.254	0.242	0.232
0.85	0.419	0.387	0.362	0.324	0.298	0.265	0.250	0.237	0.223
0.90	0.419	0.388	0.363	0.325	0.299	0.264	0.247	0.232	0.216
0.95	0.420	0.389	0.364	0.326	0.300	0.262	0.245	0.227	0.209
1.00	0.420	0.390	0.365	0.327	0.300	0.262	0.243	0.224	0.202
1.05	0.421	0.391	0.366	0.328	0.301	0.262	0.241	0.220	0.196
1.1	0.421	0.391	0.366	0.328	0.302	0.261	0.240	0.218	0.190
1.2	0.421	0.392	0.368	0.330	0.303	0.261	0.238	0.213	0.180
1.3	0.421	0.393	0.369	0.331	0.304	0.261	0.237	0.210	0.170
1.4	0.421	0.393	0.369	0.332	0.304	0.261	0.236	0.207	0.162
1.6	0.420	0.393	0.370	0.333	0.306	0.261	0.235	0.203	0.146
1.8	0.419	0.393	0.371	0.335	0.307	0.262	0.234	0.200	0.132
2.0	0.418	0.393	0.371	0.335	0.308	0.262	0.234	0.198	0.120
2.5	0.415	0.391	0.370	0.336	0.309	0.263	0.234	0.190	0.0957
3.0	0.410	0.388	0.368	0.336	0.310	0.264	0.235	0.181	0.0770
3.5	0.406	0.385	0.366	0.335	0.310	0.265	0.235	0.170	0.0629
4	0.403	0.382	0.364	0.333	0.309	0.265	0.235	0.159	0.0525
5	0.396	0.377	0.360	0.330	0.307	0.264	0.233	0.137	0.0388
7	0.384	0.367	0.351	0.324	0.302	0.261	0.224	0.101	0.0235
10	0.371	0.355	0.341	0.316	0.296	0.252	0.200	0.069	0.0138
20	0.344	0.330	0.317	0.294	0.271	0.207	0.130	0.030	0.0050
50	0.296	0.280	0.263	0.227	0.188	0.099	0.0434	0.0067	0.00097
100	0.240	0.218	0.195	0.149	0.107	0.041	0.0145	0.0019	0.00025

TABLE XIII. The reduced entropy of gas imperfection S'/Nk.

$(v/v_0)^2$	.32	.405	.5	.72	.98	1.125	1.28	1.62	2.	2.42
v/v_0	.5657	.6364	.7071	.8485	.9899	1.0607	1.1314	1.2728	1.4142	1.5556
kT/ϵ_m										
0.70	−8.816	−7.7406	−7.0399	−5.8313	−4.8227	−4.3804	−3.9672	−3.2834	−2.7417	−2.3220
0.75	−8.643	−7.6333	−6.9413	−5.7235	−4.7413	−4.2865	−3.8988	−3.2277	−2.6979	−2.2872
0.80	−8.491	−7.5360	−6.8490	−5.6415	−4.6657	−4.2185	−3.8354	−3.1761	−2.6572	−2.2547
0.85	−8.359	−7.4465	−6.7627	−5.5647	−4.5952	−4.1549	−3.7764	−3.1281	−2.6193	−2.2242
0.90	−8.239	−7.3612	−6.6814	−5.4925	−4.5293	−4.0953	−3.7212	−3.0834	−2.5807	−2.1955
0.95	−8.132	−7.2852	−6.6047	−5.4244	−4.4674	−4.0393	−3.6695	−3.0414	−2.5502	−2.1684
1.00	−8.036	−7.2116	−6.5322	−5.3600	−4.4091	−3.9865	−3.6209	−3.0020	−2.5187	−2.1428
1.05	−7.948	−7.1417	−6.4634	−5.2989	−4.3340	−3.9366	−3.5750	−2.9647	−2.4888	−2.1184
1.1	−7.866	−7.0752	−6.3979	−5.2408	−4.2838	−3.8893	−3.5316	−2.9295	−2.4605	−2.0977
1.2	−7.723	−6.9488	−6.2763	−5.1327	−4.1904	−3.8018	−3.4514	−2.8643	−2.4079	−2.0545
1.3	−7.5965	−6.8372	−6.1652	−5.0338	−4.1050	−3.7221	−3.3786	−2.8051	−2.3600	−2.0148
1.4	−7.4834	−6.7317	−6.0632	−4.9428	−4.0266	−3.6493	−3.3122	−2.7511	−2.3160	−1.9781
1.6	−7.2854	−6.5422	−5.8813	−4.7804	−3.8873	−3.5205	−3.1948	−2.6553	−2.2376	−1.9126
1.8	−7.1145	−6.3759	−5.7108	−4.6390	−3.7664	−3.4092	−3.0936	−2.5727	−2.1717	−1.8551
2.0	−6.9628	−6.2284	−5.5756	−4.5140	−3.6602	−3.3117	−3.0050	−2.5000	−2.1116	−1.8042
2.5	−6.6442	−5.9209	−5.2917	−4.2383	−3.4413	−3.1116	−2.8233	−2.3504	−1.9865	−1.6977
3.0	−6.3855	−5.6645	−5.0623	−4.0386	−3.2688	−2.9544	−2.6805	−2.2339	−1.8869	−1.6120
3.5	−6.1697	−5.4465	−4.8707	−3.8729	−3.1277	−2.8259	−2.5638	−2.1369	−1.8046	−1.5408
4	−5.9854	−5.2962	−4.7068	−3.7320	−3.0088	−2.7179	−2.4655	−2.0545	−1.7345	−1.4798
5	−5.6719	−5.0146	−4.4138	−3.5032	−2.8175	−2.5439	−2.3083	−1.9215	−1.6203	−1.3798
7	−5.2402	−4.5988	−4.0361	−3.1757	−2.5456	−2.2976	−2.0823	−1.7299	−1.4546	−1.2336
10	−4.7916	−4.1602	−3.6502	−2.8508	−2.2792	−2.0538	−1.8587	−1.5388	−1.2876	−1.0849
20	−3.9568	−3.4121	−2.9641	−2.2900	−1.8159	−1.6290	−1.4670	−1.1996	−0.9877	−0.8152
50	−3.0070	−2.5594	−2.2027	−1.6735	−1.3014	−1.1538	−1.0250	−0.8107	−0.6389	−0.4976
100	−2.3994	−2.0251	−1.7277	−1.2864	−0.9738	−0.8490	−0.7395	−0.5502	−0.4084	−0.2881
400	−1.4539	−1.1926	−0.9841	−0.6703	−0.4437	−0.3526	−0.2744	−0.1562	−0.0841	−0.0445

TABLE XIII.—(*Continued*)

$(v/v_0)^2$ / v/v_0 / kT/ϵ_m	2.88	3.125	3.38	3.92	4.5	6.125	8.	12.5	18.
	1.6971	1.7678	1.8385	1.9799	2.1213	2.4749	2.8284	3.5355	4.2426
0.70	−1.9982	−1.8619	−1.7402	−1.5323	−1.3611	−1.0393	−0.8104	−0.4954	−0.2812
0.75	−1.9695	−1.8354	−1.7155	−1.5101	−1.3406	−1.0207	−0.7924	−0.4780	−0.2642
0.80	−1.9426	−1.8105	−1.6923	−1.4894	−1.3214	−1.0035	−0.7759	−0.4621	−0.2489
0.85	−1.9172	−1.7871	−1.6704	−1.4698	−1.3033	−0.9874	−0.7606	−0.4476	−0.2352
0.90	−1.8933	−1.7650	−1.6497	−1.4512	−1.2862	−0.9723	−0.7464	−0.4342	−0.2226
0.95	−1.8705	−1.7439	−1.6301	−1.4336	−1.2701	−0.9581	−0.7331	−0.4218	−0.2112
1.00	−1.8490	−1.7239	−1.6113	−1.4169	−1.2547	−0.9446	−0.7206	−0.4103	−0.2006
1.05	−1.8285	−1.7049	−1.5936	−1.4010	−1.2400	−0.9319	−0.7088	−0.3995	−0.1909
1.1	−1.8089	−1.6867	−1.5765	−1.3857	−1.2260	−0.9197	−0.6976	−0.3893	−0.1820
1.2	−1.7723	−1.6526	−1.5446	−1.3571	−1.1998	−0.8970	−0.6768	−0.3705	−0.1658
1.3	−1.7386	−1.6212	−1.5151	−1.3306	−1.1754	−0.8761	−0.6578	−0.3536	−0.1518
1.4	−1.7074	−1.5921	−1.4877	−1.3061	−1.1530	−0.8568	−0.6403	−0.3382	−0.1395
1.6	−1.6512	−1.5396	−1.4383	−1.2616	−1.1123	−0.8220	−0.6089	−0.3108	−0.1190
1.8	−1.6017	−1.4932	−1.3947	−1.2222	−1.0762	−0.7912	−0.5813	−0.2871	−0.1027
2.0	−1.5576	−1.4518	−1.3556	−1.1870	−1.0437	−0.7636	−0.5567	−0.2661	−0.0894
2.5	−1.4647	−1.3644	−1.2729	−1.1120	−0.9748	−0.7049	−0.5044	−0.2228	−0.0656
3.0	−1.3897	−1.2934	−1.2056	−1.0507	−0.9183	−0.6568	−0.4616	−0.1888	−0.0501
3.5	−1.3265	−1.2338	−1.1489	−0.9990	−0.8705	−0.6160	−0.4254	−0.1617	−0.0394
4	−1.2724	−1.1825	−1.1002	−0.9544	−0.8293	−0.5806	−0.3940	−0.1397	−0.0318
5	−1.1833	−1.0978	−1.0194	−0.8803	−0.7605	−0.5216	−0.3415	−0.1068	−0.0220
7	−1.0520	−0.9728	−0.8999	−0.7701	−0.6579	−0.4330	−0.2639	−0.0676	−0.0122
10	−0.9176	−0.8442	−0.7766	−0.6560	−0.5513	−0.3407	−0.1873	−0.0391	−0.0064
20	−0.6714	−0.6080	−0.5494	−0.4444	−0.3530	−0.1779	−0.0772	−0.0119	−0.0018
50	−0.3790	−0.3270	−0.2796	−0.1989	−0.1369	−0.0493	−0.0171	−0.0021	−0.0003
100	−0.1939	−0.1565	−0.1253	−0.0788	−0.0490	−0.0149	−0.0048	−0.0006	−0.00013
400	−0.0236	−0.0174	−0.0128	−0.0071	−0.0040	−0.0011	−0.0004	−0.00008	+0.00002

(53) of reference 1]:

$$E' = E - E_{(v\to\infty)} = \tfrac{1}{2}N\psi^*(0) + N\chi(v, T). \quad (17)$$

Here $\frac{1}{2}\psi^*(0)$ is the potential energy (per molecule) for the entire lattice-work when the molecules are all at the centers of their cells [Eq. (47) of reference 1]:

$$\psi^*(0) = -12\epsilon_m[2.4090(v_0/v)^2 - 1.0109(v_0/v)^4] \quad (18)$$

and $\chi(v, T)$ is the average potential energy of the molecule in a cell referred to the center as zero:

$$\chi(v, T) = 12\epsilon_m[(v_0/v)^4(g_L/G) - 2(v_0/v)^2(g_M/G)]. \quad (19)$$

TABLE XIV. Liquid volume comparison.

Gas	T(°K)	kT/ϵ_m	Exptl. liquid density, g/cc	Pressure (atmos.)	v_l/v_0 exp.	v_l/v_0 calc.
Nitrogen	77.15	0.844	0.804	1	1.16	1.09
Neon	27.26	0.764	1.204	1	1.27	1.07
Argon	90	0.726	1.374	1.5	1.209	1.05
	111	0.9026	1.224	7.4	1.357	1.11
	122	0.9871	1.138	13.7	1.459	1.17
Methane	111.6	0.818	0.4245	1	1.07	1.08
	133	0.976	0.3916	4.38	1.16	1.15
	153	1.122	0.3547	11.84	1.28	1.27
	191.05	1.400	0.1615	45.8	2.82	1.77

TABLE XV. Argon.*

			pv/NkT								
		kT/ϵ_m	2.203			2.808			3.413		
		T	0°C			75°C			150°C		
Density Amagat units	v/v_0	g/cc	calc.	exp.	p(atmos.) exp.	calc.	exp.	p(atmos.) exp.	calc.	exp.	p(atmos.) exp.
316.6	2.944	0.5642	1.45	0.97	310	1.64	1.14	450	1.76	1.25	610
419.9	2.219	0.7483	1.61	1.13	470	1.87	1.36	710	2.02	1.50	980
503.6	1.851	0.8975	1.77	1.38	900	2.09	1.64	1090	2.28	1.80	1400
626.3	1.488	1.1161	2.10	2.07	1330	2.51	2.34	1820	2.74	2.32	2250

* Critical density, 0.531 g/cc; liquid density (90°K), 1.41 g/cc; solid density (40°K), 1.65 g/cc; normal volume, 22390 cc/g mole.

TABLE XVI. Nitrogen.*

			pv/NkT											
		kT/ϵ_m	2.987			3.533			4.080			4.627		
		T	0°C			50°C			100°C			150°C		
Density, Amagat units	v/v_0	g/cc	calc.	exp.	p(atmos.) exp.	calc.	exp.	p(atmos.) exp.	calc.	exp.	p(atmos.) exp.	calc.	exp.	p(atmos.) exp.
186.6	3.998	.2332	1.41	1.03	190	1.44	1.11	250	1.46	1.16	300	1.46	1.20	350
223.6	3.337	.2795	1.62	1.07	240	1.70	1.16	310	1.75	1.22	370	1.77	1.27	440
315.1	2.368	.3938	1.87	1.25	390	1.98	1.37	510	2.06	1.46	630	2.11	1.52	740
415.9	1.794	.5198	2.21	1.63	680	2.36	1.79	880	2.46	1.89	1070	2.53	1.96	1260
578.5	1.290	.7231	3.07	3.03	1750	3.28	3.17	2170	3.40	3.25	2570	3.49	3.30	2960

* Critical density, 0.311 g/cc; liquid density (77°K), 0.804 g/cc; solid density (20°K), 1.03 g/cc; normal volume, 22407 cc/g mole.

TABLE XVII. Hydrogen.*

Density, Amagat units	g/cc	v/v_0	pv/NkT kT/ϵ_m T calc.	8.20 0°C exp.	p(atmos.) exp.	calc.	9.70 50°C exp.	p(atmos). exp.	calc.	12.71 150°C exp.	p(atmos.) exp.
939.0	0.08441	1.516	3.126	2.707	2540	3.122	2.640	2932	3.118	—	—
758.1	0.06815	1.878	2.612	2.124	1610	2.630	2.098	1882	2.619	2.049	2406
675.5	0.06072	2.108	2.415	1.910	1290	2.434	1.900	1516	2.429	1.866	1952
583.1	0.05241	2.442	2.215	1.706	995	2.234	1.704	1175	2.224	1.688	1525
483.3	0.04345	2.946	1.977	1.520	735	1.976	1.525	872	1.933	1.522	1140
391.7	0.03516	3.640	1.593	1.378	539	1.542	1.386	641	1.498	1.389	842
348.8	0.03135	4.082	1.342	1.321	461	1.313	1.329	548	1.275	1.334	721

* Critical density, 0.03172 g/cc; liquid density (20°K), 0.070 g/cc; solid density, (13°K), 0.076 g/cc; normal volume, 22427 cc/g mole.

In Table XI is presented $E'/N\epsilon_m$, the reduced internal energy of gas imperfection per mole. In Figs. 4a and 4b is shown a plot of E' *vs.* v_0/v.

The correction to the specific heat

$$c_v' = \partial E'/\partial T \tag{20}$$

can be calculated by evaluating integrals similar to g_L and g_M. However, because of the extensiveness of the E' table, it was deemed more expedient simply to differentiate the E' table numerically. The dimensionless quantity c_v'/Nk is given in Table XII and shown in Fig. 5. It is to be noted that the large values for the specific heat experimentally found in the critical region are not given by the LJD equations. The reason for this is that the free volume theory does not take into account the fluctuations in local density. The "hole" theories are more accurate in this respect.

The entropy of the gas can be written in the form

$$S = S^\circ(T) - Nk\log(NkT/v_0) + Nk\log(v/v_0) + S'(v, T). \tag{21}$$

Here $S^\circ(T)$ is the entropy of the substance considered

TABLE XVIII. Argon: Internal energy of gas imperfection, E' in cal./mole.

Density, Amagat units	Density, gram/cc	v/v_0	kT/ϵ_m T calc.	2.203 0°C exp.	calc.	2.808 75°C exp.	calc.	3.413 150°C exp.
280	0.4995	3.325	− 445.1	−429	−415.4	−401.5	−386.2	−385.6
400	0.7136	2.3275	− 634.2	−600.9	−592.0	−563.8	−549.8	−539.0
520	0.9277	1.7904	− 825.7	−769.3	−768.5	−717.8	−711.8	−679.5
640	1.1418	1.4547	−1035.3	−923.8	−956.2	−851.0	−879.4	−791.3

TABLE XIX. Nitrogen: Internal energy of gas imperfection, E' in cal./mole.

Density, Amagat units	v/v_0	g/cc	kT/ϵ_m T calc.	2.987 0°C exp.	calc.	3.533 50°C exp.	calc.	4.080 100°C exp.	calc.	4.627 150°C exp.
200	3.731	0.2500	−267	−302	−252	−285	−238	−275	−226	−270
240	3.109	0.3000	−316	−360	−295	−340	−245	−328	−254	−312
280	2.665	0.3500	−370	−418	−346	−395	−322	−381	−297	−372
320	2.332	0.4000	−423	−475	−395	−449	−368	−433	−340	−422
400	1.865	0.5000	−531	−588	−495	−554	−459	−530	−424	−514
480	1.554	0.6000	−640	−693	−594	−650	−549	−616	−504	−594

TABLE XX. Argon: Specific heat of gas imperfection, c' in cal./mole/degree.

Density, Amagat units	Density, gram/cc	v/v_0	kT/ϵ_m T calc.	2.203 0°C exp.	calc.	2.808 75°C exp.	calc.	3.413 150°C exp.
280	0.4995	3.325	0.411	0.42	0.395	0.30	0.379	0.16
400	0.7136	2.3275	0.558	0.55	0.562	0.42	0.564	0.26
520	0.9277	1.7904	0.765	0.74	0.761	0.62	0.755	0.43
640	1.1418	1.4547	1.069	1.02	1.039	0.91	1.015	0.69

TABLE XXI. Nitrogen: Specific heat of gas imperfection, c' in cal./mole/degree.

Density, Amagat units	v/v_0	g/cc	kT/ϵ_m T calc.	2.987 0°C exp.	calc.	3.533 50°C exp.	calc.	4.080 100°C exp.	calc.	4.627 150°C exp.
200	3.731	0.2500	0.31	0.40	0.29	0.27	0.26	0.13	0.24	0.06
240	3.109	0.3000	0.42	0.45	0.41	0.33	0.40	0.18	0.40	0.07
280	2.665	0.3500	0.49	0.49	0.49	0.38	0.49	0.23	0.49	0.10
320	2.332	0.4000	0.55	0.56	0.55	0.45	0.55	0.27	0.55	0.14
400	1.865	0.5000	0.72	0.71	0.72	0.60	0.71	0.41	0.71	0.22
480	1.554	0.6000	0.93	0.91	0.92	0.78	0.90	0.57	0.89	0.33

TABLE XXII. Argon: Entropy of gas imperfection, S' in cal./mole/degree.

Density, Amagat units	Density, gram/cc	v/v_0	kT/ϵ_m T calc.	2.203 0°C exp.	calc.	2.808 75°C exp.	calc.	3.413 150°C exp.
280	0.4995	3.325	−0.6635	−1.234	−0.5365	−1.147	−0.4773	−1.101
400	0.7136	2.3275	−1.699	−1.861	−1.561	−1.741	−1.450	−1.671
520	0.9277	1.7904	−2.754	−2.600	−2.567	−2.433	−2.418	−2.329
640	1.1418	1.4547	−3.924	−3.480	−3.666	−3.244	−3.463	−3.085

TABLE XXIII. Nitrogen: Entropy of gas imperfection, S' in cal./mole/degree.

Density, Amagat units	v/v_0	g/cc	kT/ϵ_m T calc.	2.987 0°C exp.	calc.	3.533 50°C exp.	calc.	4.080 100°C exp.	calc.	4.627 150°C exp.
200	3.731	0.2500	−0.28	−1.05	−0.22	−1.00	−0.19	−0.96	−0.16	−0.95
240	3.109	0.3000	−0.66	−1.29	−0.59	−1.22	−0.54	−1.18	−0.48	−1.16
280	2.665	0.3500	−1.08	−1.54	−1.00	−1.46	−0.93	−1.42	−0.87	−1.39
320	2.332	0.4000	−1.49	−1.80	−1.40	−1.72	−1.32	−1.66	−1.25	−1.63
400	1.865	0.5000	−2.34	−2.38	−2.22	−2.28	−2.12	−2.20	−2.03	−2.16
480	1.554	0.6000	−3.20	−3.05	−3.05	−2.91	−2.92	−2.81	−2.82	−2.74

as a perfect gas at one atmosphere pressure and is a function only of the temperature. The function $S'(v, T)$ is the correction for gas imperfection defined in such a way that it is zero in the limit of large volume. From the generalized equation of state we obtain an expression for $S'(v, T)$:

$$S'(v, T)=[N\chi(v, T)/T]+Nk \log(G/G_\infty). \quad (22)$$

Here

$$G_\infty=\lim_{v\to\infty} G=(2\sqrt{2}\pi)^{-1}. \quad (23)$$

$S'(v, T)$ is given in Table XIII and in Fig. 6.

Table XIV compares[12] theoretical with experimental values of the volume of the liquid in equilibrium with its vapor at various temperatures. The agreement is fair, and shows the proper trend, but in view of the rapid variation of the pressure with volume in this region, this comparison does not afford a very sensitive test.

Tables XV and XVI compare calculated values of pv/NkT with experimental values obtained by Michels and co-workers[13,14] for argon and nitrogen. It is seen that the agreement with experiment is best at high densities. The direction of the discrepancies indicates that the Lennard-Jones interaction potential, Eq. (1), is a good approximation to reality for these molecules, but that the molecules are not in fact confined to cells at low densities.

Table XVII and Fig. 7 compare calculated values of pv/NkT with experimental values obtained by Michels and Goudeket[15] for hydrogen. It appears that the hydrogen molecules are more compressible than is represented by a repulsion energy varying as the inverse twelfth power of the separation distance, since hydrogen has a much lower compressibility at high density than is predicted by the theory.

The pressure of liquid argon has been measured by Bridgman.[16] Our tables allow us to make a single comparison: at a density of 1.531 g/cc ($v/v_0=1.085$), and a temperature of 138.1°K ($kT/\epsilon_m=1.114$), experimentally the pressure is 2500 kg/cm^3 and $pv/NkT=5.569$; the calculated value is $pv/NkT=1.580$. Other data for the compressed liquid at lower temperatures unhappily lie in the metastable region of the theory. However, these results are not to be regarded as conclusive proof that the theory does not describe liquids well, for the experimental measurement of volume is quite difficult, and the theoretical isotherms change quite rapidly with volume in this region.

The thermodynamical properties of argon and nitrogen were obtained by Michels and co-workers[17,18] directly from their experimental PVT data. Our values, of course, are consistent with the calculated equation of state, but in order to indicate the accuracy with which these properties can be predicted we include Tables XVIII through XXIII which compare the calculated and experimental values of the energy, specific heat, and entropy of gas imperfection. The internal energy of gas imperfection agrees somewhat more closely for argon than for nitrogen. This might be attributed to the fact that diatomic nitrogen molecules do not interact according to the spherically symmetric potential on which the theory is based. The specific heat of gas imperfection shows an increasing discrepancy with increasing temperature. This could be due to the fact that the molecules tend to roam more at high temperatures and that smearing the potential inside the cell to obtain radial symmetry is an approximation which requires improvement. In the case of the entropy of gas imperfection the trend of the disagreement shows that the theory attributes more order to the system than it actually possesses at low density, i.e., the molecules are not completely confined to their cells, but tend to roam. The theory is only satisfactory at high densities, where the molecules are more confined.

The authors wish to express their indebtedness to Mrs. Marjorie S. Herrick, who very ably directed the punched-card calculations described herein. The computing which followed the punched-card integration was performed by the computing group of the University of Wisconsin Naval Research Laboratory; in this connection we wish to thank Marjorie Leikvold (director), Alice Epstein, Dorothy Campbell, Mary Nordling, Ruth Schmidt, and LaVon Hall. The graphs were prepared by Marshall Cohen.

This work was made possible by the financial assistance of the Navy Bureau of Ordnance, under contract number NOrd 9938.

[12] In obtaining the calculated values of Tables XIV through XXIII we have used values of ϵ_m/k and r_0 obtained from viscosity data (see reference 9). These values are given in Table IX with the exception of the constants for methane, which are $\epsilon_m/k=136.5$°K and $r_0=3.882$A. The references for the experimental values are as follows: Table XIV, *The Handbook of Chemistry and Physics;* Table XV, Michels, Wijker, and Wijker (see reference 14); Table XVI, Michels, Wouters, and deBoer (see reference 13); Table XVII, Michels and Goudeket (see reference 15); Tables XVIII, XX, and XXII, Michels, Lunbeck, and Wolkers (see reference 18); Tables XIX, XXI, and XXIII, Michels, Wouters, and deBoer (see reference 17).

[13] Michels, Wouters, and deBoer, Physica **3**, 585 (1936).

[14] Michels, Wijker, and Wijker, Physica **15**, 627 (1949).

[15] A. Michels and M. Goudeket, Physica **8**, 347 (1941).

[16] P. W. Bridgman, Proc. Am. Acad. **70**, 1 (1935).

[17] See reference 13, p. 597.

[18] Michels, Lunbeck, and Wolkers, Physica **15**, 689 (1949).

THE JOURNAL OF CHEMICAL PHYSICS VOLUME 18, NUMBER 11 NOVEMBER, 1950

The Effect of Isotopic Substitution on Mass Spectra of Molecules*

OLIVER A. SCHAEFFER
Chemistry Department, Brookhaven National Laboratory, Upton, Long Island, New York
(Received August 16, 1950)

A general method for calculating the effect of isotopic substitution on mass spectra is presented. The calculation is based on the notion that the various fragment ions, formed by electron impact on a molecule, are produced by a Franck-Condon mechanism. It is assumed that those bonds will break which possess more potential energy than bond energy at the instant of ionization. The mass spectral data for a molecule are used in conjunction with the ground-state vibrational wave function to evaluate critical bond distances (distances for which the potential energy equals the bond energy). Then the mass spectral pattern for isotopic molecules can be predicted from a knowledge of the ground-state vibrational wave function of the isotopic molecule. The method is applied to the diatomic molecules $N^{14}N^{14}$, $N^{14}N^{15}$, $N^{15}N^{15}$, and $C^{12}O^{16}$, $C^{13}O^{16}$. The predicted values compare favorably with previously observed results, however, experimental errors obscure a sharp test of the predictions for these cases. New experimental values are presented for the ratios $C^{13+}/C^{13}O_2^{16+}$ and $C^{12+}/C^{13}O_2^{16+}$ from carbon dioxide and compared with predictions. Good agreement is found between ratios extrapolated to high ion accelerating voltage and predicted ones.

INTRODUCTION

THERE have been a number of determinations[1] of the effect of isotopic substitution on the mass spectral pattern of a molecule. Except for the case of hydrogen no theoretical calculations which explain these effects quantitatively appear in the literature.

When a molecule is ionized by electron impact in a mass spectrometer, a number of products are formed due to the breaking of one or more bonds in the molecule. The nature of this process has been understood for some time.[2] The first step is the removal of one or more electrons by the impinging electron sometimes accompanied by excitation of the remaining electrons. This process takes place in a time so short that the nuclei can be considered at rest. The effect on the nuclei is that they suddenly find themselves in a new potential field, that of the smaller number of electrons. Depending on the configuration of the nuclei at the time of impact, the molecule will decompose or remain intact.

Two kinds of information are required for a prediction of the probability for breaking a given bond or set of bonds. These are (1) a knowledge of which configurations of the nuclei lead to the rupture of the given bond or set of bonds and (2) the probability of finding the nuclei in a given configuration. The latter is easily obtained from the ground-state vibrational wave functions. Vibrational wave functions are available for most simple molecules from analysis of spectral data. The former type of information can be deduced from appropriate potential functions for the various ionized states. Such potential functions are in general, however, not available.

As so little is known about the potential surfaces of molecular ions, these ideas have been applied only to a calculation of the relative yields of molecular and atomic ions from hydrogen.[3] For hydrogen the potential function of the ion as well as accurate wave functions are known so that it is possible to make a theoretical prediction of the ratios X^+/X_2^+ for H_2, D_2, and T_2. The agreement between this calculation and recent experimental results[4] shows that the essential ideas on which the theory is based are valid. As potential surfaces for most molecule-ions are not, at present, available, it is not possible to predict the mass spectral patterns of other molecules or the isotope effects on the mass spectral patterns without some further approximations. It is the purpose of this article to describe an approximate method which allows a calculation of the change in mass spectral pattern on isotopic substitution without a knowledge of the potential surfaces of the ionic states. The calculation will then be applied to several simple molecules for which experimental observations are available.

THE GENERAL METHOD

The potential energy of a molecule or molecule-ion can be approximated by the form

$$V=\tfrac{1}{2}\sum_j k_j R_j^2, \qquad (1)$$

where R_j is the jth internal coordinate. This form neglects the coupling terms of the form $k_{ij}R_iR_j$ and all anharmonic terms. Such a potential does give reasonable agreement between calculated and observed vibrational frequencies for polyatomic molecules.[5] Then for each bond, i, in a given molecule ion there will be some distance, R_{ci}, such that when R_i, the bond length, is less than R_{ci}, the potential energy of the bond will be larger than the energy required to break the bond, i.e., the energy required to increase the bond length from its equilibrium value to a very large value, all other bonds being kept at their equilibrium value.

* Research conducted under the auspices of the AEC.
[1] See for example, Turkevich, Friedman, Solomon, and Wrightson, J. Am. Chem. Soc. **70**, 2638 (1948), which contains references to other work.
[2] Bleakney, Condon, and Smith, J. Phys. Chem. **41**, 197 (1937).
[3] D. P. Stevenson, J. Chem. Phys. **15**, 409 (1947).
[4] O. A. Schaeffer and J. M. Hastings, J. Chem. Phys. **18**, 1048 (1950).
[5] See for example, G. Herzberg, *Infrared and Raman Spectra* (D. Van Nostrand and Company, Inc., New York, 1945).

TABLE I. Calculated ion ratios, of isotopic diatomic molecules for various types of electronic states. Calculated ratios, $(X^+ + Y^+)/(XY^+ + X^+ + Y^+)$, for the $X-Y$ molecule.

Assumed experimental ratio $X^+/(X_2^+ + X^+)$ for the $X-X$ molecule	One bonding ionic state[a]	Two bonding states Case I[b]	Two bonding states Case II[c]	One bonding, one repulsive state[d]	All X^+ and Y^+ from repulsive states[e]
0.050	0.042	0.043	0.045	0.045	0.050
0.100	0.089	0.090	0.094	0.092	0.100
0.200	0.189	0.190	0.195	0.190	0.200

[a] For all the ions coming from the same state.
[b] For half the X^+ and Y^+ ions coming from each state, one-third the XY^+ from one state and two-thirds the XY^+ from the other.
[c] For all the X^+ and Y^+ ions coming from the same state, half the XY^+ coming from each state.
[d] For half the X^+ and Y^+ ions coming from each state, all the XY^+ coming from the same state.
[e] For all X^+ and Y^+ from states yielding no XY^+ and all the XY^+ from states yielding no X^+ or Y^+.

It will be assumed that for a given arbitrary displacement of the nuclei those bonds and only those bonds will break for which at the time of ionization

$$R_i < R_{ci}. \tag{2}$$

This assumption is the basis for the application to polyatomic molecules. It states in effect that the bonds are independent. That is, if one bond possesses a large amount of potential energy, due to its configuration, it will dissociate rather than distribute its potential energy among the other bonds.

The assumption certainly is valid for diatomic molecules. Here only one bond is involved so there is no possibility for such a molecule to distribute its potential energy. The application to diatomic molecules will furnish no test of this hypothesis but will serve as a check on the correctness of the approximations used to evaluate the R_{ci}'s.

The problem now is to evaluate the various R_{ci}'s, which would be a relatively easy matter if the appropriate potential functions for the molecule-ion were available. In place of such information, the R_{ci}'s can be considered as parameters to be evaluated by inserting values for the probabilities for breaking the bonds. The bond-breaking probabilities may be determined from the mass spectral pattern of one of the isotopic molecules. For example, the probability of breaking the bond in the molecule $X-X$ would be given by $X^+/(X^+ + X_2^+)$ where by X^+ and X_2^+ are meant the relative yields of X^+ and X_2^+ ions due to electron bombardment of X_2 molecules as measured by a mass spectrometer.

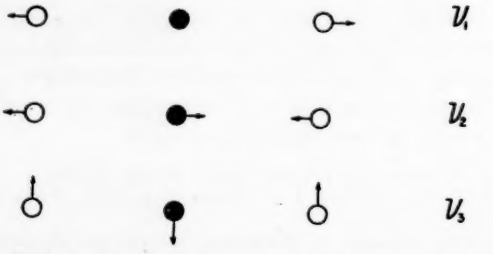

FIG. 1. The normal vibrational modes of carbon dioxide.

The R_{ci}'s are invariant to an isotopic substitution. As defined they depend on the potential surface of the molecule-ion which is negligibly influenced by an isotopic substitution for one of the nuclei. The mass spectral patterns of the other isotopic molecules can then be obtained by the use of the R_{ci}'s and the known vibrational wave functions. In effect, the calculation allows an estimate of the pattern of a molecule if the pattern of an isotopic molecule is available. For a polyatomic molecule there will usually be fewer R_{ci}'s than ionic fragments formed under electron bombardment, so that the R_{ci}'s can all be evaluated from a part of the mass spectral pattern and then the rest of the pattern calculated. For example, in the case of CO_2 there is only one R_{ci}, namely, the C—O critical distance. This can be evaluated from the ratio O^+/(total ions) and then the relative amount of C^+ can be predicted. However, such a procedure is probably very approximate as all the O^+ and C^+ probably do not arise from the same ionic state.

MATHEMATICAL FORMULATION

The vibrational wave function for the harmonic oscillations† of a polyatomic molecule can be written

$$\psi(Q) = \exp(-\tfrac{1}{2}\alpha_1 Q_1^2)\cdot\exp(-\tfrac{1}{2}\alpha_2 Q_2^2)\cdots \cdot\exp(-\tfrac{1}{2}\alpha_n Q_n^2), \tag{3}$$

where Q represents the totality of the normal coordinates, Q_i being a particular one, and

$$\alpha_i = [2\pi(m_i k_i)^{\frac{1}{2}}]/h. \tag{4}$$

The other symbols have their usual significance. The normal coordinates can be expressed in terms of internal coordinates, R, by

$$Q_k = \textstyle\sum_i J_{ki} R_i. \tag{5}$$

In terms of internal coordinates the wave function becomes

$$\psi(R) = \exp[-\tfrac{1}{2}\alpha_1(J_{11}R_1 + J_{12}R_2 + \cdots + J_{1n}R_n)^2] \cdot\exp[-\tfrac{1}{2}\alpha_2(J_{21}R_1 + J_{22}R_2 + \cdots J_{2n}R_n)^2]\cdots \cdot\exp[-\tfrac{1}{2}\alpha_n(J_{n1}R_1 + J_{n2}R_2 + \cdots J_{nn}R_n)^2]. \tag{6}$$

Let P_k be the probability of breaking the kth bond and no other bonds, and $P_{k,j}$ be the probability of breaking the kth and jth bonds simultaneously and no other bonds, and so forth, for other combinations of bonds.

Then according to the previously stated assumption (2)

$$P_k = \int_{-\infty}^{R_{ck}} \int_{R_{ci\neq k}}^{\infty} \cdots \int_{R_{cn}}^{\infty} \psi^2(R)dR \Big/ \int_{-\infty}^{\infty}\cdots\int_{-\infty}^{\infty} \psi^2(R)dR \tag{7}$$

† It should be noted that, for the heavy molecules discussed below, the harmonic oscillator approximation should be valid. Such was not the case for H_- because of the large anharmonicity of this light molecule.

TABLE II. X^+/X_2^+ ratios for the nitrogen molecules.

Molecule	Observed[a] X^+/X_2^+	Calculated X^+/X_2^+
$N^{14}N^{14}$	0.067	(Used to evaluate R_e)
$N^{14}N^{15}$	0.067	0.065
$N^{15}N^{15}$	0.061	0.063

[a] See reference 8.

and

$$P_{k,j}=\int_{-\infty}^{R_{ck}}\int_{-\infty}^{R_{cj}}\int_{R_{ci}\neq k \text{ or } j}^{\infty}\cdots\int_{R_{cm}}^{\infty}\psi^2(R)dR\Big/\int_{-\infty}^{\infty}\cdots\int_{-\infty}^{\infty}\psi^2(R)dR, \quad (8)$$

with similar expressions for the other P's. Since values for the Q's, i.e., the J's and the α's can be determined by a normal coordinate analysis of the molecule, the values of the R_{ci}'s are uniquely determined, in principle, by relations of the type (7) and (8) together with values of the P's obtained from the mass spectral pattern.

EVALUATION OF THE BOND-BREAKING PROBABILITIES FROM THE MASS SPECTRAL DATA

The determination of the P's from the mass spectral data involves certain approximations which need further discussion. It would be a simple matter to evaluate the P's accurately if only one electronic state of the ion were involved. But for most work reported in the literature the data were obtained at relatively high accelerating voltages, in the neighborhood of 50 v. For electrons of 50 v energy, molecules will be excited to a number of ionic states so that the measured ratio $X^+/(X_2^+ + X^+)$, for example, will not represent P for a single state but rather an average value of P over several states.

The values listed in Table I were calculated in order to indicate how large an error may be introduced by a calculation which assumes that all the ions originate from the same electronic state when indeed several states are involved. The body of the table lists values of $(X^+ + Y^+)/(X^+ + Y^+ + XY^+)$ for the molecule $X-Y$ whose $\alpha = 1.1$ times the α of the molecule, $X-X$, where X and Y are isotopic atoms.

To illustrate the method, part of Table I will be calculated in detail. The first row is the hypothetical case where the measured ratio, $X^+/(X_2^+ + X^+)$, for a diatomic molecule X_2 is 0.050. If all the ions came from the same ionic state, then P as defined before would just be 0.050, and R_e could be evaluated from (7). For the purposes of numerical calculation, however, the substitution of

$$\xi = (\tfrac{1}{2}\alpha)^{\frac{1}{2}}R \quad (9)$$

in (7) yields the more convenient form

$$P=\int_{-\infty}^{\xi_e}\exp(-\xi^2)d\xi\Big/\int_{-\infty}^{\infty}\exp(-\xi^2)d\xi \quad (10)$$

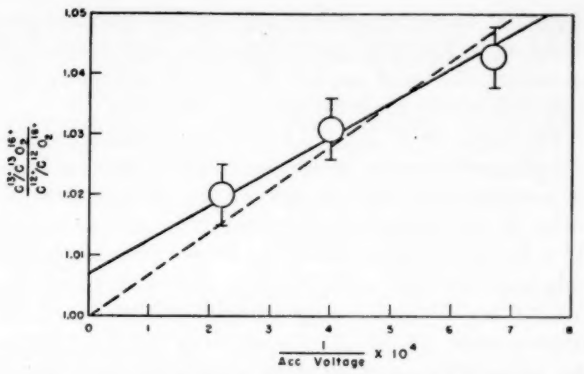

FIG. 2. The ion ratio $(C^{13+}/C^{13}O_2^{16+})/(C^{12+}/C^{12}O_2^{16+})$ as a function of the reciprocal of the ion accelerating voltage. The solid line represents the best fit to the data. The dashed line represents the best fit to the data which also extrapolates to unity at high ion accelerating voltages.

where

$$\xi_e = (\tfrac{1}{2}\alpha)^{\frac{1}{2}}R_e. \quad (11)$$

By the use of a table of the integral of the normal error curve,[6] ξ_e can be readily evaluated to be 1.163. Let P', ξ_e', and α' be the corresponding quantities for the isotopic molecule $X-Y$. Then, as $\alpha' = 1.1\alpha$, ξ_e' becomes -1.220 and P' can be evaluated from the error integral to be 0.042, the value listed in Table I.

Consider now the case where the ions originated from two states such that half the atomic ions come from each state, but one-third the molecule ions come from one state and two-thirds from the other. Then the measured ratio $X^+/(X^+ + X_2^+) = 0.050$ corresponds to two states which have P's of 0.0732 and 0.0380. The corresponding P' values are found to be 0.0634 and 0.0314 by the same method used for the single state above. The predicted ratio $(X^+ + Y^+)/(X^+ + Y^+ + XY^+)$ in this case is 0.043. For this calculation it is noted that as the over-all transition probability to a given

TABLE III. C^+/CO^+ ratios for carbon monoxide.

Molecule	Observed[a] C^+/CO^+	Calculated C^+/CO^+
$O^{12}O^{16}$	0.054	(Used to evaluate R_e)
$O^{13}O^{16}$	0.051	0.052

[a] See reference 10.

TABLE IV. C^+/CO_2^+ ratios from $C^{12}O_2^{16}$ and $C^{13}O_2^{16}$.

Electron voltage[a]	$C^{12+}/C^{13}O_2^{16+}$	$C^{13+}/C^{13}O_2^{16+}$	$\frac{C^{13+}/C^{13}O_2^{16+}}{C^{12+}/C^{12}O_2^{16+}}$
35	0.0121	0.0123	1.015
40	0.0216	0.0220	1.018
50	0.0318	0.0328	1.031
60	0.0392	0.0400	1.022
68	0.0412	0.0418	1.015

[a] Not corrected for contact potential. For these measurements the ion accelerating voltage was 4500 v.

[6] For example, *Tables of Probability Functions* National Bureau of Standards, Washington, D. C.

electronic state is dependent only on the electronic part of the wave function[7] (and hence the same for isotopic molecules) the total number of ions originating by each state will be the same for isotopic molecules.

The range of $X^+/(X_2^+ + X^+)$ listed in Table I is that encountered in most molecules. The calculation based on a single state does not deviate appreciably from the value if two states are involved both of comparable $X^+/(X_2^+ + X^+)$ ratio. However, it does deviate appreciably from the true value if one of the states either contributes no X^+ and a large fraction of the X_2^+ or if a large amount of the X^+ comes from repulsive states. An interesting point to note is that in the range of $X^+/(X^+ + X_2^+)$ considered in Table I, the largest isotope effect is obtained if the X^+ all comes from a single bound state.

For experimental data which are determined at low electron voltages there will be negligible amounts of ions contributed from repulsive states. However, there will not necessarily be negligible amounts of undissociated ions contributed from states having low probability of fragmentation. The assumption of only one state as responsible will in these cases lead to an upper limit for most isotope effects.

COMPARISON WITH EXPERIMENTAL DATA

Nitrogen

The mass spectral pattern of a mixture of $N^{14}N^{14}$, $N^{14}N^{15}$, and $N^{15}N^{15}$ has been obtained using 50-v electrons.[8] From this pattern and that of a sample of natural abundance nitrogen Mohler *et al.* were able to obtain values of X^+/X_2^+ for all three isotopic molecules. These are listed in Table II along with a set of values calculated by the preceding method assuming all the ions originate from a single state. The agreement between the experimental data and the calculated values is satisfactory. The ratios listed by Mohler and co-workers were obtained by subtracting a number of contributions to the 14 and 15 mass peaks which tends to increase the error. The observations were made by electrostatic scanning which requires a correction for discrimination.[9] Discrimination will reduce the apparent isotope effect and make the observed values approach the calculated ones. On the other hand, there are known low lying states of N_2^+ whose R_e values are so small that the states would lead to negligible fragmentation.

Carbon Monoxide

For carbon monoxide Dibeler and co-workers[10] have obtained the ratios $C^{13+}/C^{13}O^{16+}$ and $C^{12+}/C^{12}O^{16+}$ from a C^{13} enriched sample. The comparison of these observations with a calculated $C^{13+}/C^{13}O^{16+}$ ratio appears in Table III. Here again the agreement is better than one would expect as the same sort of errors are involved as discussed before for nitrogen.

Carbon Dioxide

A particularly interesting case which will test the assumption of the independence of the bonds is that of the ratios $C^{13+}/C^{13}O_2^{16+}$ and $C^{12+}/C^{12}O_2^{16+}$ from carbon dioxide. The normal modes of carbon dioxide are represented in Fig. 1. The bending mode can be neglected as there are never any large repulsive terms in its motion. The only mode capable of yielding C^+ is ν_1, to the approximation discussed before. Since for ν_1, m equals the mass of O^{16}, the value of α for $C^{13}O_2^{16}$ and $C^{12}O_2^{16}$ will be the same. Hence the observed ratios $C^{13+}/C^{13}O_2^{16+}$ and $C^{12+}/C^{12}O_2^{16+}$ should be the same. Dibeler and co-workers[10] have reported the values $C^{13+}/C^{13}O_2^{16+}=0.0542$ and $C^{12+}/C^{12}O_2^{16+}=0.0564$. Since it seemed that this non-equality might have been caused by a discrimination error in the mass spectral data, this point was investigated by redetermining the values at high accelerating voltages and with magnetic scanning at this Laboratory.

For the measurements the 60° spectrometer described elsewhere[4] was used. The CO_2 was prepared by adding sulfuric acid to a 40 percent excess C^{13} $BaCO_3$ sample obtained from Eastman Kodak Company. The ratios $C^{13+}/C^{13}O_2^{16+}$ and $C^{12+}/C^{12}O_2^{16+}$ were measured at 4500-v ion accelerating potential for several electron voltages. These appear in Table IV.

Instead of the $C^{13+}/C^{13}O_2^{16+}$ ratio being four percent smaller than the $C^{12+}/C^{12}O_2^{16+}$ ratio, the $C^{13+}/C^{13}O_2^{16+}$ ratio was found to be two percent larger than the $C^{12+}/C^{12}O_2^{16+}$ ratio. The ratio of the ratios $(C^{13+}/C^{13}O_2^{16+})/(C^{12+}/C^{12}O_2^{16+})$, was then measured at several ion accelerating voltages using 70-v electrons. Figure 2 shows a plot of this ratio as a function of the reciprocal of the ion accelerating voltage. These data fall on a straight line which extrapolates to a ratio of 1.007 at infinite accelerating voltage, a ratio larger than unity. On the other hand, the data are not inconsistent with an extrapolation to a ratio of unity. It is difficult to understand a ratio larger than unity except as an instrumental effect. The question which Fig. 2 answers negatively is whether the instrumental effect is larger than the isotope effect and obscures the latter. Figure 2 is hardly consistent with a ratio smaller than unity. It may be concluded that the ratios $C^{13+}/C^{13}O_2^+$ and $C^{12+}/C^{12}O_2^+$ are indeed equal when systematic discrimination errors are removed from the measurements.

From the results given in Tables I to IV it may be concluded that the proposed method of calculation, with its necessary approximations, leads to reasonable

[7] For a discussion of this point see N. F. Mott and H. S. W. Massey, *The Theory of Atomic Collisions* (Oxford University Press, London, 1933), first edition.

[8] Dibeler, Mohler, and Reese, J. Chem. Phys. **18**, 156 (1950).

[9] H. Washburn and C. Berry, Phys. Rev. **71**, 559 (1946).

[10] Dibeler, Wells, and Reese, Phys. Rev. **79**, 223 (1950).

agreement with experimental results available at present. It must be admitted that inaccuracies inherent in the available experimental data prevent a sharp quantitative comparison with theory. On the other hand, the assumption that the bonds are independent and that only those break which possess large amounts of potential energy at the instant of ionization is verified when instrumental systematic errors are evaluated.

Note.—After this method of calculation had been formulated, the author learned that an independent treatment of this problem, however, only applicable to diatomic molecules, was presented by D. P. Stevenson and J. W. Otvos at the Consolidated Mass Spectrometer Group Meeting, New Orleans (May, 1950).

THE JOURNAL OF CHEMICAL PHYSICS VOLUME 18, NUMBER 11 NOVEMBER, 1950

On the Stability of Gas Bubbles in Liquid-Gas Solutions

P. S. Epstein and M. S. Plesset
California Institute of Technology, Pasadena, California

(Received July 31, 1950)

With the neglect of the translational motion of the bubble, approximate solutions may be found for the rate of solution by diffusion of a gas bubble in an undersaturated liquid-gas solution; approximate solutions are also presented for the rate of growth of a bubble in an oversaturated liquid-gas solution. The effect of surface tension on the diffusion process is also considered.

INTRODUCTION

THE stability of gas bubbles in a liquid-gas solution is of concern in several problems of physical interest. Among these may be mentioned the extinction of sound or light in water by air bubbles, and the diffusion of air into the bubbles formed in the cavitating flow of a liquid.[1]

A gas bubble in a liquid-gas solution will grow or shrink by diffusion according as the solution is oversaturated or undersaturated. The resulting motion of the bubble boundary introduces a transport term in the diffusion equation which makes it very difficult to obtain an analytic solution. This effect of the motion of the medium on the diffusion process is neglected in the following analysis; the resulting approximation, however, is quite good. The physical reason for the accuracy of the approximation is that the concentration of dissolved gas in the liquid surrounding the bubble is much smaller than the gas density in the bubble, and the region in the solution around the bubble through which the diffusion process takes place is very soon much larger than the bubble itself. Under this circumstance, the size of the bubble is of little consequence so far as the configuration of the surrounding concentration in the solution is concerned. The bubble size is important only insofar as it determines the interfacial area across which the mass transfer between phases takes place.

A more significant effect on the accuracy of the numerical results obtained here arises from translatory motion of a gas bubble in a liquid. Consider, for example, the motion due to buoyancy of an air bubble of density ρ in water of density ρ'. The buoyant force is

$$F=(4\pi/3)g(\rho'-\rho)R^3,$$

where g is the acceleration of gravity and R is the bubble radius. The terminal velocity of rise of the bubble, v, is attained when this force is balanced by the force of resistance which is given approximately by Rybczynski's formula[2] to be

$$F_R=6\pi\mu' Rv\frac{2\mu'+3\mu}{3\mu'+3\mu},$$

where μ' is the coefficient of viscosity of the liquid and μ is the coefficient of viscosity of the gas. The terminal velocity is found at once and, since ρ/ρ' and μ/μ' are small, it has very nearly the value

$$v=(g/3)(\rho'/\mu')R^2.$$

Thus, an air bubble of radius $R=10^{-3}$ cm has a terminal velocity of rise in water $v=3\times10^{-2}$ cm/sec. Even this slow motion through the diffusion atmosphere around the bubble is sufficient to produce some slight acceleration of the diffusion process. Hence, the diffusion rates deduced here will be somewhat low.

A summary of the results is contained in Tables I, II and in Figs. 1–4.

MATHEMATICAL SOLUTION OF THE DIFFUSION PROBLEM

Let us suppose that at the initial time $t=0$ a spherical gas bubble of radius R_0 is placed in a liquid-gas solution in which the concentration of dissolved gas is uniform and equal to c_i. The solution will be assumed to be at constant temperature and pressure, and the dissolved gas concentration for a saturated solution at this temperature and pressure will be denoted by c_s. The center

[1] See M. S. Plesset, J. App. Mech. **16**, 277 (1949).

[2] See H. Lamb, *Hydrodynamics*, 6th edition (Cambridge University Press, London, 1932), p. 601. Rybczynski's formula should be used here rather than Stokes' formula, since the latter applies strictly to a rigid sphere in a fluid medium.

TABLE I. Times for complete solution of air bubbles in water.

f	$R_0=10^{-3}$ cm T (sec.)	T_A (sec.)	T_S (sec.)	$R_0=10^{-2}$ cm $T_A\times10^{-3}$ (sec.)	$T_S\times10^{-3}$ (sec.)	$R_0=10^{-1}$ cm $T_A\times10^{-4}$ (sec.)	$T_S\times10^{-4}$ (sec.)
0	1.05	1.25	1.17	1.25	1.24	1.25	1.25
0.25	1.44	1.67	1.46	1.67	1.64	1.67	1.66
0.50	2.21	2.50	1.96	2.50	2.41	2.50	2.49
0.75	4.58	5.00	2.99	5.00	4.60	5.00	4.95
1.00	∞	∞	6.63	∞	58.8	∞	580

The tabulated values are the times, in seconds, required for air bubbles to dissolve completely in air-water solutions at 22°C. R_0 is the initial radius of the bubble, f is the ratio of the dissolved concentration of air in the solution c_i to the dissolved concentration for a saturated solution c_s. T is time calculated from the complete solution of Eqs. (17) with surface tension neglected; T_A is the time calculated from the approximation to Eq. (17) given in Eq. (16) which also neglects surface tension; T_S is the time calculated including surface tension effects under the same approximation as is used in obtaining T_A so that the effects of surface tension are noted by comparison of T_S and T_A. It should be remarked that T and T_A are proportional to R_0^2.

TABLE II. Times of growth of air bubbles in water from R_0 to $10R_0$.

f	$R_0=10^{-3}$ cm T (sec.)	T_A (sec.)	T_S (sec.)	$R_0=10^{-2}$ cm $T_A\times10^{-2}$ (sec.)	$T_S\times10^{-2}$ (sec.)
1.25	466	496	567	496	501
1.50	228	248	266	248	249
1.75	149	165	174	165	166
2.00	110	124	129	124	124
5.00	24.6	30.9	31.7	30.9	31.0

The tabulated values are the times, in seconds, required for air bubbles in an air-water solution at 22°C to grow from R_0 to $10R_0$. The ratio of the dissolved concentration to the dissolved concentration for a saturated solution is f. T is calculated from complete solution of Eqs. (24) which neglects surface tension; T_A is calculated from the approximate solution of Eq. (23) which also neglects surface tension; and T_S is the time calculated with the same approximation except that the effect of surface tension is included.

of the gas bubble will be assumed to be at rest, and it will be taken as the origin of a spherical polar coordinate system. At any time $t>0$ when the bubble radius is R, the dissolved gas concentration c at a point in the solution at a distance r from the origin is to be found from the diffusion equation

$$\partial c/\partial t=\kappa\Delta c, \tag{1}$$

where κ is the coefficient of diffusivity of the gas in the liquid. The transport term, $\mathbf{u}\cdot\Delta c$, in which $\mathbf{u}$ is the velocity produced in the medium by bubble growth or shrinkage, has been omitted from the left-hand side of Eq. (1). A spherically symmetric solution, $c(r, t)$, of Eq. (1) is to be found which satisfies the following conditions:

$$c(r, 0)=c_i, r>R;\quad \lim_{r\to\infty}c(r, t)=c_i, t>0; \tag{2a}$$

$$c(R, t)=c_s, t>0. \tag{2b}$$

It is convenient to introduce the dependent variable

$$u=r(c-c_s) \tag{3}$$

in place of c so that Eq. (1) becomes

$$\partial u/\partial t=\kappa(\partial^2u/\partial r^2), \tag{4}$$

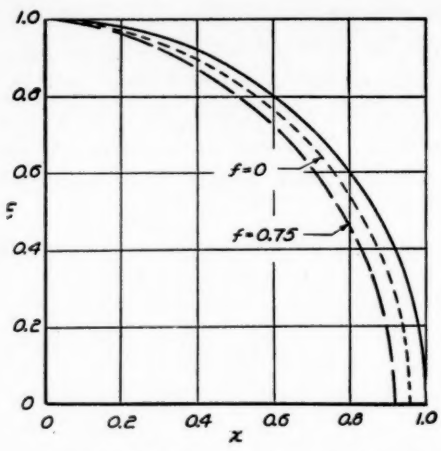

FIG. 1. Radius-time relation for dissolving bubbles neglecting surface tension. The ordinate, ϵ, is the ratio of the bubble radius to its initial radius, and the abscissa, x, is a dimensionless variable proportional to the square root of the time (compare Eq. (13)). The solid curve is the approximate quasi-static solution of Eq. (16) which, in this dimensionless form, gives the radius-time behavior for any type of gas bubble in any undersaturated solution. The dashed curves come from the more accurate Eqs. (17) and depend in form on the ratio of the saturated dissolved-gas concentration to the gas density (c_s/ρ); the value used in these curves is $c_s/\rho=0.02$, which is the value for an air-water solution at 22°C. f is the ratio of the initial dissolved-air concentration to the concentration at saturation.

with initial and boundary conditions

$$u(r, 0)=r\delta, \tag{5a}$$

$$u(R, t)=0. \tag{5b}$$

The constant δ has, of course, the value (c_i-c_s). One

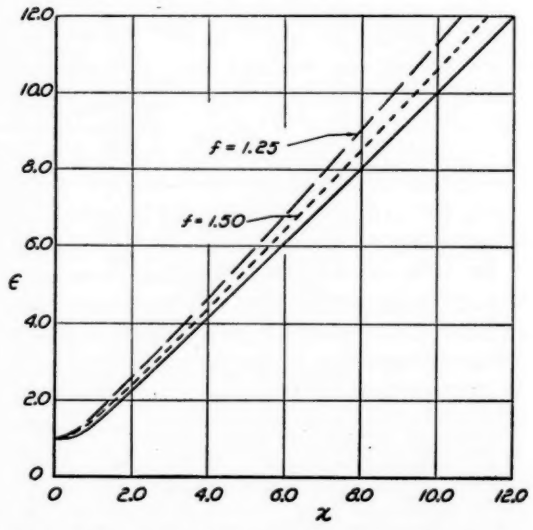

FIG. 2. Radius-time relation for growing bubbles neglecting surface tension. The solid curve is the approximate quasi-static solution of Eq. (23) and gives in dimensionless form the radius-time behavior for a bubble growing in any oversaturated solution. The dashed curves are the more accurate solution of Eqs. (24). The dimensionless variables ϵ and x are defined in Eq. (21); f is the ratio of the dissolved-gas concentration to the concentration at saturation. For the dashed curves, it has been assumed that $c_s/\rho=0.02$.

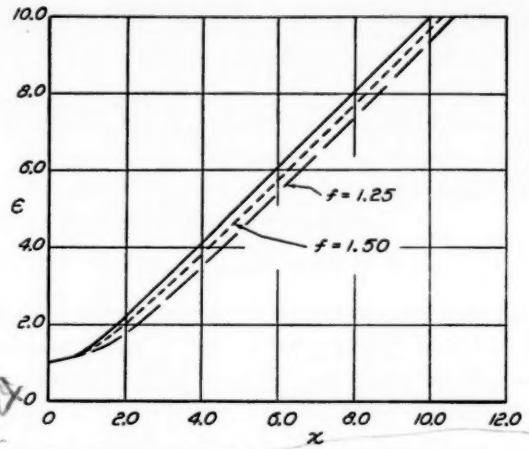

FIG. 3. Radius-time relation for dissolving bubbles with and without surface tension. The solid curve gives the radius-time behavior for a gas bubble in an undersaturated solution with surface tension neglected (Eq. (16)). The dashed curves include the effect of surface tension and are drawn for an initial bubble radius $R_0=10^{-3}$ cm; the surface tension constant is for an air-water combination, and $c_s/\rho=0.02$.

need only make a linear shift in the r-coordinate by

$$\xi=r-R$$

in order to make the problem identical with a familiar problem in heat conduction which has the solution[3]

$$u(r,t)=\frac{\delta}{2(\pi\kappa t)^{\frac{1}{2}}}\int_0^\infty (R+\xi')\{\exp[-(\xi-\xi')^2/4\kappa t] -\exp[-(\xi+\xi')^2/4\kappa t]\}d\xi'. \quad (6)$$

The quantity of interest is the concentration gradient at $r=R$. One finds directly from (6) that

$$(\partial u/\partial r)_R=\delta\{1+R/(\pi\kappa t)^{\frac{1}{2}}\};$$

and, since $(\partial c/\partial r)_R=(\partial u/\partial r)_R/R$, one has

$$\left(\frac{\partial c}{\partial r}\right)_R=\delta\left\{\frac{1}{R}+\frac{1}{(\pi\kappa t)^{\frac{1}{2}}}\right\}. \quad (7)$$

Thus, the mass flow into the bubble per unit time has the value

$$\frac{dm}{dt}=4\pi R^2\kappa\left(\frac{\partial c}{\partial r}\right)_R=4\pi R^2\kappa\delta\left\{\frac{1}{R}+\frac{1}{(\pi\kappa t)^{\frac{1}{2}}}\right\}. \quad (8)$$

Now Eq. (8) is a solution of the diffusion problem which is valid only for a stationary bubble boundary. It is, however, as has been discussed above, a reasonable physical approximation to use this result for a bubble boundary which changes in time by diffusion. Then, if ρ is the density of the gas in the bubble, one has

$$dm/dt=4\pi R^2\rho(dR/dt), \quad (9)$$

[3] See, for example, H. S. Carslaw, *Introduction to the Mathematical Theory of the Conduction of Heat in Solids* (Dover Publications, New York 1945), p. 158.

so that, from Eq. (8),

$$\frac{dR}{dt}=\frac{\kappa\delta}{\rho}\left\{\frac{1}{R}+\frac{1}{(\pi\kappa t)^{\frac{1}{2}}}\right\}. \quad (10)$$

In addition to the coefficient of diffusivity, κ, the physical constants which enter are the ratio of the saturated dissolved gas concentration to the gas density

$$d=c_s/\rho,$$

and the ratio of the initial dissolved gas concentration to the concentration at saturation

$$f=c_i/c_s.$$

The differential Eq. (10) is readily solved, and the two cases of an undersaturated solution, $0\leqq f<1$, and of an oversaturated solution, $f>1$, will be considered separately.

Bubble Dissolving in an Undersaturated Solution

Equation (10) may be written in the form

$$\frac{dR}{dt}=-\alpha\left\{\frac{1}{R}+\frac{1}{(\pi\kappa t)^{\frac{1}{2}}}\right\} \quad (11)$$

where now α is a positive constant with the value

$$\alpha=\kappa(c_s-c_i)/\rho=\kappa d(1-f). \quad (12)$$

It is convenient to put Eq. (11) in dimensionless form. With

$$\epsilon=R/R_0, \quad x^2=(2\alpha/R_0^2)t, \quad (13)$$

the differential equation becomes

$$d\epsilon/dx=-x/\epsilon-2\gamma, \quad (14)$$

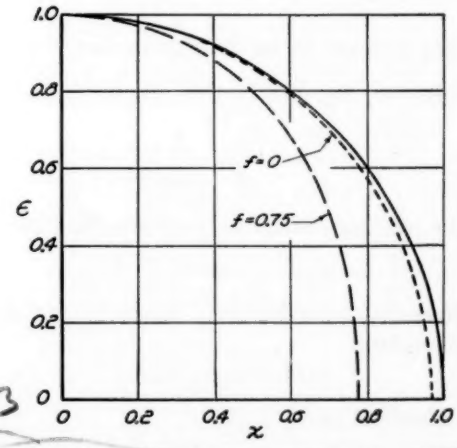

FIG. 4. Radius-time relation for growing bubbles with and without surface tension. The solid curve gives the radius-time behavior for a gas bubble in an oversaturated solution with surface tension neglected (Eq. (23)). The dashed curves include the effect of surface tension; for these curves the initial bubble radius has been taken to be 10^{-3} cm; the surface tension constant is that of an air-water combination; and $c_s/\rho=0.02$.

where

$$\gamma=\left(\frac{c_s-c_i}{2\pi\rho}\right)^{\frac{1}{3}}. \tag{15}$$

It is to be noted that the constant γ is in general small compared to x/ϵ when enough time has elapsed for significant diffusion to take place, so that an approximate solution may be obtained by neglecting γ. This neglect is equivalent to omitting the second term of Eq. (11) in which the time appears explicitly. This approximate solution is

$$\epsilon^2=1-x^2. \tag{16}$$

A solution to the complete equation may also be readily found. Since Eq. (14) is homogeneous, it is convenient to express the solution in parametric form. One then finds in a straightforward manner that

$$\epsilon=e^{-\gamma z}\{\cos[(1-\gamma^2)^{\frac{1}{2}}z] -\gamma(1-\gamma^2)^{-\frac{1}{2}}\sin[(1-\gamma^2)^{\frac{1}{2}}z]\}; \tag{17a}$$

$$x=e^{-\gamma z}(1-\gamma^2)^{-\frac{1}{2}}\sin[(1-\gamma^2)^{\frac{1}{2}}z]. \tag{17b}$$

The scale of the parameter z has been fixed so that $z=0$ when $x=0$ and $\epsilon=1$. A comparison of the approximate solution (16) with the accurate solution (17) is given graphically in Fig. 1, and it is evident that the approximation is fairly good. Herein is contained a justification of the remark in the introduction that the diffusion concentration c is rapidly adjusted to a quasi-static distribution.

The time required for a bubble to dissolve completely is given from Eq. (16) by $x=1$, and from Eqs. (17) by $x=\exp[-\gamma(1-\gamma^2)^{-\frac{1}{2}}\cos^{-1}\gamma]$. In either case, the time for complete solution is proportional to R_0^2. Some numerical values for times of complete solution are given in Table I for air bubbles in water where the constants have been fixed by taking $\kappa=2\times10^{-5}$ cm^2 sec.$^{-1}$, and from the solubility of air at 22°C, $c_s/\rho=0.02$.

Bubble Growth in an Oversaturated Solution

For this case, Eq. (10) may be written in the form

$$\frac{dR}{dt}=\alpha\left\{\frac{1}{R}+\frac{1}{(\pi\kappa t)^{\frac{1}{2}}}\right\} \tag{18}$$

where the positive constant α now has the value

$$\alpha=\kappa(c_i-c_s)/\rho=\kappa d(f-1). \tag{19}$$

The differential equation may again be put into dimensionless form

$$d\epsilon/dx=(x/\epsilon)+2\gamma \tag{20}$$

by the substitutions

$$\epsilon=R/R_0;\quad x^2=(2\alpha/R_0^2)t. \tag{21}$$

The constant γ now is given by

$$\gamma=\left(\frac{c_i-c_s}{2\pi\rho}\right)^{\frac{1}{3}}. \tag{22}$$

The approximate solution obtained with the neglect of γ is

$$\epsilon^2=1+x^2, \tag{23}$$

and the accurate solution of Eq. (20) is readily found to be

$$\epsilon=e^{\gamma z}\{\cosh[(1+\gamma^2)^{\frac{1}{2}}z] +\gamma(1+\gamma^2)^{-\frac{1}{2}}\sinh[(1+\gamma^2)^{\frac{1}{2}}z]\}; \tag{24a}$$

$$x=e^{\gamma z}(1+\gamma^2)^{-\frac{1}{2}}\sinh[(1+\gamma^2)^{\frac{1}{2}}z]. \tag{24b}$$

A graphical comparison of the solutions given by Eq. (23) and Eqs. (24) is given in Fig. 2, and it is evident from both solutions that ϵ varies linearly with x when x is large. In fact, one finds from Eqs. (24)

$$\epsilon\approx[\gamma+(1+\gamma^2)^{\frac{1}{2}}]x,\quad \epsilon, x\gg1. \tag{25}$$

A tabulation of the times of growth from R_0 to $10R_0$ for air bubbles in water at 22°C is presented in Table II.

Effect of Surface Tension on the Diffusion

If the surface tension constant for the given gas-liquid combination is σ, then the equation of state for a gas bubble of radius R in a liquid at pressure p, and temperature T, is

$$p+2\sigma/R=(B/M)\rho(R)T \tag{26}$$

where $\rho(R)$ is the gas density in the bubble, M is the molecular weight of the gas, and B is the universal gas constant. Thus,

$$\rho(R)=\frac{M}{BT}p+\frac{2M\sigma}{BT}\frac{1}{R}, =\rho(\infty)+\tau/R, \tag{27}$$

where $\rho(\infty)$ is the density of the gas under the same conditions of pressure and temperature with a gas-liquid interface of zero curvature, and

$$\tau=2M\sigma/BT. \tag{28}$$

The mass of gas in the bubble is

$$m=\frac{4\pi}{3}R^3\rho(R)=\frac{4\pi}{3}R^3\rho(\infty)+\frac{4\pi}{3}R^2\tau \tag{29}$$

so that

$$\frac{dm}{dt}=4\pi R^2\frac{dR}{dt}\left\{\rho(\infty)+\frac{2\tau}{3R}\right\}. \tag{30}$$

Equation (30) now replaces Eq. (9). The equality of (8) and (30) gives the differential equation for the bubble radius

$$\frac{dR}{dt}=\frac{\kappa(c_i-c_s)}{\rho(\infty)+2\tau/3R}\left\{\frac{1}{R}+\frac{1}{(\pi\kappa t)^{\frac{1}{2}}}\right\}. \tag{31}$$

The dissolved concentration, c_s, which is in equilibrium

with the gas density $\rho(R)$, is given by

$$c_s/\rho(R)=d, \quad c_s=[\rho(\infty)+\tau/R]d, \tag{32}$$

where the value of d is the same as that used in the previous formulation since it may be shown that d is not affected by surface tension effects. As before, the initial dissolved concentration, c_i, is conveniently expressed in terms of f by the relation

$$c_i/\rho(\infty)=fd. \tag{33}$$

Equation (31) may now be written

$$\frac{dR}{dt}=-\kappa d\frac{1-f+\tau/(R\rho(\infty))}{1+2\tau/(3R\rho(\infty))}\left\{\frac{1}{R}+\frac{1}{(\pi\kappa t)^{\frac{1}{2}}}\right\}, \tag{34}$$

and the following dimensionless variables

$$\epsilon=R/R_0, \quad x'^2=(2\kappa d/R_0^2)t, \tag{35}$$

put this equation in the form

$$\frac{d\epsilon}{dx'}=-\frac{(1-f)+\delta/\epsilon}{1+2\delta/3\epsilon}\left\{\frac{x'}{\epsilon}+2b\right\}, \tag{36}$$

where

$$\delta=\tau/[R_0\rho(\infty)], \quad b=(d/2\pi)^{\frac{1}{2}}. \tag{37}$$

An approximate solution corresponding to Eqs. (16) and (23) except for the inclusion of surface tension is found by neglecting the small constant b in Eq. (36). This solution is

$$1-\epsilon^2-2\delta\left[\frac{1}{1-f}-\frac{2}{3}\right](1-\epsilon)+\frac{2\delta^2}{1-f}\left[\frac{1}{1-f}-\frac{2}{3}\right]\ln\frac{\delta+(1-f)}{\delta+(1-f)\epsilon}=x'^2(1-f). \tag{38}$$

When $0\leq f<1$, one may put

$$x^2=x'^2(1-f) \tag{39a}$$

in Eq. (38). The resulting function $\epsilon(x)$ when $R_0=10^{-3}$ cm is compared graphically in Fig. 3 with the corresponding solution without surface tension given by Eq. (16). The time of complete solution with surface tension is given in Table I for air bubbles in water, where as before the constants have the values $\kappa=2\times10^{-5}$ cm^2 sec.$^{-1}$, $d=0.02$.

When $f>1$, the substitution

$$x^2=x'^2(f-1) \tag{39b}$$

may be used in Eq. (38) and the resulting function $\epsilon(x)$ for $R_0=10^{-3}$ cm is compared graphically in Fig. 4 with the corresponding solution without surface tension given by Eq. (23). Numerical values for the growth of air bubbles in oversaturated water with the effect of surface tension included are given in Table II.

The special case $f=1$ is of interest. If surface tension is neglected, a bubble of any radius would be stable against diffusion in a saturated solution. Such a bubble actually dissolves because of surface tension, and its behavior in time is found by putting $f=1$ in Eq. (36). The solution with neglect of the term containing the constant b is

$$1-\epsilon^3+\delta(1-\epsilon^2)=(3\delta/2)x'^2, \tag{40}$$

and the time to complete solution is given by

$$x'^2=(2/3\delta)(1+\delta). \tag{41}$$

Numerical values determined from Eq. (41) are given in Table I where the constants have the values appropriate for air bubbles in water at 22°C.

Letters to the Editor

THIS section will accept reports of new work, provided these are terse and contain few figures, and especially few half-tone cuts. The Editorial Board will not hold itself responsible for opinions expressed by the correspondents. Contributions to this section should not exceed 600 words in length and must reach the office of the Managing Editor not later than the first of the month preceding that of the issue in which the letter is to appear. No proof will be sent to the authors. The usual publication charge ($8.00 per page) will not be made and no reprints will be furnished free.

The Theory of Open-Tube Distillation Column

MARCEL BERTRAND AND MARCEL RINFRET
Department of Chemistry, University of Montreal, Montreal, Canada
August 14, 1950

FOR total reflux and ideal reflux conditions, the H.E.T.P. of an open-tube distillation column was found by Westhaver[1] to be $11vr^2/48D$ where v is the radially averaged velocity, r the radius, and D the molecular diffusion coefficient of the vapor stream.

The graphical representation of the above formula should give a straight line passing through the origin.

The authors[2] have found that the H.E.T.P. varies proportionately with the average velocity of the vapor stream but that the straight line which represents that proportionality does not pass through the origin.

The experiments were conducted in a highly insulated column as suggested by Westhaver.[1]

The results are summarized in Table I and in Fig. 1.

We think that the fact that the curve does not pass through the origin can be explained by a retardation of the equilibrium between the flow of vapor and the reflux film.

The ratio of the number of vapor molecules condensing on a surface, per second, to the total number incident on the surface may be defined as the "condensation coefficient" of the vapor at the surface.

Alty[3] has shown experimentally that the condensation coefficient is not always unity, as one can see in Table II. It can be noted that the molecules which have a zero dipole moment have a condensation coefficient of unity; on the other hand, the coefficient is small for molecules of large dipole moment.

We believe that the attainment of equilibrium is proportional to the number of collisions per second on the liquid surface and also to the efficiency of the collisions. In fact, all the collisions are not efficient according to Alty's results.

By the kinetic theory the number of collisions per second is equal to the number of molecules multiplied by the average velocity of those molecules.

TABLE I.

Binary mixtures	Vapor stream velocity cm/sec.	H.E.T.P. cm
$CHCl_3-CCl_4$	1.11	61.3
	4.31	95.3
	7.38	122.0
	13.87	193.7
$CH_3OH-C_2H_5OH$	4.15	42.2
	12.38	54.2
	16.48	61.9
	24.71	72.2
$C_6H_6-C_2H_4Cl_2$	11.30	24.1
	16.83	26.6
	22.61	31.4
	28.38	39.4

TABLE II.

Substances	Condensation coefficient
Benzene	1.0
Carbon tetrachloride	1.0
Benzoic acid	0.29
Water	0.036
Ethyl alcohol	Small

TABLE III.

Constituents	Averaged velocity cm/sec.	Molar fraction	Number of collisions/ cm^2/sec.	Collisions of mixture
$CHCl_3$	24572	0.16	3930	22150
CCl_4	21691	0.84	18220	
C_6H_6	30916	0.36	11130	28690
$C_2H_4Cl_2$	27441	0.64	17560	
CH_3OH	47791	0.14	6690	39870
C_2H_5OH	38587	0.86	33180	

In Table III are summarized the number of collisions which were calculated for our binary mixtures. We can consider that (1) the retardation is greater when there are less collisions and (2) and still greater when they are less efficient.

Now, if we compare the results shown in Fig. 1 with those in Table III we can come to the conclusion that: (1) The retardation for the $CHCl_3-CCl_4$ mixture is the greatest because the number of collisions is small and, for $CHCl_3$, not very efficient, because the $CHCl_3$ has a large dipole moment and therefore a small condensation coefficient. (2) The retardation for the $CH_3OH-C_2H_5OH$ mixture is almost as large because the efficiency of the very large

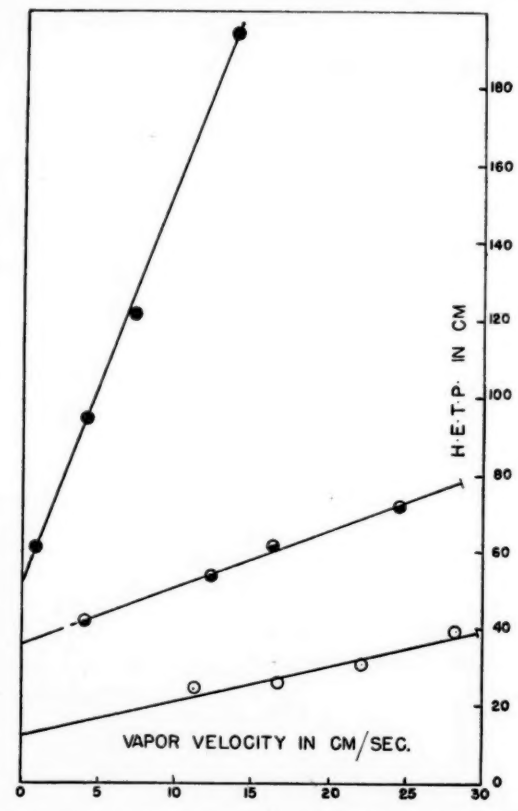

FIG. 1. ● $CHCl_3-CCl_4$. ◓ $CH_3OH-C_2H_5OH$. ○ $C_6H_6-C_2H_4Cl_2$.

number of collisions is very small for ethyl alcohol, according to Alty's results, and we can presume the same effect for methyl alcohol which has about the same dipole moment as ethyl alcohol. (3) The retardation of the $C_6H_6-C_2H_4Cl_2$ mixture is small because the number of collisions is large and only the ethylene chloride has a condensation coefficient less than unity.

[1] J. W. Westhaver, Ind. and Eng. Chem. **34**, 126 (1942).
[2] M. Bertrand, Ph.D. thesis, University of Montreal (1950).
[3] T. Alty, Nature **139**, 374 (1937).

Nuclear Magnetic Resonance in Methane*

J. T. Thomas, N. L. Alpert, and H. C. Torrey
Physics Department, Rutgers University, New Brunswick, New Jersey
August 16, 1950

NUCLEAR magnetic resonance studies of materials with more than one phase in the solid state have been carried on in this laboratory as a continuation of the earlier work done by one of us.[1]

The most interesting and complete results have so far been obtained in methane. Plots of the thermal relaxation time (T_1) and of the line width (ΔH) *vs.* absolute temperature are shown in Figs. 1 and 2, respectively.

The technique used has been the pulse method recently described by Torrey.[2] All of the data reported here were taken using a new nuclear resonance cryostat designed and constructed in this laboratory. This cryostat operates on the principle of adiabatic isolation commonly used in specific heat measurements. The cryostat and associated equipment permit the variation, control, and measurement of temperature to within better than 0.1°K in the vicinity of 20°K and lower, and to within better than 0.2°K in the vicinity of 80°K and lower.

The line-width data obtained here on methane do not agree with those previously reported.[1] This is not the case for other materials for which we have obtained close checks. In view of the comparatively qualitative nature of the data taken in those early, exploratory experiments on methane, this is not surprising. The absence of any change in line width at the λ-point at 20.4°K eliminates the possibility of a rotational transformation, as originally suggested by Pauling.[3] This conclusion is in agreement with the x-ray observations of Mooy.[4]

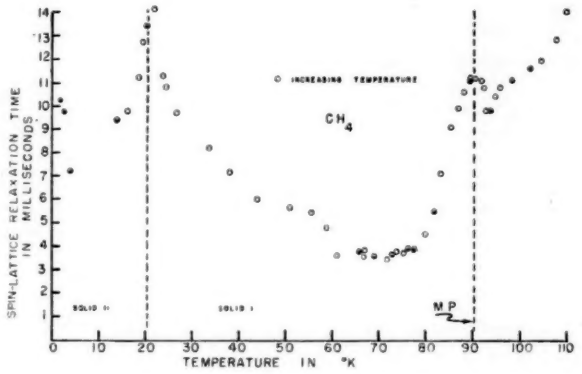

FIG. 1.

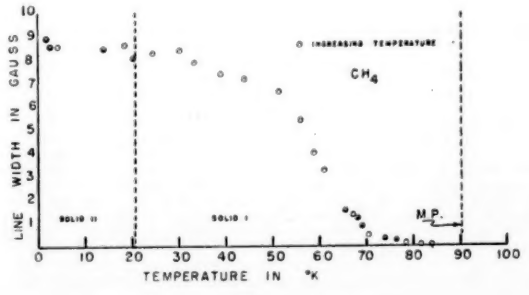

FIG. 2.

The data for T_1 are more complex. The values reported here are reproducible to about one percent above 65°K and to about five percent below 65°K where the line becomes broad. The salient features are: (1) The extremely small value of T_1 in the vicinity of 2 to 4°K. (2) The behavior of T_1 is anomalous in the vicinity of the λ-point and there may be a small discontinuity in T_1 near the λ-point. This will be studied further. (3) There are two dips in T_1 in the solid state, rather than one as might be expected on the basis of the Bloembergen, Purcell, Pound[5] theory. (4) T_1 is continuous across the melting point. (5) The small dip in T_1 just above the melting point is unexpected on the basis of existing theories.

At first we suspected the presence of paramagnetic impurity, particularly oxygen, which might explain (1) above.[6] Since we did not know the impurities in the sample, we condensed a new sample from a tank of Matheson c.p. (better than 99 percent) methane, which is supposed to contain traces of ethane, nitrogen, and carbon dioxide, but no oxygen. This showed roughly the same relaxation times at helium temperatures and gave about the same variation with temperature, according to a few spot checks at various temperatures. We plan to obtain an even purer sample to study this factor as well as other possible impurity effects.

Although data have not yet been taken between 4.2 and 14°K, there is apparently a minimum in T_1 in this range. If we assume that this dip is due to a decrease in the characteristic time[5] τ_c, we obtain values of τ_c which would require the line width to be much narrower than observed in this range. Other explanations are under study. The minimum at 73°K is qualitatively consistent with the line-width data, as predicted by the Bloembergen, Purcell, Pound theory. On the basis of this theory, τ_c is almost constant from about 30°K to about 55°K, after which it starts dropping rapidly almost up to the melting point. There is apparently sufficient activity in the solid at the melting point so that the additional Brownian motion in the liquid phase has little or no effect on τ_c.

A more detailed account of this work as well as our results on other substances will be submitted for publication in the near future.

* This work has been supported by the joint program of the ONR and AEC, by the Research Corporation, by the Rutgers University Research Council, and by the Radio Corporation of America.
[1] N. L. Alpert, Phys. Rev. **75**, 398 (1949).
[2] H. C. Torrey, Phys. Rev. **76**, 1059 (1949).
[3] L. Pauling, Phys. Rev. **36**, 430 (1930).
[4] H. H. Mooy, Leiden Comm. **19**, 213d (1931).
[5] Bloembergen, Purcell, and Pound, Phys. Rev. **73**, 679 (1948).
[6] N. Bloembergen, Physica **XV**, 386 (1949).

The Infra-Red Spectrum and Molecular Structure of HNCS

L. H. Jones and Richard M. Badger
Gates and Crellin Laboratories of Chemistry, California Institute of Technology, Pasadena, California*
August 7, 1950

FROM an examination of the microwave spectra of four isotopic species of isothiocyanic acid, Beard and Dailey[1] recently obtained the following values for the molecular parameters in the ground vibrational state:

$$r_{C-S}=1.57\pm0.01\text{A}; \quad r_{N-C}=1.21\pm0.01\text{A};$$
$$r_{N-H}=1.2\ \pm0.1\text{A}; \quad \angle\text{HNC}=112°\pm10°.$$

These C−S and N−C distances are not unexpected, but the N−H distance is abnormally long and the HNC angle abnormally

small.[2] The errors in locating the hydrogen atom from the microwave data are, of course, rather large; indeed we believe they are much larger than are indicated here.

The infra-red spectrum of isothiocyanic vapor has recently been examined in this laboratory and the coarse rotational structure of the first overtone of the N−H vibration at 6914 cm^{-1} has been resolved with a vacuum grating instrument. The large rotational constant was found to be 43.1±0.4 cm^{-1} in the ground state. The frequency of the N−H fundamental is 3530 cm^{-1} as against 3534 cm^{-1} found[3] for HNCO.

Because of the practical equality of these frequencies it is reasonable to believe that the N−H distance in HNCS does not differ appreciably from the 0.99A recently found[3] for HNCO. Using this distance and the C−S and N−C distances reported by Beard and Dailey, it is found that an HNC angle of 138°40′±1° is required to account for the rotational constant mentioned above. This angle is quite compatible with the observed hybrid structure of the NH bands, which would be difficult to account for if the angle were in the neighborhood of 112°.

The HNC angle is HNCS is about 10° larger than in HNCO which indicates that of the three resonant structures:

$$N^+\equiv C-S^- \qquad N=C=S \qquad N^--C\equiv S^+$$
$$\diagup \quad H \qquad \diagup \quad H \qquad \diagup \quad H$$

the third is less important than the analogous structure in HNCO. This is in agreement with general chemical experience which indicates that structures with a carbon-sulfur triple bond are less important than others.

* Contribution No. 1446 from the Gates and Crellin Laboratories.
[1] C. I. Beard and B. P. Dailey, J. Chem. Phys. **15**, 762 (1947).
[2] L. Pauling, *Nature of the Chemical Bond* (Cornell University Press, Ithaca, New York, 1945).
[3] Jones, Shoolery, Shulman, and Yost, J. Chem. Phys. **18**, 990 (1950).

The Infra-Red Absorption Spectrum of Isothiocyanic Acid (HNCS)

C. Reid
National Research Council, Ottawa, Canada
August 7, 1950

THE infra-red absorption spectrum of isothiocyanic acid has been studied in the region 400 to 4000 cm^{-1}, for comparison with that of isocyanic acid (HNCO) of which a more detailed study has recently been made.[1]

The isothiocyanic acid was prepared by cooling dry potassium thiocyanate to −10°C and slowly adding glacial phosphoric acid while passing a stream of dry nitrogen through the reaction vessel. The gas was condensed at −70°C, and fractionated from a bath at 0° to purify it. HCN was the most troublesome impurity.

At 0°C isothiocyanic acid has a vapor pressure of a few millimeters only, and at higher temperatures rapid decomposition or polymerization to a reddish solid occurs in the condensed phase. By heating quickly above 0°C, however, it is possible to obtain vapor pressures up to 5 cm. At this pressure the vapor is stable at room temperature, although occasionally polymerization occurs after a few hours.

The absorption spectrum was measured using a Perkin-Elmer Model 12*B* instrument with a 10-cm absorbing path, and gas pressures ranging from 1 to 50 mm. The spectrum obtained is shown in Fig. 1.

On the basis of comparisons with the normal vibrational frequencies of HNCO, COS, and of the NCS ion,[2] the assignments in Table I have been obtained. The labeling of normal vibrations is as follows: ν_1=N−H stretching; ν_2=asymmetric CNS stretching; ν_3=symmetric CNS stretching; ν_4=N−H bending; ν_5=in-plane CNS bending; ν_6=out-of-plane CNS bending. Diagrams of the normal vibrations are given in reference 1.

TABLE I. Observed infra-red absorption bands of HNCS.

ν_{vac} observed cm^{-1}	Assignment and band type		Approximate relative intensity
469	$\nu_5(a')$	Irregular hybrid	125
600	$\nu_6(a'')$	Irregular ⊥ (?)	200
817(?)	$\nu_4(a')$	Resolved hybrid	75
995	$\nu_3(a')$	∥, *P R*	50
1145	$\nu_2-\nu_4(A')$	∥, *P R*	12
1963	$\nu_2(a')$	∥, *P R*	1000
2540	$\nu_2+\nu_6(A')$	Irregular ⊥ (?)	2.5
2830	$\nu_2+\nu_4(A')$	Irregular (?)	12
2912	$\nu_2+\nu_3(A')$	Irregular (?)	4
3536	$\nu_1(a)$	Resolved hybrid	90
4130	$\nu_1+\nu_6(A')$	Irregular (?)	12

The positions of the two lowest frequency fundamentals are uncertain by about ±10 cm^{-1} since the values given are approximate centers of irregular bands in which the widely spaced ⊥ components are interlaced. The origin of ν_4 was tentatively located by the assignment of the series of parallel sub-bands with K=1, 2, and 3, respectively, centered at 810, 773, and 712 cm^{-1}. Each of these sub-bands shows *P* and *R*, but no *Q* structure. In view of the

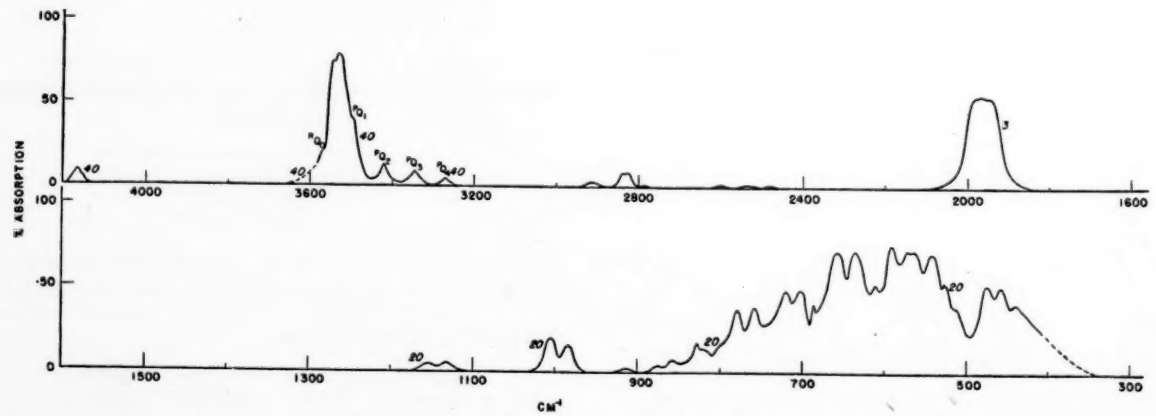

FIG. 1. Infra-red absorption spectrum of HNCS. The figures in italics are the product of gas pressure in centimeters of mercury times path length in centimeters at which the band was observed.

complexity of the spectrum in this region the correctness of the ν_4-assignment is by no means certain.

The rotational fine structure of the band ν_1 allows the identification of several of the Q branches of the perpendicular component, from which an approximate value of the rotational constant A may be determined. The assignments of the Q branches are given in Table II. The band center of ν_1 is given as 3530 cm^{-1} in a recent publication by Jones, Shoolery, Shulman, and Yost.[3]

TABLE II. Fine structure of the band ν_1.

ν_{vac}	Assignment	$\Delta\nu$
3570	RQ_0	
		77
3493	PQ_1	
		76
3417	PQ_2	
		74
3343	PQ_3	
		71
3272	PQ_4	

Beard and Dailey[4] have calculated the molecular parameters for HNCS from the frequency of the rotational transition $J=1 \rightarrow J=2$ in the microwave region. B values were obtained for each of the five isotopic molecules, $HNC^{12}S^{32}$, $DNC^{12}S^{32}$, $HNC^{13}S^{32}$, $DNC^{13}S^{32}$, and $HNC^{12}S^{34}$ and by use of these the following molecular geometry was calculated:

$$r(H-N)=1.20A; \quad r(N=C)=1.21A;$$
$$r(C=S)=1.57A; \quad \sphericalangle HNC=112°.$$

The small moment of inertia for a molecule with the above dimensions is readily shown to be $I_A=1.775\times10^{-40}$ g cm^2, corresponding to an A value 15.77 cm^{-1}.

From the spacing of the $\perp$ component of ν_1, however, we obtain* $A-B\simeq37.50$ or, using Beard and Dailey's B value of 0.1957, $A=37.70$.

Since our measurements can hardly be more than five to ten percent in error, it is clear that Beard and Dailey's model is unsatisfactory. There is another unsatisfactory feature of this model. The N−H stretching frequency in HNCS is almost identical with that in HNCO (3536 as compared with 3531 cm^{-1}), and both of these values are abnormally high for N−H stretching frequencies. Accordingly we would expect an unusually short, rather than the abnormally long N−H bond length suggested by Beard and Dailey.

The following parameters fit our result for the A value and Beard and Dailey's B value for $HNC^{12}S^{32}$ quite well and are consistent with our accurately determined value for the N−H bond length of 1.00$_0$A in HNCO.

$$r(H-N)=1.00\pm0.01A; \quad r(N=C)=1.21A;$$
$$r(C=S)=1.57A; \quad \sphericalangle HNC=132°\pm3°.$$

The very high ratio of A to B value in this molecule makes the calculation of molecular parameters from B values of isotopic molecules particularly susceptible to error. Furthermore, apart from purely experimental errors, the use of B_0 rather than B_e values in this kind of calculation may introduce further errors when these B_0 values are used to construct models of identical geometry.

[1] G. Herzberg and C. Reid, presented at the Faraday Society Symposium on Spectroscopy and Molecular Structure (September, 1950).
[2] P. F. Bartunek and E. F. Barker, Phys. Rev. **48**, 516 (1935); L. Kahovec and K. W. F. Kohlrausch, Zeits. f. physik. Chemie **B37**, 421 (1937).
[3] Jones, Shoolery, Shulman, and Yost, J. Chem. Phys. **18**, 990 (1950).
[4] C. J. Beard and B. P. Dailey, J. Chem. Phys. **15**, 762 (1947).
* In the light of L. H. Jones and R. M. Badger's result [J. Chem. Phys. **18**, 1511 (1950), preceding letter] (the author acknowledges gratefully the opportunity to see their letter in manuscript form), it seems probable that the convergence in the ν-values (Table II), which we did not at first take into account, is in fact significant. If we allow for it, we find $A_0=39.2\pm2$ cm^{-1}. Using our $r(N-H)$ value of 1.00±0.01, this gives a bond angle of 138°36′±3° in substantial agreement with Jones and Badger's value. It is felt, nevertheless, that the latter authors' value is much more reliable than our own in view of the higher resolution attainable by them.

Comment on "Theoretical Explanation of the Chemical Effects of Ultrasonics"

ALFRED WEISSLER
Naval Research Laboratory, Washington, D.C.
August 28, 1950

IN this interesting communication[1] Miss Griffing proposes that the magnitude of the ultrasonic-chemical effect is determined by the ratio of specific heats and the thermal conductivity of the dissolved gas.

However, an experimental observation exists which cannot be explained by this theory. It is well established that, if the aqueous solution is saturated with CO_2, ultrasonic irradiation fails to produce such effects as chlorine liberation,[2] luminescence,[3] or depolymerization.[4] Yet in non-aqueous solutions saturated with CO_2, irradiation does produce the characteristic effect of depolymerization (for example, of polystyrene dissolved in toluene,[4] and of rubber dissolved in xylene[5]); this does not occur in degassed solutions. The CO_2 inside the cavitation bubbles has practically the same ratio of specific heats at a given frequency, whether surrounded by toluene or water,[6] but the chemical reaction occurs in one case and not in the other.

Perhaps the true explanation involves the influence of the gas on the violence of collapse of cavitation bubbles. If the gas can react with the solvent, or else liquefy or dissolve readily, much of the collapse-energy may be absorbed and rendered unavailable for disruption of other molecules.

[1] V. Griffing, J. Chem. Phys. **18**, 997 (1950).
[2] Weissler, Cooper, and Snyder, J. Am. Chem. Soc. **72**, 1769 (1950).
[3] E. N. Harvey, J. Am. Chem. Soc. **61**, 2392 (1939).
[4] A. Weissler, J. App. Phys. **21**, 171 (1950).
[5] K. Shibata, Reports, Tokyo Imp. Ind. Research Inst. Lab. **35**, No. 3, 1 (1940).
[6] V. O. Knudsen and E. Fricke, J. Acous. Soc. Am. **12**, 255 (1940).

Effect of Small Refractive Index Differences between the Solution and the Solvent on Light-Scattering Molecular Weight

ROLAND RIVEST AND MARCEL RINFRET
Laboratory of Physical Chemistry, University of Montreal, Montreal, Canada
August 7, 1950

THE light-scattering molecular weight of a solute is given by the familiar Debye's equation:

$$\tau=\frac{32\pi^3}{3N\lambda^4}\left(\frac{n-no}{c}\right)^2 n^2 \frac{c}{(1/M)+2Bc}$$

where τ—turbidity due to the solute, λ—wave-length of the primary beam, N—Avogadro's number, n—refractive index of solution, no—refractive index of solvent, c—concentration of solute in gram per cubic centimeter of solution, M—molecular weight of solute, B—constant dependent upon the solvent chosen for the experiments.

When the solute is a polymer, one has to take into account the dissymetry of the light scattered because of the interference effect in the backward and forward directions.[1]

We used the Debye's equation for the determination of the molecular weight of GR-S rubber in solution in toluene. The molecular weight obtained was far too high, since the viscosity molecular weight was found to be 125,000 at 25°C, and the light-scattering molecular weight was found equal to one million.

We repeated our experiments many times with great care, and always obtained the same result. We did other light-scattering measurements on GR-S using carbon tetrachloride and ethylene chloride as solvents. The results obtained with these solutions were in good agreement with the viscosimetric determinations.

We noted that the unexpected results described above were obtained with solutions of small refractive index difference with the

solvent. We assumed that this small difference was responsible for such results.

From Debye's equation it appears that, when the refractive index difference between the solution and the solvent is very small, the turbidity of the solution must be also very small.

We planned an experiment to have another test of the value of Debye's equation for very small refractive index differences. Using tetrachlorethane as a solvent and cellulose acetate as a solute we obtained what was desired, because the values of the refractive indices of both are very close to each other. We made the value of $n-no$ very close to zero by the addition of ethylene chloride to the solution. We prepared a mixture of solvents of the same composition and we presumed that the turbidity due to the solute would be very small because of the negligible value of $n-no$.

The turbidity of the solution was found to be one time and a half that of the solvent mixture. This yields a value of about ten million for the molecular weight compared with a viscosity molecular weight of 60,000 for the same polymer.

TABLE I.

Solvent	Solute	$\left(\frac{n-no}{c}\right)^2$	Molecular weight (Light scattering)	(Viscosity)
Ethylene chloride	GR-S	27.2 $\times 10^{-3}$	140,000	125,000
Carbon tetrachloride	GR-S	14.4 $\times 10^{-3}$	120,000	125,000
Toluene	GR-S	3.1 $\times 10^{-3}$	1,000,000	125,000
Tetrachloroethane Ethylene chloride	Cellulose acetate	0.036 $\times 10^{-3}$	10,000,000	60,000

Table I gives the value of light-scattering molecular weight compared with viscosity molecular weight. For each solution we give the value of $[(n-no)/c]^2$.

The results of turbidity measurements are in good agreement with viscosimetric determinations for the first solutions where the value of $[(n-no)/c]^2$ is large enough. When this value decreases, the difference between viscosimetric and light-scattering determinations increases very rapidly.

The results tabulated in Table I indicate that Debye's equation is correct only under certain conditions and one of those conditions is to have a large enough value of $n-no$.

[1] P. J. Debye, J. Phys. Colloid Chem. **51**, 18 (1947).

The Structure of Nitrosyl Chloride from the Microwave Absorption Spectrum

H. J. BERNSTEIN
Division of Chemistry, National Research Council, Ottawa, Canada
September 13, 1950

THE recent note[1] on the microwave absorption of NOCl gave the values for the moments of inertia listed in Table I.

TABLE I.

	Microwave NOCl[35]	Microwave NOCl[37]	Electron diffraction NOCl[35.5]
I_C	152.59 ±0.04	153.05 ±0.08	156.7
I_B	147.33 ±0.03	148.12 ±0.08	147.7
I_A	5.27 ±0.07	4.93 ±0.16	9.05

Those obtained by electron diffraction[2] are listed for comparison. (All moments of inertia are expressed in units of 10^{-40} c.g.s.)

Calculation of the molecular dimensions from the microwave data leads to a bond distance for NO in NOCl which is less than 1.080A. This is so much less than 1.150A which is the NO distance[3] in the nitric oxide molecule that it would seem to be an unlikely value for the NO distance. The entropy at 298°K calculated[4] with the electron diffraction value of the least moment of inertia agrees within the experimental error with the observed value, whereas the entropy calculated with the least moment of inertia obtained from microwave absorption gives a value which is 1.0 entropy unit lower than the observed value. This is well beyond the discrepancy permitted by experimental error.

The observed frequencies for the transitions between rotational levels were used for determining I_C and I_B whereas I_A was found from the sum rule ($I_C=I_B+I_A$) since the data are not sufficiently accurate to obtain I_A from the frequency reported for the $1_{-1}\rightarrow 2_{-2}$ transition.

The microwave value for I_A obtained from the sum rule is not compatible with the geometry of the molecule nor the observed value of the entropy, whereas the value of I_A determined by electron diffraction is quite suitable.

Higher accuracy in determining the frequencies in the microwave spectra is needed before a value for I_A can be obtained with an accuracy which is comparable to that obtained by electron diffraction, *viz.*, $9.05\pm0.50\times10^{-40}$ c.g.s. unit.

[1] Pietenpol, Rogers, and Williams, Phys. Rev. **77**, 741 (1950).
[2] J. A. A. Ketelaar and K. J. Palmer, J. Am. Chem. Soc. **59**, 2629 (1937).
[3] G. Herzberg, *Diatomic Molecules* (Prentice-Hall, Inc., New York, 1939), p. 490.
[4] W. G. Burns and H. J. Bernstein (in press).

Thermodynamic Functions for Fluorine

GEORGE M. MURPHY AND JOHN E. VANCE
Chemistry Laboratories of Washington Square College, New York University, New York, New York
September 21, 1950

MOLECULAR data were used by us[1] some years ago to calculate the entropy, free energy, and heat capacity of fluorine gas. Our results, however, were subject to slight uncertainties since the value of the internuclear distance of the molecule came from a preliminary electron diffraction result of Brockway[2] and the vibrational frequency, in the absence of a direct spectroscopic measurement, had to be estimated by the use of Badger's rule.[3]

These two sources of uncertainty have now been removed, as Rogers, Schomaker, and Stevenson[4] have reported a more precise electron diffraction result and, recently, Andrychuk[5] has observed the Raman spectrum of gaseous fluorine. It has thus seemed useful to recalculate our 1939 results using the new molecular constants. At the same time, we have thought it worth while to use the revised values of the natural constants, Avogadro's number, Planck's constant, etc. For the latter purpose, we have taken the working formulas given by Wagman *et al.*[6]

Our earlier values for the internuclear distance and vibrational frequency, with their estimated probable errors were $r_0=1.45\pm0.05$A; $\omega_0=856\pm17$ cm^{-1}; the revised values are $r_0=1.435\pm0.01$A; $\omega_0=892.1\pm2$ cm^{-1}. With the latter data, we have calculated the thermodynamic quantities shown in Table I by the

TABLE I. Thermodynamic functions of fluorine gas, F_2 (in cal./mole).

T, °K	$-(F^0-H_0^0)/T$	S^0	Cp^0
298.16	41.412	48.484	7.466
300	41.455	48.530	7.474
400	43.510	50.734	7.853
500	45.139	52.519	8.135
600	46.498	54.020	8.331
800	48.696	56.453	8.566
1000	50.446	58.379	8.691
1200	51.905	59.970	8.763
1400	53.156	61.325	8.809
1600	54.253	62.503	8.839
1800	55.228	63.546	8.860
2000	56.108	64.480	8.876

well-known methods for the rigid rotator-harmonic oscillator molecular model. In comparing our present results with the earlier ones, it will be observed that the latter are larger in each case. The differences in the free energy function, $-(F^0-H_0^0)/T$ range from 0.08 to 0.14 cal./mole, the two figures referring to 298.16° and 2000°, respectively. For the entropy, the corresponding differences are 0.09 to 0.16 and for the heat capacity, 0.06 to 0.00. It should be remembered, however, that these variations are from two sources: change in the fundamental natural constants and change in the molecular constants.

Lack of a reliable value for the heat of dissociation of fluorine into atoms or the heat of dissociation for another fluorine containing molecule prevents us from recalculating equilibria involving fluorine or fluorine compounds. This difficulty was discussed in our earlier paper and has been considered more recently by Gaydon,[7] Potter,[8] and Nathans.[9] It appears that this source of uncertainty can only be removed when further experimental data are available.

[1] G. M. Murphy and J. E. Vance, J. Chem. Phys. **7**, 806 (1939).
[2] L. O. Brockway, J. Am. Chem. Soc. **60**, 1348 (1938).
[3] R. M. Badger, J. Chem. Phys. **2**, 128 (1934); **3**, 710 (1935).
[4] Rogers, Schomaker, and Stevenson, J. Am. Chem. Soc. **63**, 2610 (1941).
[5] D. Andrychuk, J. Chem. Phys. **18**, 233 (1950).
[6] Wagman, Kilpatrick, Taylor, Pitzer, and Rossini, J. Research Nat. Bur. Stand. **34**, 143 (1945).
[7] A. G. Gaydon, *Dissociation Energies and Spectra of Diatomic Molecules* (Dover Publications, Inc., New York, 1950).
[8] R. L. Potter, J. Chem. Phys. **17**, 957 (1949).
[9] M. W. Nathans, J. Chem. Phys. **18**, 1122 (1950).

The Infra-Red Spectra of Propane and 2,2-Dideuteropropane

H. L. McMURRY AND V. THORNTON
Phillips Petroleum Company, Research Division, Bartlesville, Oklahoma
June 29, 1950

IN an earlier paper[1] the frequency assignments for the vibrational modes of propane were discussed in the light of the infra-red spectra of 1-deuteropropane and 2-deuteropropane. We have since obtained the spectrum of a sample of 2,2-dideuteropropane estimated to be 98 percent pure.[2] This spectrum, together with that of propane for comparison, is shown in Fig. 1.

The new data show that the three type B_1 bands below 1350 cm^{-1} in the propane spectrum have analogs at markedly lower frequencies in the 2,2-dideuteropropane spectrum.[3] The changes on going from propane to 2,2-dideuteropropane are 1336 to 1199, 1053 to 964, 923 to 850 cm^{-1}. These modes, belonging to species B_1, involve rocking motions of the CH_3 groups and the CH_2 (or CD_2) group about axes normal to the plane of the carbons, and the unsymmetrical C−C−C stretching motion. Since the frequencies of all three modes are sensitive to substitution of CD_2 for CH_2, the CH_2 rocking motion in propane is seen to interact strongly with the CH_3 rocking and unsymmetrical C−C−C stretching motions. It is, therefore, unrealistic to describe the low frequency modes of species B_1 in propane as specific group vibrations.

The present data, together with available Raman data, permit reasonable assignments for the approximate frequencies of all the modes belonging to species A_1 and B_1 in both propane and 2,2-dideuteropropane. These are given in Table I. The ratios for

TABLE I. Frequencies of the A_1 and B_1 modes in propane and 2,2-dideuteropropane.

Symmetry	Propane frequency[a]	2,2-Deuteropropane frequency[a]	Propane mode[c,d]
A_1	2940 (cm^{-1})	2920 (cm^{-1})	CH_3 u. st.
	2940	2920	CH_3 sy. st.
	2940	2160	CH_2 (CD_2) sy. st.
	1460	1460	CH_3 u. def.
	1460	1062	CH_2 (CD_2) def.
	1380	1380	CH_3 sy. def.
	1155(?)	1140(?)	CH_3 r. plus C−C−C sy. st.
	870	850	C−C−C sy. st. plus CH_3 r.
	372[b]	370 (est.)	CCC def.
B_1	2940	2920	CH_3 u. st.
	2940	2920	CH_3 sy. st.
	1460	1460	CH_3 u. def.
	1380	1380	CH_3 sy. def.
	1336	1199	CH_2 (CD_2) r. plus CH_3 r. and C−C−C u. sy. st.
	1053	964	CH_2 (CD_2) r. plus CH_3 r. and C−C−C u. sy. st.
	923	850	C−C−C u. sy. st. plus CH_3 r. and CH_2 (CD_2) r.

[a] Where bands are nearly superposed the frequency is generally near the center of the absorption. Bands of doubtful origin are indicated by (?), estimated values for unobserved frequencies by (est.).
[b] Obtained for gaseous propane by J. R. Nielsen and C. M. Richards (unpublished).
[c] The abbreviations u., sy., st., def., r. stand for unsymmetrical, symmetrical, stretching, deformation, and rocking, respectively. When the mode in 2,2-dideuteropropane involves the CD_2 this is placed after CH_2 in parenthesis, i.e., $CH_2(CD_2)$.
[d] Where possible the modes are characterized by the most important group motions involved in them. They are given in more detail in Table I of reference 1.

TABLE II. Moments of inertia of propanes.[a]

	I_x	I_y	I_z
$CH_3CH_2CH_3$	67.6	17.3	59.6
$CH_3CD_2CH_3$	70.4	21.9	61.3

[a] The z axis is the symmetry axis. The x and y axes are principal axes normal to the z axis, and normal to the plane of the carbons and in this plane, respectively. The units are atomic weight times angstroms squared. The C−C and C−H (or C−D) distances are 1.54 and 1.09A, respectively. All angles are tetrahedral except the C−C−C angle which is 111°30′ (see K. S. Pitzer, J. Chem. Phys. **12**, 310 (1944).

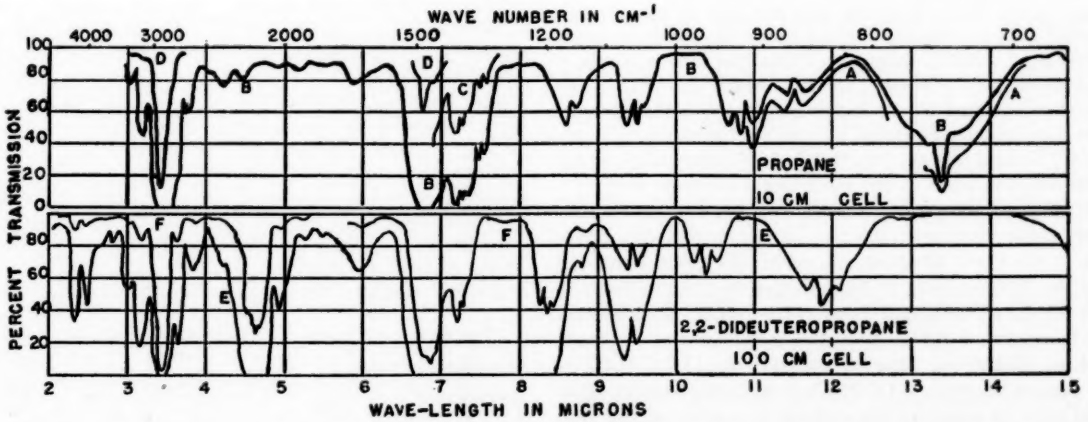

FIG. 1. Infra-red spectra of propane and 2,2-dideuteropropane A, 760 mm; B, 620 mm; C, 100 mm; D, 25 mm; E, 100 mm; F, 20 mm.

the frequency products for the 2,2-dideuteropropane modes to those for propane are 0.52 and 0.75 for the A_1 and B_1 species, respectively. These compare with 0.50 and 0.74, respectively, obtained from the Teller-Redlich equation[4] using the moments of inertia in Table II.

The help of Dr. F. E. Condon in supplying the 2,2-dideuteropropane is acknowledged. Dr. F. E. Frey and Dr. F. W. Crawford encouraged this work.

[1] McMurry, Thornton, and Condon, J. Chem. Phys. **17**, 918 (1949).
[2] Details as to preparation and purity will be published later in the *Journal of the American Chemical Society*.
[3] Band shapes are important in identifying analogs (see reference 1).
[4] F. Halverson, Rev. Mod. Phys. **19**, 87 (1947).

Note on the Rotational Isomers of 1,2-Dihalogenoethanes

SAN-ICHRO MIZUSHIMA AND YONEZO MORINO
Chemical Laboratory, Faculty of Science, Tokyo University, Bunkyo-ku, Tokyo, Japan
September 5, 1950

So far we have explained the change of Raman and infra-red spectra of 1,2-dihalogenoethanes with the change of state on the basis of the rotational isomer theory (hereafter abbreviated as R.I.T.); in other words, we have explained it from the difference of the equilibrium ratio of rotational isomers in different states of aggregation.[1] In this note we shall answer the questions raised by some investigators against R.I.T. (1) The inconsistency of the intensity of Raman lines assigned to one molecular form (*trans*-form) was pointed out to exist among the Raman spectra in the gaseous, liquid, and solid states. However, the exact intensity measurements of Raman lines reported in our papers[1] have been made only for the two lines described in the text, and the figures given in our tables refer to the visually estimated intensities as usually. Therefore, the intensity of weak lines of the gaseous spectrum which are not sufficiently exposed tends to be underestimated. So also is the case for the strong lines of the overexposed liquid spectrum. This gives rise to the apparent inconsistency of the intensity of lines estimated visually. (2) Bishui[2] reported that the Raman line at 1056 cm^{-1} of 1,2-$C_2H_4Br_2$ is totally depolarized in contradiction to R.I.T., but Neu, Ottenberg, and Gwinn[3] found the corresponding line of 1,2-$C_2H_4Cl_2$ to be polarized ($\rho=0.47$) as would be predicted by R.I.T. It is desirable to repeat the polarization measurement on the 1056-cm^{-1} line of 1,2-$C_2H_4Br_2$. (3) Bishui's result[2] that the intensity ratio of the two lines, 660 cm^{-1} (*trans*-form) and 551 cm^{-1} (gauche form), of 1,2-$C_2H_4Br_2$ changed only slightly between 30° and 95°C also cannot offer evidence in disproof of R.I.T., since the energy difference between the rotational isomers of this substance in the liquid state is very small (0.75 kcal./mole) according to our measurement[4] and that of Rank, Kagarise, and Axford.[5] (4) Bishui[6] considered that too many Raman frequencies were observed below 1100 cm^{-1} for 1,1-$C_2H_4Cl_2$ which should have no rotational isomer according to our view. However, all these Raman frequencies can reasonably be assigned to the vibrations of only one molecular form. We may tentatively assign 168 cm^{-1} to the torsional vibrations, 275, 322, and 408 cm^{-1} to the skeletal deformation vibrations, 640 and 688 cm^{-1} to the stretching vibrations of C—Cl, and 905, 977, and 1054 cm^{-1} to the C—H deformation and the C—C stretching vibrations, the last frequency probably corresponding to the C—C vibration. Therefore, his experimental result that the disappearance of Raman lines on solidification was observed for 1,2-$C_2H_4Cl_2$ and not for 1,1-$C_2H_4Cl_2$ affords good evidence in support of R.I.T. According to the association theory proposed by Bishui, we have to consider that 1,2-$C_2H_4Cl_2$ is strongly associated, while 1,1-$C_2H_4Cl_2$ is not associated at all in the liquid state. It would be very difficult to understand this conclusion by any of the existing molecular theories.

In conclusion, we want to add that R.I.T. is supported not only by spectroscopic data, but also by the experimental results of electron diffraction, dielectric constant, and entropy.[1]

[1] See, for example, Mizushima, Morino, Watanabe, Shimanouchi, and Yamaguchi, J. Chem. Phys. **17**, 591 (1949).
[2] B. M. Bishui, Ind. J. Phys. **22**, 253 (1948).
[3] Neu, Ottenberg, and Gwinn, J. Chem. Phys. **16**, 1004 (1948).
[4] Morino, Mizushima, Kuratani, and Katayama, J. Chem. Phys. **18**, 754 (1950).
[5] Rank, Kagarise, and Axford, J. Chem. Phys. **17**, 1354 (1949).
[6] B. M. Bishui, Ind. J. Phys. **22**, 319 (1948).

The Infra-Red Spectrum of Nitrosyl Fluoride

E. A. JONES AND P. J. H. WOLTZ
K-25 Research Laboratories, Carbide and Carbon Chemicals Divisions, Union Carbide and Carbon Corporation, Oak Ridge, Tennessee*
August 8, 1950

The infra-red spectrum of nitrosyl fluoride, which so far as the present authors can determine has not been previously reported, has been studied throughout the region 260 to 7000 cm^{-1}. Of the nitrosyl halides, measurements have been reported by Bailey and Cassie[1] on NOCl and a reinvestigation of this molecule, as well as a report on NOBr, has recently been given by Bernstein and Powling.[2] The data on NOF were obtained with a Perkin-Elmer Model 12C spectrometer equipped with LiF, NaCl, KBr, and KRS-5 prisms. The sample was prepared in a fluorothene[3] test tube by the direct fluorination of nitric oxide. NOF readily attacks glass; therefore, the techniques reported earlier[3,4] for studying corrosive fluorine compounds in the infra-red region were used.

The frequencies of the observed bands are given in Table I, together with the relative intensities and tentative assignments.

TABLE I. Frequencies of infra-red bands in the spectrum of NOF.

Observed frequency (cm^{-1})	Assignment	Calculated frequencies (cm^{-1})	Intensity[a]
521	ν_2	—	100
767	ν_3	—	100
1038	$2\nu_2$	1042	8
1282	$\nu_2+\nu_3$	1288	11
1511	$2\nu_3$	1534	6
1844	ν_1	—	100
2365	$\nu_1+\nu_2$	2365	13
2613	$\nu_1+\nu_3$	2611	11
3087	$\nu_1+\nu_2+\nu_3$	3132	1
3635	$2\nu_1$	3688	14
4176	$2\nu_1+\nu_2$	4209	1
4441	$2\nu_1+\nu_3$	4455	1
5417	$3\nu_1$	5532	2

[a] Relative intensity on the basis of 100 for the strongest bands.

NOF is a bent unsymmetrical molecule having three fundamental modes of vibration. It is believed that the strong infra-red bands located at 521, 767, and 1844 cm^{-1} are ν_2, ν_3, and ν_1, respectively, where ν_2 corresponds to the asymmetric mode of the YX_2 model. Each of the fundamental bands exhibits three maxima with an average $P-R$ separation of 32 cm^{-1}.

Measurements in the regions 1038, 1282, and 1510 cm^{-1} were complicated by the presence of impurity bands. The information on these bands may, therefore, be somewhat in doubt. On the other hand, reasonable assignments can be made for these bands on the basis of the assigned fundamentals.

Further details on this work will be reported later.

* This document is based on work performed for the AEC by Carbide and Carbon Chemicals Division, Union Carbide and Carbon Corporation, Oak Ridge, Tennessee.
[1] C. R. Bailey and A. B. D. Cassie, Proc. Roy. Soc. **145**, 336 (1934).
[2] Presented at Symposium on Molecular Structure and Spectroscopy, The Ohio State University, Columbus, Ohio (June 15, 1950).
[3] J. S. Kirby-Smith and E. A. Jones, J. Opt. Soc. Am. **39**, 780 (1949).
[4] Jones, Parkinson, and Murray, J. Chem. Phys. **17**, 501 (1949).

The Propagation of Order in the Simple Cubic Lattice

TAKEHIKO OGUCHI
Tokyo Institute of Technology, Oh-okayama, Tokyo, Japan
August 28, 1950

WE have obtained the correlation probabilities,[1] as a measure of the propagation of order in an Ising model of ferromagnetism of the simple cubic lattice, in the form of power series valid at low and high temperatures, respectively. The correlation probability between a spin on the zeroth site and that on the nth site at a distance of n sites away in the same line of the crystal from the zeroth site is defined by

$$C(0, n)=f(0, n)/f, \tag{1}$$

where f is an ordinary partition function and $f(0, n)$ is a partition function to be taken over the configurations allowed by the restriction by which the spins on zeroth site and nth site have the same polarities.

For low temperatures, both f and $f(0, n)$ are obtained by counting the configurations.[2] Thus, we have found

$$\begin{aligned}
C(0,1)&=1-2\beta^6-10\beta^{10}+14\beta^{12}-70\beta^{14}+176\beta^{16}-626\beta^{18}\cdots\\
C(0,2)&=1-2\beta^6-12\beta^{10}+16\beta^{12}-88\beta^{14}+212\beta^{16}-790\beta^{18}\cdots\\
C(0,3)&=1-2\beta^6-12\beta^{10}+16\beta^{12}-90\beta^{14}+216\beta^{16}-818\beta^{18}\cdots\\
C(0,4)&=1-2\beta^6-12\beta^{10}+16\beta^{12}-90\beta^{14}+216\beta^{16}-820\beta^{18}\cdots
\end{aligned} \tag{2}$$

and to terms of order β^{18}

$$\begin{aligned}
C(0, n)&=C(0, 4), \qquad n\geq 5.\\
\beta&=\exp(-2K), \quad K=J/2kT.
\end{aligned} \tag{3}$$

J is the energy gained if two neighbors change from an antiparallel to a parallel position. $C(0, 1)$ agrees with the one obtained by van der Waerden which is quoted in the paper of Ashkin and Lamb.[1]

For high temperatures the treatment is different from that for low temperatures. The partition function is transformed as follows.

$$f=\sum_{\mu_i=\pm 1}\exp\Big(K\sum_{\langle i,k\rangle}\mu_i\mu_k\Big)=(\cosh K)^{2N}\sum_{\mu_i=\pm 1}\prod_{\langle i,k\rangle}(1+\mu_i\mu_k\kappa). \tag{4}$$

$$\kappa=\tanh K, \tag{5}$$

where μ_i is the spin component on ith site, which is capable of taking the values, $+1$ or -1. $\sum_{\langle i,k\rangle}$ or $\prod_{\langle i,k\rangle}$ means that the sum or product is carried out over all connecting lines between the direct neighbors, and $\sum_{\mu_i=\pm 1}$ means that the sum is carried out over all spins. (The total number of spins is M.) In developing the product, we get a series consisting of various products. But after it is summed over all values of the μs, most of the terms will vanish. The only non-vanishing terms are those which consist of the pairs forming closed polygons in the same way as for the case of the dual transformation.[3] Thus the partition function is expressed in the following form.

$$f=2^N(\cosh K)^{3N}\left[1+3N\kappa^4+22N\kappa^6+\left(\frac{9}{2}N^2+\frac{375}{2}N\right)\kappa^8\cdots\right] \tag{6}$$

and

$$f^{1/N}=2(\cosh K)^3(1+3\kappa^4+22\kappa^6+192\kappa^8\cdots). \tag{7}$$

Equation (7) is the same result as that which D. Ter Haar[4] has obtained by the method of Opechowsky[5] up to terms of order K^6.

In the expression of $f(0, n)$, besides the closed polygons mentioned above, those lines consisting of successive pairs which have their terminals at zeroth spin and nth spin also contribute as non-vanishing terms. From (1) we have

$$\left.\begin{array}{lccccccc}
C(0,1)=\frac{1}{2}(1+\kappa & +4\kappa^3 & & +40\kappa^5 & & +456\kappa^7 & & \cdots\\
C(0,2)=\frac{1}{2}(1 & +\kappa^2 & +12\kappa^4 & & +176\kappa^6 & & +2348\kappa^8 & \cdots\\
C(0,3)=\frac{1}{2}(1 & & +\kappa^3 & +24\kappa^5 & & +504\kappa^7 & & \cdots\\
C(0,4)=\frac{1}{2}(1 & & & +\kappa^4 & +40\kappa^6 & & +1156\kappa^8 & \cdots\\
C(0,5)=\frac{1}{2}(1 & & & & +\kappa^5 & +60\kappa^7 & & \cdots\\
C(0,6)=\frac{1}{2}(1 & & & & & +\kappa^6 & +84\kappa^8 & \cdots\\
C(0,7)=\frac{1}{2}(1 & & & & & & +\kappa^7 & \cdots\\
C(0,8)=\frac{1}{2}(1 & & & & & & & +\kappa^8\ \cdots
\end{array}\right\}. \tag{8}$$

In order to calculate the paramagnetic susceptibility χ, we must add the energy due to the external magnetic field H to the partition function (4). Thus

$$\begin{aligned}
f&=\sum_{\mu_i=\pm 1}\exp\Big(K\sum_{\langle i,k\rangle}\mu_i\mu_k+C\sum_i\mu_i\Big)\\
&=(\cosh K)^{3N}(\cosh C)^N\sum_{\mu_i=\pm 1}\prod_{\langle i,k\rangle}(1+\mu_i\mu_k\kappa)\prod_i(1+\mu_i\tanh C).
\end{aligned} \tag{9}$$

$$C=mH/kT, \tag{10}$$

where m is the magnetic moment of each spin. Considering that the susceptibility is proportional to the coefficient of $(\tanh C)^2$ in $\log f$, we obtain

$$\frac{2N\mu^2}{J}\frac{1}{\chi}=\frac{1}{K}(1-6\kappa+6\kappa^3-6\kappa^3+30\kappa^4-54\kappa^5+318\kappa^6\cdots). \tag{11}$$

The theoretical paramagnetic Curie point K_p, which is obtained from the asymptote of (11), is given by

$$1-6\tanh K_p=0, \quad K_p=0.168. \tag{12}$$

The results of the ordering influence of more complicated configurations and those of other lattice types will be published in the *Journal of the Physical Society of Japan*.

The author desires to give his sincere thanks to Professors Y. Takagi and R. Kubo for their kind guidance in the course of this work.

[1] J. Ashkin and W. E. Lamb, Jr., Phys. Rev. **64**, 159 (1943).
[2] H. A. Kramers and G. H. Wannier, Phys. Rev. **60**, 263 (1941).
[3] G. H. Wannier, Rev. Mod. Phys. **17**, 50 (1945).
[4] D. Ter Haar, Phys. Rev. **76**, 176 (1949).
[5] W. Opechowsky, Physica **4**, 181 (1937).

The Heat of Dissociation of Carbon Monoxide

GEORGE GLOCKLER
Department of Chemistry and Chemical Engineering, State University of Iowa, Iowa City, Iowa*
September 5, 1950

THE heat of sublimation of carbon L(C) has been determined lately by three different investigators.[1-3] If in these experiments the equilibrium vapor pressure of carbon is measured, then the atomic heat of dissociation of carbon monoxide D_0(CO) is about 255 kcal. The ordinary heat of formation[4] of carbon monoxide is 27.2019 kcal. at 0°K, and the heat of dissociation[5] of oxygen molecules is 117.16 kcal. D_0(CO) must be less than the

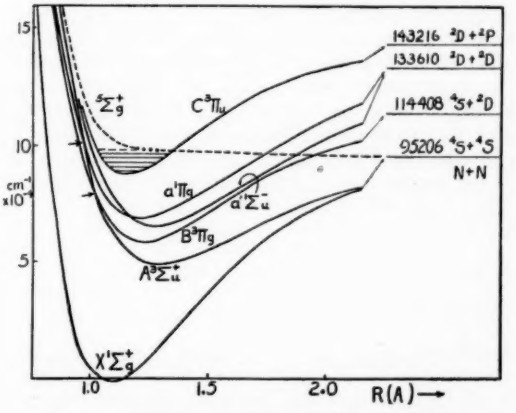

FIG. 1. Energy level diagram of carbon monoxide.

dissociation limit observed from predissociations[6] (11.11 ev) and D_0(CO) = 11.08 ev has been adopted, giving less weight to the determintion of L(C) by Marshall and Norton.[3]

The above value of $D_0(CO)$ has been used to construct the energy diagram of CO shown in Fig. 1. The distinctive feature is a repulsive state arising from $C(^3P)+O(^3P)$ at 89397 cm^{-1} or 11.08 ev and reaching about 89700 cm^{-1} or 11.12 ev at $r=1.2$A. Toward smaller distances it rises and at 1.1A it is about 93500 cm^{-1} or 11.60 ev. This repulsive level is supposed to predissociate $C'\Sigma^+$ ($v=0$, $K=29$) at 93536 cm^{-1}, $B'\Sigma^+$ ($v=0$, $K=38$) at 89700 cm^{-1}, $B'\Sigma^+$ ($v=1$, $K=18$) at 89650 cm^{-1}, and $b^3\Sigma^+$ ($v=0$, $K=55$) at about this height. The vibration levels $v=1$ of $C'\Sigma^+$ (~94008 cm^{-1}), $v=2$ of $B'\Sigma^+$ (~90940 cm^{-1}) are affected by the crossing of this assumed repulsive state and no bands arising from them have been found as yet.[7] The repulsive state may perhaps cause the effects observed, not only by predissociation but also by dissociating molecules possessing energies in this region by virtue of a greater transition probability. All other irregularities in the spectrum of CO are considered to be perturbations. $A'\Pi$ is an example.[8] The state $b^3\Sigma^+$ ($v=2$) at about 88140 cm^{-1} is crossed by $a'^3\Sigma^+$ at $r\doteq1.02$A leading to strong perturbation which may be the reason for its absence at that point.[8]

It is suggested that this energy diagram can serve as a start to explain all perturbations and so-called predissociations of the CO molecule provided the simple Morse curves are replaced by others involving the rotational changes mentioned by Oldenberg.[9]

* Financial support was received from ONR under Contract N-8 onr 79400.

1 Brewer, Gilles, and Jenkins, J. Chem. Phys. **16**, 797 (1948).
2 Simpson, Thorn, and Winslow, AEC Argonne National Laboratory, Report of Chemistry Division ANL-4264 (1949).
3 A. L. Marshall and F. J. Norton, J. Am. Chem. Soc. **72**, 2166 (1950).
4 *Selected Values of Properties of Hydrocarbons* (National Bureau of Standards, Circular C461, 1947).
5 G. Herzberg, *Molecular Spectra and Molecular Structure. I. Spectra of Diatomic Molecules* (D. Van Nostrand Company, Inc., New York, 1950).
6 A. G. Gaydon, *Dissociation Energies and Spectra of Diatomic Molecules* (John Wiley and Sons, Inc., New York, 1947).
7 References 5 and 6 give all of the literature references used.
8 Reference 6, p. 186.
9 O. Oldenberg, Zeits. f. Physik **56**, 563 (1929).

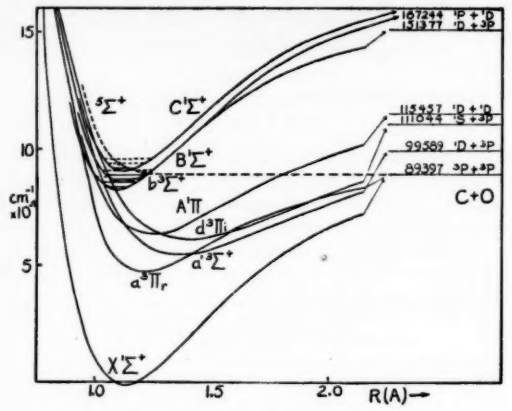

FIG. 1. Energy level diagram of nitrogen.

The Heat of Dissociation in Nitrogen

GEORGE GLOCKLER
Department of Chemistry and Chemical Engineering, State University of Iowa, Iowa City, Iowa*
September 5, 1950

AN estimate of the heat of dissociation of nitrogen is made by comparing this molecule with the isoelectronic carbon monoxide. The force constants[1] are $k(N_2)=2.29$ and $k(CO)=1.89$ megadynes/cm. The internuclear distances[2] are $R(N_2)=1.095$A and $R(CO)=1.128$A. The currently discussed heats of dissociation[2,3] are $D(N_2)=9.764$ or 7.384 ev and $D(CO)=9.61$ or 11.1 ev. The latter value fits the determinations of the heat of sublimation of carbon[4] (preceding note). From a comparison of these properties one would expect that the heat of dissociation of nitrogen should also be greater than either of the above values. If the term values of N_2 are compared with the ones of CO arranged in order of magnitude,[2] then it is found that they stand in the ratio 1.0655:1. The second highest terms [$A^3\Sigma_u^+$ (50206) for N_2 and $a^3\Pi_r$ (48688) for CO] do not follow this rule. However, the term $a'(^1\Sigma_u^-)$ for N_2 can be calculated to be 66380 cm^{-1} from $d^3\Pi_i$ (62299.4) of CO. Gaydon estimates it to be around 65000 to 67000 cm^{-1}. Applying the rule to $D(N_2):D(CO)$ with $D(CO)=11.08$ ev yields $D(N_2)=11.80$ ev. This value has been used to construct an energy diagram for nitrogen (Fig. 1). It is supposed that a repulsive state starts from the $^4S+^4S$ level (95206 cm^{-1}) and crosses $C^3\Pi_u$ just below 97946 cm^{-1} at the dissociation limit.[2,3] The breaking-off points on account of predissociation in $v'=1$, 2, 3, 4 at $K=65$, 55, 43, and 28 lie on this repulsive curve at about 1.195, 1.223, 1.253, and 1.281A, respectively. These points were found from the work of Büttenbender and Herzberg[5] and sketching the probability functions of the oscillator onto the corresponding vibration levels. It may be that this proposed repulsive state has a greater transition probability than other states at about 11 ev and hence other states may not appear. The $A^3\Sigma_u^+$-state perturbs $B^3\Pi^g$ ($v=12$) at 79385 and the $a'\Pi_g$ ($v=9$) at 84787 cm^{-1}. In Fig. 1 these crossings happen at 74000 and 98000, respectively. It must be remembered that these simple Morse curves do not give quite the correct picture of the potential energy of the molecule. It is suggested that the value $D(N_2)=11.8$ ev mentioned here deserves consideration and that this diagram can serve as basis for explaining all the perturbations and so-called predissociations of the nitrogen molecule. An early value of $D(N_2)\doteq11.5$ ev by Sponer[6] was based on electron impact experiments and hence less accurate. The possibility that active nitrogen is really nitrogen atoms must again be considered.[7]

* Financial support was received from ONR under Contract N-8 onr 79400.

1 K. W. F. Kohlrausch, *Der Smekal-Raman Effekt* (Verlag. Julius Springer, Berlin, 1931).
2 G. Herzberg, *Molecular Spectra and Molecular Structure. I. Spectra of Diatomic Molecules* (D. Van Nostrand Company, Inc., New York, 1950).
3 A. G. Gaydon, *Dissociation Energies and Spectra of Diatomic Molecules* (John Wiley and Sons, Inc., New York, 1947).
4 Reference 3, p. 184.
5 G. Büttenbender and G. Herzberg, Ann. d. Physik **21**, 577 (1935).
6 H. Sponer, Zeits. f. Physik. **34**, 622 (1925).
7 R. J. Strutt, Proc. Roy. Soc. **85**, 219 (1911).